METALLOPHTHALOCYANINES AS PHOTOCATALYSTS FOR TRANSFORMATION OF CHLOROPHENOLS AND SELF-ASSEMBLED MONOLAYERS FOR ELECTROCHEMICAL DETECTION OF THIOLS AND CYANIDES

A thesis submitted in fulfilment of the requirements for the degree of

DOCTOR OF PHILOSOPHY

of

RHODES UNIVERSITY

by

KENNETH IKECHUKWU OZOEMENA
{M.Sc (Chem.), M.Sc (Pharm. Chem.), Lagos}

November 2002

DEDICATION

To my dear papa, Mr. Celestine Echefu Ozoemena (who passed on barely two months after I arrived South Africa for this degree programme) and mama, Mrs. Helen Ada Ozoemena, for their love and uncompromising obsession with my education.

ACKNOWLEDGMENTS

First, I would like to thank Almighty God through our Lord and Saviour Jesus Christ for this and great things He has always done. I owe an immeasurable debt of gratitude to my supervisor, Prof. Tebello Nyokong, for giving me the opportunity to work with her, and making research such fun. It is her unequalled supervision and painstaking attention to details that brought me this far. I am greatly honoured to be associated with such a rare gem of an academic.

I wish to give special thanks to my beautiful wife, Rita, for her thoughtfulness, invaluable support, patience and encouragement. To every member of Ozoemena's family, especially my siblings, and all Obinikpa-umuokpara for their prayers and moral supports. It woud not have been possible for me to get to this stage of education without the care and nurture of Okai's Okoronyeama, and particularly the Okoroike's family. Ndi umere nnem, I salute you! To dedem Columba and Simeon and families, I hope I have not disappointed you. I can never thank you well enough. Engr. Kevin Obiodu, dedem Josiah, Lukman, Innocent, Chidi and their families, and all my great inlaws, Ezinne G.N. Agwu and family, I thank you with all my heart.

I will remain eternally grateful to the Andrew Mellon Foundation for the PhD scholarship, and the National Research Foundation (NRF) for financial assistance. I am thankful to Dr. Sci. Nina Kuznetsova (a photochemist who visited from Organic Intermediates and Dyes Institute, Moscow, Russia) and Dr. Philippe Westbroek (electrochemist from Ghent University, Ghent, Belgium) for lavishly sharing their wealth of knowledge with me. To all academic and technical staff of Chemistry Department, Rhodes University, you are simply wonderful. All my friends and colleagues (too numerous to mention by names) in the Chemistry department for the challenging intellectual interactions we have shared over these thirty-three months, thank you a million times! Finally, I wish to acknowledge all the helpful discussions (oral and e-mail) with several academics, and especially the constructive criticisms and concerns raised by referees of the published works from this thesis. Thank you guys.

ABSTRACT

Photochemical properties of sulphonated phthalocyanine complexes of aluminium, zinc, tin and silicon, and octa-carboxyphthalocyanine complexes of aluminium and zinc have been investigated. These water-soluble metallophthalocyanine (MPc) complexes, especially the sulphonated aluminium and zinc phthalocyanines, were found to be good photosensitisers for the transformation of the toxic mono-, tri- and penta-chlorophenols in aqueous solutions. The efficiency of MPc sensitiser towards photo-transformation of chlorophenols depends on its effectiveness to generate singlet oxygen as well as its photostability.

Octa-substituted thiol-derivatised phthalocyanine complexes of cobalt, iron and zinc were synthesized and their spectral and electrochemical properties investigated. The photochemical properties of the zinc phthalocyanine complexes in non-aqueous solutions were comparable to those in literature.

Ultrathin films of the octasubstituted thiol-derivatised phthalocyanine complexes of cobalt, iron and zinc were, for the first time, immobilized onto gold electrodes using the self-assembling technique. Surface electrochemistry indicates that the ultrathin films are surface-confined self-assembled monolayer (SAM) species. Gold electrodes modified with the redox-active SAMs of cobalt and iron phthalocyanine complexes proved to be potential electrochemical sensors for the detection of thiols (L-cysteine, homocysteine and penicillamine) and thiocyanate in aqueous solutions (pH 4). The limits of detection for the thiols and thiocyanate were in the range of ~ 10^{-7} and 10^{-6} mol dm^{-3}, respectively. The modification process was reproducible and the modified electrodes showed good stability and, if stored in pH 4 buffer solutions, could be used for the analysis of thiols and thiocyanate for about a month without the need for recalibration. Etching of gold marred electrochemical detection of cyanide with the MPc-SAM-modified gold electrodes. Interestingly, however, kinetic and equilibria studies revealed strong interaction of octabutylthiophthalocyaninatoiron (II), FeOBTPc, with cyanide in both DMF and DMSO solutions.

TABLE OF CONTENTS

Title Page		i
Dedication		ii
Acknowledgments		iii
Abstract		iv
Table of contents		v
List of abbreviations		xi
List of symbols		xiv
List of figures		xvi
List of schemes		xxiii
List of tables		xxiv

CHAPTER 1:

INTRODUCTION 1

1.1	**Metallophthalocyanines: General Introduction**	2
1.1.1	Historical perspective	2
1.1.2	Structure of metallophthalocyanines	2
1.1.3	Synthesis of metallophthalocyanines	3
1.1.4	Electronic absorption spectra of metallophthalocyanines	8
1.1.5	General applications of metallophthalocyanines	11
1.1.6	Aims of thesis	12
1.2	**Overview of Properties of Chlorophenols, Cyanide, Thiols and Thiocyanate.**	13
1.2.1	Chlorophenols	13
1.2.2	Cyanide	15
1.2.3	Thiocyanate	17
1.2.4	Thiols: L-cysteine, homocysteine and penicillamine	18

1.3	**Photochemical Processes: An Overview**	22
1.3.1	Basic concepts	22
1.3.2	Basic photochemistry of metallophthalocyanines	24
1.3.3	Singlet oxygen	27
1.3.3.1	Basic chemistry	27
1.3.3.2	Singlet oxygen quantum yields	28
1.3.4	Photodegradation studies of chlorophenols	33
1.4	**Electrochemistry: An Overview**	36
1.4.1	Basic concepts	36
1.4.1.1	The electrode-solution interface	37
1.4.1.2	Classification of electroanalytical techniques	38
1.4.1.3	Faradaic and non-Faradaic proceeses	39
1.4.1.4	The electrochemical cell	40
1.4.1.5	Mass transport processes	41
1.4.2	Cyclic voltammetry	42
1.4.2.1	Reversible process	43
1.4.2.2	Irreversible process	46
1.4.2.3	Quasi-reversible process	47
1.4.2.4	Electrocatalysis using cyclic voltammetry	47
1.4.3	Square wave voltammetry	49
1.4.4	Spectroelectrochemistry	50
1.4.5	Electrochemistry of metallophthalocyanines	51
1.4.6	Electrocatalytic properties of metallophthalocyanines	51
1.5	**Chemically Modified Electrodes**	54
1.5.1	General methods of modifying electrode surfaces	54
1.5.2	SAM–modified electrodes: An overview	56
1.5.2.1	Thiol-derivatised phthalocyanine self-assembled monolayers	59
1.5.2.2	Blocking and electroactive monolayers	60
1.5.2.3	Conditions for a successful monolayer formation	61

1.5.2.4 Characterization of SAM-modified electrodes 65
1.5.2.5 Application of SAM-modified electrodes 68

1.6 Summary of Aims of Thesis 70

CHAPTER 2:

EXPERIMENTAL 71

2.1 Materials 72
2.2 Instrumentation 73
2.3 Synthesis 74
2.3.1 Synthesis of metallo-tetrasulphophthalocyanine complexes, ($MPcS_4$) 74
2.3.2 Synthesis of sulphonated metallophthalocyanine complexes containing mixtures of differently substituted complexes, $MPcS_{mix}$ 77
2.3.3 Synthesis of octa-carboxymetallophthalocyanine complexes, (MOCPc) 80
2.3.4 Synthesis of thiol-derivatised metallophthalocyanine complexes 81
2.3.4.1 Synthesis of 4,5-dichlorophthalonitrile 81
2.3.4.2 Synthesis of disubstituted thiol-derivatised phthalonitriles 83
2.3.4.3 Synthesis of metal-free octasubstituted thiol-derivatised phthalocyanine complexes 85
2.3.4.4 Synthesis of octasubstituted thiol-derivatised metallophthalocyanine complexes 85

2.4 Methods 92
2.4.1 Singlet oxygen determination and photobleaching 92
2.4.2 Photosensitized transformation of chlorophenols 95
2.4.3 Kinetics and equilibria of interaction with cyanide 96
2.4.4 Electrochemical methods 97
2.4.5 Self-assembling techniques 98
2.4.5.1 Apparatus 98
2.4.5.2 Electrode pre-treatment and formation of MPc self-assembled monolayer 98

RESULTS AND DISCUSSION

CHAPTER 3:

SYNTHESIS AND CHARACTERIZATION OF METALLOPHTHALOCYANINE COMPLEXES

3.1	**Synthesis and Spectroscopic Properties**	101
3.1.1	Sulphonated metallophthalocyanine complexes	102
3.1.2	Octacarboxy metallophthalocyanine complexes (MOCPc)	106
3.1.3	Thiol-derivatised metallophthalocyanine complexes	107
3.1.3.1	4,5-disubstituted thiol-derivatised phthalonitrile complexes	107
3.1.3.2	Metal-free octasubstituted thiol-derivatised metallophthalocyanine complexes	108
3.2	**Photochemical Properties**	117
3.2.1	Water-soluble metallophthalocyanine complexes	117
3.2.1.1	Singlet oxygen quantum yields	117
3.2.1.2	Photostability	119
3.2.2	Thiol-derivatised zinc phthalocyanine complexes	120
3.2.2.1	Singlet oxygen quantum yields	120
3.2.2.2	Photostability	122
3.3	**Electrochemical Properties**	125
3.3.1	Thiol-derivatised zinc phthalocyanine complexes	125
3.3.2	Thiol-derivatised cobalt phthalocyanine complexes	132
3.3.3	Thiol-derivatised iron phthalocyanine complexes	135

CHAPTER 4:

PHOTOSENSITISED TRANSFORMATION OF CHLOROPHENOLS IN THE PRESENCE OF WATER-SOLUBLE METALLOPHTHALOCYANINE COMPLEXES 139

4.1 Photosensitised Transformation of 4-Chlorophenol 140

4.1.1 The pH studies 140

4.1.2 Rates and quantum yields of 4-CP photo-oxidation 141

4.1.3 Kinetic Studies. 146

4.2 Photosensitized Transformation of Polychlorophenols 151

4.2.1 Relative efficiency of sensitized oxidation of polychlorophenols 151

4.2.2 The pH dependence 154

4.2.3 Efficiency of Type I and Type II processes 160

CHAPTER 5:

SURFACE ELECTROCHEMICAL CHARACTERIZATION OF METALLOPHTHALOCYANINE SELF-ASSEMBLED MONOLAYERS ON GOLD ELECTRODES 166

5.1 Passivation of Gold Surface Reaction 168

5.2 Interfacial Capacitance 173

5.3 Passivation of Underpotential Deposition of Copper 175

5.4 Passivation of Heterogeneous Electron Transfer Processes 178

5.5 Nernstian Factors for Electroactive Monolayer 181

5.5.1 Reversibility and activation of the $M^{(III)}Pc$ / $M^{(II)}Pc$ couple 181

5.5.2 The pH effect on the $[M^{(III)}Pc(-2)]^{+}$ / $[M^{(II)}Pc(-2)]$ couple 189

5.5.3 Surface coverage 193

5.6 Reproducibility and Stability of Thio-MPc SAMs 199

5.7 The Fate of Carbon-Sulfur Bond During Self-Assembling 199

CHAPTER 6:

ELECTROCATALYTIC BEHAVIOUR OF MPC-SAM MODIFIED GOLD ELECTRODES TOWARDS THIOLS, THIOCYANATE AND CYANIDE 202

6.1 Electrocatalytic Oxidation of Thiols 203

6.1.1 Activation of MPc-SAM modified gold electrode 203

6.1.2 Detection of thiols: L-cysteine, homocysteine and penicillamine 208

6.2 Electrocatalytic Oxidation of Thiocyanate 220

6.3 Interaction of Cyanide with MPc-SAM-Modified Gold Electrodes 228

6.4 Reproduciblity and Stability of the MPc-SAM-Modified Gold Electrodes 231

CHAPTER 7:

SPECTROSCOPIC STUDIES ON THE INTERACTION OF CYANIDE WITH THIOL-DERIVATISED METALLOPHTHALOCYANINE COMPLEXES 234

7.1 Interaction with Octabutylthiophthalocyaninatoiron(II) 235

7.1.1 Spectroscopic studies 235

7.1.2 Kinetics and equilibria 237

7.2 Interaction of Cyanide with other Thiol-derivatised Iron and Cobalt Phthalocyanine Complexes 243

CONCLUSION 246

REFERENCES 251

LIST OF ABBREVIATIONS

ADMA	=	Tetrasodium α,α-(anthracene-9,10-diyl) dimethylmalonate
AFM	=	Atomic force microscopy
Ag	=	Silver wire pseudo-reference electrode
Ag|AgCl	=	Silver/silver chloride reference electrode
$AlPcS_4$	=	Aluminium (II) tetrasulphophthalocyanine
$AlPcS_{mix}$	=	Aluminium (II) sulphonated (mixed) phthalocyanine
AlOCPc	=	Octacarboxy phthalocyaninato aluminium (II).
ClAlPc	=	Chloroaluminium phthalocyanine
$(Cl)_2SnPc$	=	Bis (dichloro) phthalocyaninatotin(IV)
CME	=	Chemically modified electrode
CoOBTPc	=	Octabutylthiophthalocyaninato cobalt (II).
CoOHETPc	=	Octa-(hydroxyethylthio) phthalocyaninato cobalt (II)
C.E.	=	Counter electrode
$(CN)_2FeOBTPc$	=	Bis(cyano) octabutylthiophthalocyaninato iron (II)
$(DMF)_2FeOBTPc$	=	Bis(dimethylformamido) octabutylthiophthalocyaninato-iron (II)
CV	=	Cyclic voltammetry
CV	=	Cyclic voltammogram
4-CP	=	4-chlorophenol
DABCO	=	Diazabicyclooctane
DBU	=	1,8-diazabicyclo[5.4.0] undec-7-ene
DMA	=	Dimethylacetamide
DMF	=	Dimethylformamide
DMSO	=	Dimethylsulfoxide
DPBF	=	1,3-diphenylisobenzofuran
EQCM	=	Electrochemical quartz chemical balance
FTIR	=	Fourier transform infrared
FeOBTPc	=	Octabutylthiophthalocyaninato iron (II)
FeOHETPc	=	Octa-(hydroxyethylthio) phthalocyaninato iron (II)

GCE	=	Glassy carbon electrode
H_2OBTPc	=	Metal-free octabutylthio phthalocyanine
H_2OMPPc	=	Metal-free octa-(4-methylphenythio) phthalocyanine
HOMO	=	Highest occupied molecular orbital
^{1}H NMR	=	Proton nuclear magnetic resonance
IHP	=	Inner Helmholtz plane
IR	=	Infrared
ic	=	Internal conversion
isc	=	Intersystem crossing
L.B.	=	Langmuir-Blodgett
LMCT	=	Ligand-to-metal charge transfer
LoD	=	Limit of detection
MLCT	=	Metal-to-ligand charge transfer
MOCPc	=	Metallated octacarboxy phthalocyanine
MOBTPc	=	Metallated octacarboxy phthalocyanine
MOHETPc	=	Metallated octa-(hydroxyethylthio) phthalocyanine
MPc	=	Metallophthalocyanine
^{3}MPc*	=	Excited triplet state of the MPc photosensitiser
MPc-SAM	=	Metallophthalocyanine-self assembled monoyer
MP	=	Metalloporphyrin
$MPcS_4$	=	Metallated tetrasulphophthalocyanine
$MPcS_{mix}$	=	Metallated sulphonated phthalocyanine
OHP	=	Outer Helmholtz plane
$(OH)_2$SiPc	=	Bis(dihydroxo) phthalocyaninatosilicon(IV)
$(OH)_2$SnPc	=	Bis(dihydroxo) phthalocyaninatotin(IV)
OSWV	=	Osteryoung square wave voltammogram
OTTLE	=	Optically transparent thin layer electrode
Pc	=	Phthalocyanine
PCP	=	Pentachlorophenol
PDT	=	Photodynamic therapy
Pp	=	Porphyrin

PVC	=	Polyvinyl chloride
QCM	=	Quartz crystal microbalance
RAIRS	=	Reflection-absorption infrared spectroscopy
R.E.	=	Reference electrode
SAM	=	Self-assembled monolayer
SCE	=	Standard calomel electrode
SECM	=	Scanning electrochemical microscopy
SEM	=	Scanning electron microscopy
SERS	=	Surface enhanced raman spectroscopy
$SiPcS_{mix}$	=	Silicon sulphonated (mixed) phthalocyanine
$SnPcS_{mix}$	=	Tin sulphonated (mixed) phthalocyanine
STM	=	Scanning tunneling microscopy
SWV	=	Square wave voltammetry
TBAP	=	Tetrabutylammonium perchlorate
TCP	=	Trichlorophenol
THF	=	Tetrahydrofuran
UV-Vis	=	Ultraviolet-visible
UPD	=	Underpotential deposition
XPS	=	X-ray photoelectron spectroscopy
ZnPc	=	Zinc phthalocyanine
$ZnPcS_4$	=	Zinc (II) tetrasulphopthalocyanine
$ZnPcS_{mix}$	=	Zinc (II) sulphonated (mixed) phthalocyanine
ZnOCPc	=	Octacarboxy phthalocyaninato zinc (II).
ZnOBTPc	=	Octabutylthiophthalocyaninato zinc (II)
ZnOHETPc	=	Octa-(hydroxyethylthio) phthalocyaninato zinc (II)
ZnOMPPc	=	Octa-(4-methylphenythio) phthalocyaninato zinc (II)
W.E.	=	Working electrode

LIST OF SYMBOLS

α	=	Fraction of light absorbed
Φ_{Δ}	=	Singlet oxygen quantum yield
Φ_{Q}	=	Quantum yield of the quencher
Φ_{Chp}	=	Chlorophenol quantum yield used to represent any of the chlorophenols
$\Phi_{4\text{-}Cp}$	=	4-Chlorophenol quantum yield
Φ_{TCP}	=	Trichlorophenol quantum yield
Φ_{PCP}	=	Pentachlorophenol quantum yield
Φ_{p}	=	Photobleaching quantum yield
Φ_{Δ}^{MPc}	=	Singlet oxygen quantum yield in the presence of a metallophthalocyanine
Φ_{Q}^{MPc}	=	Quantum yield of the quencher in the presence of a metallophthalocyanine
ε	=	Extinction coefficient
Γ	=	Surface coverage or concentration
Γ_{ibf}	=	Ion barrier factor
π	=	Pi bonding
λ	=	Wavelength
π^*	=	Anti pi-bonding
A	=	Absorbance
A_o	=	Initial absorbance
A_f	=	Final absorbance
A_{eq}	=	Equilibrium absorbance
$A_{QM}(CTAC)$	=	Q band absorbances of the monomeric MPc complex in cetyltrimethylammonium chloride
$A_{QM}(H_2O)$	=	Q band absorbances of the monomeric MPc complex in water

A_t	=	Absorbance at time, t.
A_∞	=	Absorbance for the complete formation of the dicyano complex.
c	=	Speed of light
C	=	Capacitance
C_t	=	Concentration of chlorophenol at time, t.
C_T	=	Total interfacial capacitance.
C_m	=	Monolayer capacitance
C_o	=	Initial concentration of chorophenol
C_{Ox}	=	Concentration of the oxidized form of an analyte
C_{Red}	=	Concentration of the oxidized form of an analyte
C_s	=	Specific interfacial capacitance
d	=	Diameter
D	=	Diffusion coefficient
D_{Ox}	=	Diffusion coefficient of the oxidized form of an analyte
D_{Red}	=	Diffusion coefficient of the oxidized form of an analyte
E_{pa}	=	Anodic peak potential
E_{pc}	=	Cathodic peak potential
E	=	Potential
E^o	=	Standard potential
$E_{1/2}$	=	Half-wave potential
E_{fwhm}	=	Potential corresponding to full-width at half-maximum
ΔE_p	=	Anodic-to-cathodic peak potential separation
ΔE_s	=	Potential step size
f	=	Frequency
F	=	Faraday's constant
h	=	Plank's constant
Hz	=	Hertz
I_{abs}	=	Absorbed light
i_{ch}	=	Charging current
i_{pa}	=	Anodic peak current

i_{pc}	=	Cathodic peak current
k_d	=	Natural decay constant
k_f	=	Rate of forward reaction
k_q	=	Physical quenching constant
k_r	=	Chemical quenching constant
k_r	=	Rate of reverse/backward reaction
k_{obs}	=	Observed rate constant
K	=	Equilibrium constant
K	=	Kelvin
N	=	Number of electron
N_A	=	Avogadro's constant
O_2 ($^3\Sigma_g$)	=	Triplet state oxygen
O_2 ($^1\Delta_g$)	=	Singlet state oxygen
q	=	Electrical charge
Q	=	Electrical charge
Q_{Bare}	=	Integrated electrical charge due to bare gold electrode
Q_{SAM}	=	Integrated electrical charge due to MPc-SAM-modified gold electrode
r	=	Radius of electrode
R	=	Universal gas constant
S	=	Surface area of UV-Vis cell irradiated
Sub	=	Substrate
$Sub_{(ox)}$	=	Oxidised substrate
T_{filter}	=	Light transmitted through interference filter
T_{MPc}	=	Light transmitted through metallophthalocyanine solution
ν	=	Scan rate
V	=	Volts

LIST OF FIGURES

Figure 1.1:	The geometric structures of metallophthalocyanie and Metalloporphyrin	3
Figure 1.2:	Typical electronic absorption spectra of metallophthalocyanine and metalloporphyrin	8
Figure 1.3:	Molecular structures of chlorophenols.	13
Figure 1.4:	Molecular structures of L-cysteine and its derivatives.	19
Figure 1.5:	Model of the electrode-solution double layer region	37
Figure 1.6:	A conventional three-electrode cell	40
Figure 1.7:	A typical cyclic voltammogram.	43
Figure 1.8:	Cyclic voltammogram showing catalytic behaviour of a catalyst (e.g. MPc) towards the electro-oxidation of an analyte.	49
Figure 1.9:	Representation of a thiolate-on-gold SAM	58
Figure 1.10:	Typical cyclic voltammogram obtained for a bare gold electrode in sulphuric acid soution.	64
Figure 2.1:	A diagrammatic representation of photochemical set-up.	92
Figure 3.1:	The Q band electronic absorption spectra of the sulphonated metallophthalocyanine complexes.	104
Figure 3.2:	Variation of absorbance with concentration and Beer's law behaviour for $AlPcS_{mix}$, **15,** (A) and $SnPcS_{mix}$, **17,** (B) in pH 7.	105
Figure 3.3:	Electronic absorption spectra of AlOCPc, **20** and ZnOCPc, **21.**	107
Figure 3.4:	Electronic absorption spectra of AlOCPc and ZnOCPc.	109
Figure 3.5:	Variation of absorbance with concentration and Beer's law behaviour for ZnOMPPc (**34**) in DMF.	110
Figure 3.6:	Electronic absorption spectrum of CoOBTPc (**33**) in chloroform.	112
Figure 3.7:	Electronic absorption spectra of FeOBTPc (**35**) and FeOHETPc (**36**) in non-aqueous solutions.	114

Figure 3.8: Electronic absorption spectra of [$(CN)_2$FeOBTPc] (**38**) in DMF and DMSO. 115

Figure 3.9: Comparative FTIR spectra of FeOBTPc (**35**), $(DMF)_2$FeOBTPc (**37**) and $(CN)_2$FeOBTPc, (**38**) showing the characteristic Fe-O and Fe-CN vibration bands. 116

Figure 3.10: Typical decay of ADMA following irradiation of the Q band of **15** in aqueous buffer solution at different irradiation times. 118

Figure 3.11: Photo-degradation mechanism of MPc 120

Figure 3.12: Typical decay of DBPF following irradiation of the Q band of ZnOMPPc (**34**) in DMF solution at different irradiation times. 121

Figure 3.13: The kinetic curves for the photobleaching of ZnOMPPc (**34**) in DMF saturated with air and oxygen and containing DABCO. 124

Figure 3.14: Cyclic and Osteryoung square wave voltammograms of ZnOMPPc (**34**) in DMF. 125

Figure 3.15: Plot of anodic peak currents of ZnOMPPc (**34**) against the square root of scan rate. 127

Figure 3.16: Comparative cyclic and Osteryoung square wave Voltammograms of ZnOMPPc **34** in DMF. 129

Figure 3.17: Changes in spectral features observed for complex ZnOMPPc (**34**) in DMF during controlled potential reduction 131

Figure 3.18: Cyclic voltammogram of CoOBTPc, **33**, in DMF, and plot of peak currents against the square root of scan rate. 132

Figure 3.19: Cyclic and Osteryoung square wave voltammograms of $(DMF)_2$FeOBTPc, **32**, in DMF. 136

Figure 3.20: Cyclic and Osteryoung square wave voltammograms of FeOHETPc, **36**, in DMF. 137

Figure 4.1: Dependence of quantum yields on pH for the photo-transformation of 4-CP in the presence of AlPcSmix, **15**. 140

Figure 4.2: Dependence of concentration of 4-CP on photolysis time in the presence of the sensitisers; $ZnPcS_4$ (**10**), AlOCPc (**20**), $AlPcS_4$ (**9**), ZnOCPc (**21**), $AlPcS_{mix}$ (**15**) and $ZnPcS_{mix}$ (**16**). 141

Figure 4.3: Changes in absorbance of ZnOCPc, **21** with time in the Absence and presence of 4-CP. 144

Figure 4.4: Typical HPLC traces for the photo-oxidation of 4-CP before and after 16 min of photolysis. 145

Figure 4.5: Effects of addition of singlet oxygen quencher (sodium azide) on the rate of photo-transformation of different concentrations of 4-CP. Sensitiser = $AlPcS_{mix}$, **15**. 147

Figure 4.6: Plots of $1/\Phi_{4\text{-}CP}$ vs 1/[4-CP] for the photo-transformation of 4-CP in the presence of $AlPcS_{mix}$, **15** and $ZnPcS_{mix}$, **16**. 148

Figure 4.7: Kinetic curves for the photo-oxidation of TCP sensitised by $SnPcS_{mix}$ (**17**), $SiPcS_{mix}$ (**18**), $AlPcS_4$ (**9**), $ZnPcS_{mix}$ (**16**) and $AlPcS_{mix}$ (**15**) under pH 7 conditions. 151

Figure 4.8: Kinetic curves for the photo-degradation of $SiPcS_{mix}$ (**18**), $AlPcS_4$ (**9**), $AlPcS_{mix}$ (**15**), $ZnPcS_{mix}$ (**16**) and $SnPcS_{mix}$ (**17**) in the presence of PCP under pH 7 conditions. 153

Figure 4.9: The pH dependence of quantum yield for the transformation of TCP and relative yields of 2,5-dichloro-1,4-benzoquinone using $AlPcS_{mix}$ (**15**) as sensitiser. 154

Figure 4.10: Electronic absorption spectral changes observed during photolysis of solutions of PCP and TCP in the presence of $AlPcS_{mix}$ (**15**) as sensitiser at PH 7. 156

Figure 4.11: Typical HPLC traces for the photo-transformation of TCP before and after 3.5 and 7 min of photolysis. 157

Figure 4.12: Electronic absorption spectral changes observed during photolysis of PCP in the presence of $AlPcS_{mix}$ (**15**). 158

Figure 4.13: Effects of addition of singlet oxygen quencher (sodium azide) on the rate of photo-transformation of PCP in the presence and absence of sodium azide using $AlPcS_{mix}$ (**15**). 161

Figure 4.14: Plots of $1/\Phi_{TCP}$ vs 1 / [TCP] and $1/\Phi_{PCP}$ vs 1/[PCP] for the photo-transformation of TCP and PCP in the presence of $AlPcS_4$, **9** and $AlPcS_{mix}$ (**15**). 164

Figure 5.1: Cyclic voltammogram obtained for bare gold electrode in sulphuric acid soution. 168

Figure 5.2: Cyclic voltammograms of gold electrode before and after coating with the SAMs of CoOHETPc (**40**), CoOBTPc (**33**), FeOHETPc (**36**), FeOBTPc (**35**), ZnOMPPc (**34**) and ZnOBTPc (**32**). 169

Figure 5.3: Cyclic voltammograms of gold electrode before and after deposition of FeOBTPc-SAM and FeOHETPc-SAM. 174

Figure 5.4: Cyclic voltammograms showing the responses of gold electrode to underpotential deposition of copper before after coating with the SAMs of CoOHETPc (**40**), CoOBTPc (**33**), FeOHETPc (**36**), FeOBTPc (**35**), ZnOMPPc (**34**) and ZnOBTPc (**32**). 175

Figure 5.5: Cyclic voltammograms showing the responses of gold electrode to $Fe(NH_4)(SO_4)_2$ in $HClO_4$ before and after coating with SAMs of CoOHETPc (**40**), CoOBTPc (**33**), FeOHETPc (**36**), FeOBTPc (**35**), ZnOMPPc (**34**) and ZnOBTPc (**32**). 178

Figure 5.6: Cyclic voltammograms showing the responses of gold electrode to the redox chemistry of $Fe(NH_4)(SO_4)_2$ in $HClO_4$ before and after coating with SAMs of (b) CoOBTPc, **33** (c) ZnOBTPc, **32** (d) FeOBTPc, **35** and (e) H_2OBTPc, **30**. 180

Figure 5.7: Surface cyclic voltammograms of the SAMs of MOBTPc and MOHETPc (M = Co or Fe) on gold electrodes. 182

Figure 5.8: Cyclic voltammograms showing the dependence of peak currents on scan rate of the CoOHETPc-SAM-modified gld electrode. 184

Figure 5.9: Surface cyclic voltammograms of MOBTPc-SAM-modified gold electrode before and after repetitive cycling in DMF. 186

Figure 5.10: Plots of the peak current versus scan rate for the anodic peaks of the $[Fe^{(III)}Pc(-2)]^{+}/[Fe^{(II)}Pc(-2)]$ redox processes of the activated and inactivated FeOBTPc-SAM-modified gold electrode. 188

Figure 5.11: Surface Osteryoung square wave voltammetric responses of CoOHETPc with changes in pH, and plot of potential versus pH. 189

Figure 5.12: Surface Osteryoung square wave voltammetric responses of FeOBTPc and FeOHETPc with changes in pH. 191

Figure 5.13: Reductive desorption cyclic voltammetry peaks of gold electrodes before and after modification with the SAMs of CoOBTPc, CoOHETPc, ZnOBTPc and ZnOMPPc. 195

Figure 5.14: Reductive desorption cyclic voltammetry peaks of ZnOBTPc and ZnOMPPc-SAM-modified gold electrode. 196

Figure 5.15: Schematic representations of the possible orientations adopted by SAMs of MOHETPc and MOBTPc on gold electrodes. 200

Figure 6.1: Cyclic voltammetric responses of FeOBTPc-SAM-modified gold electrode in pH 4 solution of L-cysteine before and after several minutes of cycling. 203

Figure 6.2: Cyclic voltammograms of FeOBTPc-SAM-modified gold electrode in pH 4 solution before and after activation. 205

Figure 6.3: Cyclic voltammograms of L-cysteine using gold electrode modified with CoOBTPc-SAM. 209

Figure 6.4: Cyclic voltammograms of FeOBTPc-SAM-modified gold Electrode in pH 4 solution before and on addition of increasing concentrations of L-cysteine. 210

Figure 6.5: Voltammograms of homocysteine and penicillamine on CoOBTPc-SAM and FeOBTPc-SAM-modified gold electrodes. 212

Figure 6.6: Examples of cyclic voltammograms of L-cysteine, homocysteine and penicillamine on FeOHETPc-SAM and CoOHETPc-SAM modified gold electrodes. 213

Figure 6.7: Cyclic voltammetric responses of FeOHETPc-SAM-modified gold electrodes before and after addition of varying concentrations of homocysteine. 214

Figure 6.8: Relationship between i_p and $\nu^{1/2}$ at CoOBTPc-SAM-modified gold electrode for varying concentrations of L-cysteine. 215

Figure 6.9: Cyclic voltammetric responses of the oxidation peak current of penicillamine on FeOHETPc-SAM-modified gold electrode on continuous scanning. 218

Figure 6.10: UV-Vis spectral changes of FeOBTPc and FeOHETPc before and after addition of L-Cysteine. 219

Figure 6.11: Voltammograms of CoOBTPc-SAM and FeOHETPc-SAM on increasing concentrations of thiocyanate. 221

Figure 6.12: Relationship between i_p and $\nu^{1/2}$ of thiocyanate at CoOBTPc-SAM-modified gold electrode. 222

Figure 6.13: Relationship between i_p and [SCN^-] at CoOBTPc-SAM modified gold electrode. 222

Figure 6.14: Cyclic voltammetric responses of thiocyanate on CoOBTPc-SAM modified gold electrode on continuous cycling. 223

Figure 6.15: Cyclic voltammetric responses of CoOBTPc-SAM-modified gold electrodes in the presence of thiocyanate at pH 4 and 9. 224

Figure 6.16: UV-Vis spectral changes of CoOHETPc in DMSO before and after addition of SCN^-. 225

Figure 6.17: Osteryoung square wave voltammetric responses of CoOHETPc-SAM- modified gold electrode before and after addition of increasing cyanide concentrations. 228

Figure 6.18: Electrocatalytic oxidation of L-cysteine at CoOBTPc-SAM electrode before and after 5 days dry storage in nitrogen. 232

Figure 6.19: Theoretical and experimental calibration plots between peak current and L-cysteine concentration at CoOBTPc-SAM electrode before and after several days of storing in pH 4 buffer. 233

Figure 7.1: Absorption spectral changes observed on addition of cyanide to FeOBTPc, **35** in DMSO and $(DMF)_2$FeOBTPc, **37** in DMF. 235

Figure 7.2: Absorption spectral changes observed 15 minutes after addition of cyanide to a solution of $(DMF)_2$FeOBTPc, **37**. 236

Figure 7.3: Plots of log $[(A_{eq} - A_o) / (A_\infty - A_{eq})]$ vs log [CN^-] for the formation of $[CN)_2FeOBTPc]^{2-}$ in DMSO and DMF. 238

Figure 7.4: Typical plots of $\ln(A_\infty - A_t)$ vs time for the coordination of CN^- to FeOBTPc, **35** in DMSO. 240

Figure 7.5: Variation of observed rate constants with concentration for the formation of $[CN)_2FeOBTPc]^{2-}$ in DMSO and DMF. 241

Figure 7.6: Absorption spectral changes observed before and 20 minutes after addition of cyanide to a solution of FeOBTPc, **36** in DMSO. 243

Figure 7.7: Q band absorption spectral changes observed for CoOBTPc, **33** and CoOHETPc, **40** before and after addition of cyanide. 245

LIST OF SCHEMES

Scheme 1.1:	The general synthetic routes for metallophthalocyanine.	4
Scheme 1.2:	The synthetic route for peripherally octasubstituted MPcs from substituted phthalonitrile.	5
Scheme 1.3:	The synthetic route for tetrasulphonated MPcs.	6
Scheme 1.4:	The synthetic route for octacarboxy-MPcs.	7
Scheme 1.5:	The synthetic route for axial-ligated MPcs	7
Scheme 1.6:	Electronic transitions for phthalocyanine and porphyrin showing the origin of the Q and B bands.	9
Scheme 1.7:	Charge transfer transitions between the metal and Pc ring.	10
Scheme 1.8:	Simplified Jablonski diagram showing the various modes of excitation and relaxation in a chromophore.	22
Scheme 1.9:	Type I and Type II photoreaction mechanisms in MPc sensitiser.	26
Scheme 1.10:	Molecular orbital diagrams showing the electronic distribution in triplet and singlet oxygen and Lewis structure showing the Zwitterion character of singlet oxygen.	28
Scheme 1.11:	A simplified energy level diagram of ring-oxidized and ring-reduced metallophthalocyanine species.	52
Scheme 2.1:	Synthesis of water-soluble MPc complexes	76
Scheme 2.2:	Synthetic routes for the bis(hydroxy) phthalocyanine complexes of tin and silicon.	77
Scheme 2.3:	Synthetic route for the dichlorophthalonitrile	82
Scheme 2.4:	Synthetic routes for the thiol-derivatised phthalonitriles	83
Scheme 2.5:	Synthetic routes for the thiol-derivatised phthalocyanines	86
Scheme 4.1:	Proposed mechanistic pathway for the photo-tranformation of PCP in aqueous solution using MPc sensitiser	162

LIST OF TABLES

Table 1.1:	The diagnostic criteria for reversible, irreversible and quasi-reversible cyclic voltammetric processes.	48
Table 2.1:	Calculation of fraction of light (α) absorbed by a typical MPc photosensitiser	94
Table 3.1:	List of MPc complexes studied in this thesis.	101
Table 3.2	Singlet oxygen quantum yield and percentage photodegradation data of various water-soluble MPc sensitisers	119
Table 3.3:	Φ_Δ and of Φ_p values of ZnPc and its thiol-derivatised complexes	122
Table 3.4:	Comparison of redox potentials for **34** with those for **32** and other ZnPc complexes.	126
Table 3.5:	Comparison of redox potentials for CoOBTPc with those of other CoPc complexes	134
Table 3.6:	Comparison of redox potentials of $(DMF)_2$FeOBTPc, **37** with those of other FePc and complexes	138
Table 4.1:	Photosensitisation data for 4-CP transformation in the presence of various water-soluble MPc sensitisers	143
Table 4.2:	Photosensitisation data for TCP and PCP transformation in the presence of various water-soluble MPc sensitisers	152
Table 5.1:	Summary of ion-barrier factor (Γ_{ibf}), interfacial capactance (C_s), and surface coverage (Γ) of the MPc-SAMs	171
Table 5.2:	Voltammetric data of the SAMs of MOBTPc and MOHETPc	185
Table 6.1:	Comparative peak potential (E_p) and limit of detection (LoD) for the electrocatalysed reactions of L-cysteine, homocysteine and penicillamine.	211
Table 6.2:	Comparative peak potential (E_p) and limit of detection (LoD) for the electrocatalysed reactions of thiocyanate	220
Table 7.1:	Kinetics and Equilibrium data for the axial exchange reaction of cyanide with iron (II) phthalocyanine complexes	239

CHAPTER 1

INTRODUCTION

1.1 Metallophthalocyanines: General Introduction

1.1.1 Historical Perspective

Metallophthalocyanine (MPc) complexes are very versatile class of organic compounds that have established themselves as great commercial, industrial and biomedical materials.[1] They were discovered by accident in 1928 during the course of industrial production of phthalimide at the Grangemouth plant of the Scottish Dyes Ltd, which later became part of the Imperial Chemical Industries (ICI).[2,3] The production process of phthalimide involves passing ammonia into a molten phthalic anhydride in glass-lined iron vessels. History has it that in the course of a certain preparation, the glass-lined vessel cracked thereby exposing the reaction to the outer steel casing. This exposure resulted in the formation of traces of dark blue impurity in the phthalimide. The blue material was analysed at Imperial College by Linstead[4] and found to be iron phthalocyanine (FePc), the structure of which was confirmed by Robertson[5,6] using X-ray diffraction techniques. Linstead named the compound 'phthalocyanine' (*phthalo* from its precursor, 'phthalic acid' derivative, and *cyanine* from the Greek word 'blue').

1.1.2 Structure of Metallophthalocyanine

Metallophthalocyanine is a planar, 18 π-electron macrocyclic aromatic compound, consisting of four isoindole subunits linked together by aza nitrogen atoms.[6] Its structure {Figure 1.1 (A)} closely resembles that of the biologically important metalloporphyrin (MP){Figure 1.1 (B)}, except:

- porphyrins ring system is made up of pyrrole units instead of the isoindole, and
- carbon atoms instead of the nitrogen atoms link pyrrole units in porphyrins.

Like the porphyrins, a host of metal cations, ranging from the groups I and II to the lanthanide and actinides,[1,7-10] can be introduced into the central cavity of the phthalocyanine (Pc). Today, more than seventy MPc complexes are known.[2]

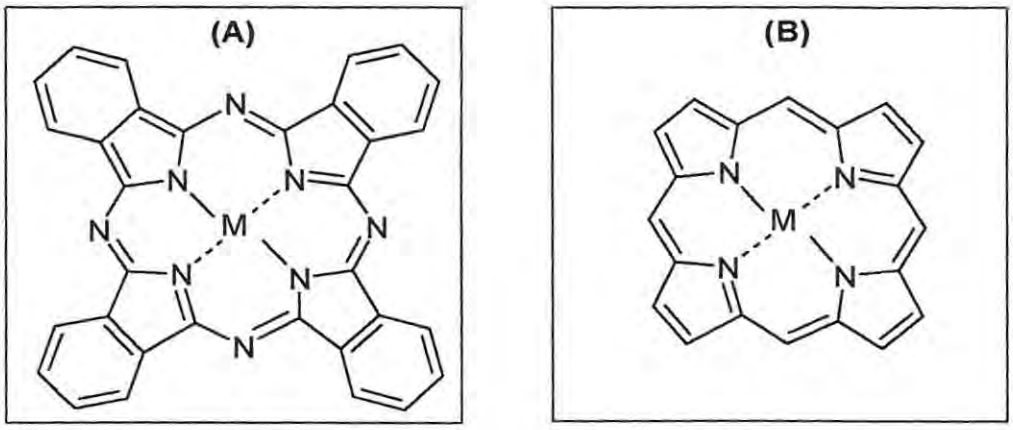

Figure 1.1: Geometric structures of (A) metallophthalocyanine and (B) metalloporphyrin complexes; M represents the metal center of the macrocycles.

1.1.3 Synthesis of Metallophthalocyanines

The common synthetic routes[11,12] for the preparation of metallophthalocyanine complexes are shown in Scheme 1.1. Basically, these routes involve heating a mixture of metal salt (or metal) and (i) phthalic anhydride (**1**), or (ii) o-cyanobenzamide (**2**), or (iii) diiminoisoindoline (**3**) or (iv) phthalonitrile (**4**) in the presence of various reagents to give the MPc complex. The phthalic anhydride route requires inexpensive starting materials, thus making it the preferred route for large-scale production of MPc complexes.[2] The phthalonitrile route, on the other hand, is expensive but gives high purity products. Thus, the phthalonitrile route is used for the synthesis of MPcs used for technology applications where high quality and high purity and not cost are the major considerations. Recently,

reports on the use of microwave irradiation for the synthesis of MPc complexes have been reported.[13,14] The micro-wave technique is fast and eliminates the use of solvents.

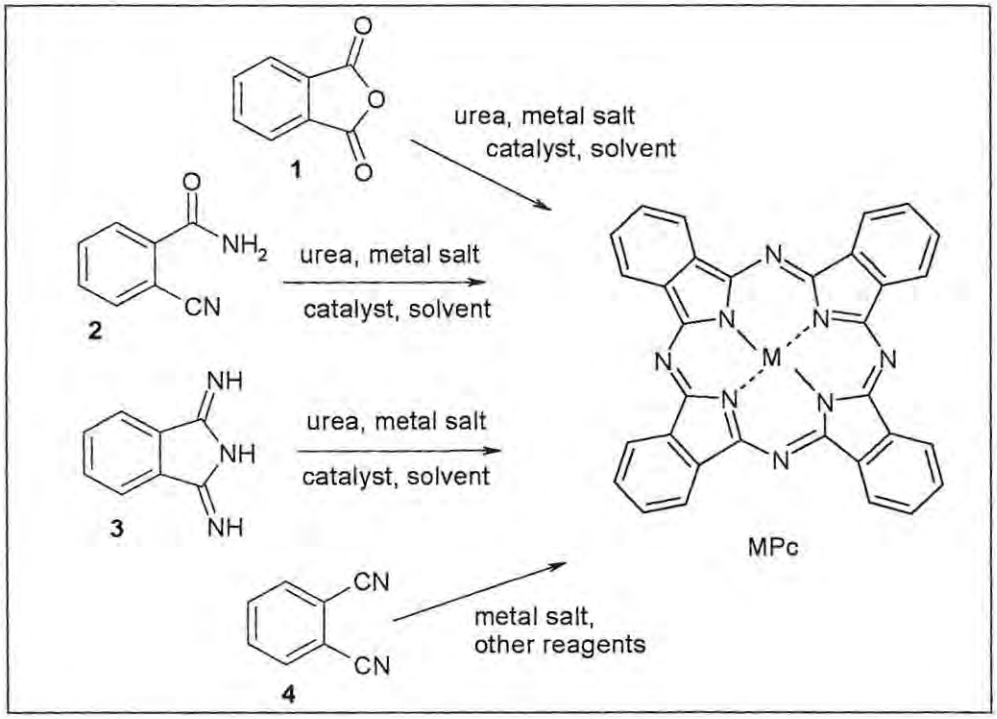

Scheme 1.1: General synthetic routes for metallophthalocyanine.[2,11,12]

Due to strong intermolecular cohesion, most unsubstituted MPcs are non-melting, insoluble solids. However, introduction of substituents on the Pc rings dramatically changes their basic properties, such as electrochemistry and solubility.[15-20] A substituted MPc complex is obtained by cyclotetramerisation of the appropriate substituted phthalonitrile derivative, thereby making it possible for the introduction of up to four substituents into each of the four benzo subunits. For example, the soluble, peripherally octasubstituted MPc ($MPcR_8$, where R = substituent) complexes (Scheme 1.2) are normally synthesized from the disubstituted phthalonitrile (**5**) and the metal salt.[17,21]

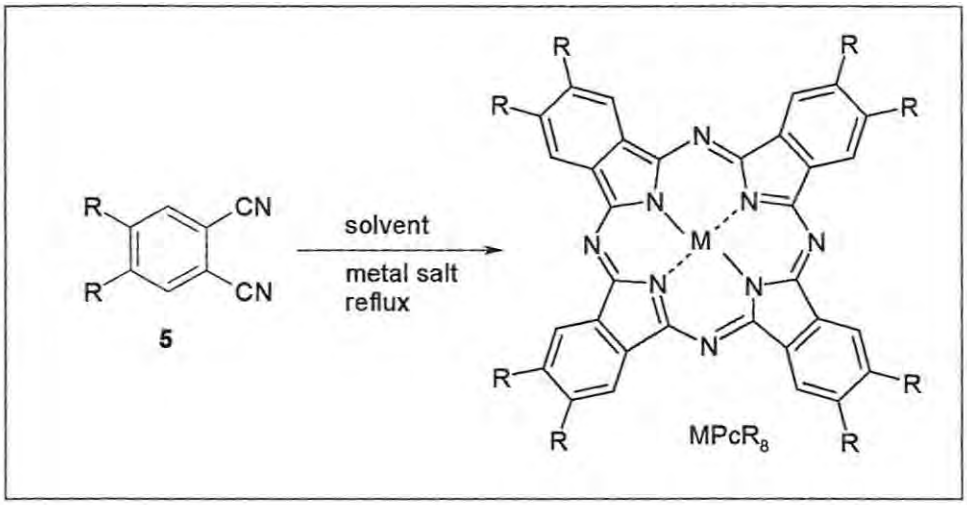

Scheme 1.2: Synthetic route for peripherally octasubstituted MPcs from substituted phthalonitrile.[17,21]

Scheme 1.2 is popular[22] for the preparation of the peripherally octasubstituted thiol-derivatised metal-free, H_2PcR_8, (where R = alkanethiols) and metallated ($MPcR_8$)[23] phthalocyanine complexes described in this thesis.

Water-soluble MPc complexes are obtained by the introduction of sulphonic,[24] carboxylic[25,26] or phosphonic[27] acid groups on the annellated benzene rings. Tetrasodium salt of metallo-tetrasulphophthalocyanine ($MPcS_4$) is synthesized using the Weber and Bush method[24] wherein the monosodium salt of the 4-sulphonic acid (**6**) and appropriate metal salt are refluxed in nitrobenzene in the presence of a catalyst, Scheme 1.3. Direct sulphonation[28] of unsubstituted MPc also leads to a water-soluble mixture of sulphonated complexes, equation 1.1

$$MPc \xrightarrow{"SO_3"} MPc(SO_3H)_n \qquad 1.1$$

where n = 1,2,3 or 4

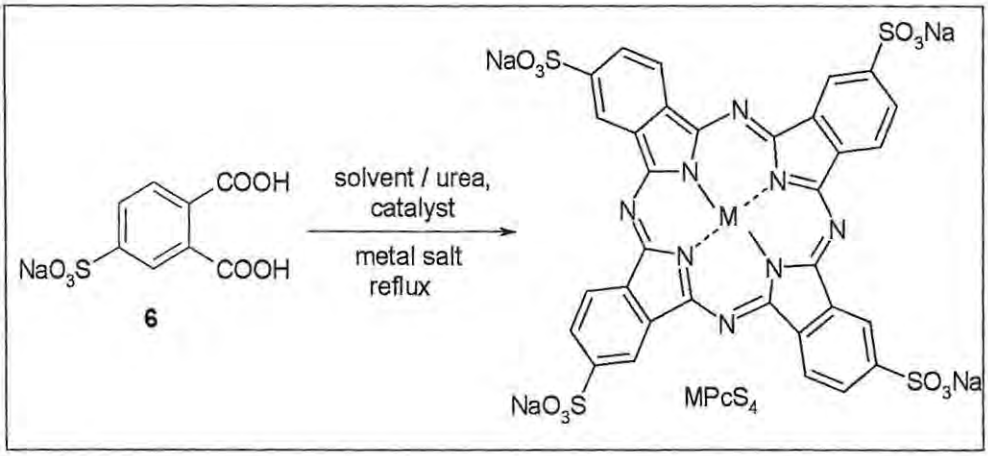

Scheme 1.3: Synthetic route for tetrasodium salt of metallotetrasulphophthalocyanine ($MPcS_4$).[24]

Octacarboxymetallophthalocyanine (MOCPc) complex is obtained from its tetra-amide intermediate product, tetra-amidometallophthalocyanine (MTAPc) using benzene-1,2,4,5-tetracarboxylic dianhydride (pyromellitic dianhydride, 7) and 1,8-diazabicyclo[5.4.0]undec-7-ene (DBU) as a catalyst,[26] Scheme 1.4. Water-soluble MPcs containing non-transition metal centers are essential in photosensitized reaction such as photodynamic therapy (PDT) and photo-oxidation reactions in aqueous environments. In this work, Schemes 1.3 - 1.5 and equation 1.1 were employed for the preparation of MPc complexes used for the photo-transformation of chlorophenols in aqueous solution (discussed in Chapter 4).

Axial ligand substituents can be introduced onto an appropriate cation (example Fe^{2+}) held within the central cavity of the MPc, Scheme 1.5. The axial-ligated MPc is obtained by refluxing the uncoordinated MPc in a coordinating solvent or other axial ligands (L).[29,30]

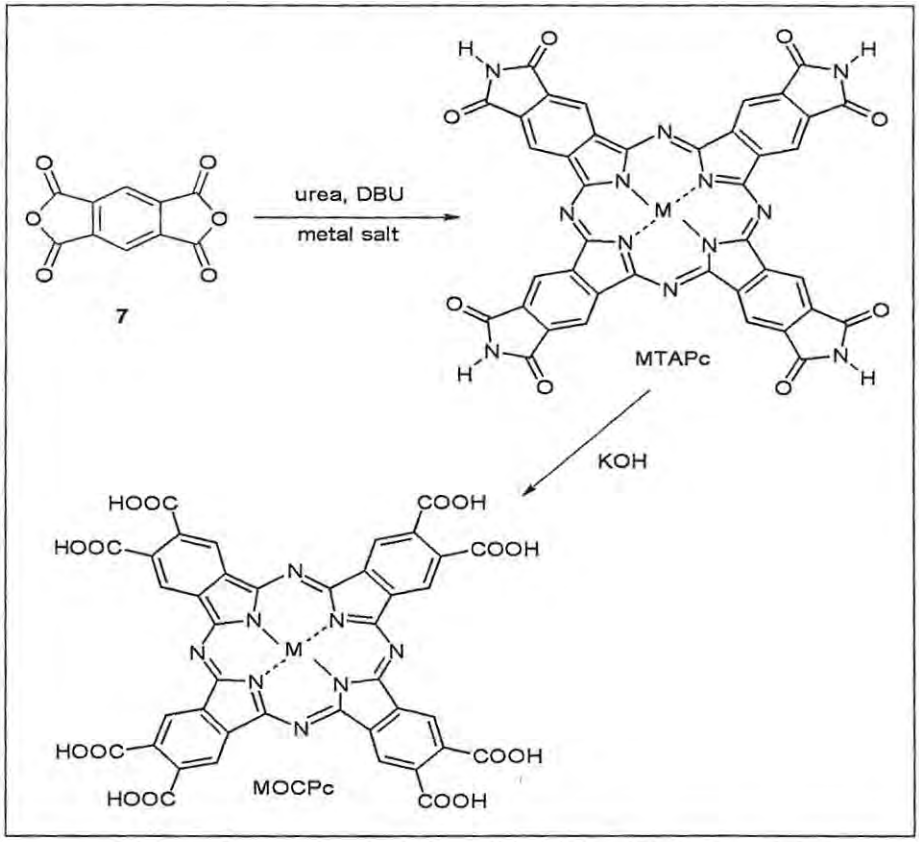

Scheme 1.4: Synthetic route for water-soluble octacarboxy-metallophthalocyanine, MOCPc.[26]

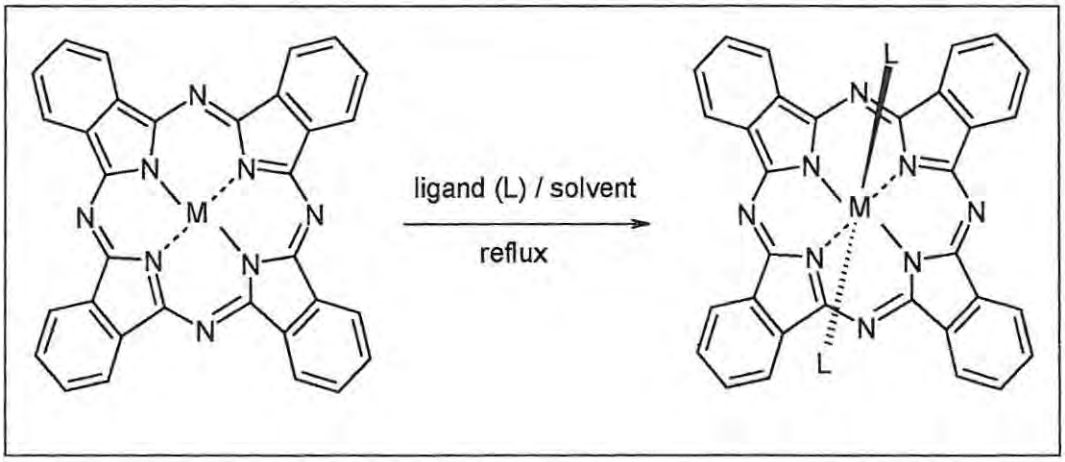

Scheme 1.5: Synthetic route for axial-ligated MPcs.[29,30]

1.1.4 Electronic Absorption Spectra of Metallophthalocyanines

Figure 1.2 shows the ultraviolet-visible (UV-Vis) absorption spectra of typical metallopthalocyanine (Figure 1.2A) and metalloporphyrin (Figure 1.2B).

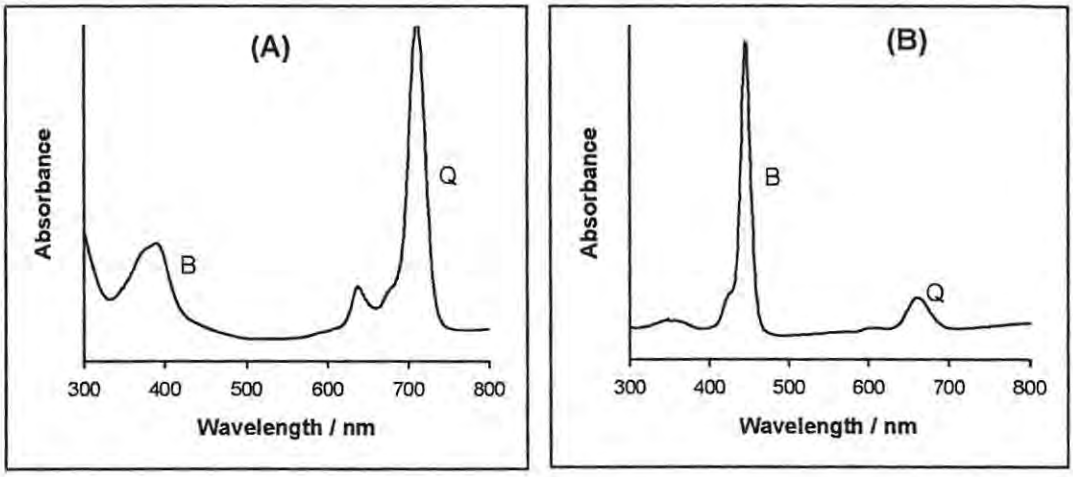

Figure 1.2: Typical electronic absorption spectra of (A) metallophthalocyanine and (B) metalloporphyrin.

These spectra are characterized by distinct bands, which arise primarily from the π-π^* transitions[31] within the delocalised phthalocyanine or porphyrin ring system. The isolated single band in the far-red end of the visible region, which appears around 600-700 nm regions, is known as the Q band. The less intense bands in the blue end of the UV region (near 300-500 nm) are called the B (or Soret) bands.[32,33] The origins of these first two π-π^* transitions are depicted in Scheme 1.6.

According to the Gouterman's four orbital model,[34] the spectra of MPc complexes are due to transition of electrons from the highest occupied molecular orbital (HOMO) (π) to the lowest unoccupied molecular orbital (LUMO) (π^*). The Q and B bands arise from transitions from the HOMO, $a_{1u}(\pi)$ (Q band), and $a_{2u}(\pi)$ and b_{2u} (B bands) to the

LUMO, e_g orbital.[32] Unlike with MPc, the spectrum of a typical metalloporphyrin (MP) shows a weak Q and an intense B band. This discrepancy is because the HOMOs of the

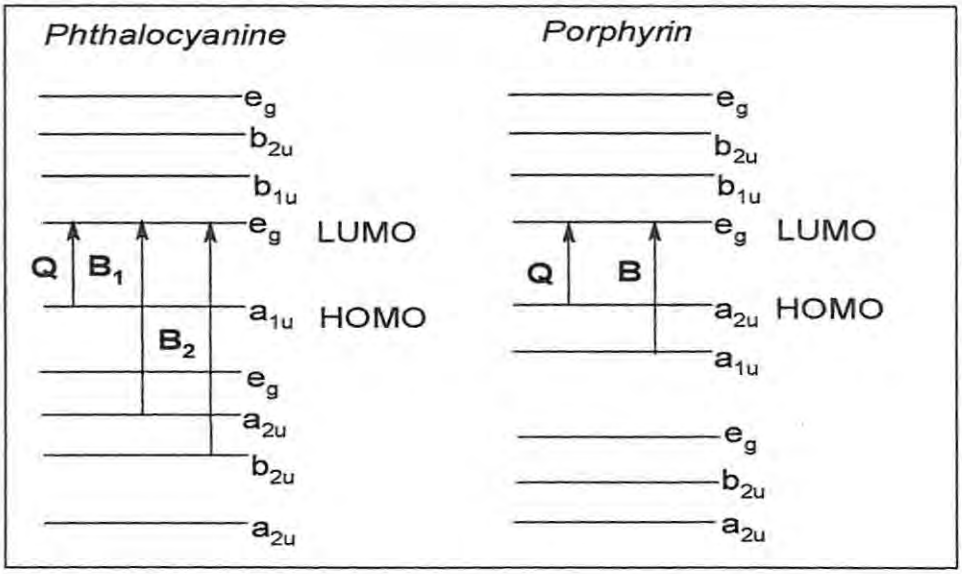

Scheme 1.6: Electronic transitions for phthalocyanines and porphyrins showing the origin of the Q and B bands.

phthalocyanines are widely separated (a_{1u} lies well above the a_{2u}) while those of the porphyrins are accidentally degenerate (a_{1u} and a_{2u} are very close together). This accidental degeneracy in porphyrins results in extensive configuration interaction for transitions to the same e_g (LUMO).[32,34] Thus, phthalocyanines exhibit significant red shift in energy and intensification of the Q band relative to the B band, compared to the porphyrins. These spectral features explain why porphyrins are red in colour while phthalocyanines are either blue or green. Also, since phthalocyanines are made up of isoindoles rather than pyrroles, they have longer conjugated pathway around the ring structure and therefore absorb at wavelengths longer than porphyrins. The Q band of

porphyrins occurs in the regions of ~ 650 nm, while for phthalocyanines longer wavelengths are observed.

UV-Vis spectra of MPcs are mostly recorded in solutions such as concentrated acids, coordinating {such as pyridine, dimethyl formamide (DMF) and dimethyl sulphoxide (DMSO)} and non-coordinating {benzene, tetrahydrofuran (THF) and chloroform ($CHCl_3$)} solvents. In addition, both vapour phase spectra[32] and solid phase spectra, as thin films[35] and crystals[36] have been reported. There are other absorption bands observed in the spectra of MPc, which have been assigned to the charge transfer transitions (CTT). If the central metal has d-orbital lying within the HOMO-LUMO gap (Scheme 1.7) there is a possibility for the CTT, either metal to ligand (MLCT) or ligand to metal (LMCT). CTT mostly occur as weak absorption bands in the near infrared (NIR) region or between the Q and B bands, normally in the 400-500 nm regions.[8,32,37]

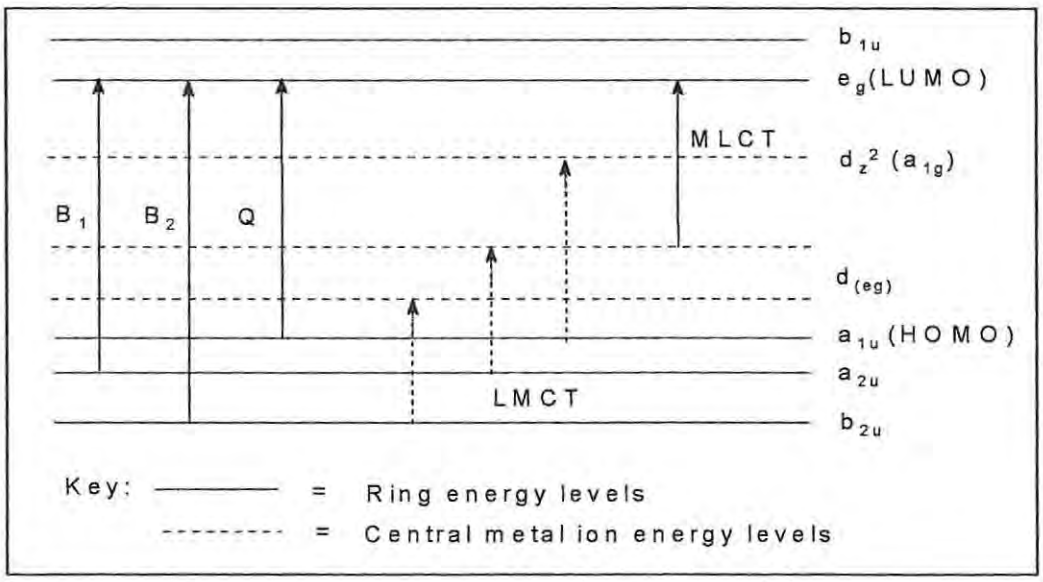

Scheme 1.7: Charge transfer transitions (CTT) between metal and phthalocyanine ring.

At this juncture, it is important to note that axial coordination of different ligands to MPcs and their resulting spectral changes has been an important and specialized area of research.[30,38-56] Owing to their excellent coordinating and catalytic activities, phthalocyanine complexes of cobalt and iron have been the most intensively studied.[30,38,56] As a modest contribution to this interesting field, this work also investigated the interaction of cyanide with novel thiol-derivatised FePc complexes.

1.1.5 General Applications of Metallophthalocyanines

Rarely in history has there been one type of molecule that has such a wide variety of applications as the phthalocyanine (Pc). Most of the applications of Pc complexes stem from their diverse chemical, structural, electronic and optical properties. Because of their remarkable chemical stability, beautiful bright blue to green colours, high tinctorial strength and excellent fastness to light,[2,3] phthalocyanines have been used mainly as dyestuffs for jeans and other clothings, inks in ballpoint pens, and paints for plastics and metal surfaces. Today, they have been shown to possess properties that have attractive applications including ink jet printing,[2] electrophotography,[2,57] photocopying and laser printing,[2,3] electrochromic display devices,[58-60] optical computer re-writable discs and information storage systems,[61-63] liquid crystal display devices,[64,65] photovoltaic cells,[66,67] fuel cells,[68] molecular electronics,[69] semi-conductor devices,[70-73] electronic and chemical sensors,[74-76] catalysis,[48,77-82] photosensitisation,[83-86] in particular photodynamic therapy (PDT).[84,87-91] Such is the interest in these macrocyclic complexes that much work has been focused on the formulation of thin films of phthalocyanines using techniques such as Langmuir-Blodgett (L-B),[73,92-96] spin-coating[95-97] and, more recently, the fabrication of

phthalocyanine monolayers via self-assembling.[95,96,98-104] The areas of application mentioned above are by no means an exhaustive, or even close to comprehensive list of new areas of technology where phthalocyanines are being applied. New applications of Pc complexes are reported on a constant basis.

1.1.6 Aim of Thesis

The major thrust of this thesis is the search for potential applications of hydrophilic sulphonated MPcs and hydrophobic thiol-derivatised MPcs in the fields of

- ***Photocatalysis***: Photosensitized transformation of chlorophenols, which are known industrial and environmental pollutants.
- ***Electroanalysis***: Development of electrodes modified with ultrathin films; self-assembled monolayers (SAMs) of MPc complexes suitable for possible detection of molecules of biological and environmental importance; thiols (L-cysteine, homocysteine and penicillamine) and cyanides (thiocyanate and cyanide).

1.2 Overview of Properties of Chlorophenols, Cyanide, Thiols and Thiocyanate.

1.2.1 Chlorophenols

The chlorinated phenols, 4-chlorophenol (4-CP), trichlorophenol (TCP) and pentachlorophenol (PCP), (Figure 1.3) are well-known[105-108] recalcitrant pollutants of

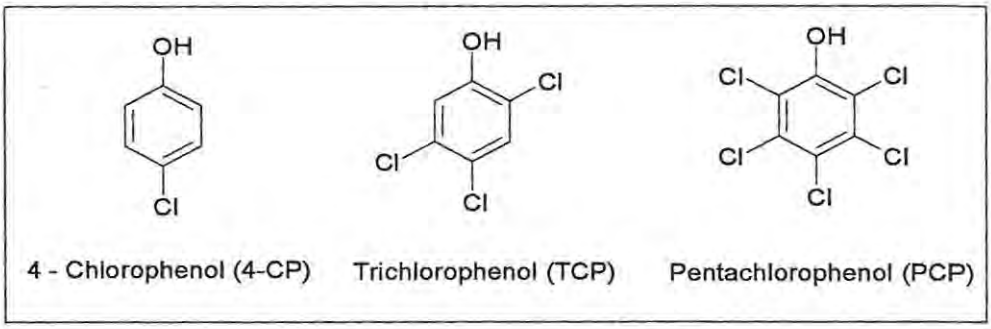

Figure 1.3: Molecular structures of chlorophenols studied in this work.

waste and natural waters. Because of their toxicity, persistence and bioaccumulation in aquatic organisms, they are listed among top priority pollutants by both the European Union[109] and the United States of America.[110] The polychlorophenols (TCP and PCP), are commonly used in a wide variety of agricultural and industrial applications as pesticides, germicides, fungicides, herbicides, molluscides, algicides and insecticides.[111] They became commercially important in the 1930s but were only recognized as environmental pollutants in the 1960s.[112] Hitchman et al.[112] have elegantly reviewed the various methods for the degradation of chlorophenols. These range from biological to photochemical processes.

The toxicity and resistance of chlorophenols to degradation increase with the number of halogen substituents.[110-115] As a model pollutant, 4-CP is the most studied of all the chlorophenols, and has also become a standard for evaluating experimental

parameters for photocatalysis and examining the mechanism and efficiency of degradation of chlorophenols and other chlorinated aromatics.[116-129]

There have been several reports on the degradation of chlorophenols under UV irradiation.[111,130-133] Unfortunately, direct irradiation of these complexes in water has been found to generate some intermediate compounds (e.g., polychlorinated dibenzo-*p*-dioxins) that are as toxic or even more toxic and persistent than the parent pollutant. On the other hand, the use of semi-conductive photocatalysts (such as TiO_2) and photosensitisers [116,134-137] has resulted in the production of less harmful photoproducts.

Tetrasulphophthalocyaninatoiron (II), $FePcS_4$, has been intensively employed as a catalyst in the chemical oxidation of chlorinated phenols using hydrogen peroxide (H_2O_2) or potassium monopersulphate ($KHSO_5$) as oxidant.[138-143] In these studies,[138-143] the products of trichlorophenol oxidation were reported as dichlorobenzoquinone, chloromaleic acid, chlorofumaric acid, maleic acid, fumaric acid and several oxidative coupling products. Phthalocyanine complexes containing non-transition metal centers have proved to be very efficient photosensitiser for use in PDT[84,87-91] but their use in photosensitized transformation of chlorophenols has received little attention. In neutral solutions, the final product of phenol and 4-chlorophenol photo-oxidation using MPc photosensitisers in the presence of oxygen is *p*-benzoquinone.[85,86] In alkaline solutions, the *p*-benzoquinone is further degraded to carbon dioxide, maleic and / or fumaric acids.

Aim of thesis

In this thesis, the use of sulphonated AlPc, ZnPc, SiPc and SnPc as photocatalysts for the degradation of chlorophenols in aqueous solutions is explored. Sulphonated SiPc

and SnPc complexes have not been reported; hence their synthesis and photosensitising properties are reported in this work.

1.2.2 Cyanide

Cyanide, either free or bound to metals, is released into the environment through various activities such as electroplating, metal finishing, petroleum and chemical industries, and mining operations.[144] The extreme toxic effects of cyanide poisoning, which start from dizziness, then fainting and finally death, are well known.[144] Deaths arising from cyanide poisoning are compatible with blood cyanide concentrations of 1.0 - 2.0 mg l^{-1} and above. This explains why many environmental authorities such as the Australian and New Zealand Environmental and Conservation Council (ANZECC), limit the maximum allowable concentration of CN^- in fresh and marine waters to 5.0 μg l^{-1}.

The extreme toxicity of CN^- in humans partially arises when it binds to the iron (III) porphyrins in the respiratory enzyme, cytochrome oxidase,[145] and prevents respiration. There are several clinical methods[146] for treating cyanide poisoning. In the USA, for instance, sodium nitrite[147] is injected intravenously to cause the oxidation of the poisoned blood's iron (II) haemoglobin into the high cyanide-affinity iron (III) methaemoglobin form.[148] This is followed by the injection of sodium thiosulphate which serves as a massive sulphur source for the body's rhodonase enzymes that transforms the CN^- into the less toxic thiocyanate, SCN^-.

MPc complexes, especially those of iron and cobalt, are known to coordinate with CN^-. FePc complexes, in particular, have received much attention because of their strong tendency to undergo axial ligation with CN^- [30,46,47] Also, FePc is usually considered

analogous to the haem group of haemogloblin and myoglobin, hence the study of its axial coordination with cyanide is of utmost importance in the search for anti-cyanide drugs. One of the major reasons for the extensive studies of the axial reactivity of FePc complexes with biomolecules is the belief that it may contribute to a better understanding of the reactivity of the structurally related and biologically important porphyrins.

Kinetics and equilibria for the axial exchange reaction between cyanide and MPc or metalloporphyrin complexes in non-aqueous[30,46,47] and aqueous [53] environments are known. Axial-ligation in MPc and porphyrin complexes is known[43,44] to be step-wise, which results in the formation of a highly reactive five-coordinate intermediate. The overall ligand substitution may be conveniently represented by reactions 1.2 and 1.3, where L and E represent the leaving and entering ligands, respectively. L is usually the solvent molecule (e.g. DMF and DMSO) while E is the target ligand (e.g. CN^-).

$$(L)_2MPc \underset{k_{-1}}{\overset{k_1}{\rightleftharpoons}} L(MPc) + L \qquad 1.2$$

$$L(MPc) + E \underset{k_{-2}}{\overset{k_2}{\rightleftharpoons}} (L)(E)MPc \qquad 1.3$$

The rate law for axial exchange reactions 1.2 and 1.3 is generally given[38] by equation 1.4.

$$k_{obs} = \frac{k_1 k_2[E] + k_{-1}k_{-2}[L]}{k_{-1}[L] + k_2[E]} \qquad 1.4$$

Since solvent L is always in excess, it can be assumed that k_{-1} [L] >> k_2 [E], then equation 1.4 may be written as equation 1.5,

$$k_{obs} = \frac{k_1 k_2[E] + k_{-1}k_{-2}[L]}{k_{-1}[L]} \qquad 1.5$$

which can further be simplified to equation 1.6

$$k_{obs} = \frac{k_1 k_2[E]}{k_{-1}[L]} + k_{-2} \qquad 1.6$$

Representing k_1k_2/k_{-1}[L] = k_f and k_{-2} by k_r equation 1.6 becomes

$$k_{obs} = k_f[E] + k_r \qquad 1.7$$

The k_f values for the coordination of CN^- to $Fe^{II}Pc$ were reported[30] as 17.5 and 0.2 dm^{-3} mol^{-1} s^{-1} for the first and second CN^-, respectively; while the equilibrium constants, K, were 3.0 x 10^3 and 5.7 x 10^2 dm^3 mol^{-1} for the first and second CN^-, respectively.

Aim of thesis

There has been no study on the effects of the axial reactivity of cyanide with FePc substituted with alkanethiol groups. To this end, and as a step towards the development of anti-cyanide drugs, this research work in part examines the equilibra and kinetics of the interaction of cyanide with FePc complex substituted with sulphur group, and compares the results with those previously reported for FePc complexes.[30,46,47]

1.2.3 Thiocyanate

Thiocyanate (SCN^-) is found in many industrial and biological applications.[149-152] Although it is less toxic than CN^-, it is harmful to aquatic life and has been known to block the iodine uptake by thyroid gland. As a detoxification product of hydrogen cyanide (HCN), thiocyanate in the body fluids has been used to monitor HCN from tobacco smoke, fire atmospheres and certain vegetables containing cyanogenic glucosides.[149] A chemical test to distinquish between smokers and nonsmokers is essential in many epidemiologic studies. Thiocyanate has proved to be a good "smokers'

implicator" since high levels of it (in the range of ~ 10^{-5} – 10^{-3} mol dm^{-3}) in biological samples such as saliva and urine correlate to excessive cigarette smoking.[149-152]

Although colorimetry and spectrophotometry have been used to detect thiocyanate, the use of potentiometric techniques based on ion-selective electrodes (ISEs) has been attracting great attention. Recently, graphite electrodes coated with polyvinyl chloride (PVC) containing transition metal macrocycles (including MPcs) have been used for the detection of the thiocyanate ion, SCN^- in biological fluids.[150,151]

Aim of thesis

There has not been any study on either the electrocatalytic activity of electrodes modified with SAMs of alkylthio-substituted MPc complexes or their catalytic activity towards thiocyanate detection. One of the aims of this thesis is to study the electrocatalytic behaviour of the SAMs of the thiol-derivatised CoPc and FePc complexes towards detection of thiocyanate with a view to improving sensitivity.

1.2.4 Thiols: Cysteine, Homocysteine and Penicillamine

The thiols (R-SH), cysteine and its derivatives (Figure 1.4), play important roles within physiological systems, and are also present in various cosmetics and pharmaceutical preparations.[153-157] Cysteine {(R)-2-amino-3-mercaptopropanoic acid} is a sulphur-containing α-amino acids, which is one of about 20 amino acids commonly found in natural proteins. Cysteine is a crucial substrate for protein synthesis, and rate-determining precursor for glutathione. Glutathione is the most abundant non-protein thiol and it is known for its wide-ranging functions within the cell including regulation of cell

growth and maintenance of immune function and scavenging of free radicals and peroxides,[153,155] which helps protect the brain and liver from damage due to alcohol and

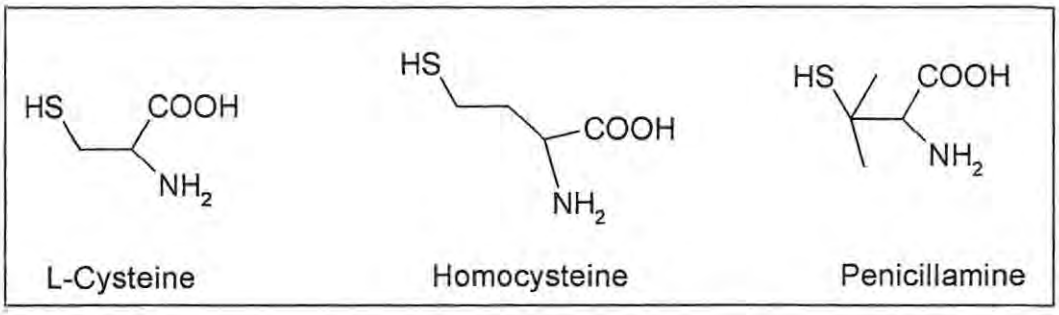

Figure 1.4: Molecular structures of thiols (L-cysteine, homocysteine and penicillamine) studied in this work.

drugs.[157] The ability of cysteine and glutathione to scavenge free radicals has been a major significance in medicine. The depletion of cysteine and glutathione in the body is accompanied by premature arteriosclerosis, leukaemia, cervical cancer, liver disease, sepsis, diabetes and several other disorders.[153-155,158] Abnormally high levels of cysteine, in particular, in body fluids have been implicated in the pathological conditions such as Alzheimer's and Parkinson's diseases, acquired immune deficiency syndrome (AIDS) related dementia and stroke.[153] Although it is being contested[155] whether monitoring cysteine or glutathione in isolation can give definitive evidence for the onset of any of the above debilitating conditions, nevertheless it has been postulated that these thiols can be powerful biomarkers in post diagnosis supervision of patients, in that monitoring their levels within physiological fluids could provide the clinician hard data from which to gauge the effectiveness or response of the patient to subsequent treatments.

Homocysteine (Figure 1.4) has recently risen to greater prominence because of its implication in cardiovascular disease rather than its antioxidant properties. Homocysteine

is a critical regulatory intermediate during the methionine metabolism and a precursor for cysteine.[153] Plasma homocysteine concentrations in the (5 – 15) x 10^{-6} mol dm^{-3} range are considered normal in fasting subjects. Slightly higher plasma homocysteine levels, known as hyperhomocysteinemia, are associated with greater risk of cardiovascular and cerebrovascular diseases. Major causes of moderate homocysteinemia are chronic renal failure and deficiencies in specific vitamins including folate, vitamins B_{12} and B_6.[153,254] On the other hand, very high concentrations of homocysteine in plasma and urine are a clinical indicator of the genetic disease commonly referred to as homocystinuria, whose sufferers are known to be highly susceptible to heart diseases. Although the use of plasma homocysteine as a biomaker for an individual's susceptibility to homocystinuria is not common, efforts are being made towards the developments of protocols to enable easy detection of this thiol in physiological and pharmaceutical products.[155]

Penicillamine (β,β-dimethylcysteine; 3-mercaptovaline) (Figure 1.4) is the acid degradation product of β-lactam antibiotics. It is a chelating agent, which is widely used in medicine for the elimination of copper in the treatment of Wilson's disease, heavy metal poisonings and many other diseases such as cystinuria and rheumatoid arthritis.[156,159,160] New and efficient methods for monitoring its levels in biological fluids and pharmaceutical preparations are of current interests.

Several methods that have been used for the analysis of the above thiols, and these include chromatography, fluorimetry, and electrochemistry.[154-156,160] However, most of these methods are not necessarily simple. Many electrochemical studies have been devoted to the study of these complexes using bare electrode materials such as mercury,[161-166] platinum and gold,[161,167-169] carbon,[170] and boron-doped diamond,[171] and

electrode materials modified with metalloporphyrin and metallophthalocyanine complexes.[55,78,172-177] At most conventional electrodes, the oxidation of these thiols occurs at extreme positive potentials coupled with slow electron transfer. However, when MPc-chemically modified electrodes (MPc-CMEs) are employed, a considerable reduction in the oxidation potentials of these thiols, with a remarkable acceleration in the rate of electron transfer, is observed.[176, 178]

The greatest obstacles that still hamper the applications of most MPc-CMEs to biological analysis of species, such as L-cysteine and its derivatives, include rapid loss of sensitivity due to leaching or deactivation of MPc catalysts, and poor detection limits (arising from large background currents).

Aim of thesis

There has been no study on the application of electrodes modified with SAMs of alkylthio-substituted MPcs for the oxidation of thiols. This work, for the first time, attempts to probe into the self-assembling features of these MPc complexes on gold electrode as well as their electrocatalytic behaviour toward the oxidation of cysteine and other thiols. Since the FePc and CoPc are the most active complexes for thiol electrooxidation,[172] this study is devoted to alkanethiol-derivatised phthalocyanine complexes of Co and Fe only.

1.3 Photochemical Processes: An Overview

1.3.1 Basic Concepts

Photochemistry is concerned with the biomolecular interaction of a quantum of light and a molecule (chromophore) and the subsequent chemical and physical changes which result from this interaction.[91,179-181] The photophysical processes, which follow molecular excitation by light absorption, can be conveniently represented using the so-called Jablonski diagram, Scheme 1.8. Illumination of the chromophore (e.g. MPc) with

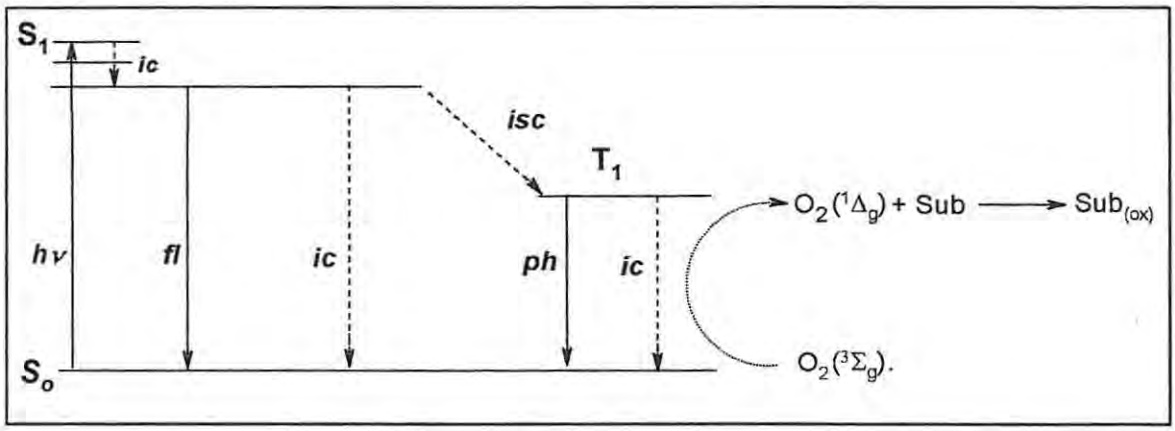

Scheme 1.8: Simplified Jablonski diagram showing the various modes of excitation and relaxation in a chromophore. hν = energy of absorption, S_o = ground state energy level, S_1 = excited state energy level, fl = fluorescence, ph = phosphorescence, isc = intersystem crossing, ic = internal conversion.

light of appropriate wavelength, leads to energy of absorption (hν), and subsequently to excitation from the ground state energy level (S_o) to the excited state energy level (S_1). To place itself in equilibrium with the surrounding medium, the excited molecule soon loses its excitation energy by deactivation via radiative (energy loss in the form of light) and radiationless (energy loss in the form of heat, shown by the dotted arrows) processes.

These physical deactivation processes can be any of the following; fluorescence (fl), phosphorescence (ph), intersystem crossing (isc) and internal conversion (ic). Whereas isc involves a change of spin, ic does not. The radiative, triplet to singlet transitions are quantum mechanically "forbidden" since a change of spins is required, they however occur to a very small extent. Therefore, triplet excited states generally have longer lifetimes (~ order of seconds) than the singlet excited states (10^{-10} - 10^{-6} seconds).[180] In oxygenated environments, the chromophore easily transfers its energy to ground state triplet molecular oxygen, $^3O_2$ or O_2 ($^3\Sigma_g$), to yield the excited state singlet oxygen, $^1O_2$ or $O_2(^1\Delta_g)$, which can react with organic substrate (Sub).[83-91,182,183]

The concept of energy transfer can be represented by equation 1.8, where D* is the excited molecule.

$$A + D^* \longrightarrow D + A^* \qquad 1.8$$

In this process, an excited donor molecule, D*, collapses to its ground state with the simultaneous transfer of its electronic excitation to an acceptor molecule, A, which is thereby promoted to an excited state.[179,180] Thus, photosensitization may simply be described as a process whereby a molecule or an atom absorbs radiant energy, becomes electronically excited in the process, and then passes the energy onto another molecule or atom, without itself reacting.

Quantum Yields:

Quantum yield (Φ) is a measure of the how much any photoproduct (X) is produced per quanta of light absorbed,[179] mathematically defined by equations 1.9 and 1.10).

$$\Phi_X = \frac{\text{number of molecule (X) formed / } cm^3s^{-1}}{\text{number of quanta absorbed / } cm^3s^{-1}} \qquad 1.9$$

$$\text{i.e.} \quad \Phi_X = \frac{d[X]/dt}{I_{abs}} \qquad 1.10$$

where I_{abs} is the amount of photon of light absorbed by the sensitiser.

The 'overall quantum yield' is to a photochemist what 'overall yield' is to an organic chemist. Owing to the major role singlet oxygen plays in both PDT and photo-oxidation processes, the interest of scientists is focused on the singlet oxygen quantum yield (Φ_Δ). For usable sensitisers, the Φ_Δ value should lie between 0.2 and 0.8. Other quantum yields such as the fluorescence (Φ_F) and the triplet states (Φ_τ) of the MPc sensitisers are also important, since their values directly or indirectly affect the values for Φ_Δ.

1.3.2 Basic Photochemistry of Metallophthalocyanines

Irradiation of phthalocyanine dimers at wavelengths shorter than 300 nm (UV region) is known[184] to induce photoredox dissociations leading to monomeric phthalocyanines with oxidized or reduced metal centers or ligand radical species. UV irradiation of the monomers, on the other hand, induces redox reactions that have been characterized as abstractions of hydrogen from the solvent or appropriate hydrogen donors, shown by equation 1.11.

$$MPc \underset{\cdots\cdots}{\overset{h\nu}{\rightleftharpoons}} {}^*MPc \xrightarrow{SH_2} MPc\text{-}H^{\cdot} + SH^{\cdot} \qquad 1.11$$

These hydrogen abstractions have been related to the population of a reactive $n\pi^*$ state by the absorption of UV light. An important characteristics of the photoprocesses induced

with visible light absorptions is that quantum yields of product formation are larger than those determined with UV light.

Phthalocyanine complexes of the non-transition metals are very useful class of sensitisers because of their chemical stability and high absorption wavelengths in the 650 –700 nm. The excited singlet states of phthalocyanine $^1\pi$-π^* have a higher energy (1.8-1.9 eV) than the triplet states $^3\pi$-π^* (1.1 – 1.3 eV), but their lifetimes are only several nanoseconds. Thus, the triplet states $^3\pi$-π^* are more significant for photochemical reaction. Titanium dioxide (TiO_2) semiconductor is one of the most efficient photocatalysts for the degradation of chlorophenols.[116-128] Due to its large band gap ($E_g \cong$ 3.2 eV), its use in photocatalytic processes is limited to the UV regions where only approximately 4% of the solar radiation can be utilized. To overcome this advantage, photosensitisers (such as metallophthalocyanines[85,86]) that absorb in the visible region are used.

The photochemical reactions of MPc complexes that generate excited singlet oxygen, O_2 ($^1\Delta_g$) (which is the oxidative species in photo-induced oxidative processes[83,91,182,183]) are represented in Scheme 1.9. Singlet oxygen is generated by energy transfer from the excited triplet state of the photosensitiser (^{3}MPc*) to ground state triplet oxygen, $^3O_2$ or O_2 ($^3\Sigma_g$), through the so-called Type II photo-oxidation process. The energy required for the triplet to singlet transition in oxygen is 0.98eV (~94 kJ mol^{-1}), which corresponds to a wavelength of ~1270 nm.[84,182,183] This implies that a relatively low energy is required to obtain singlet oxygen. For efficient generation of singlet oxygen, the MPc photosensitiser energy should be higher than that of the O_2 ($^1\Delta_g$). This prerequisite holds for MPc complexes with triplet energies ranging from 1.12-1.31

eV (~ 26-30 Kcal mol^{-1}) for MPcs containing non-transition metal and heavy metal centres. For example, the triplet energies for the tetrasulphophthalocyanine complexes of aluminium ($AlPcS_4$) and zinc ($ZnPcS_4$) are 1.20eV and 1.12eV, respectively.[182]

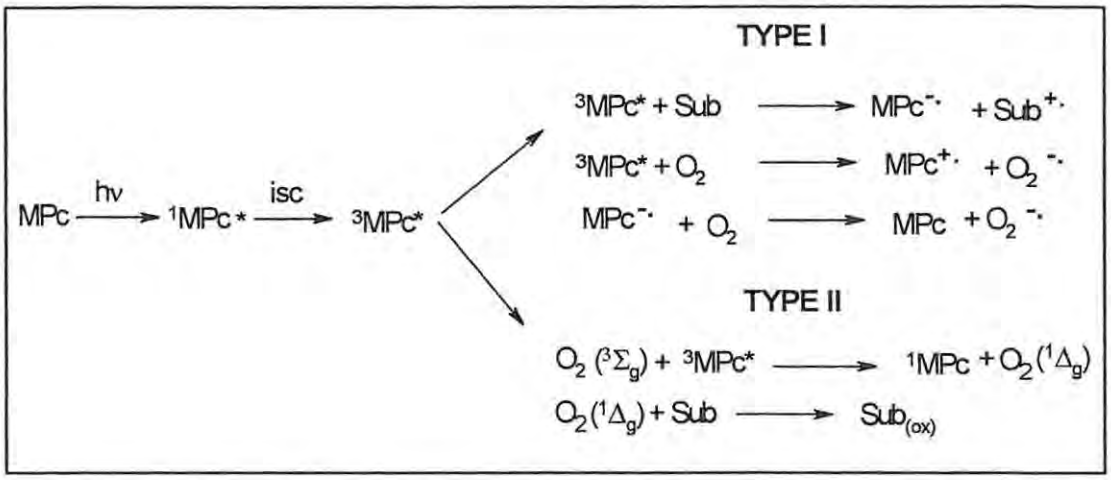

Scheme 1.9: Type I and Type II photoreaction mechanisms in a metallophthalocyanine (MPc) photosensitiser.

In Type I process, ^{3}MPc* can react directly with organic substrate (Sub) or molecular oxygen by electron transfer to generate the reduced $MPc^{-\cdot}$ or oxidized $MPc^{+\cdot}$, respectively. Types I and II reactions depend on substrate and oxygen concentrations, respectively. It is generally believed that the route via singlet oxygen (Type II) is the predominating process in PDT and photo-oxidation of many biological and environmental substrates.

The excited singlet oxygen, O_2 ($^1\Delta_g$), is the species involved in the photocatalytic degradation of phenols using MPc complexes as catalysts, hence its chemistry relevant to photolysis is discussed in the following section. It is hoped that this will help the reader appreciate the importance of this molecule in the photo-oxidation processes.

1.3.3 Singlet Oxygen

1.3.3.1 Basic Chemistry

The ground state oxygen possesses two unpaired electrons located separately in the outermost antibonding orbitals (Scheme 1.10). In the presence of a magnetic field, the spins of the electrons can be revealed to be in one of three possible configurations; both spins aligned up, both spins aligned down, or one up and one down. Because of these three possible states the ground state of oxygen is called a triplet state.[91] The two degenerate half-filled molecular orbitals of the oxygen create an electron "sink", which explains why oxygen will accept an electron from the excited photosensitiser. The extreme reactivity of singlet oxygen, on the other hand, is due to the pairing of two electrons into one of the π^*_{2p} antibonding orbital (Scheme 1.10).

In the ground state, the electrons are distributed according to the Hund's rule, in the p_x and p_y antibonding orbitals. However, since these orbitals are degenerate and electrons have aligned spins, the quantum numbers of each electron are identical and thus are forced to occupy separate orbitals to comply with the Pauli exclusion principle. Interaction with excited photosensitiser causes the spin of one electron to invert, making its quantum numbers unique, allowing them to pair together into the antibonding orbital which destabilizes the molecule. The lifetime of O_2 ($^1\Delta_g$) is larger in organic solvents (~ 10 - 100 μs) than in aqueous environment (~ 2 μs) because the energy of O-H stretching in water molecules nearly equals the excited state energies of O_2 ($^1\Delta_g$). The energy dissipates as heat by the stretching and vibrational motions of water molecules.[91]

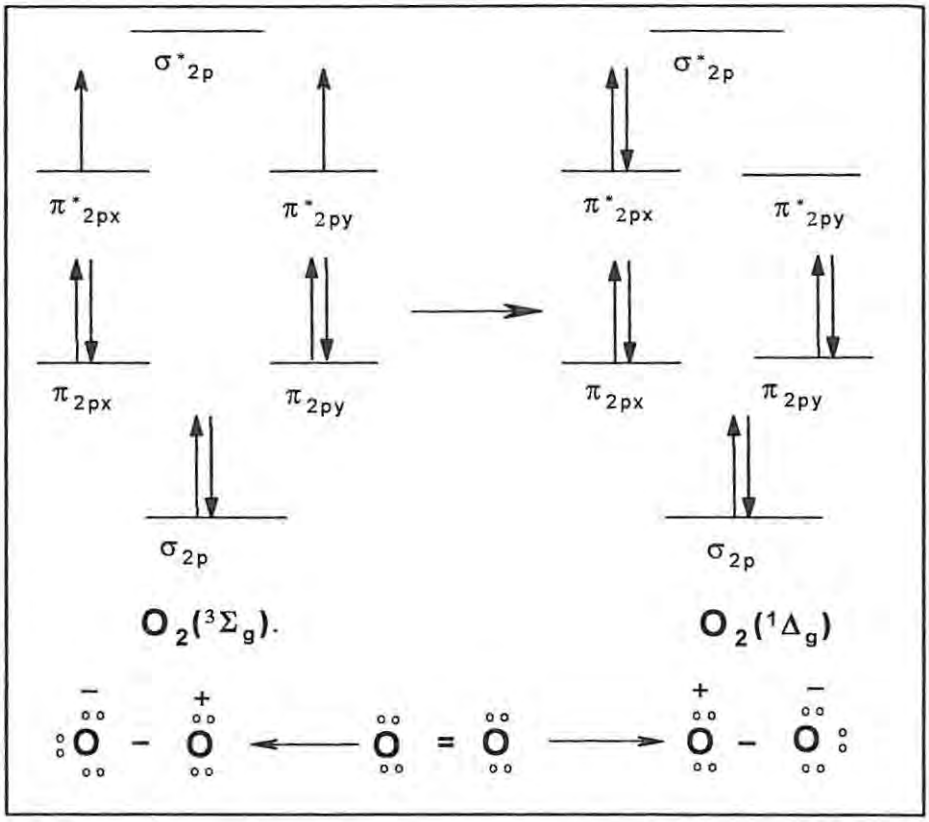

Scheme 1.10: Molecular orbital diagrams showing the electronic distribution in triplet and singlet oxygen (top). Lewis structure showing the Zwitterion character of singlet oxygen (bottom).

1.3.3.2 Singlet Oxygen Quantum Yields

As has been indicated earlier, the major determining factor for assessing the effectiveness of any MPc as a photosensitiser is the overall singlet oxygen quantum yield, Φ_{Δ}. Some of the factors, which affect the efficient generation of singlet oxygen by MPc complex, include:

(i) ***Aggregation***: The photosensitizing effectiveness of MPc complexes is substantially reduced by aggregation in solution.[32,84,182,185-187] Aggregation reduces the lifetimes of the excited MPc complex, most probably due to enhanced radiationless excited state dissipation,[182] and therefore reduces

the Φ_Δ value. Aggregation in MPc is charaterised by such spectral effects as band broadening, blue shift of the Q band and splitting of the Q band. Aggregation is a result of four main processes,[32] viz: direct linkage between two or more phthalocyanine rings (i.e. intramolecular interaction),[188] covalent bonding between the metals as μ-oxo-links (especially MPc complexes of Fe and Si),[68,189] sand-witch type complexation where two MPcs share one central metal,[190-192] or by weak association whereby the peripheral substituents hold two rings in space.[193]

(ii) ***Photobleaching:*** This is the destruction or degradation of the photosensitiser molecule by light-mediated processes. The rate of photobleaching or its quantum yield (Φ_P) is a measure of the stability of the MPc sensitiser in a given environment.[91] Photobleaching generally depends on factors such as structure, concentration, solvent and light intensity. There have been different reports on the dependence of photobleaching on oxygen, with some researchers showing dependence on singlet oxygen,[194,195] independence on ground state oxygen,[196,197] or indifferent to either conditions.[195]

The Φ_Δ value can be determined via physical and chemical means.[198-200] In this work, the Φ_Δ values of various water-soluble phthalocyanine complexes of aluminium, zinc, tin and silicon were determined using photochemical methods. In photochemical method, a solution containing photosensitiser (MPc), oxygen and quencher (a singlet oxygen sensitive compound, also known as singlet oxygen scavenger or quencher) is irradiated and the decay of the quencher is followed spectroscopically. The chemical

quenchers employed were 1,3-diphenylisobenzofuran (DPBF)[200] in DMF and tetrasodium α,α'-(anthracene-9,10-diyl) bimethylmalonate (ADMA)[198] in aqueous media. These quenchers are pure and efficient complexes that react quickly with singlet oxygen as soon as it is produced. Other chemical quenchers that can be used in organic solvents for this purpose include furans, derivatives of anthracene, guanine and bilirubin.[200-202] Kraljic and El Mohsni[203] have also devised the use of N,N-dimethyl-4-nitrosoaniline (abbreviated as RNO) as chemical quencher for singlet oxygen in aqueous solution.

The decay of the quenchers can be directly correlated to Φ_Δ using equations 1.12 - 1.16, where Q represents the quenchers, DPBF or ADMA;

$$O_2\,(^1\Delta_g) \xrightarrow{k_d} O_2\,(^3\Sigma_g^-) \qquad \text{(Natural decay)} \qquad 1.12$$

$$O_2\,(^1\Delta_g) + Q \xrightarrow{k_r} \text{Oxidation Products} \qquad \text{(Chemical reaction)} \qquad 1.13$$

$$O_2\,(^1\Delta_g) + Q \xrightarrow{k_q} O_2\,(^3\Sigma_g^-) + Q \qquad \text{(Physical quenching)} \qquad 1.14$$

$$MPc + O_2\,(^1\Delta_g) \longrightarrow O_2\,(^3\Sigma_g^-) + MPc \qquad \text{(Physical quenching)} \qquad 1.15$$

$$MPc + O_2\,(^1\Delta_g) \longrightarrow \text{Oxidation products} \qquad \text{(Chemical reaction)} \qquad 1.16$$

where k_d is the natural decay constant of singlet oxygen, k_r and k_q represent the rate constants for the chemical reaction and physical quenching of singlet oxygen by the quencher, respectively. DPBF and ADMA are known[198,200] to be mainly chemical quenchers hence equation 1.14 may be ignored. The interaction of the MPcs with singlet oxygen is negligible compared to the rate of reaction of the latter with the quenchers, thus equations 1.15 and 1.16 can also be ignored.

The rate of disappearance of the quencher, Q in the presence of O_2 ($^1\Delta_g$) is given by equation 1.17

$$\frac{-d[Q]}{dt} = k_r[Q][O_2(^1\Delta_g)] \qquad 1.17$$

Applying the steady-state approximation for [O_2 ($^1\Delta_g$)], and then rearranging gives equation 1.18

$$O_2(^1\Delta_g) = \Phi_\Delta \frac{I_{abs}}{k_d + k_r[Q]} \qquad 1.18$$

Substituting equation 1.18 into 1.17 gives 1.19

$$\frac{-d[Q]}{dt} = \Phi_\Delta \frac{k_r[Q]I_{abs}}{k_d + k_r[Q]} \qquad 1.19$$

Equation 1.10 may be written as equation 1.20 for the quencher

$$-d[Q]/dt = I_{abs}\Phi_Q \qquad 1.20$$

Substituting 1.20 into 1.19 and cancelling out I_{abs} gives 1.21

$$\Phi_Q = \Phi_\Delta \frac{k_r[Q]}{k_d + k_r[Q]} \qquad 1.21$$

At high [Q], the reaction kinetics is zero, i.e. independent of [Q]; a situation not suitable for this work. For the desired first order kinetics, low [Q] (~10^{-5} mol dm^{-3}) was employed. Thus, it can be assumed that $k_d >> k_r$ [Q], and equation 1.21 becomes equation 1.22

$$\Phi_Q = \Phi_\Delta \frac{k_r[Q]}{k_d} \qquad 1.22$$

In the presence of any MPc sensitiser, equation 1.22 may be written for Φ_Δ^{MPc} as equation 1.23

$$\Phi_{\Delta}^{MPc} = \Phi_{Q}^{MPc} \frac{k_d}{k_r[Q]^{MPc}} \quad 1.23$$

where Φ_Q^{MPc} and $[Q]^{MPc}$ are the quantum yield and concentration of the quencher in the presence of the MPc, respectively. Equation 1.23 may also be written for a reference (e.g. ZnPc) whose Φ_Δ is known as equation 1.24.

$$\Phi_{\Delta}^{Ref} = \Phi_{Q}^{Ref} \frac{k_d}{k_r[Q]^{Ref}} \quad 1.24$$

The ratio of the equation 1.23 over 1.24 (the comparative method[185,200]) gives equation 1.25.

$$\Phi_{\Delta}^{MPc} = \Phi_{\Delta}^{ref} \frac{\Phi_{Q}^{MPc}[Q]^{ref}}{\Phi_{Q}^{ref}[Q]^{MPc}} \quad 1.25$$

The reference MPc complexes used in this work are those of $AlPcS_{mix}$ (Φ_Δ = 0.38 in water) and ZnPc (Φ_Δ = 0.56 in DMF). Φ_Q can be obtained using the relationship[200] shown in equation 1.26

$$\Phi_{Q} = \frac{(C_o - C_t)V}{I_{abs}t} \quad 1.26$$

where C_o and C_t are the concentrations of the quencher prior to and after irradiation, respectively. C_o and C_t may be conveniently replaced by absorbances, A_o and A_t. V is the volume of the sample in the cell; t is the irradiation or photolysis time. I_{abs} is given as

$$I_{abs} = \frac{aSI}{N_A} \quad 1.27$$

where α is the fraction of light absorbed, S is the cell area irradiated, I is the light intensity from the lamp and N_A is the Avogadro's constant. Assuming that S and V are

the same, then substituting 1.27 into 1.26, and then 1.26 into 1.24, equation 1.28 is obtained.

$$\Phi_{\Delta}^{MPc} = \Phi_{\Delta}^{ref} \frac{(C_o - C_t)^{MPc}(\alpha t)^{ref}[Q]^{ref} I^{ref}}{(C_o - C_t)^{ref}(\alpha t)^{MPc}[Q]^{MPc} I^{MPc}} \qquad 1.28$$

The value of I is constant if the same interference filters are used for both reference and sample, and so can be cancelled out in equation 1.28.

1.3.4 Photodegradation Studies of Chlorophenols

Photodegradation of monochlorophenols in aqueous solution[85,86] and trichlorophenol in organic solution[204] using MPc sensitisers is known. Although the photo-transformation kinetics of chlorophenols were not reported by these authors,[85,86,204] the route via singlet oxygen (Type II, Scheme 1.9) is the dominating process in sensitized photo-oxidation processes.[84-91,135,200] In the 1970s, Foote and co-workers,[205,206] showed that phenolic compounds, such as α-tocopherol and triphenylphenol, scavenge O_2 ($^1\Delta_g$) more by physical quenching than by chemical reaction (i.e. $k_q > k_r$) in organic solvents. Tratnyek and Holgné[207] obtained rate constant, k_r, for O_2 ($^1\Delta_g$) reaction with various chlorophenols, but failed to establish the quenching constants (k_q) for these species in water. To provide a qualitative insight into the mechanism of the reaction of chlorophenols with O_2 ($^1\Delta_g$) in aqueous environment, it is important to provide a means of predicting the respective values of both k_r and k_q.

Replacing Q with chlorophenol (Chp) in equation 1.21 without neglecting physical quenching (k_q), the quantum yield for the transformation of a chlorophenol (Φ_{Chp}) may be given as equation 1.29.

$$\Phi_{Chp} = \Phi_{\Delta} \frac{k_r[Chp]}{k_d + (k_r + k_q)[Chp]} \qquad 1.29$$

Rewriting equation 1.29 as its double reciprocal and rearranging gives equation 1.30.

$$\frac{1}{\Phi_{Chp}} = \frac{1}{\Phi_{\Delta}}\left(\frac{k_r + k_q}{k_r} + \frac{k_d}{k_r[Chp]}\right) \qquad 1.30$$

According to the equation 1.30, a plot of $1 / \Phi_{ChP}$ versus $1 / [Chp]$ gives the slope as $k_d / k_r\Phi_{\Delta}$. The k_r value can be obtained from the slope if k_d and Φ_{Δ} are known. The total rate constants $(k_r + k_q)$ can then be obtained from the intercept, $(k_r + k_q) / k_r\Phi_{\Delta}$.

In addition to the Type II pathway (Scheme 1.9) photodegradation of phenols and chlorophenol substrates (Sub) can occur through the formation of superoxide anion radical ($O_2^{-\cdot}$) by photo-induced electron transfer (i.e. the so-called Type I mechanism), equations 1.31 – 1.34.

$$^3MPc^* + O_2 \longrightarrow MPc^{+\cdot} + O_2^{-\cdot} \qquad 1.31$$

$$MPc^{+\cdot} + Sub \longrightarrow MPc + Sub_{(ox)} \qquad 1.32$$

$$O_2^{-\cdot} + Sub\text{-}H \longrightarrow HO_2^- + Sub^{\cdot} \qquad 1.33$$

$$Sub_{(ox)},\ HO_2^-,\ Sub^{\cdot} \longrightarrow \text{further reactions} \qquad 1.34$$

Type I mechanism has also been proposed by Kasuga et al.[204] for the photo-degradation of trichlorophenol in aerated organic solvents using tetra-*tert*-butyl zinc phthalocyanine, equations 1.35 – 1.40.

$$MPc \xrightarrow{h\nu} MPc^* \qquad 1.35$$

$$MPc^* + O_2 \longrightarrow MPc^{+\cdot} + O_2^{-\cdot} \qquad 1.36$$

$$MPc^{+\cdot} + O_2^{-\cdot} \longrightarrow MPc + O_2 \qquad 1.37$$

$$O_2^{-\cdot} + TCP \longrightarrow HO_2^{\cdot} + TCP^- \qquad 1.38$$

$$TCP^- + MPc^{+\cdot} \longrightarrow TCP^{\cdot} + MPc \qquad 1.39$$

$$TCP^{\cdot} + HO_2^{\cdot} \longrightarrow \text{Oxidised products} \qquad 1.40$$

In this case, the superoxide anion radical ($O_2^{-\cdot}$) generated by photo-induced electron transfer from the excited metallophthalocyanine (MPc*) complex, attacks the unionized TCP molecule to give its anion (TCP^-) and the reactive hydroperoxyl radical ($HO_2^{\cdot}$). The photocatalytic activity of MPc complexes towards transformation of chlorophenols in water has not received much attention.

From the above knowledge, the photochemistry part of this research work is aimed at:

- Synthesizing water-soluble MPc complexes and investigating their photosensitizing properties towards the generation of singlet oxygen as a first step towards their effectiveness as photosensitisers.
- Studying the applicability of these complexes towards the photo-degradation of chlorophenols in aqueous solutions.
- Investigating relative efficiencies of Type I and Type II photo-oxidation processes (since both of them may operate simultaneously) towards the photosensitized transformation of chlorophenols.

1.4 Electrochemistry: An Overview

1.4.1 Basic Concepts

Electrochemistry may generally be defined as the study of chemical reactions to produce electric power or, alternatively, the use of electricity to effect chemical processes or systems.[208] Thus, electrochemical techniques are simply the interplay between electricity and chemistry, namely the measurements of electrical quantities, such as current, potential, and charge, and their relationship to chemical parameters. The use of these electrical measurements for analytical purposes has found a wide range of applications in industrial quality control, biomedical analysis and environmental monitoring.[209]

Unlike many chemical measurements, which involve homogeneous bulk solutions, the fundamental electrochemical reactions are heterogeneous in nature as they take place at interfaces, usually electrode-solution boundaries. The electrode creates a phase boundary that differentiates otherwise identical solute molecules; those at a distance from the electrode, and those close enough to the surface of the electrode to participate in the electron transfer process.[208-210]

The work described in this thesis employed two electroanalytical techniques, cyclic voltammetry (CV) and Osteryoung square wave voltammetry (OSWV). They were employed in the characterization of alkanethiol-derivatised metallophthalocyanine complexes and investigation of the surface electrochemistry of gold electrodes modified with the self-assembled monolayers of these metallophthalocyanines (MPc-SAM), as well as the electrocatalytic oxidation of thiols and thiocyanate using these MPc-SAM

modified gold electrodes. A closer look at the electrode processes and these two electroanalytical techniques follows.

1.4.1.1 The Electrode-Solution Interface

The definitive picture of the electrode-solution interface, also known as the "electrical double layer", is given in Figure 1.5. The currently accepted model was produced by Stern,[210-214] and is a development from the Helmholtz model (which regards the interface as a single capacitor) and the Guoy-Chapman model (which explains the interface as a Boltzman distribution of ions).

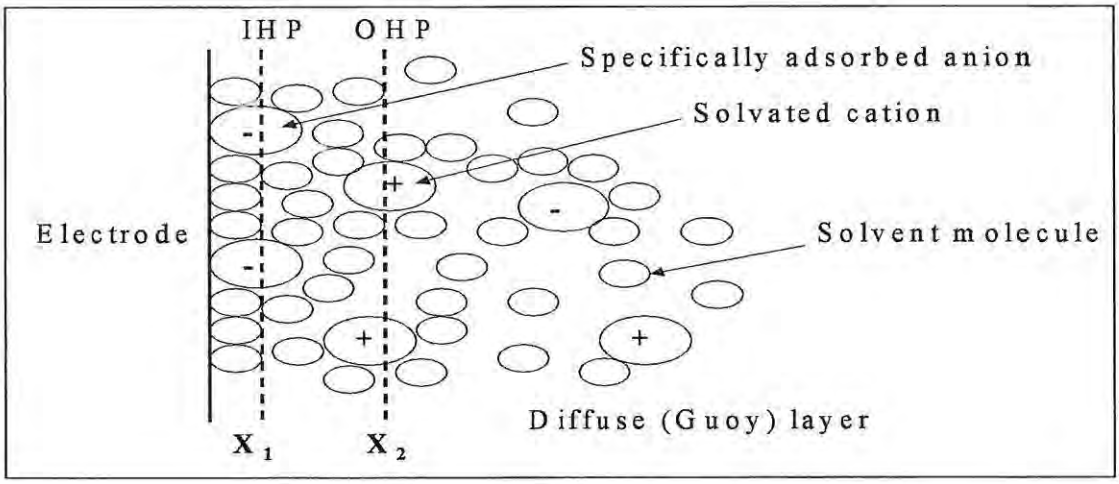

Figure 1.5: Model of the electrode-solution double layer region

As shown in Figure 1.5, the electrical double layer is a complex structure of several distinct parts. The inner layer (closest to the electrode) where the contact-adsorbed ions (not fully solvated) and solvent molecules sit is called the Inner Helmholtz Plane (IHP). The outer layer, the Outer Helmholtz Plane (OHP) is the imaginary plane passing through the solvated cations. The solvated cations are nonspecifically adsorbed

(i.e. noncontact-adsorbed) and are attracted to the surface by long-range coulombic forces. These planes cannot be measured exactly, nor do they strictly exist, but the distance from the electrode to the IHP (x_1) will be the radius of the ion and to the OHP (x_2) will be about two water molecules plus the radius of the cation.[209,211] Both IHP and OHP represent the compact layer, which is strongly held by the electrode, and can survive even when the electrode is pulled out of the solution.[209] The layer, a three-dimensional region of scattered ions, which extends from the OHP to the bulk solution, is referred to as the 'diffuse layer' or Guoy layer. The ion distribution in the diffuse layer is a consequence of the balance between the disorder caused by the random thermal motion and order due to the electrostatic force of the attraction and repulsion from the electrode surface. Beyond the diffuse layer, it becomes impossible for the ions in the homogeneous bulk solution to 'feel' the presence of the electrode.[210]

1.4.1.2 Classification of Electrochemical Techniques

Electrochemical techniques can be divided into two classes: bulk and interfacial techniques. Bulk techniques are based on the phenomena that occur in the core of the solution, for example, conductimetry. By contrast, interfacial techniques are based on the phenomena taking place at the electrode-solution interface.

Interfacial techniques are further classified into equilibrium (e.g. potentiometric measurements) and dynamic methods. The dynamic methods are sub-classified into controlled-potential and controlled-current methods. The controlled-potential methods are indisputably more popular and include a vast array of techniques such as voltammetry, bulk electrolysis and chronoamperometry. The controlled-potential techniques involve

current measurement, while potential is controlled. In this research, all electroanalytical experiments were performed using the controlled potential techniques. The advantages [209] for using these techniques include high sensitivity and selectivity towards electroactive species, wider linear range, portable and low cost instrumentation.

1.4.1.3 Faradaic and Non-Faradaic Processes

In controlled potential experiments, a current response corresponding to the concentration of the analyte oxidized or reduced at the electrode-solution interface is obtained. This current response is obtained by monitoring the transfer of electrons during the redox process of the target analyte as represented by equation 1.41:

$$Ox + ne^- \rightleftharpoons Red \qquad 1.41$$

where Ox and Red represent the oxidized and reduced forms of the analyte, respectively, while n is the number of electrons transferred. The current resulting from the oxidation or reduction of the analyte is termed the Faradaic current since it obeys the Faraday's laws.

For a thermodynamically controlled reversible process the applied potential of the electrode (E) is given by the well-known Nernst equation, equation 1.42

$$E = E^o + \frac{2.303RT}{nF}\log\frac{C_{Ox}}{C_{Red}} \qquad 1.42$$

where E^o = standard potential of the redox couple

R = universal gas constant

T = temperature (K)

n = number of electrons transferred

F = Faraday's constant

NB: At 25°C, 2.303RT/F = 0.05916V.

In contrast to Faradaic currents, non-Faradaic currents arise from processes that do not involve electron transfer reactions across the electrode-solution interface, that is no oxidations or reductions occur.[208-211] Non-Faradaic currents originate mostly from the electrical capacitance present at the interface. The electrical double layer behaves like an ordinary (parallel plate) capacitor. Like any capacitor, the charge (q) is directly proportional to the effective potential (E) according to equation 1.43

$$C = \frac{q}{E} \qquad 1.43$$

where C stands for the capacitance (in Farads, F)

1.4.1.4 The Electrochemical Cell

A three-electrode electrochemical cell (Figure 1.6) is usually employed in dynamic electrochemical experiments. The working (or indicator) electrode, W.E., is

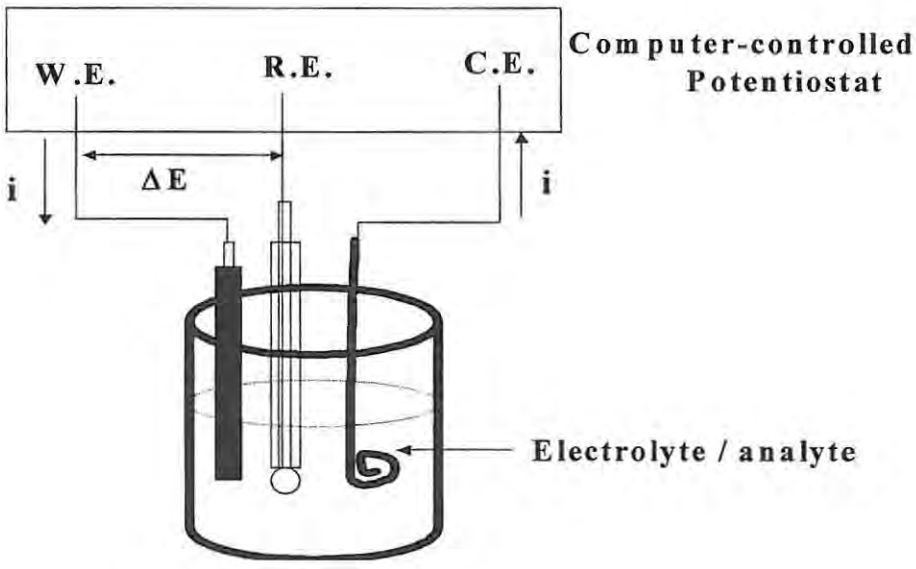

Figure 1.6: A diagrammatic representation of a conventional three-electrode cell

where the electrochemical reaction being studied takes place. R.E. is the reference electrode, while counter electrode, C.E., completes the electric circuit. The best reference electrode is one whose potential does not shift from equilibrium (i.e. non-polarisable). To maintain low current densities and, thus, minimize its polarization, reference electrode with very large surface area is used. The complete elimination of reference electrode polarization is only feasible with modern potentiostatic instrumentation based on operational amplifiers. The potentiostat maintains a potential difference, ΔE, between the R.E. and W.E. and supplies the current, i, needed for affecting the changes occurring at W.E. [208,211]

There are several reference electrodes employed in electroanalytical experiments, silver|silver chloride (Ag|AgCl) being the most popular. This consists of a piece of silver wire anodized with silver chloride in a glass tube. The wire is in contact with concentrated KCl or NaCl solution. A semi-permeable salt-bridge protects the electrode from the bulk of the solution.[215] Counter electrodes are commonly platinum wire, loops, gauze or foil. Working electrodes are commonly mercury, carbon and 'inert' metals, particularly platinum and gold.

1.4.1.5 Mass Transport Processes

The movement of charged and neutral species in electrochemical cells is fundamentally important. The three modes of transport to the electrode surface are diffusion, migration and convection.[208-214]

Diffusion is mass transport resulting from the spontaneous movement of analyte species from regions of high concentrations to those of lower ones, with the aim of

minimizing concentration differences. Diffusion can be described using mathematics, hence it is easier to treat a wide variety of electrochemical phenomena. The rate of diffusion of any chemical species is related to its diffusion coefficient, D ($\sim 10^{-5}$ cm^2 s^{-1} for most small organic or inorganic molecules or ion).[208] Fick's second law (equation 1.44) allows the calculation of changes in concentration with time.

$$\frac{\delta c}{\delta t} = D.\left(\frac{\delta^2 c}{\delta x^2}\right) \qquad 1.44$$

where c = concentration of diffusing species, t = time and x = distance

Migration is the movement of charged particles under the influence of an electric field. In most voltammetric experiments, the contribution of migration to mass transport of the target analyte is eliminated by the addition of large excess of easily ionisable salt (supporting electrolyte). The supporting electrolyte dissociates to produce inert anions and cations, which become the migration current carriers thus releasing the electroactive analyte (if charged) from migration effects.[208]

Convection is a mass transport due to movement of the solution as a whole. It is driven by stirring, solution flow, rotation or vibration of electrode.

1.4.2 Cyclic Voltammetry

Cyclic voltammetry is a most widely applied electroanalytical technique for examining the nature or route of an electrochemical reaction in detail. Its popularity stems, among others, from its relative experimental simplicity and ability to offer a rapid location of redox potentials of the target electroactive species, and convenient evaluation of the effect of media on the redox processes.[208, 216] The experiment allows one to scan the potential of a stationary working electrode in an unstirred solution back after reaching

a certain value, E_s, the so-called switching potential. The resulting current-potential plot (represented in Figure 1.7) is termed a *cyclic voltammogram*. As exemplified in the

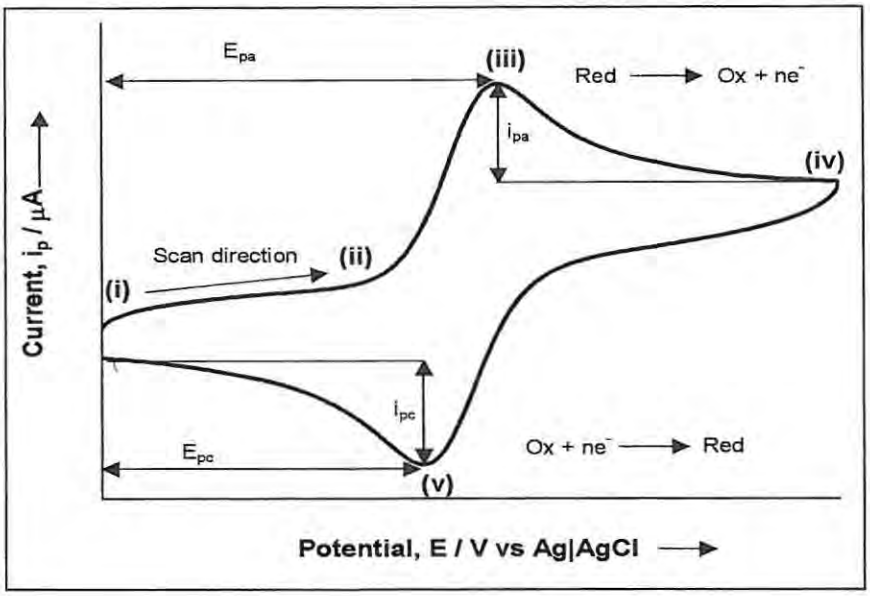

Figure 1.7: A typical cyclic voltammogram.

diagram, the reductant (Red) is oxidised in the forward scan to its oxidized (Ox) species, which in turn is re-reduced during the reverse scan. Information obtainable from cyclic voltammogram include the anodic (E_{pa}) and cathodic (E_{pc}) peak potentials, and anodic (i_{pa}) and cathodic (i_{pc}) peak currents. Cyclic volammetric processes could be reversible, quasi-reversible and irreversible.

1.4.2.1 Reversible Process

A reversible electrochemical process is the one in which the electroactive species, oxidized (or reduced) in the forward scan is reduced (or oxidized) in the backward / reverse scan (equation 1.45).

$$Red \rightleftharpoons Ox + ne^- \qquad 1.45$$

Reversibility is an indication that the process is in equilibrium, meaning that the Nernst equation is obeyed at all potentials. A typical voltammogram for a reversible process is shown in Figure 1.7. In the Figure, the starting point (i) is selected such that no current flows when the circuit is closed. From point (i), the voltage is scanned in the anodic direction; when point (ii) is reached, oxidation of 'Red' starts and the current increases with increasing electrode potential until point (iii), where depletion of substrate at the electrode leads to decrease in current and the observation of a peak. The direction of the voltage sweep is changed at point (iv) and a peak is observed at (v) on the cathodic sweep, which corresponds to the reduction of 'Ox'. Since there are no coupled chemical reactions in this case, no other cathodic peaks are observed and the second cycle can differ from the first only slightly due to changes in concentrations of Red and Ox at the electrode. The kinetics of electron transfer is fast such that mass transport is the determining rate, even at small overpotentials. Reversibility is a direct and straightforward manner of probing the stability of an electroactive species. An unstable species reacts as it is formed and thus producing no current wave in the reverse scan. A stable species, on the other hand, remains in the vicinity of the electrode surface and produces a current wave of opposite polarity to that of the forward scan. In Figure 1.7 for example, the flow of Faradaic current is not observed until at a potential in the (ii) region is reached. If the potential were to be reversed at this point (ii) and returned to the initial value (i), a flat voltammogram having approximately constant levels of anodic (forward scan) and cathodic (reverse scan) currents would be observed. These currents are due to

the capacitive charging current of the working electrode's double layer, which can be estimated using equation 1.46:

$$C = \frac{\Delta i}{2\nu} \qquad 1.46$$

Where C(F) is the capacitance, Δi (A) is the difference between the cathodic and anodic currents, and ν is the scan rate (Vs^{-1}).

At 25°C, the peak current of a reversible process is given by the Randles-Sevcik equation, 1.47

$$i_p = (2.69\text{x}10^{-5})n^{3/2}Ac(D\nu)^{1/2} \qquad 1.47$$

where i_p = peak current (A)

n = number of electrons transferred

A = electrode area (cm^{-2})

C = concentration (mol cm^{-3})

D = diffusion coefficient (cm^2 s^{-1})

ν = scan rate (Vs^{-1})

A linear plot of i_p vs $\nu^{1/2}$ indicates that the currents are controlled by planar diffusion to the electrode surface. The ratio of the anodic (i_{pa}) to the cathodic (i_{pc}) currents is equal to one for a totally reversible process. Deviation from unity indicates the presence of chemical reaction involving either Ox or Red, or both. The average of the two peak potentials gives the half-wave potential ($E_{1/2}$), i.e. the potential where the current is half of its limiting value, equation 1.48.

$$E_{1/2} = \frac{E_{pa} + E_{pc}}{2} \qquad 1.48$$

where E_{pa} and E_{pc} are the anodic and cathodic peak potentials , respectively. $E_{1/2}$ may also be represented by

$$E_{1/2} = E^{o'} - \frac{RT}{nF}\ln\frac{D_{Ox}}{D_{Red}} \qquad 1.49$$

The formal potential of the redox couple ($E^{o'}$) can be estimated from the equation where the ratio of the diffusion coefficients, D_{Ox} and D_{Red}, is approximately unity. The separation between two peak potentials, ΔE_p, for a reversible couple is given by equation 1.50 and can be used to obtain the number of electrons (n) transferred.

$$\Delta E_p = E_{pa} - E_{pc} = \frac{RT}{nF} \qquad 1.50$$

ΔE_p is independent of the scan rate, and at 25°C equation 1.50 can be simplified to equation 1.51.

$$\Delta E_p = \frac{RT}{nF} = \frac{0.059V}{n} \qquad 1.51$$

At appropriate conditions (i.e. at 25°C, first cycle voltammogram) the standard rate constant (k^o) for the heterogeneous electron transfer process can be estimated.[208,217]

1.4.2.2 Irreversible Process

An irreversible cyclic voltammetric process shows a single oxidation or reduction peak, with a weak or no reverse wave. When a reverse wave is present, it is widely separated from the forward scan. Irreversibility arises from the sluggish electron exchange of redox species with the working electrode,[218] thus making the Nernst equation invalid. The peak current, i_p, for irreversible process is given by equation 1.52.

$$i_p = (2.99\text{x}10^5)n(\alpha n)^{1/2}Ac(Dv)^{1/2} \qquad 1.52$$

where α is the rate of electron transfer. For a totally irreversible system, ΔE_p is calculated from equation 1.53:

$$\Delta E_p = E^{o'} - \frac{RT}{\alpha nF}\left[0.78 - \ln\frac{k^o}{D^{1/2}}\ln\left(\frac{\alpha nF}{RT}\right)^{1/2}\right] \qquad 1.53$$

where all the symbols are as already defined above. At 25°C, the peak potential (E_p) and the half-peak potential ($E_{1/2}$) differ by $0.048/\alpha n$.

1.4.2.3 Quasi-Reversible Process

Unlike the reversible process in which the current is purely mass transport-controlled, currents due to quasi-reversible process are controlled by a mixture of mass transport and charge transfer kinetics.[209,216] Because mass transport plays a part in controlling the concentration of the redox couple, the expressions outlined for reversible processes above also apply for quasi-reversible.[216] The slight differences in three cyclic voltammetric processes are summarized in Table 1.1.

1.4.2.4 Electrocatalysis Using Cyclic Voltammetry

Electrocatalysis using cyclic voltammetry is characterized by an enhancement of either the cathodic or anodic currents, or an absence of a reverse peak, and / or a shift in redox potentials to lower values.[209] Hypotheticcal cyclic voltammograms showing the electrocatalytic behaviour of a catalyst (e.g. an MPc molecule with an electroactive central metal) towards the oxidation of an analyte (A) are shown in Figure 1.8.[55,76,78,82]

Table 1.1: The diagnostic criteria for reversible, irreversible and quasi-reversible cyclic voltammetric processes.

Parameter	Cyclic Voltammery Process		
	Reversible	Irreversible	Quasi-reversible
E_p	Independent of ν	Shifts cathodically by $30/\alpha n$ mV for a 10-fold increase in V	Shifts with ν
$E_{pc} - E_{pa}$	~ 59 n mV at 25°C and independent of ν	_	May approach 60/n mV at low ν but increases as ν increases
$i_p / \nu^{1/2}$	Constant	Constant	Virtually independent of ν
i_{pa} / i_{pc}	Equals 1 and independent of ν	No current on the reverse side	Equals 1 only for $\alpha = 0.5$

The active form of the MPc ($M^{(III)}Pc$) is generated which then reacts with the analyte. In cases where the chemical reaction is fast, and all the analyte is electro-oxidised ($A_{oxidised}$), there will be a very small or no return peak. Electrocatalysis in Figure 1.8 is characterized by enhancements in current and shifts of potential to lower values.

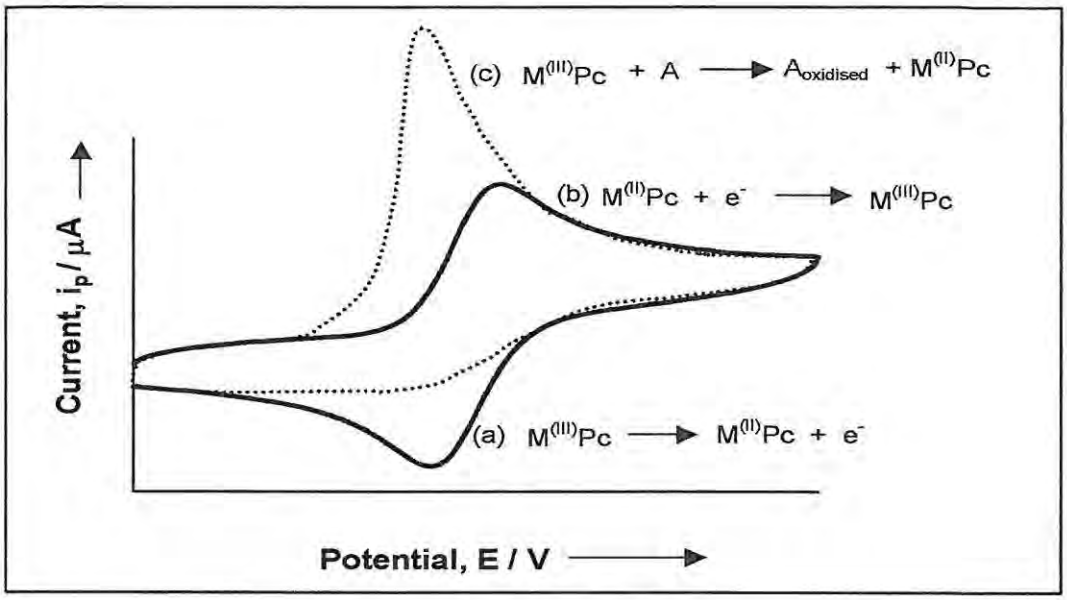

Figure 1.8: Hypothetical cyclic voltammogram showing catalytic behaviour of a catalyst (e.g. MPc) towards the electro-oxidation of an analyte.

1.4.3 Square Wave Voltammetry

Square wave voltammetry is a technique, which depends on excitation functions that combine the features of a large amplitude square wave modulation with a single staircase waveform. During each square wave cycle, the current is sampled twice, at the end of the forward and reverse scans. When the current function ($\delta i = i_1 - i_2$) is plotted against the average potential of each waveform cycle, peak-shaped voltammograms are obtained. This current function is symmetrical around the half-wave potential meaning that the peak potential occurs at the $E_{1/2}$ value of the redox couple.[208,219,220] The scan rate, ν, of a square wave voltammetry experiment is given by equation 1.54.

$$\nu = f.\Delta E_s \qquad 1.54$$

where f is the square wave frequency (Hz) and ΔE_s is the potential step size.

The major advantages of this powerful electrochemical technique include the use of faster scan rates compared to conventional differential pulse voltammetry, superior ability to reject capacitive charging currents and excellent sensitivity. Its popularity is on the increase by the availability of software packages capable of digital simulations of the corresponding current-potential waves. In this research, a computer-aided Osteryoung square wave voltammetry was employed.

1.4.4 Spectroelectrochemistry

As the name suggests, spectroelectrochemistry is a technique that relies on the coupling of optical and electrochemical methods. The development of optically transparent electrodes (OTEs) [209,211,212,218,221,222] has made it possible to observe spectral changes simultaneously with electrochemical perturbations.

There are three groups of OTE: (a) metal minigrids, which comprises several wires of platinum, gold, silver, etc.; (b) thin films of semiconductors or metals or glass and (c) reticulated vitreous carbon. Thin layer cells that incorporate these electrodes are termed optically transparent thin layer electrode (OTTLE) cells. The technique is extremely useful for studies such as the elucidation of reaction mechanism, kinetics of formation and decay of species, and UV-Vis spectra of electrogenerated species in solutions. The working volumes of OTTLE cells range between 30-50 μL and complete electrolysis takes place in few seconds.[209,213,214] The number of electrons transferred during the redox process can be determined using the Faraday's law, given by equation 1.55

$$n = \frac{Q}{FVc} \qquad 1.55$$

where Q = amount of charge passed (C), V = volume of OTTLE cell (L). Other constants are as defined previously.

1.4.5 Electrochemistry of Metallophthalocyanines

The redox chemistry of MPc complexes is commonly observed using electrochemical,[16-20,223-225] (particularly cyclic voltammetry), photochemical,[226-228] or spectroelectrochemical methods.[32,191,227,228] The neutral form of MPc exists as a dianion, designated as Pc(-2).[231] Reduction and oxidation reactions can occur at either the Pc ring or central metal or both. Oxidation at the Pc ring in MPc(-2) occurs by successive loss of one or two electrons from the HOMO resulting in the formation of the $[MPc(-1)]^{+\cdot}$ and $[MPc(0)]^{2+\cdot}$ cation radicals, respectively. The formation of $[MPc(-1)]^{+\cdot}$ creates a hole in the $a_{1u}(\pi)$ level, thus permitting an allowed transition from the low-lying, $e_g(\pi)$ level. The presence of $[MPc(-1)]^{+\cdot}$ is normally characterized by the loss in the intensity of the Q band, formation of weak bands in the 700-825 nm region, and a broad band near 500 nm. The band around 700 nm is usually associated with the dimerisation of the radical species.[232-237]

Reduction of the Pc ring occurs by the successive gain of one to four electrons by the LUMO of the MPc complex, resulting in the formation of MPc(-3), MPc(-4), MPc(-5) and MPc(-6) species.[223,231,238-247] Scheme 1.11 shows the energy level for one-electron ring reduced or ring oxidized MPc complex.

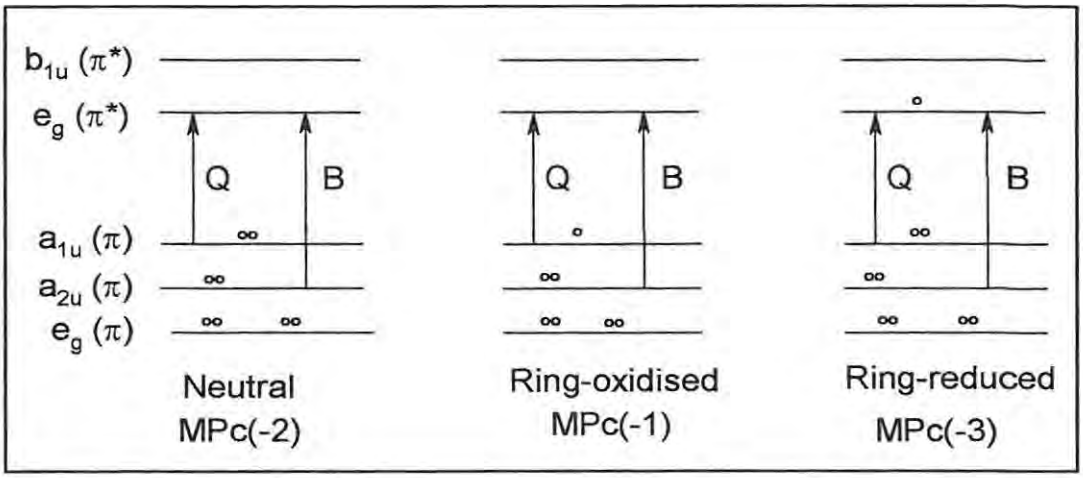

Scheme 1.11: A simplified energy level diagram of ring-oxidized and ring-reduced metallophthalocyanine species.

Depending on its position on the Periodic Table, the central metal ion of the MPc may or may not undergo redox processes. The main group MPcs (example, ZnPc and MgPc) and transition metal MPcs (example, NiPc) whose metal ions have no accessible d-orbital levels lying in the HOMO-LUMO gap are redox-inactive with respect to their metal centers.[16,223,243-246,248-250] Thus, all redox processes occur exclusively on the Pc rings for these complexes. The potential separation between the first ring oxidation and first ring reduction (ΔE^o) in voltammetric experiment is about 1.6V for non-transition metal phthalocyanines, which corresponds to the magnitude of the energy difference between the HOMO and LUMO.[32,243]

On the other hand, the redox processes of the redox-active transition metal MPcs (such as the FePc and CoPc complexes) occur both on the metal and the Pc rings, depending on the factors within the environment such as solvent, electrolyte, axial

ligands and ring substituents.[8,33,223,247,251,252] Metal oxidation or reduction is characterized by a shift in Q band without much reduction in intensity.[253]

1.4.6 Electrocatalytic Properties of Metallophthalocynines

Owing to their dual π donor-acceptor function, MPcs have established themselves as electrocatalysts per excellence.[172,254-260] They have been known to exhibit good electrocatalytic activity (both in homogeneous and heterogeneous phases) towards various technologically important redox reactions. The catalytic activity is mediated by redox process centered at the central metal and/or ring [254-260] and electrocatalytic activities are normally observed at potentials close to the formal potential of the MPc. The established[55,76,78,82,255,257] mechanism for the metal oxidation-mediated catalytic oxidation of an analyte (A) to an oxidation product (A_{ox}) is given by equations 1.56 and 1.57.

$$M^{(II)}Pc(-2) \longrightarrow M^{(III)}Pc(-2) + e^- \qquad 1.56$$

$$M^{(III)}Pc(-2) + A \longrightarrow M^{(II)}Pc(-2) + A_{ox} \qquad 1.57$$

For a ring oxidation mediated process,[173] equations 1.58 – 1.60 have been proposed for L-cysteine oxidation using phthalocyanine complexes of rhodium (RhPc) and ruthenium (RuPc).

$$MPc(-2) \longrightarrow [MPc(-1)]^{+\bullet} + e^- \qquad 1.58$$

$$2\,[MPc(-1)]^{+\bullet} \longrightarrow ([MPc(-1)]^{+\bullet})_2 \qquad 1.59$$

$$([MPc(-1)]^{+\bullet})_2 + A \longrightarrow MPc(-2) + A_{ox} \qquad 1.60$$

1.5 Chemically Modified Electrodes

According to International Union of Pure and Applied Chemistry (IUPAC),[261] a chemically modified electrode (CME) can be defined as "an electrode made of a conducting or semiconducting material that is coated with a film of a chemical modifier and that by means of Faradaic (charge transfer) reactions or interfacial potential differences (no net charge transfer) exhibits chemical, electrochemical, and/or optical properties of the film". In other words, the attachment of specific molecule to the surface of an electrode imparts on the electrode some chemical, electrochemical or other desirable properties not available at the unmodified electrode.[261-264]

In this work, gold working electrodes modified with MPc-SAMs were studied; hence a closer look at the CMEs follows.

1.5.1 General Methods of Modifying Electrode Surfaces

Electrode surfaces are modified using the following methods:

Chemisorption

In this method, the chemical film is strongly and ideally irreversibly adsorbed (chemisorbed) onto the electrode surface.[261-266] Electrode modification using self-assembled monolayer (see discussion in Section 1.5.2) falls into this category.

Covalent Bonding

This method employs a linking agent (e.g. an organosilane) to covalently attach one to several monomolecular layer of the chemical modifier to the electrode surface.[261,267,268]

Composite

The composite method is simply the mixing of chemical modifier with an electrode matrix material. The fabrication of carbon paste electrodes is based on this method.[257,269-273]

Polymer Film Coating

Coating of electrode surfaces with polymer films is perhaps the most versatile approach of modifying electrode surfaces. The following are some of the techniques used to deposit polymer films onto electrode surface.[261,264]

(a) Dip-dry coating: the immersion of the electrode in a solution of the polymer for a period sufficient for spontaneous film formation to occur by adsorption. Thereafter, the electrode is withdrawn from the solution and the solvent is allowed to dry off.

(b) Drop-dry coating (or solvent evaporation): a few droplets of the polymer solution are applied to the electrode surface and the solvent allowed to dry out.

(c) Spin-coating (or spin-casting): involves the evaporation of a drop of a polymer solution on an electrode surface by rotating at high speeds using centrifugal force.

(d) Electropolymerisation: the electrode surface is immersed in a concentrated solution (~ 10^{-3} mol dm^{-3}) of the modifier solution followed by repetitive voltammetric scanning within a specific potential window. The first scan is different from the subsequent scan indicating the formation of new species

(polymer) on the electrode surface as opposed to simple electrodeposition.[255,274,275]

Langmuir-Blodgett Technique

Invented by Langmuir and Blodgett in the 1930s, this technique involves forming an ordered monolayer or multiplayer films at the air/water interface (in a special trough) and then transferring the films to the substrate (electrode) surface.[95,96,264] This technique was first satisfactorily applied to phthalocyanine complexes in the early 1980s by Roberts' group[92] at Durham.

1.5.2 Self-Assembled Monolayer-Modified Electrodes: An Overview

General:

The self-assembling technique may simply be defined as the spontaneous adsorption of an appropriate molecule (such as a thiol species) from its solution directly onto the surface of an appropriate substrate (such as gold), forming an ultrathin film.[208,276,277] Self-assembled monolayers (SAMs) have succinctly been described as "organized molecular assemblies or ultrathin films (one molecule thick) whose spontaneous formation and stability depend on favourable, if weak, intermolecular forces, as well as forces between each of the individual component molecules and the solid substrate or support".[208] Interest in SAMs has been focused mostly on the following systems: chlorosilanes on silicon or glass,[277-281] carboxylic acids on metal oxides [282,283] and organosulphur (thiols, sulphides, disulphides, and related moieties) compounds on gold.[266,284-305]

SAMs are an incredible means of extending the function of an electrode. The self-assembling technique has been recognized for over 50 years[306] but has not been as popular as the Langmuir-Blodgett (L.B) technique. The interest in SAM was revived in the early 1980s by Sagiv and co-workers,[278,279] and Allara and Nuzzo.[284] However, it was the different articles in 1987 by various groups [285-289] and in 1988 by Whitesides and co-workers[290-295] that have resulted in the flood of research on thiol SAMs today.

The self-assembling technique offers a number of advantages over other film formation techniques. These advantages include:[307]

(a) The adsorption to the electrode surface is spontaneous; resulting in thermodynamically equilibrated final film structures.

(b) SAM film is less susceptible to desorption since the adsorbate is covalently linked to the substrate.

(c) The adsorbate does not have to be 'compatible' with water, unlike for example the L.B. technique.

(d) No special equipment is required for SAM, hence less expensive to fabricate.

(e) The orientation of the film (lying flat or standing perpendicular to the substrate) can be controlled, for example by the formation of mixed monolayer.

***Thiolates on gold*:**

From the standpoint of electrochemistry, it is believed[208,276,277] that the most important class of SAMs is formed by the chemisorption of thiolates on gold (Figure 1.9). Apart from gold, other coinage metals such as silver, platinum and copper can also serve

as effective support materials for organosulphur SAMs.[281,308,309] The choice of gold for thiol SAMs is based on the following considerations:[310]

(a) Gold is a relatively inert metal; it does not have a stable oxide under ambient conditions.[266,310]

(b) Gold has a strong specific interaction with sulphur that allows the formation of monolayers in the presence of many other functional groups.[310] The bond strength between sulphur and gold atom is in the range of 40-50 kcal mol^{-1} [311,312] This high affinity of gold for sulphur also permits the incorporation of a diverse range of functional groups into the SAM or onto the exposed surface of the SAM.[266]

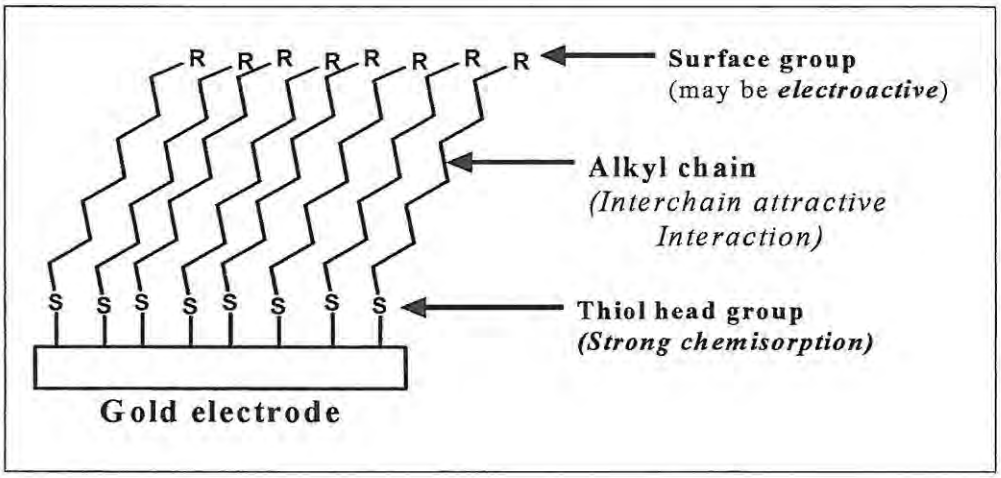

Figure 1.9: Representation of a thiolate-on-gold SAM.

(c) Long-chain alkanethiols form densely packed, crystalline or liquid crystalline monolayers on gold. Attractive van der Waals forces between the alkyl chains enhance the stability and order of the SAM. These chains are tilted slightly from

the substrate surface (~ 20-30°), resulting in the formation of a densely packed, highly ordered monolayer (Figure 1.9).

The detailed chemistry concerning the nature of the bond between the gold surface and the thiol, and the reaction leading to that bond has been a subject of much interest.[208,276,277,303,309,310,313] However, it is generally accepted that the gold-thiolate bond is due to the cleavage of the S-H bond. The sulphides (i.e. thioethers, as in this work), on the other hand form monolayers on gold surfaces with the C-S bonds intact.[303,309]

The properties of SAMs as described above are very attractive in many fields in which phthalocyanines are being applied. Thus, the major part of the work described in this thesis is based on self-assembling properties of alkanethiol-derivatised metallophthalocyanine complexes (MPc-SAMs) on gold electrodes for potential applications in electroanalysis. The following discussion is on SAMs of phthalocyanines and alkanethiols. Specific references on the structurally similar complexes, porphyrins deposited on gold surfaces will be noted where appropriate.

1.5.2.1 Thiol-Derivatised Phthalocyanine Self-Assembled Monolayers

In the last 15 years, the modification of gold electrodes with SAMs of alkanethiols has been studied.[266,284-305] The field has also been reviewed by various workers.[28,266,312,314,315] However, because of the difficulty and multistep reactions involved in their synthesis, phthalocyanines substituted with sulphur groups are rather few.[22,23,97,316] Hence, the response of electrodes on which thiol-derivatised phthalocyanines have been assembled has not received much attention. It is mainly the research groups of Cook [98-101] and Lieberman,[102-104] which are actively involved in the

synthesis of thiol-deriavatised phthalocyanines for the fabrication of SAMs. Cook and co-workers[98-101] have made phthalocyanine complexes that contain one pendant thiol functional group. However, the noticeable limitation of such complexes is that the large phthalocyanine molecules are attached to the substrate by one tether, and consequently the rings are tilted at various unpredictable angles to the surface of the substrates. To force the phthalocyanine rings to lie flat to the surface (as in this work), Li et al.[102-104] have either arranged short thiol tethers around the periphery of the phthalocyanines or attached such short tethers to the central metals of the phthalocyanines.

1.5.2.2 Blocking and Electroactive Monolayers

One important feature of an alkanethiolate SAM is its ability to limit access of solution-phase molecules (both electrolyte ions and redox couples) to the electrode surface. When this barrier phenomenon is observed, the electrode is said to be 'passivated' or 'blocked' by the monolayer.[208,276,277] Thus, the shortest distance between the electroactive species in solution and the electrode is increased by a length similar to the thickness of the monolayer. This increase in distance severely affects the heterogeneous electron transfer, imposing a tunneling mechanism. Applications of a blocked electrode include:[208,276,277]

(a) Enhancement of the Faradaic current of the adsorbed species relative to the charging current in voltammetric analytical experiments.

(b) The possibility to study electron tunneling over a well-defined distance and through a well-defined medium.

(c) Fabrication of blocking monolayer with chemically selective sites, which is the basis of an electrochemical sensor.

There are two basic approaches to the formation of an electroactive monolayer.[266] Either a redox center is bonded to preformed SAM or the redox center is modified to contain thiol moieties, which bond to the gold surface. The redox center, like the enzymes, can be attached onto the preformed SAMs via electrostatic binding or covalent attachment. The most extensively studied electroactive SAMs are probably those containing ferrocene redox centers, due to the synthetic accessibility of these complexes.[208,276,277]

Li et al.[102-104] have synthesized metallophthalocyanine complexes of copper and silicon containing eight peripheral short thiol legs with the objective of fabricating electronic devices. Recently, several workers[317-319] have formed flat-oriented metal phthalocyanine and porphyrin monolayers by first forming a thiol-derivatised SAMs containing peripheral N-donor atoms (such as amine and pyridine) and then attaching the metal phthalocyanine and porphyrin complexes to the nitrogen group via axial coordination to the central metal. Pilloud et al.[307] have successfully attached iron porphyrins to a preformed monolayer of dimercaptoalkanes. Several other metalloporphyrins have also been anchored to gold surfaces.[320-321]

1.5.2.3 Conditions for a Successful Monolayer Formation

Basically, the integrity of a quality SAM can be ascertained by

(i) Coverage: the coverage achievable on the electrode surface by a thiol adsorbate is a monolayer (e.g. MPc ~ 10^{-10} mol cm^{-2}).[208,265,276,277,322-328]

(ii) Substantial reduction of interfacial capacitance (in the range 1-5 $\mu F\ cm^{-2}$ for most alkanethiol SAMs) to values more than an order of magnitude smaller than the typical capacitance for bare gold.[276,277]

(iii) Non-existence of pinholes and defects. A *pinhole* is a site at which the electrode surface is exposed to the electrolyte, while a *defect* is a site at which molecules or ions can approach the electrode surface at a distance shorter than the normal thickness of the SAM. Unfortunately, most SAMs are associated with a certain density of pinholes or defects.[208,276,277]

Thus, to achieve the most blocking or highly oriented monolayer on gold substrate, the following factors are considered in the self-assembling process:[276,277]

(a) ***Substrate morphology*:**

The topography of the underlying gold surface influences the integrity of the SAM.[255,276,277,329] Studies have shown that the most important criterion for obtaining a SAM with minimum defects is a surface with the lowest microscopic roughness. A recent report by Losic et al.[329] has established that the important factor in fabricating a defect-free SAM is not the amount of alkanethiol adsorbed but the number of grain boundaries in the surface. Roughness leads to SAMs with poor uniformity as well as far less stability to electrochemical cycling.

(b) ***Cleaning Procedures*:**

Cleaning procedures for the gold substrate include

(i) Strong heating in gas-air flame to the point of incandescence.[330,331]

(ii) Immersion of the substrate in solutions of powerful oxidants. Three popular oxidizing cleaners are

- The " Piranha" solution (3:1 ratio of concentrated H_2SO_4 and 30% H_2O_2 heated to ca. 100°C).
- Chromic acid (potassium or sodium dichromate in concentrated H_2SO_4 at room temperature) is used when the substrate may be damaged by the "Piranha" solution.[296]
- Dilute "aqua regia" (3:1:4 ratio of concentrated HCl, concentrated HNO_3 and water).[332]

The substrate is thoroughly wetted with water after exposure to either of these oxidants.

(iii) Exposure to argon ion plasmas and oxygen plasmas, or ozone/UV radiation removes organics efficiently from the gold surface.[276,277]

(iv) Electrochemical cycling: A final check of surface cleanliness is obtained by placing the electrode in ca. 0.5 mol dm^{-3} H_2SO_4 and scanning the potential between – 0.5 and +1.5V vs Ag|AgCl.[276,277,329] Repeated scanning removes any organic contaminant left preceding cleaning treatments. Terminating the potential scan at a potential negative of the 'oxide-stripping peak', i.e. the cathodic peak due to gold (Figure 1.10) ensures that the gold surface is oxide-free. Clean gold is characterized by a sharp rise in anodic current to a peak near + 1.1V vs standard calomel electrode (SCE), a single oxide stripping peak near + 0.9V vs SCE, and a reproducible cyclic voltammogram (CV) on successive scans.[276,277,313]

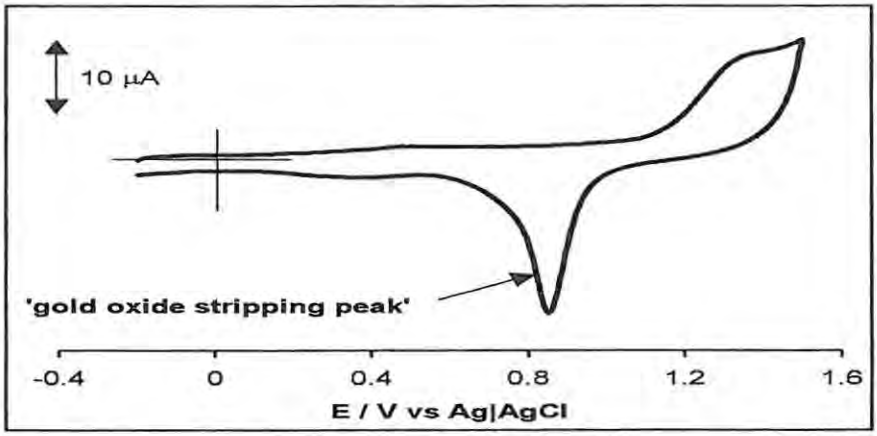

Figure 1.10: Typical cyclic voltammogram obtained for a bare gold electrode in 0.1 mol dm^{-3} H_2SO_4 at scan rate = 100 mV s^{-1}.

(c) ***Thiol Purity*:**

The influence of impurities present in the adsorbate on the behaviour of a SAM is not well known. However, electroactive impurities that co-adsorb onto the SAM are readily detected by cyclic voltammetry.[276,277]

(d) ***Deposition Solvent:***

All common organic solvents (such as ethanol, toluene, tetrahydrofuran and methylene chloride) have been employed for SAM preparation. Ethanol is a choice solvent for most thiols because of its faint odour, low toxicity, and availability in pure form and ability to reduce gold oxide. Unfortunately, most metallophthalocyanine complexes are insoluble in ethanol, thus limiting their deposition from other organic solvents, for example, toluene or toluene/methylene chloride.[103,104] The choice of solvent is most critical when mixed monolayer is prepared since the composition of the SAM is dependent on both the solvent and deposition solution.[276,277,313]

(e) ***Deposition Concentration, Time and Temperature:***

Typically at millimolar concentrations, a thiol monolayer assembles on gold in seconds at room temperature. Longer deposition times are required for lower concentrations of the thiol (~ 10^{-6} mol dm^{-3} range) because of mass transport limitations of the thiol to the surface. Longer deposition times at room temperature allow the monolayer to rearrange into a more highly ordered structure. The use of higher concentrations (>10^{-3} mol dm^{-3}) of thiols and temperature (ca. 60°C) has been reported [276] for the formation of mixed SAMs.

(f) ***Monolayer Annealing:***

Thermal annealing (or heating) of the SAM during or after self-assembly helps break out the metastable disordered states of the SAM.[276] Monolayer annealing can also be carried out using cyclic voltammetry. In this method, the SAM-coated electrode is subjected to a cyclic voltammetry experiment and then re-immersing the electrode in the deposition solution. Multiple immersions followed by cyclic voltammetry experiments lead to a noticeable drop in the oxide stripping current, and hence pinhole area. The cyclic voltammetry experiment is believed to shock the SAM so that subsequent immersion can cause adsorption of more thiols and a restructuring of the existing chains.

1.5.2.4 Characterization of SAM-Modified Electrodes

A number of techniques are being employed for the characterization of chemically modified electrodes, especially the SAM-modified electrodes. Electrochemical methods, particularly cyclic voltammetry, provide an effective means for

interrogating the integrity of a SAM on gold electrode. For electroactive SAMs, diffusion has no influence on the cyclic voltammetry experiment, since the redox centers are close to the electrode surface. Thus, unlike in experiments with diffusion-controlled currents, the peak current, i_p (μA), is directly proportional to the scan rate, ν (Vs^{-1}) equation 1.61.[276,277]

$$i_p = \frac{n^2F^2A\Gamma}{4RT}\nu \qquad 1.61$$

where A is the surface area of the electrode surface (cm^2), Γ is the surface coverage (mol cm^{-2}) given by equation 1.62.

$$\Gamma = \frac{Q}{nFA} \qquad 1.62$$

All the symbols have their usual meaning. It is important to note that even though the electrode surface may appear perfectly flat, the presence of microscopic surface steps, holes, kinks, and terraces yield a real surface area that is larger than the geometric area.[333]

The cathodic to anodic peak separation (ΔE_p) is theoretically zero for the surface-confined electroactive species, while the peak is symmetrical with a peak half-width (ΔE_{fwhm}) of 3.53R / nF, or 90.6 / n mV at 25°C.

The coverage can also be estimated by both reductive (equation 1.63) and oxidative (equation 1.64) desorptions in 0.5 mol dm^{-3} KOH.

$$Au\text{-}SC_nX + ne^- + M^+ \longrightarrow Au^o + XC_nS^-M^+ \qquad 1.63$$

$$Au\text{-}SC_nX + 4OH^- \longrightarrow Au^o + XC_nSO_2^- + 3e^- + 2H_2O \qquad 1.64$$

where M^+ cation from the electrolyte is usually included in the desorption equation because the peak is sensitive to the identity of the cation.

The total interfacial capacitance, C_T, which is approximately equal to the monolayer capacitance, C_m, is given by equation 1.65.

$$C_T \approx C_m = \frac{i_{ch}}{\nu A} \qquad 1.65$$

where i_{ch} is the charging current (μA) while A is the surface area of the electrode. For most alkanethiol SAMs, C_T lie in the 1-5 $\mu F\ cm^{-2}$ range, more than an order of magnitude smaller than the typical capacitances for bare gold.[276,277] C_T is an essential tool for examining the ion permeability through the SAM, since it provides the answers as to how "closed-packed" and "defect-free" the monolayer is.[289,307,329] The lower the C_T value the less defects there are in the SAM, and hence the lower the permeability to the ions of the electrolyte. C_T is usually independent of the scan rates.

The absence of pinholes in SAMs is usually indicated by the inhibition of gold surface oxidation, probably by the exclusion of water.[276,277] The area under the well-defined reduction peak commonly referred to as the "oxide removal or stripping peak" (see Figure 1.10) is regarded as the true measure of the total pinhole area available for an undisturbed penetration of ions present in the working solution. Comparison of the total charges under the oxide striping peak at the bare gold (Q_{Bare}) and the SAM-modified gold electrode (Q_{SAM}) gives the so-called "ion barrier factor" (designated herein as Γ_{ibf}), equation 1.66:

$$\Gamma_{ibf} = 1 - \frac{Q_{SAM}}{Q_{Bare}} \qquad 1.66$$

The total charge, Q(μC) is obtained by integrating the currents (μAs^{-1}). The blocking manifestation of a SAM can also be determined by either the inhibition of metal deposition (using $CuSO_4$) on gold electrode or the suppression of simple Faradaic

processes of redox probes such as $Ru[(NH_3)_6]^{3+}$, $Fe[(CN)_6]^{4-}$ and $Fe[(H_2O)_6]^{3+}$.[208,276,277,286]

Characterization methods, which are based on nonelectrochemical techniques[95,96,101-104,276,277,298] include the reflection-absorption infrared spectroscopy (RAIRS), X-ray photoelectron spectroscopy (XPS), surface enhanced raman spectroscopy (SERS), atomic force microscopy (AFM), scanning tunneling microscopy (STM), scanning electron microscopy (SEM), ellipsometry, and electrochemical quartz crystal microbalance (EQCM).

1.5.2.5 Applications of SAM-Modified Electrodes

Considerable interest has lately been placed on SAMs of organothiols on gold surfaces both from analytical prospects and fundamental studies points of view. Fundamentally, they have been used for studying the theory of heterogeneous electron transfer.[334,335] From the analytical point of view, they have extensively been applied in the fabrication of a variety of biosensors,[302,336] immunosensors,[337-339] DNA hybridisation biosensors,[340] enzyme biosensors [266,341] and metal ion sensors.[305] SAMs are especially relevant to electrochemical phenomenon in corrosion, electroanalysis and electrocatalysis. Although, actual application of MPc-SAMs has barely been reported, new thiol-derivatised Pcs have been designed, synthesized and formulated as SAMs for potential applications in electronic devices [102-104] and chemical sensing.[98-101,342,343]

Inspite of the popularity of the MPcs as efficient electrocatalysts for the detection and analysis of a variety of molecules, their use as electroactive SAMs still remain unexplored. The search for new electroactive thiol-derivatised MPc-SAMs for actual

application in electroanalysis and electrocatalysis constitutes the major aim of this part of research work. To this end, new alkanethiol-derivatised MPc complexes of Fe and Co centers were synthesized, characterized and fabricated as SAMs on gold electrodes. Their practical applications as electrochemical sensors were also investigated using the biologically important molecules, L-cysteine and its derivatives (homocysteine and penicillamine) as well as the thiocyanate.

1.6 Summary of Aims of Thesis

The aims of the thesis are summarized as follows:

a) Synthesis and comparative study of the photosensitizing properties of water-soluble, sulphonated and carboxyphthalocyanine complexes of aluminium, zinc, tin and silicon.

b) The study of the kinetics of photo-transformation of the environmentally important 4-chlorophenol and polychlorophenols in water in the presence of water-soluble metallophthalocyanine photosensitisers.

c) Synthesis and investigation of the photochemical and electrochemical properties of alkanethiol-derivatised metallophthalocyanine complexes for potential use as electrocatalysts.

d) Fabrication and development of surface electrochemical techniques for characterizing thiol-derivatised metallophthalocyanine complexes immobilized onto gold electrodes as self-assembled monolayers (SAMs).

e) Development of gold electrodes modified with the SAMs of alkanethiol-derivatised metallophthalocyanine complexes of iron and cobalt, for use in the detection of the biologically important thiols (L-cysteine, homocysteine and penicillamine), thiocyanate and cyanide.

f) The study of the kinetics and equilibria of interaction of alkanethiol-derivatised iron and cobalt phthalocyanine complexes with cyanide in non-aqueous environment.

CHAPTER 2

EXPERIMENTAL

2.1 Materials

Dimethylsulphoxide (DMSO), dimethylformamide (DMF), cobalt acetate, zinc acetate, ammonium chloride, silver nitrate, sodium hydroxide, iron (II) chloride tetrahydrate, potassium ferrocyanide, potassium ammonium sulphate, perchloric acid, ethanol, sulphuric acid, nitric acid, ethanol, methanol, acetonitrile (high pressure liquid chromatography, HPLC, grade), fuming sulphuric acid (30% SO_3^-), chloroform ($CHCl_3$), toluene, tetrahydrofuran (THF), potassium nitrate, and potassium chloride were purchased from SAARCHEM (PTY) Ltd (South Africa). Potassium cyanide (KCN) was purchased from May & Baker. Sodium perchlorate ($NaClO_4$) was from BDH. Potassium bromide was from Merck. Potassium thiocyanate (KSCN) and thionyl chloride ($SOCl_2$) were obtained from Riedel-de-Haën AG. 4-Sulphophthalic acid, 4-chlorophenol (4-CP), trichlorophenol (TCP), pentachlorophenol (PCP), 1,4-benzoquinone (*p*-benzoquinone), 2,5-dichloro-1,4-benzoquinone, 2,3,5,6-tetrachloro-1,4-benzoquinone (chloranil), 4-chlorocatechol, 4-chlororesorcinol, L-cysteine, homocysteine, penicillamine, butanethiol, 4-methylthiophenol, 4,5-dichlorophthalic acid, diphenylisobenzofuran (DPBF), diazabicyclo-octane (DABCO), 1,8-diazabicyclo[5.4.0]undec-7-ene (DBU) cetyltrimethylammonium chloride, sodium azide, formamide, thionyl chloride, acetic anhydride and potassium carbonate were purchased from Sigma-Aldrich. Hydroquinone was obtained from May & Baker while phenol was from BDH. Tetrasodium α,α-(anthracene-9,10-diyl) dimethylmalonate (ADMA) and zinc phthalocyanine (ZnPc) were gifts respectively from Drs. V. Negrimovsky and V. Derkacheva (from Organic Intermediates and Dyes Institute, Moscow, Russia). Aluminium phthalocyanine chloride (ClAlPc) was purchased from Eastman Kodak. DMF was freshly distilled after drying

over alumina, before use. DMSO was dried over alumina before use. Tetrabutylammonium perchlorate (TBAP) was recrystallized from ethanol and used as an electrolyte for all electrochemical measurements. Ferrocene (BDH) was recrystallised from ethanol before being employed as an internal standard for electrochemical measurements. All pH phosphate buffer tablets and powders were purchased from Sigma-Aldrich.

2.2 Instrumentation

Proton Nuclear Magnetic Resonance (^{1}H NMR) spectroscopy, UV-Visible spectroscopy, Fourier Transform Infrared (FTIR) and elemental analyses were used to characterize the synthesized complexes. ^{1}H NMR (400 MHz) were recorded using the Bruker EMX 400 NMR spectrometer in $CDCl_3$. UV-Visible spectra were recorded using a Varian 500 UV-Vis-NIR spectrophotometer and FTIR spectra (KBr pellets) were obtained on a Perkin-Elmer spectrum 2000 FTIR spectrometer. Elemental analyses were performed with a Carlo Erba NA 1500 Nitrogen Analyzer at the University of the Western Cape, Cape Town, South Africa.

2.3 Synthesis

2.3.1 Synthesis of Metallo-tetrasulphophthalocyanine Complexes, ($MPcS_4$), (Scheme 2.1A).

Monosodium salt of 4-sulphopthalic acid (**6**).[240]

The synthesis of **6** is summarized in Scheme 2.1A. A mixture of 30% 4-sulphophthalic acid **8** (24.6 g, 0.1 mol) and NaOH (4.0 g, 0.1 mol) was placed in a flask and left for 24 hours to allow the product to crystallize out of the solution. The pale pink product was filtered off under pressure, washed with water and allowed to dry in the open. Yield: (24.4 g, 91%). IR [(KBr) ν_{max}/cm^{-1}]: 3436, 3078, 2652 and 2535 (O-H), 1745 and 1700 (C=O), 1598, 1575, 1493 and 1437 (C–C), 1398, 1378, 1284, 1246 and 1170 (C–O and/or O–H), 1070, 1043, 975, 912, 857, 826, 792 and 720 (C–H).

Metallo-tetrasulphophthalocyanine complexes ($MPcS_4$) [24,141]

A mixture of monosodium salt of 4-sulphophthalic acid **6** (4.32 g, 16 mmol), ammonium chloride (0.47 g, 9.0 mmol), urea (5.80 g, 97 mmol), ammonium molybdate (0.068 g, 0.06 mmol), and required metal salt (4.8 mmol): {i.e. $AlCl_3$ for aluminium (III) tetrasulphopthalocyanine $AlPcS_4$ (**9**) and $ZnSO_4$ for zinc (II) tetrasulphopthalocyanine $ZnPcS_4$ (**10**)} was ground together in a mortar until homogeneous. Nitrobenzene (4 cm^3) was placed in a three-necked round-bottomed flask fitted with a thermometer and a condenser and heated to 180°C. The solid mixture was added slowly to the heated nitrobenzene under stirring over a period of 1 hour at 180-200°C. The mixture was heated for 7 hours at 200°C. The dark solid cake was finely ground in a centrifuge tube and washed several times with methanol until the odour of nitrobenzene was no longer

detected. The resulting powder was dissolved in 100 cm^3 of 1.0 mol dm^3 HCl saturated with NaCl and briefly heated to boiling. The mixture was cooled to room temperature, filtered, dissolved in 0.1 mol dm^{-3} NaOH (70 cm^3) and then heated to 80°C. After a quick separation of the solid impurities by centrifugation, NaCl (27.0 g) was added to the slurry filtrate and heated at 80°C with stirring until the evolution of ammonia gas was complete (detected with litmus paper or stirring rod previously dipped in conc. HCl). The crystallized product was separated by centrifugation and this last process was repeated twice. The product was then washed with 80% ethanol until it was chloride-free (detected by testing with 1.0 mol dm^{-3} $AgNO_3$). The product was heated under reflux in 20 cm^3 absolute ethanol for 4 hours, cooled to room temperature and filtered. The final product was dried in an oven at ~ 120°C overnight.

$AlPcS_4$ (9): Yield: (80%). Anal.: Calcd. for $C_{32}H_{12}N_8O_{12}S_4Na_4Al(Cl).8H_2O$: C, 34.08: H, 2.49: N, 9.95%. Found: C, 33.01: H, 1.73: N, 9.98. IR [(KBr) ν_{max}/cm^{-1}]: 3461 (O-H), 1638 (C=C), 1577, 1523, 1497, 1399, 1342, 1193, 1148, 1111, 1076, 1032 (S=O), 925, 830, 755, 699.

$ZnPcS_4$ (10): Yield: (44%). Anal.: Calcd. for $C_{32}H_{12}N_8O_{12}S_4Na_4Zn.3H_2O$: C, 36.94: H, 1.16: N, 10.78%. Found: C, 36.01: H, 0.73: N, 10.66. IR [(KBr) ν_{max}/cm^{-1}]: 3448, 1638, 1577, 1523, 1397, 1338, 1195, 1148, 1111, 1076, 1037 (S=O), 925, 830, 755, 699.

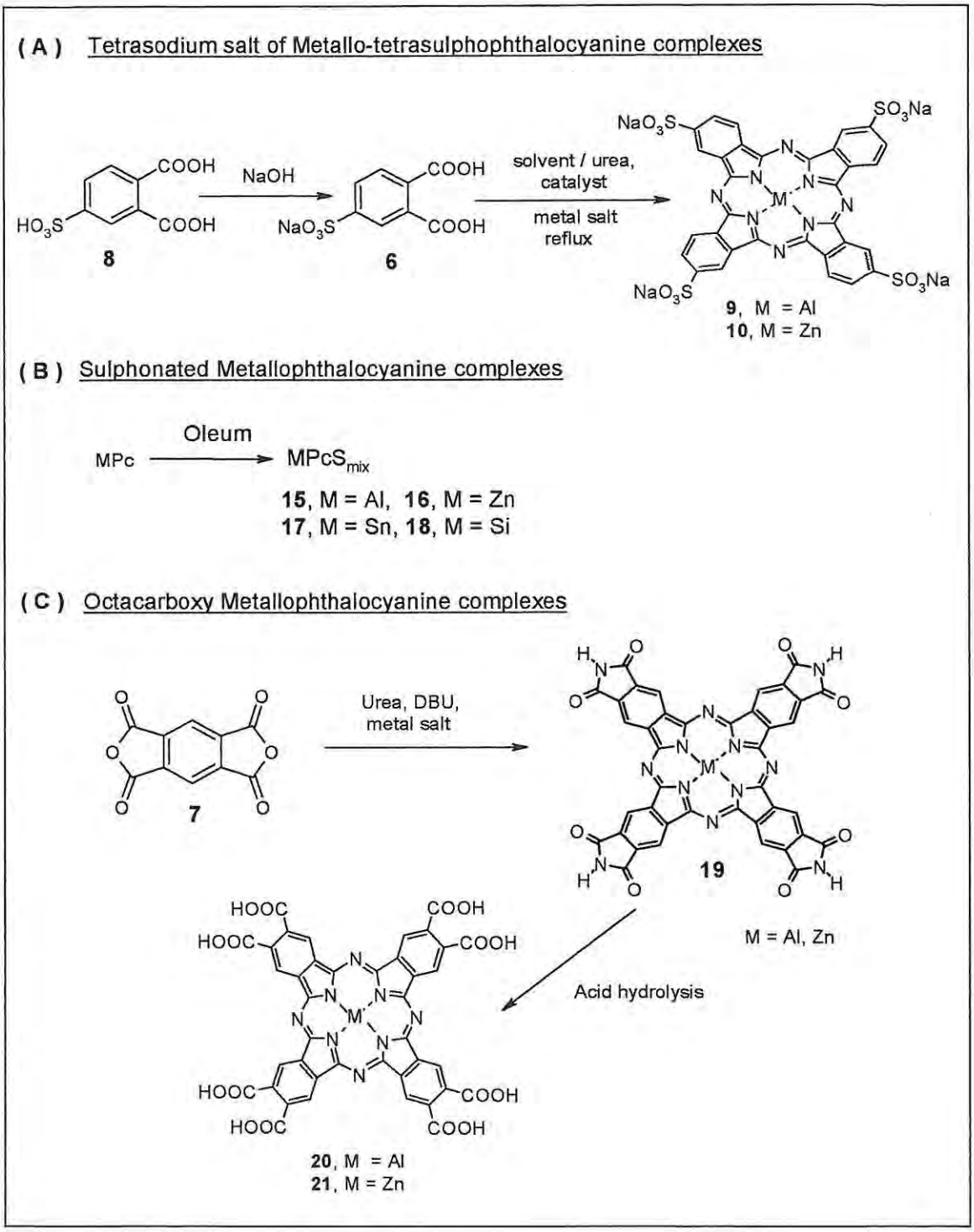

Scheme 2.1: Synthesis of water-soluble metallophthalocyanine complexes.[24,26,28,141]

2.3.2 Synthesis of Sulphonated Metallophthalocyanine Complexes Containing Mixtures of Differently Substituted Complexes, $MPcS_{mix}$, (Scheme 2.1B)

Bis(hydroxy)phthalocyaninatotin(IV), [(OH)$_2$SnPc] **(12)** *(Scheme 2.2).*[344]

The synthesis is a two-step process involving firstly the preparation of the dichlorophthalocyaninatotin(IV) complex $(Cl)_2SnPc$ **(11)** and then hydrolysing it to the

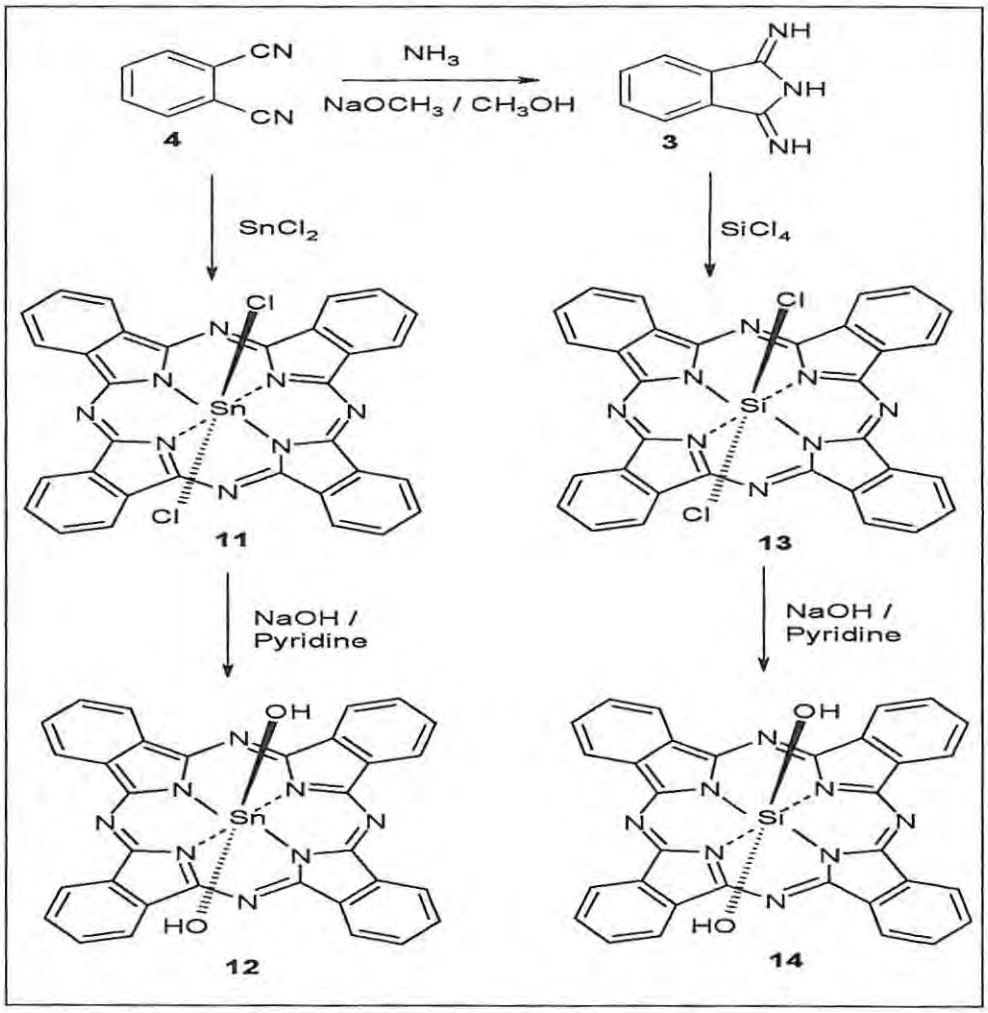

Scheme 2.2: Synthetic routes for bis(hydroxy)phthalocyanine complexes of tin and silicon.[344]

$(OH)_2SnPc$ (**12**) complex (Scheme 2.2). The $(Cl)_2SnPc$ was obtained using literature methods[344] by reacting anhydrous $SnCl_2$ (40 mmol) with phthalonitrile **4** (124 mmol) in 1-chloronaphthalene (200 cm^3) under reflux for about 4 hours. After slowly cooling to room temperature, the solution was filtered and the resulting solid washed with benzene in a Soxhlet apparatus for 24 hours giving 94% yield. The pure purple crystalline product (**11**) was hydrolyzed by mixing it (3.15 g, 4.48 mmol) with NaOH (0.69 g, 17.25 mmol), dissolved in a mixture of pyridine (17 cm^3) and water (65 cm^3), and heating under reflux for 5 hours. After slowly cooling the mixture, the blue solid $(OH)_2SnPc$ (**12**) was filtered off, washed with water and dried. Yield: (55-60%). The complex gave satisfactory spectroscopic data as reported in the literature.[344]

Bis(hydroxy)phthalocyaninatosilicon(IV) [$(OH)_2SiPc$] (**14**) *(Scheme 2.2).*[344]

Unlike the tin complex, the [$(OH)_2SiPc$] follows the 1,3-diiminoisoindoline **3** rather than the phthalonitrile route (Scheme 2.2).[344] The 1,3-diiminoisoindoline **3** was obtained by heating under reflux a mixture of phthalonitrile **4** (0.75 g, 6.00 mmol), methanol (7 cm^3) and sodium methoxide (0.013 g) for 7 hours, while bubbling ammonia. The mixture was filtered and the green product precipitated from methanol with water (20 cm^3), filtered and dried at 60°C in vacuo. A mixture of complex **3** (0.62 g, 4.30 mmol) and dry quinoline (2 cm^3) was stirred at room temperature for 10 min, after which $SiCl_4$ (0.2 cm^3, 2.8 mmol) was added and heated under reflux in a nitrogen atmosphere. 6 mol dm^{-3} HCl (20 cm^3) was then added to the mixture, the resulting product was filtered and treated in a Soxhlet extractor with methanol until a clear extract was obtained. The pure product, $(Cl)_2SiPc$, (**13**) was dried at 110°C, then its fine powder was hydrolysed by

heating under reflux, in a 1:1 mixture of pyridine and 25% NaOH (20 cm^3) for 10 hours. The mixture was then filtered, washed with water and dried at 110°C overnight to give pure $(OH)_2SiPc$ (**14**) complex. Yield: (55-60%). The complex gave satisfactory spectroscopic data as reported in the literature.[344]

General sulphonation procedure *(Scheme2.1B).*[28]

Following literature methods,[28] the required unsubstituted MPc complex {M = aluminium (ClAlPc) or zinc (ZnPc) or tin [$(OH)_2SnPc$] (**12**) or silicon [$(OH)_2SiPc$] (**14**)} (0.20 mmol) was placed in a round-bottomed flask, stirred and heated to 100°C. Oleum or fuming sulfuric acid (0.50 cm^3 containing 30% SO_3) was slowly added and the mixture stirred vigorously at 100°C. After 25 minutes, the mixture was quenched by adding about 4 g of crushed ice onto it. The resulting mixture was adjusted to pH 7.0-7.5 using 1.0 mol dm^{-3} NaOH solution to give a deep blue solution. The solution was evaporated to dryness and the residue Soxhlet extracted using methanol (20 cm^3) for 12 hours. Finally, the solvent was removed by evaporation and the solid product oven-dried at 100°C.

$AlPcS_{mix}$ (15): Yield: (78%). IR [(KBr) ν_{max}/cm^{-1}]: 3432 and 3200 (O-H), 1730, 1634 and 1498, 1398, 1332, 1231, 1173, 1113, 1031 (S=O), 916, 753, 724. UV-Vis [pH 7, λ_{max}/nm (log ε)]: 348 (4.74) and 675 (5.26);

$ZnPcS_{mix}$ (16): Yield: (56%). IR [(KBr) ν_{max}/cm^{-1}]: 3447 and 3210 (O-H), 1733, 1624, 1545, 1390, 1220, 1205, 1144, 1088, 1040 (S=O), 979, 905, 746, 716. UV-Vis [pH 7, λ_{max}/nm (log ε)]: 343 (4.68) and 667 (5.38).

$SnPcS_{mix}$ (17): Yield: (64%). IR [(KBr) ν_{max}/cm^{-1}]: 3462 and 3206 (O-H), 1728, 1583, 1398, 1308, 1198, 1136, 1078, 1040 (S=O), 884, 850, 808, 746, 716, 634, 566. UV-Vis [pH 7, λ_{max}/nm (log ε)]: 348 (4.96) and 691 (5.24).

$SiPcS_{mix}$ (18): Yield: (42%). IR [(KBr) ν_{max}/cm^{-1}]: 3466 and 3418 (O-H), 1642, 1618, 1573, 1386, 1288, 1193, 1133, 1040 (S=O), 896, 830, 620. UV-Vis [pH 7, λ_{max}/nm (log ε)]: 315 (5.88) and 672 (5.23).

2.3.3 Synthesis of Octa-carboxymetallophthalocyanine Complexes, (MOCPc) *(Scheme 2.1C).*[26]

A mixture of benzene-1,2,4,5-tetracarboxylic dianhydride (pyromellitic dianhydride, **7**) (3.75 g, 17.25 mmol), urea (19.5 g, 0.33 mol), DBU (0.1 g, 0.7 mmol) and metal salt (23.5 mmol): {i.e. $AlCl_3$ for octacarboxyphthalocyaninatoaluminium(III), (AlOCPc) (**20**) and zinc acetate for zinc(II) octacarboxyphthalocyaninatozinc(II), (ZnOCPc) (**21**)} was placed in 100-ml two-necked flask fitted with a reflux condenser and a thermometer and heated at 250°C under reflux for about 20 minutes, the reaction mixture was fused after this time. The fused product was washed with water, acetone and 6 mol dm^{-3} HCl. After drying, the tetra-amide product (**19**) (2.70 g) was heated under reflux with 20% H_2SO_4 (2.70 cm^3) for 3 days. The product was washed with 200 cm^3 portions of 5% H_2SO_4, 100 cm^3 portions of water and then acetone by centrifugation. After drying in air, the blue product was purified by multiple chromatography on an alumina column using 2% aqueous NaOH as eluent and reprecipitated each time with 20% HCl. The pure product (**20** or **21**) is filtered and then dried at 110°C overnight.

AlOCPc (20): Yield: (8.8%). Anal.: Calcd. for $C_{40}H_8N_8O_{17}Na_9Al.2H_2O$: C, 42.03: H, 1.06: N, 9.81%. Found: C, 41.93: H, 1.36: N, 9.78%. IR [(KBr) ν_{max}/cm^{-1}]: 3416 (O-H), 3230 (C-H), 1700 (C=O), 1638, 1619, 1500 and 1448 (C-C), 1379, 1284, 1247 and 1188 (C-O and/or O-H), 1158, 1128, 1073, 1044, 1013, 994, 907, 823 and 720 (C-H). UV-Vis [pH 10, λ_{max}/nm (log ε)]: 356 (4.90) and 690 (5.26);

ZnOCPc (**21**): Yield: (12%). Anal.: Calcd. for $C_{40}H_8N_8O_{16}Na_8Zn.2H_2O$: C, 42.06: H, 1.06: N, 9.81%. Found: C, 42.23: H, 0.98: N, 9.69%.IR [(KBr) ν_{max}/cm^{-1}]: 3416 (O-H), 3230 (C-H), 1698 (C=O), 1638, 1619, 1570 and 1448 (C-C), 1394, 1283, 1246 and 1181 (C-O and/or O-H), 1086, 1040, 1013, 979, 906 and 720 (C-H). UV-Vis [pH 10, λ_{max}/nm (log ε)]: 348 (4.96) and 690 (5.26).

2.3.4 Synthesis of Thiol-Derivatised Metallophthalocyanine Complexes

2.3.4.1 Synthesis of 4,5-dichlorophthalonitrile (26) (Scheme 2.3).[22]

4,5-Dichlorophthalic anhydride (**23**)

Following established literature methods,[22] a mixture of 4,5-dichlorophthalic acid (**22**) (25 g, 0.106 mmol) and acetic anhydride (35 cm^3) was heated under weak reflux for 5 hours while slowly distilling off of acetic acid. After cooling, the white crystalline product was filtered and thoroughly washed with petroleum ether (40-60°C) and then air-dried. Yield: (21.6 g, 92%). IR [(KBr) ν_{max}/cm^{-1}]: 1824, 1782 (anhydride)

4,5-Dichlorophthalimide (**24**)

A suspension of 4,5-dichlorophthalic anhydride (**23**) (22 g, 0.100 mmol) in formamide (30 cm^3) was heated under reflux for 3 hours. After cooling, the precipitate was filtered, washed with water and then air-dried to give a light yellow product. Yield: (21.1g, 98%). IR [(KBr) ν_{max}/cm^{-1}]: 1775, 1713 (imide)

4,5-Dichlorophthalamide (**25**)

A suspension of 4,5-dichlorophthalimide (**24**) (20 g, 0.91 mmol) was stirred in 25% ammonium hydroxide solution (300 cm^3) at room temperature. After 24 hours, 33%

ammonium hydroxide solution (100 cm^3) was added and stirring was continued for another 24 hours. The precipitate was filtered, washed with water and dried at 60°C to give a yellowish product. Yield: (15.3 g, 72%). IR [(KBr) ν_{max}/cm^{-1}]: 1657, 1620 (amide).

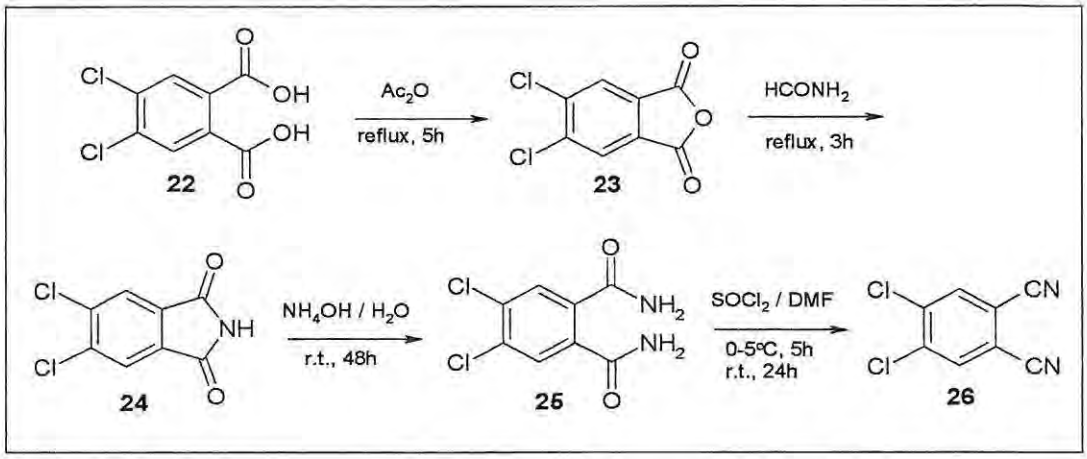

Scheme 2.3: Synthetic route for dichlorophthalonitrile.[22]

***4,5-Dichlorophthalonitrile* (26)**

Freshly distilled thionyl chloride (70 cm^3) was added under stirring, and in the presence of nitrogen gas, to dry distilled DMF (100 cm^3) at 0°C. After 2 hours, 4,5-dichlorophthalamide (**25**) (15 g, 0.065 mmol) was added and the mixture stirred for 5 hours at 0-5°C, and then at room temperature for 24 hours. The mixture was then added to ice water (~ 500 cm^3), filtered and washed with water (5 x 100 cm^3). Finally the product was recrystallised twice from methanol and then dried giving a light yellow 4,5-dichlorophthalonitrile (**26**). Yield: (8.74 g, 71%). IR [(KBr) ν_{max}/cm^{-1}]: 2236 (nitrile).

2.3.4.2 Synthesis of Disubstituted Thiol-derivatised Phthalonitriles (Scheme 2.4)

***4,5-Dibutylthiophthalonitrile* (27).**[22,23]

Dry DMSO (15 cm^3) contained in flat-bottomed flask was first heated to 45°C under stirring in the presence of dry nitrogen gas for about 5 min. Butanethiol (3 cm^3, 28 mmol) was added immediately, then after 2 minutes, 4,5-dichlorophthalonitrile (**26**) (1.10 g, 5.58 mmol) was added. The solution was refluxed for 15 minutes, then dry fine-powdered K_2CO_3 (8 x 40 mmol, every 5 min) was added. The mixture was stirred at 45°C

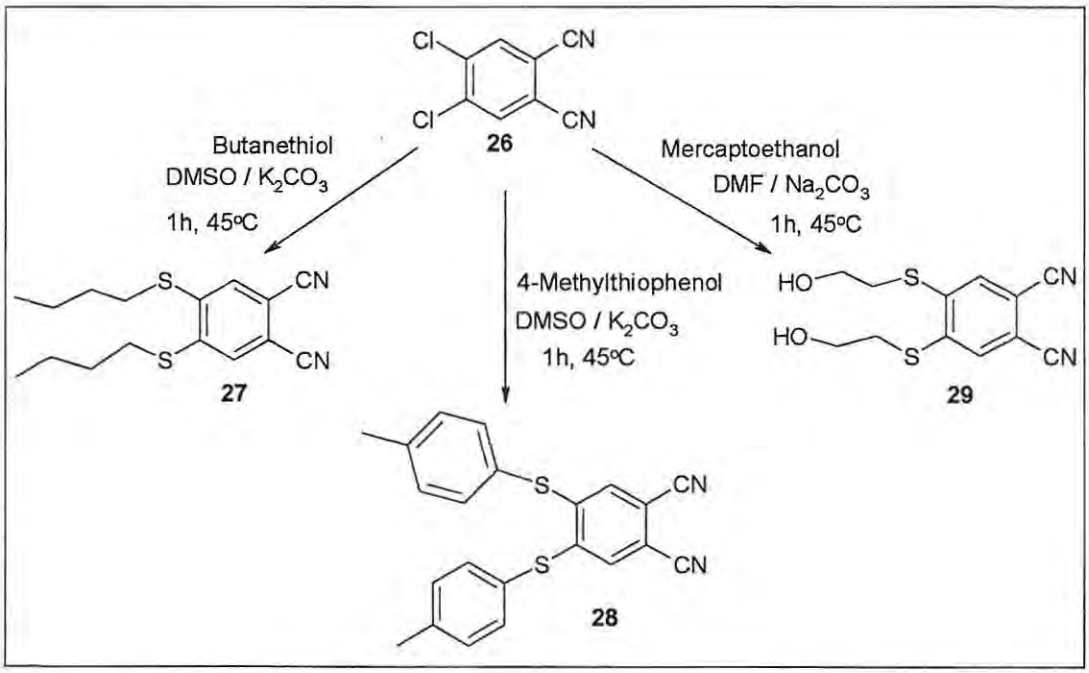

Scheme 2.4: Synthetic routes for the thiol-derivatised phthalonitrile complexes used in this work.[22,23]

for an extra 40 minutes. After cooling the product was poured into a mixture of ice chips-water (~ 350 g). The precipitate was filtered, and recrystallised from 85 cm^3 methanol to give a white product (**27**), which was dried between filter papers. Yield: (1.46 g, 86%).

IR [(KBr) ν_{max}/cm^{-1}]: 3077, 2958, 2929 and 2871 (CH), 2228 (C≡N), 1562, 1509, 1459, 1376, 1342, 1266, 1226 (RSR), 1116, 932, 893, 865, 734, 686, 528. ^{1}H NMR [$CDCl_3$, 400 MHz]: δ 7.43 (s, 2H, benzene), 3.10 (t, 4H, SCH_2), 1.74 (m, 4H, CH_2-CH_2-CH_2, 1.53 (m, 4H, CH_2-CH_2-CH_2-CH_3), 0.98 (t, 6H CH_3).

***4,5-Di (4-methyl phenylthio) phthalonitrile* (28).**[22,23]

The same synthetic procedure as for complex **27** above was employed, except for the use of 4-methylphenylthiol instead of butanethiol. Yield: (1.93 g, 93%). Anal.: Calcd. for $C_{22}H_{16}S_2N_2$: C, 70.97: H, 4.30: N, 7.53%. Found: C, 70.38: H, 4.18: N, 7.48%. IR [(KBr) ν_{max}/cm^{-1}]: 3237, 1638, 1618 and 1563 (Ph), 1492, 1459 and 1394 (CH_3-), 810 (1,4- Ph), 732, 708 and 628 (S-Ph). ^{1}H NMR [$CDCl_3$, 400MHz]: δ 7.36 (d, 4H, phenyl), 7.26 (d, 4H, phenyl), 7.01 (s, 2H, phenyl), 2.23 (s, 6H, methyl).

***4,5-Di(hydroxyethylthio)phthalonitrile* (29).**[345-347]

Dry DMF (15 cm^3) contained in a flat-bottomed flask was first heated to 50°C under efficient stirring and in the presence of dry nitrogen gas. After about 5 min, 2-mercaptoethanol (1.5 g, 19.2 mmol) and 4,5-dichlorophthalonitrile (**26**) (1.68 g, 8.54 mmol) were added. After 15 min, dry fine-powdered Na_2CO_3 (24 x 40 mmol, every 5 min) was added. The reaction mixture was stirred at 50°C for an extra 48 hours and then after cooling the reddish-brown mixture was poured into a mixture of ice chips-water (~ 350 g). The precipitate was filtered to give a sticky solid. Yield: (1.86 g, 78%). IR [(KBr) ν_{max}/cm^{-1}]: 3420 (OH), 2924 and 2878 (C-H), 2221 (C≡N), 1558, 1482, 1459, 1410, 1269, 1223, 1112, 1056, 1006, 930, 884, 822, 620.

2.3.4.3 *Synthesis of Metal-free Octasubstituted Thiol-derivatised Phthalocyanine Complexes, (Scheme 2.5, Route I).*[22]

The required 4,5-disubstituted thiol-derivatised phthalonitrile complex (**27** or **28**) (1 mmol) was heated under reflux in pentanol (50 cm^3) in the presence of DBU (1 mmol) for 48 hours. After cooling, methanol (50 cm^3) was added and the green precipitate filtered off by centrifugation. The impure phthalocyanine products, octabutylthiophthalocyanine, H_2OBTPc (**30**), octa(4-methylphenylthio)phthalocyanine, H_2OMPPc (**31**) were respectively purified in a Soxhlet apparatus using methanol and then acetone and dried at 60°C.

H_2OBTPc (30): Yield (64 %). IR (KBr), ν_{max}/cm^{-1}: IR (KBr) ν_{max}/cm^{-1}: 2956, 2926 and 2867 (CH_2), 1591 (Ph), 1462, 1406, 1371 and 1332 ($CH_3CH_2CH_2CH_2$-), 740, 700 (S-CH_2). UV-Vis ($CHCl_3$, λ_{max}/nm): 329, 360, 447, 671, 700, 732.

H_2OMPPc (31): Yield (72 %). IR (KBr), ν_{max}/cm^{-1}: 3238, 1638 and 1618 (Ph), 1490, 1402 and 1370 (CH_3-), 805 (1,4- Ph), 745, 700 and 622 (S-Ph). UV-Vis ($CHCl_3$, λ_{max}/nm): 344, 438, 644, 675, 710, 737.

2.3.4.4 *Synthesis of Octasubstituted Thiol-derivatised Metallophthalocyanine Complexes, (Scheme 2.5)*

Octabutylthiophthalocyanine complexes of zinc* (32) *and cobalt* (33), *(MOBTPc)

(Scheme 2.5, Route II)

A DMF suspension (10 ml) of the H_2OBTPc (**30**), (~ 0.1 mmol) and the metal acetate (0.2 mmol) was heated under stirring (130°C with for about 15 minutes for zinc complexes, ZnOBTPc (**32**) and at 180°C for about 60 minutes for cobalt complex, CoOBTPc (**33**). After cooling to room temperature, the solution was poured into ice-

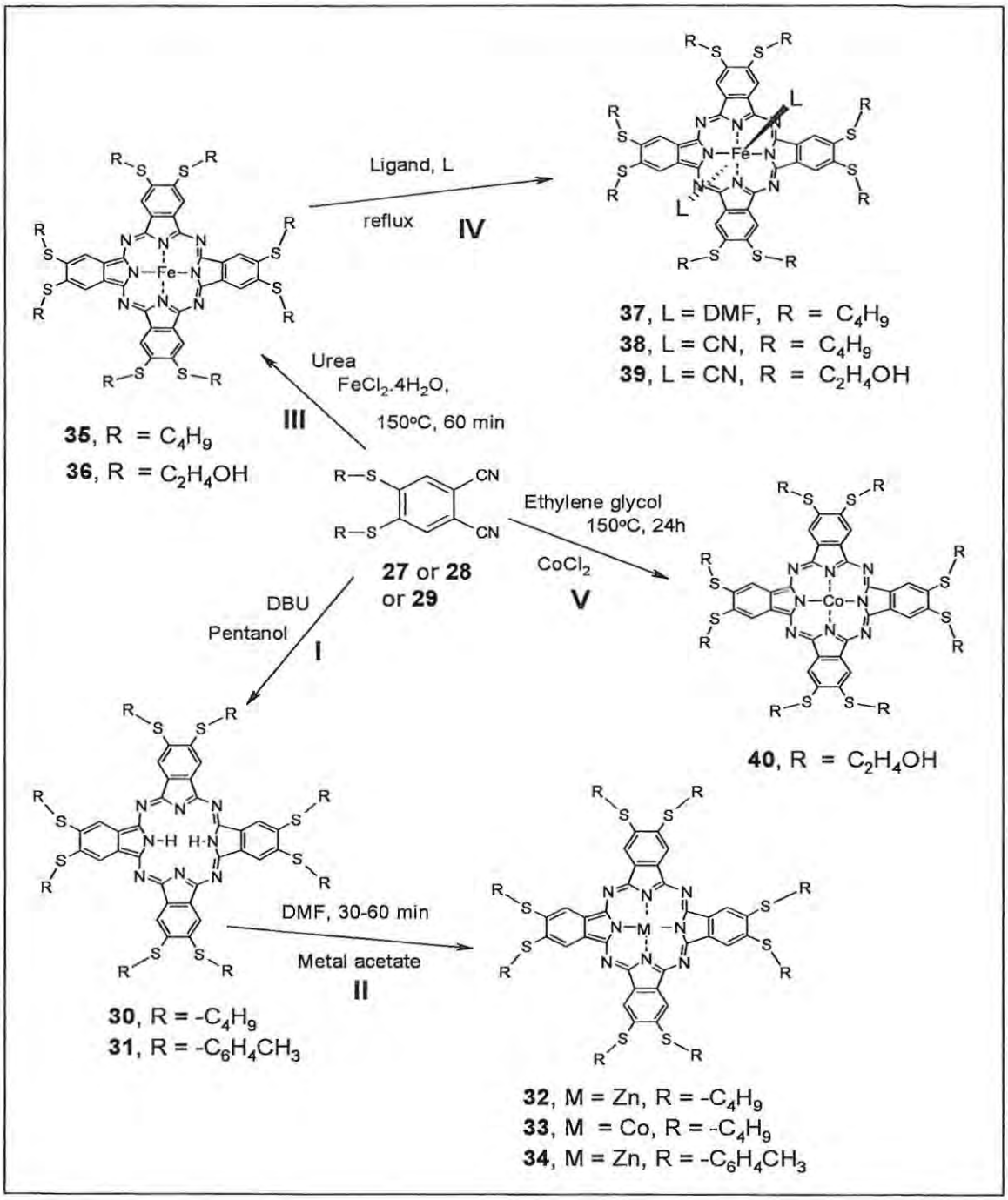

Scheme 2.5: Synthetic routes for the thiol-derivatised metal-free and metallated phthalocyanine complexes used in this work.[22,23,29,237,316,345-347]

water mixture (20 ml). The precipitated product was collected by centrifugation and washed with water and methanol. The green products were purified by chromatography on a silica gel column with chloroform or chloroform/DMF mixture (9:1) as eluent.

ZnOBTPc (32): Yield (88%). Anal: Calcd. for $C_{64}H_{80}N_8S_8Zn$: C, 59.86: H, 6.39: N, 8.73%. Found: C, 59.73: H, 6.36: N, 8.35. IR (KBr) ν_{max}/cm^{-1}: 2956, 2926 and 2867 (CH_2), 1591 (Ph), 1462, 1406, 1371 and 1332 ($CH_3CH_2CH_2CH_2$-), 740, 700 (S-CH_2). ^1H NMR [$CDCl_3$, 400MHz]: δ 7.60 (s, 8H, Pc), 3.10 (t, 16H S**C**$\mathbf{H_2}$), 1.74 (m, 16H, CH_2-**C**$\mathbf{H_2}$-CH_2, 1.53 (m, 16H, CH_2-CH_2-**C**$\mathbf{H_2}$-CH_3), 0.98 (t, 24H **C**$\mathbf{H_3}$). UV-Vis ($CHCl_3$, λ_{max}/nm (logε): 328 (4.73), 363 (4.89), 637 (4.64), 708 (5.36)

CoOBTPc (33): Yield 0.076g (62%). Anal: Calcd. for $C_{64}H_{80}N_8S_8Co$: C 60.24, H,6.28, N,8.78 Found: C,60.22, H,7.19 N,8.67. IR (KBr) ν_{max}/cm^{-1}: 2958, 2926, 2856, 1596, 1543, 1504, 1412, 1379, 1320, 1262, 1215, 1094, 1094, 1070, 1024, 965, 868, 803, 750 and 705. UV-Vis [$CHCl_3$, λ_{max}/nm (logε)]: 324 (5.01), 423 (4.38), 704 (5.06).

***Octa(4-methylphenylthio)phthalocyaninatozinc(II)*, ZnOMPPc (34)**

The same procedure as for the ZnOBTPc (**32**) was adopted, except **31**, instead of **30**, was employed. Yield (83%). Anal: Calcd. for $C_{88}H_{72}N_8S_8Zn$: C, 67.63: H, 4.61: N,7.17%. Found: C, 67.57: H, 4.41: N, 6.96. IR (KBr), ν_{max}/cm^{-1}: 3238, 1638 and 1618 (Ph), 1490, 1402 and 1370 (CH_3-), 805 (1,4- Ph), 745, 700 and 622 (S-Ph). ^1H NMR [$CDCl_3$, 400MHz]: δ 7.98 (s, 8H, Pc), 7.43 (d, 16H, phenyl), 7.31 (d,16H, phenyl), 1.24 (s, 24H, methyl). UV-Vis ($CHCl_3$, λ_{max}/nm (log ε): 328 (4.68), 363 (4.85), 640 (4.60), 715 (5.30).

Octabutylthiophthalocyaninatoiron(II), (FeOBTPc) **(35)**

(Scheme 2.5, Route III)

Better yields were obtained for this complex by direct synthesis rather than using the unmetallated complex. A mixture of 4,5-dibutylthiophthalonitrile (**27**) (0.10 g, 0.33 mmol.), $FeCl_2.4H_2O$ (0.02 g, 0.08 mmol) and urea (0.032 g, 0.5 mmol) was heated and stirred at 150°C for 90 minutes under nitrogen atmosphere. After cooling to room temperature, the reaction mixture was treated with hot ethanol and filtered by centrifugation. The dark green crude product was purified using column chromatography by first dissolving in chloroform and then eluting from silica gel column with chloroform. The first band was collected and the solvent removed under reduced pressure to give pure product (**35**). Yield: (0.09 g, 88 %). Anal.: Calcd. for $C_{64}H_{80}N_8S_8Fe.8H_2O$: C, 54.24: H, 6.78: N, 7.91%. Found: C, 54.58: H, 6.47: N, 7.91. IR [(KBr) ν_{max}/cm^{-1}]: 3447, 2958, 2863, 1589, 1500, 1455, 1412, 1375, 1325, 1263, 1215, 1185, 1073, 960, 865, 803, 746, 700. UV-Vis [(DMSO, λ_{max}/nm (log ε)]: 348 (5.88) and 676(4.97); UV-Vis [(DMF, λ_{max}/nm (log ε)]: 356 (5.08), 449 (4.59), 620 (4.61), 684 (5.06).

Octa(hydroxyethylthio)phthalocyaninatoiron(II), (FeOHETPc) **(36)**

(Scheme 2.5, Route III).

FeOHETPc (**36**) was prepared following similar procedure as for the FeOBTPc (**35**) above. A mixture of 4,5-(hydroxyethylthio)phthalonitrile, **29** (0.50 g, 1.78 mmol.), $FeCl_2.4H_2O$ (0.09 g, 0.36 mmol) and urea (0.04 g, 0.63 mmol) was heated and stirred at 150°C for 90 minutes under nitrogen atmosphere. After cooling to room temperature, the reaction mixture was heated for about 10 minutes in ethanol and filtered by

centrifugation. It was then washed with hot ethanol several times until the yellow coloration was removed. This was followed with successive washings in hot water, methanol, acetone and finally in diethylether (once) before drying in vacuo at 80°C for 2 hours. Yield: (0.33 g, 66%). Anal.: Calcd. for $C_{48}H_{48}N_8S_8Fe.10H_2O$: C, 42.48: H, 3.54: N, 8.36%. Found: C, 42.49: H, 3.52: N, 8.50. IR [(KBr) ν_{max}/cm^{-1}]: 3411 (OH), 2920-2850 (CH_2), 1710, 1593, 1410, 1330, 1280, 1070, 950, 873, 745, 700, 605. UV-Vis (Varian 500) [(DMSO, λ_{max}/nm (log ε)]: 354 (5.75) and 685(4.84); UV-Vis [(DMF, λ_{max}/nm (log ε)]: 348 (5.10), 450 (4.20), 620 (4.58), 685 (5.08).

Bis(dimethylformamide)octabutylthiophthalocyaninatoiron(II), ((DMF)$_2$FeOBTPc) (**37**), *(Scheme 2.5, Route IV)*

This complex was prepared by stirring FeOBTPc (**35**) (0.05 g, 0.040 mmol) in DMF (10ml) at 100°C for 3 hours under nitrogen atmosphere. The resulting green solution was evaporated under vacuum resulting to a dark green solid, which was then washed with water, acetone and then dried in vacuo to give the pure product (**37**). Yield: (0.046g, 93%). Anal.: Calcd. for $C_{70}H_{94}N_{10}O_2S_8Fe.2H_2O$: C, 57.78: H, 6.47: N, 9.63%. Found: C, 57.63: H, 6.51: N, 9.52. IR [(KBr) ν_{max}/cm^{-1}]: 3425, 2927, 2867, 1688, 1593, 1500, 1460, 1413, 1378, 1325, 1215, 1189, 1120, 1073, 958, 880, 850, 781, 746 and 705. UV-Vis [(DMF, λ_{max}/nm (log ε)]: 356 (5.08), 449 (4.59), 620 (4.61), 684 (5.06)

***Bis(cyano)octabutylthiophthalocyaninatoiron(II), $(CN)_2$FeOBTPc),* (38)**

(Scheme 2.5, Route IV)

The FeOBTPc (**35**) (0.05 g, 0.04 mmol) was mixed with excess potassium cyanide (0.05 g, 0.77 mmol) and refluxed in DMF (5 cm^3) for 3 hours under nitrogen atmosphere. The brilliant green solution was evaporated to dryness and the solid washed with hexane. The solid was then recrystallised twice from acetone to give the pure green complex (**38**). Yield: (0.041 g, 82%). Anal.: Calcd. for $K_2C_{66}H_{80}N_{10}S_8Fe.10H_2O$: C, 50.02: H, 4.98: N, 8.83 %. Found: C, 50.07: H, 5.06: N, 8.85 IR [(KBr) ν_{max}/cm^{-1}]: 3433, 2958, 2869, 2169 (ν_{Fe-CN}), 1592, 1512, 1458, 1407, 1381, 1216, 1131, 1073, 960, 872, 804, 781, 747 and 701. UV-Vis [(DMSO, λ_{max}/nm (log ε)]: 368m, 408w, 445w, 468w, 620m and 686s (5.10); UV-Vis [(DMF, λ_{max}/nm (log ε)]: 366m, 408w, 445w, 468w, 620m and 686s (5.08). (Where m = medium, w = weak and s = strong absorptions).

***Bis(cyano) octa(hydroxyethylthio)phthalocyaninatoiron(II), $(CN)_2$FeOHETPc,* (39)**

(Scheme 2.5, Route IV)

The method used for the $(CN)_2$FeOBTPc (**38**) complex described above was also employed for the synthesis of $(CN)_2$FeOHETPc (**39**). IR [(KBr) ν_{max}/cm^{-1}]: 3407, 3163, 2950, 2732, 2298, 2169 (ν_{Fe-CN}), 2093, 2062, 2073, 1628, 1512, 1404, 1310, 1216, 1120, 1063, 1039, 1007, 832, 780, 753 and 703. UV-Vis [(DMSO, λ_{max}/nm (log ε)]: 368m, 443w, 462w, 622m and 690 (5.10)

Octa(hydroxyethylthio)phthalocyaninatocobalt(II), (CoOHETPc) **(40)**.[316,347]

(Scheme 2.5, Route IV)

A mixture of 4,5-(hydroxyethylthio)phthalonitrile (**29**) (0.30 g, 1.07 mmol.), anhydrous $CoCl_2$ (0.04 g, 0.36 mmol) and urea (0.04 g, 0.31 mmol) and ethylene glycol (6 cm^3) was heated and stirred at 160°C for 24 hours under nitrogen atmosphere. After cooling to room temperature, the reaction mixture was heated for about 10 minutes in ethanol and filtered by centrifugation. The dark-green precipitate was treated with boiling acetic acid, water and acetone, and finally purified by chromatography from silica gel column with DMSO as eluent. Yield: (0.09 g, 30%). The complex gave satisfactory spectroscopic data as reported in the literature.[316,347]

2.4 Methods

2.4.1 Singlet Oxygen Determination and Photobleaching

The photochemical experiments were carried out in a 1cm pathlength spectrophotometric cell, fitted with a tight-fitting stopper using the set-up shown in Figure 2.1. Typically, a volume of 3.0 cm^3 of the solution (with or without bubbled oxygen)containing the MPc photosensitiser (~10^{-6} mol dm^{-3}), or MPc plus the appropriate singlet oxygen quencher (ADMA or DPBF ≈ 3×10^{-5} mol dm^{-3}), was added to the cell and

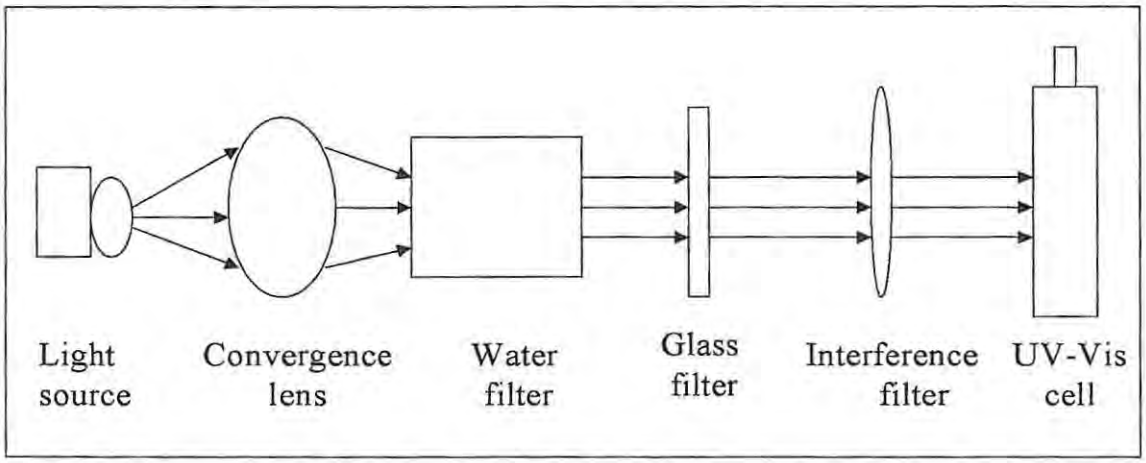

Figure 2.1: A diagrammatic representation of the photochemical set-up used in this work.

then photolysed in the Q band region of the dye. The set-up in Figure 2.1 is comprised of the General Electric Quartz line Lamp (300W), 600 nm glass cut-off filter (Schott) to eliminate light of wavelength less than 600nm, water filter to filter off the UV and far infra red radiation and interference filters (Intor 670 nm with bandwidth 20 nm was used for the water-soluble MPc complexes while the 700 nm and 40 nm bandwidths was used for the organic solvent-soluble thiol-derivatised ZnPc complexes (**32** and **34**). Light intensities at these wavelengths (~ 3-5 x 10^{16} photons $s^{-1}cm^{-2}$) were measured with a

Power meter (Lasermate/A LD 30, Coherent Auburn, USA). The light intensity was recorded in J s^{-1} A^{-1} (where A is the surface area of the detector) but was first converted to J s^{-1} cm^{-2} and then to photons $s^{-1}cm^{-2}$ using equation 2.1.

$$\Delta E_{\text{at wavelength } \lambda} = \frac{hc}{\lambda} \qquad 2.1$$

where E = Energy of light

h = Plank's constant

c = Speed of light

λ = Wavelength of the interference filter

The number of photons of light transmitted per second per unit square centimeter was obtained by dividing the total energy (E) read by the power meter by the energy at the wavelength of interest, λ.

The wavelength of interference filter was chosen such that it was close to the Q-band absorption of the metallophthalocyanine being studied. To determine the fraction of light that passes through the filter and is actually absorbed by the MPc complex, equation 2.2 was used.

$$\alpha = \frac{\Sigma T_{\text{filter}} \left(1 - T_{\text{MPc}}\right)}{\Sigma T_{\text{filter}}} \qquad 2.2$$

where α = fraction of the overlap integral of the light absorbed by the MPc sensitiser

T_{filter} = light transmitted through the interference filter (as a fraction of unity)

T_{MPc} = light transmitted through the MPc solution.

Table 2.1 shows a sample result obtained in this work for determining α using equation 2.2., where α = 0.66. Appropriate solutions (pH 10 aqueous solution and DMF for the

water-soluble MPc complexes (**9, 10, 15 - 18**) and organic solvent-soluble thiol-derivatised ZnPc complexes **32** and **34**, respectively) were used to determine the quantum yields of singlet oxygen and photobleaching in air (without bubbled oxygen) and oxygen (bubbled oxygen) using the relative method with $AlPcS_4$ as reference and ADMA as singlet oxygen scavenger (for water-soluble MPc complexes), while ZnPc was used as reference and DPBF as chemical quencher for singlet oxygen for the water-insoluble MPc complexes.

Table 2.1: Calculation of the fraction of light (α) absorbed by a typical MPc photosensitiser.

λ / nm	T_{filter}	T_{MPc}	$1-T_{MPc}$	$T_{filter}(1-T_{MPc})$
650	0.1508	0.527	0.473	0.0713
660	0.7511	0.179	0.821	0.6167
670	0.7546	0.119	0.881	0.6648
680	0.7293	0.250	0.750	0.5470
690	0.3506	0.717	0.283	0.0992
700	0.3683	0.891	0.109	0.0402
	$\Sigma = 3.1047$			$\Sigma = 2.0392$

To avoid possible chain reactions induced by ADMA and DPBF in the presence of singlet oxygen the absorbance of these quenchers were maintained at approximately 0.6 ($\sim 3\times10^{-5}$ mol dm^{-3}) as reported elsewhere.[200] Solutions of the MPc photosensitiser

(absorbance ca. 1 at the irradiation wavelength, ~ 1×10^{-5} mol dm^{-3}) containing the appropriate quencher were prepared in the dark and irradiated in the Q band region using the setup described above. All experiments were performed at room temperature.

2.4.2 Photosensitized Transformation of Chlorophenols

The photo-transformation study was carried out with a set-up (Figure 2.1) similar to that used for the determination of quantum yields of singlet oxygen and photobleaching described above. The solutions to be photolysed were introduced in a 1cm path length UV-Vis cell fitted with a tight-fitting stopper. Typically, a volume of 3.0 cm^3 of the solution containing the metallophthalocyanine photosensitiser (~10^{-6} mol dm^{-3}) and polychlorophenol (TCP or PCP, 2.0 x 10^{-5} to 7.0 x 10^{-5} mol dm^{-3}), was added to the cell and then photolysed in the Q band region; oxygen was bubbled through the cell for 20 min before each illumination period.

Photo-transformations of the substrates were analysed by both electronic absorption spectrophotoscopy and reverse phase high-pressure liquid chromatography (HPLC). The separation of substrates and photoproducts were achieved using a mobile phase consisting of an acidified mixture of 60 : 40 water : methanol (for the 4-CP) and acidified methanol, acetonitrile and water in the ratio of 20:30:50 for the polychlorophenols (TCP and PCP). The volume of injected samples was 20 μl, and the elution rate was 0.1cm^3 min^{-1}. Spectra-Physics HPLC apparatus, spectra series P100, equipped with an analytical column GL Wakosil C18 (150 x 1 mm) and connected to variable wavelength UV-Vis detectors (set at λ = 254 nm) was employed. A Perkin-Elmer 561 chart recorder was connected to the HPLC apparatus. Electronic absorption

spectra were recorded with a Cary 500 UV-Vis-NIR spectrophotometer. The pH measurements were carried out with the Beckman ϕ 50 pH meter.

2.4.3 Kinetics and Equilibria of Interaction with Cyanide

Equilibrium and kinetic studies for the interaction between cyanide and thiol-derivatised phthalocyanines of Fe and Co were run at constant temperature (25.0 ± 0.5°C) and monitored with the Varian 500 UV-Vis-NIR spectrophotometer. A detailed study was undertaken using the $(DMF)_2FeOBTPc$ (**37**) complex. Cyanide binding was followed by monitoring the increase in the absorption intensity at 686 nm following the addition of cyanide to a DMSO solution of FeOBTPc (**35**) or DMF solution of complex **37**. The latter is, of course, equivalent to studying cyanide binding to complex **35** in DMF. Typically, a known volume of the DMSO or DMF solution of the phthalocyanine complex was added to a 1 cm pathlength spectrophotometric cell, then a known volume of the DMF or DMSO solution of the potassium cyanide was added to the cell and the changes in absorption spectra monitored with time. For the kinetic studies the concentration of the MPc complex was maintained at ~ $3x10^{-6}$ mol dm^{-3}. The concentration was determined from the extinction coefficients of the Q band of complex **37** in DMF $\{\varepsilon_{684} = (1.2 \pm 0.1) \times 10^5$ dm^3 mol^{-1} $cm^{-1}\}$ and complex **35** in DMSO $\{\varepsilon_{676} = (9.4 \pm 0.1) \times 10^4$ dm^3 mol^{-1} $cm^{-1}\}$. The cyanide concentrations, determined by titration with silver nitrate,[348] were varied from 1.8×10^{-4} to 3.0×10^{-3} mol dm^{-3}. Since the concentrations of cyanide were larger than those for the phthalocyanine complexes, pseudo-first-order conditions were assumed for the kinetic studies.

2.4.4 Electrochemical Methods

Electrochemical data for the solution electrochemistry of the thiol-derivatised MPc complexes were obtained under purified nitrogen gas with BioAnalytical System (BAS) 100 B/W Electrochemical Workstation. For characterization of the MPc complexes, cyclic voltammograms (CVs) and Osteryoung square wave voltammograms (OSWVs) were collected using a conventional three-electrode set-up (Figure 1.6) with a glassy carbon electrode (GCE, 3.00mm diameter) as a working electrode, a platinum wire counter electrode, and a silver wire pseudo-reference electrode. All potentials were referenced internally to the ferrocinium/ferrocene (fc^+/fc) redox couple. The potentials of the fc^+/fc couple were measured against the silver-silver reference and the half-wave potential ($E_{1/2}$) values obtained were subtracted from the $E_{1/2}$ values vs Ag wire for MPc complexes to give $E_{1/2}$ vs fc^+/fc for MPc, as described before.[349] The potential for the fc^+/fc couple has been reported [224] to be 0.46 V vs saturated calomel electrode (SCE) in DMF. The $E_{1/2}$ values for fc^+/fc vs SCE were added to $E_{1/2}$ for MPc complexes vs fc^+/fc to give $E_{1/2}$ vs SCE. TBAP (0.1 mol dm^{-3}) was used as supporting electrolyte. The concentration of the MPc complexes was maintained at 1×10^{-4} mol dm^{-3} in DMF. The parameters for the OSWV were: step potential 4 mV; square wave amplitude 25 mV at a frequency of 15 Hz. All experiments were done under nitrogen atmosphere, with nitrogen 5.0 from MESSER. Spectroelectrochemical experiment was used to characterize ZnOMPPc (**34**). An optically transparent thin-layer electrode (OTTLE) cell was constructed as described by Hartl and Deněk.[222] The working and counter electrodes of the cell were platinum grits while a piece of silver wire served as a pseudo-reference electrode. The OTTLE cell was connected to a BAS CV 27 voltammograph. Solutions of

the ZnOMPPc (**34**) were introduced into the cell and electrolysis was performed at the appropriate potentials. Spectral changes arising from the electrolysis were monitored with UV-Vis-NIR spectrophotometer .

2.4.5 Self-Assembling Technique

2.4.5.1 Apparatus

Solid phase electrochemistry experiments were also recorded using a BioAnalytical System (BAS) 100 B/W Electrochemical Workstation. However, for the conventional three-electrode system (Figure 1.6) used, the working electrode was either bare gold (r = 0.8 mm, BAS) or the thiol-derivatised MPc-SAM-modified gold electrode. An Ag|AgCl (3.0 mol dm^{-3} KCl) was used as a reference electrode and a platinum wire wound into a spiral as a counter electrode. The gold electrode was modified using the self-assembling technique described below. The same parameters for the OSWV used for the solution electrochemistry were also employed here. A WTW® pH meter was used for pH measurements. All experiments were performed at 25.0 ± 0.5 °C.

2.4.5.2 Electrode Pre-treatment and Formation of MPc Self-Assembled Monolayer (MPc-SAM).[276,277,307,329,330]

Prior to use, the gold electrodes were first polished using aqueous slurries of alumina (<10 micron) on a SiC-emery paper (type 2400 grit), and then to a mirror finish on a Buehler felt pad. The electrode was then placed in ethanol and subjected to ultrasonic vibration to remove residual alumina particles that are trapped at the surface. Finally the electrode was etched for about two minutes in a hot "Piranha" solution {1:3

(v/v) 30% H_2O_2 and concentrated H_2SO_4} and then rinsed with copious amounts of ultrapure Millipore water followed by ethanol and the deposition solvent. A 1:3:4 HNO_3 / HCl / H_2O solution was sometimes used in place of the "Piranha" solution, since both serve the same purpose. This treatment serves to eliminate possible organic contaminants on the electrode. The cleanliness (removal of the gold oxides) of each electrode surface was finally established by placing the electrode in 0.5 mol dm^{-3} H_2SO_4 and scanning the potential between –0.5 and 1.0V vs Ag|AgCl at a scan rate of 50 mV s^{-1} until a reproducible scan was obtained. This pre-treatment procedure is known[276,329] to give an electrode with the best surface for adsorption of SAMs of alkanethiols. Following this pretreatment, the electrode was rinsed with toluene and immediately placed in a 5 ml of toluene solution of the thiol-derivatised MPc (1.0×10^{-3} mol dm^{-3}) for 24 hours at ambient temperature. Upon removal from the deposition solution, the electrodes were thoroughly rinsed with toluene prior to electrochemical experiments. Other common solvents such as dichloromethane, THF, chloroform are also suitable for use as deposition solvents for the CoOBTPc (**33**), FeOBTPc (**35**), ZnOBTPc (**32**) and ZnOMPPc (**34**) complexes. The deposition solvent used for the CoOHETPc (**40**) and FeOHETPc (**36**) complexes was DMSO.

CHAPTER 3

SYNTHESIS AND CHARACTERIZATION OF METALLOPHTHALOCYANINES

3.1 Synthesis and Spectroscopic Properties

Table 3.1 is a summary list of the metallophthalocyanine (MPc) complexes studied in this thesis.

Table 3.1: List of metallophthalocyanine (MPc) complexes studied in this thesis, their abbreviations and numbers as well as their Q band maxima.

MPc Complex Abbreviation*	MPc Complex Number	Q band maxima / nm
$AlPcS_4$	**9**	675 (pH 7, 10)
$ZnPcS_4$	**10**	667 (pH 7, 10)
$AlPcS_{mix}$	**15**	675 (pH 7, 10)
$ZnPcS_{mix}$	**16**	667 (pH 7, 10)
$SnPcS_{mix}$	**17**	691 (pH 7, 10)
$SiPcS_{mix}$	**18**	671 (pH 7, 10)
AlOCPc	**20**	690 (pH 10)
ZnOCPc	**21**	690 (pH 10)
H_2OBTPc	**30**	700, 732 ($CHCl_3$)
H_2OMPPc	**31**	710, 737 ($CHCl_3$)
ZnOBTPc	**32**	708 ($CHCl_3$)
CoOBTPc	**33**	704 ($CHCl_3$)
ZnOMPPc	**34**	715 ($CHCl_3$)
FeOBTPc	**35**	684 (DMF), 676 (DMSO)
FeOHETPc	**36**	685 (DMSO)
$(DMF)_2FeOBTPc$	**37**	684 (DMF)
$(CN)_2FeOBTPc$	**38**	686 (DMF)
$(CN)_2FeOHETPc$	**39**	690 (DMSO)
CoOHETPc	**40**	685 (DMSO)

*PcS_4 = tetrasulphopthalocyanine; PcSmix = sulphonated (mixed) phthalocyanine,
OCPc = octacarboxyphthalocyanine; OBTPc = octabutylthiophthalocyanine;
OMPPc = octa(4-methylphenylthio)phthalocyanine; OHETPc = octa(hydroxyethylthio)phthalocyanine.

3.1.1 Sulphonated Metallophthalocyanine Complexes

The most common water-soluble MPc complexes are the sulphonates, $MPcS_n$ (where M = metal ion, n = 1, 2, 3 and 4). These complexes are soluble in water since they are negatively charged. Depending on the synthetic procedure employed, sulphonation results in the common tetrasulphonated MPc ($MPcS_4$) [24] complexes as well as the MPc complexes containing a mixture of the di-, tri- and tetra-sulphonated derivatives, $MPcS_{mix}$ (where mix = 2, 3 and 4).[28,186,350-352]

The spectroscopic characteristics of sulphonated MPc complexes in aqueous solutions are well established.[24,28,186,350-352] These complexes exhibit aggregation properties, the extent of which, depends on such factors as the degree of sulphonation, isomeric composition, nature of central metal ion, concentration, temperature, pH, ionic strength, and solvent. The aggregation phenomenon is usually associated with the appearance of two peaks in the Q band region of the electronic absorption spectra; the low-energy absorption band near 670 nm being attributed to the monomeric species while the high-energy absorption band near 630 nm is associated with the dimeric species. Studies have shown[352] that $AlPcS_{mix}$ preparations consisting of the least number of isomeric species showed greater tendency to form aggregates and dimers, whereas the more complex preparations consisting of a higher number of differently substituted products show more monomeric behaviour in aqueous solutions.

All the sulphonated MPc complexes of aluminium ($AlPcS_4$, **9** and $AlPcS_{mix}$, **15**) and zinc ($ZnPcS_4$, **10** and $ZnPcS_{mix}$, **16**) presented in this work are known.[24,28,350-352] They were synthesized and duly characterized following the established procedures. The sulphonated complexes of tin ($SnPcS_{mix}$, **17**) and silicon ($SiPcS_{mix}$, **18**) have not been

reported, they were also synthesized and characterised following procedures used for the aluminium (**15**) and zinc (**16**) analogues.[28] The IR characteristic bands of the S=O vibrations appeared in the 1030 – 1040 cm^{-1} region. The other bands that are common to MPc complexes were observed in the regions of 1730 – 1470 cm^{-1} (C–C stretching vibrations of the aromatic ring) and 810 – 700 cm^{-1} (C–H out-of-plane deformations). The Si–O and Sn–O appeared weakly at 830 and 567 cm^{-1}, respectively. These spectral properties are consistent with literature reports.[344]

Since the purpose for synthesizing these water-soluble non-transition MPc complexes is to investigate their photochemical properties and the effects of their irradiation in the visible region, a further investigation of their Q band properties is desirable. The location and broadness of the Q band give information on the aggregation behaviour of MPc. MPc sensitisers that form dimers and aggregates show lower photosensitisation efficiency.[185-187,351] Aggregation and dimerisation reduce the lifetimes of the MPc's excited state, most probably due to enhanced radiationless excited state dissipation.[182,185] The Q band absorption maxima of sulphonated MPc complexes in aqueous solution (pH = 7 or 10) studied in this work are presented in Table 3.1 while the spectra in pH 10 are shown in Figure 3.1. Alkaline solution (pH 10) was chosen because it is the most convenient pH for their application in the photo-degradation of chlorophenol. It is evident from Figure 3.1 that $AlPcS_{mix}$ (**15**) showed a sharp Q band at 675 nm (with no detectable dimer peak) and a vibronic band at 630 nm; characteristics of monomeric behaviour. In contrast, all the other five complexes (**9**, **10**, **16** - **18**) showed either dimer peaks or broad shoulder at the high-energy side of the absorption band around 630 nm, typical of aggregation of MPc complexes in aqueous solutions.[350] The

effect of concentration on the absorption spectra of the complexes was also investigated using the Beer's law (Figure 3.2). As expected, Beer's law was obeyed for the monomeric $AlPcS_{mix}$ (**15**) species in the studied concentration range of $\sim 10^{-6} - 10^{-4}$ mol dm^{-3}. Figure 3.2A (inset) shows Beer's law behaviour for the 10^{-6} mol dm^{-3} concentration range. The other complexes showed strong deviation from the Beer's law at concentration $>10^{-5}$ mol dm^{-3} as shown in Figure 3.2B (inset), using $SnPcS_{mix}$ as a typical example.

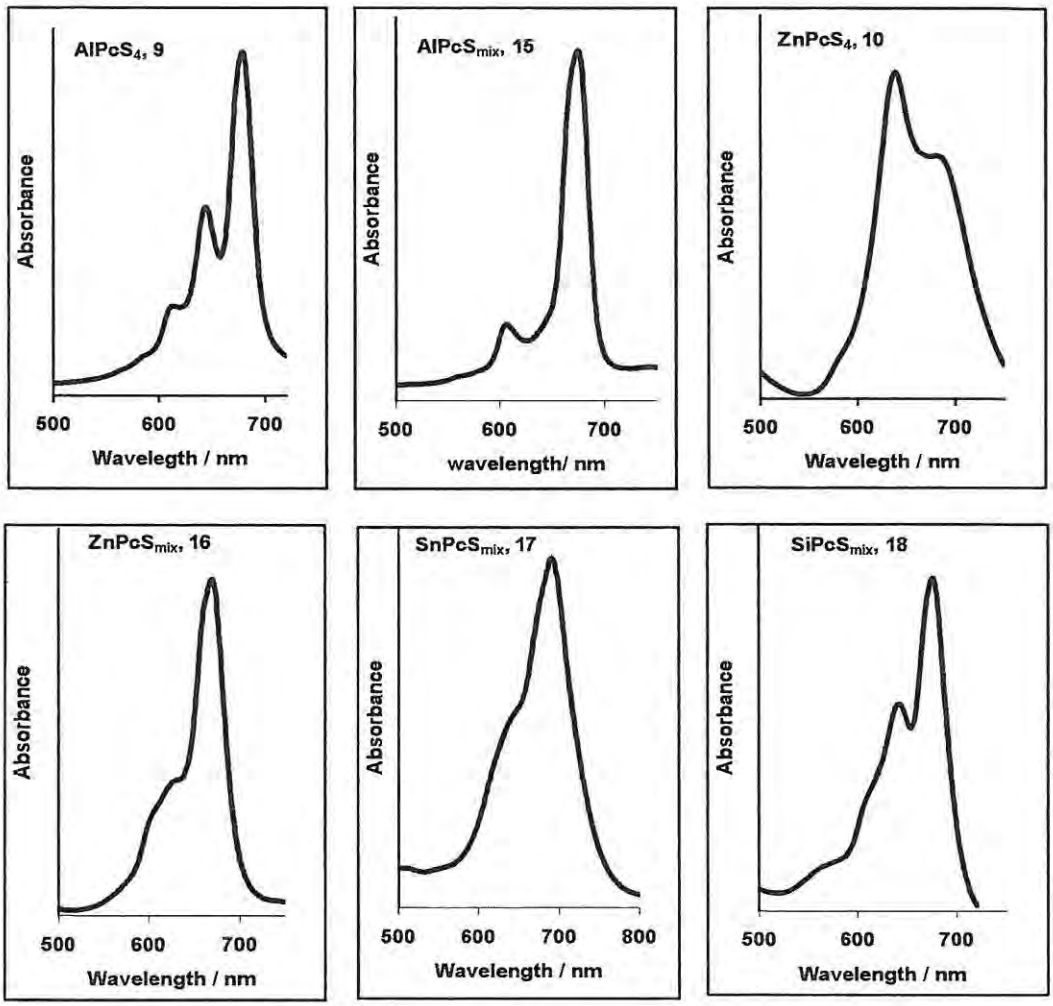

Figure 3.1: The Q band electronic absorption spectra of the sulphonated metallophthalocyanine complexes in pH 10 studied in this work.

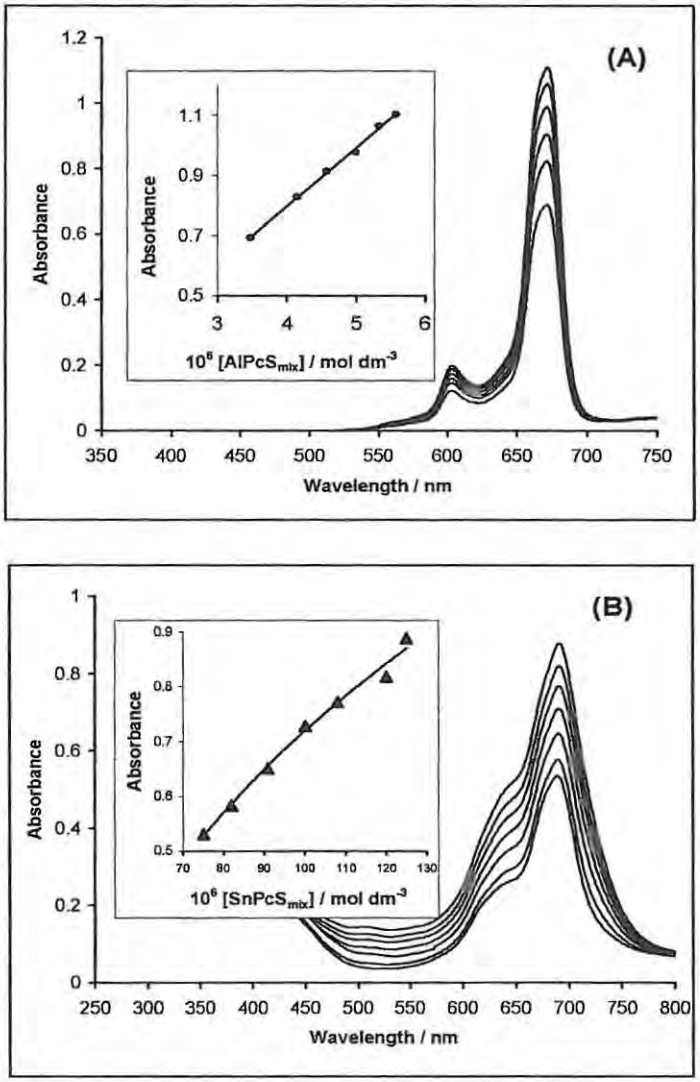

Figure 3.2: Variation of absorbance with concentration and Beer's law behaviour for $AlPcS_{mix}$, **15,** (A) and $SnPcS_{mix}$, **17,** (B) in pH 7.

Positively charged detergents, such as cetyltrimethylammonium chloride (CTAC),[86,200,353] are normally added to solutions of photosensitisers in order to form monomeric species. The increase in the low energy component of the Q band in the

presence of these cationic surfactants may be used to assess the degree of aggregation of the MPc under investigation. In this study, CTAC was used to estimate the degree of aggregation of these water-soluble complexes using equation 3.1.[352]

$$\text{Aggregation (\%)} = \frac{A_{QM}(\text{CTAC}) - A_{QM}(H_2O)}{A_{QM}(\text{CTAC})} \times 100 \qquad 3.1$$

where A_{QM}(CTAC) and $A_{QM}(H_2O)$ denote the Q band absorbances of the monomeric MPc complex (5×10^{-6} mol dm^{-3}) in CTAC and pH 10 solutions, respectively. Degrees of aggregation, obtained by using this approach were about 0% for **15**, 33% for **9,** 15% for **16**, 5% for **18** and 21% for **17** complexes. The degree of aggregation for **15** and **9** were studied previously[352] in the DMSO / phosphate-buffered saline at MPc concentration of 5×10^{-7} mol dm^{-3} and found to be zero and 37%, respectively; values approximately similar to the ones obtained here. The zero value for the $AlPcS_{mix}$ (**15**) is an indication of the pure monomeric nature of this complex in aqueous solution.

3.1.2 Octacarboxy Metallophthalocyanine Complexes (MOCPc)

The octacarboxy metallophthalocyanine (MOCPc) complexes of aluminium (AlOCPc, **20**) and zinc (ZnOCPc, **21**) were synthesised by the established methods;[26,354] the only slight modification being the use of acid rather than the reported alkaline hydrolysis of the tetra-amide product (**19**) to the final MOCPc complex. Attempts on the use of the reported alkaline hydrolysis for **20** and **21** were not successful as the impurities were difficult to remove even on multiple column chromatography, whereas acid hydrolysis was successful. The analytical data of **20** and **21** (as assigned in the experimental section) are in good agreement with the reported values of FTIR, electronic spectra and elemental analyses. MOCPc complexes are characterised by their monomeric,

sharp Q bands. The UV-Vis spectra of both complexes (Figure 3.3) showed monomeric behaviour (sharp Q band, conformation to the Beer's law up to ~ 10^{-4} mol dm^{-3} and 0% degree of aggregation).

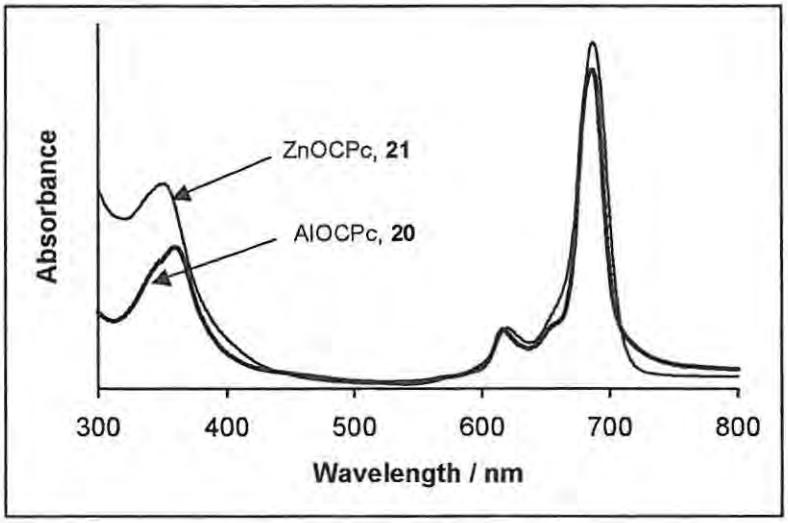

Figure 3.3: Electronic absorption spectra of AlOCPc, **20** and ZnOCPc, **21** in pH 10 aqueous solution.

3.1.3 Thiol-derivatised Metallophthalocyanine Complexes

3.1.3.1 4,5-Disubstituted Thiol-derivatised Phthalonitrile Complexes

The 4,5-disubstituted thiol-derivatised phthalonitriles complexes, 4,5-dibutylthiophthalonitrile (**27**), 4,5-di (4-methylphenylthio) phthalonitrile (**28**) and 4,5-di (hydroxyethylthio) phthalonitrile (**29**) (Scheme 2.4) were obtained from the precursor, 4,5-dichlorophthalonitrile (**26**). The precursor (**26**) was synthesized according to the method of Wöhrle et al.[22] as shown in Scheme 2.3. The synthesis of the thiol derivatives (**27 - 29**) was also according to the published method,[22] except that a milder condition, 45°C, was employed instead of the usual 90°C, which resulted in better yields of up to 86%. It is observed from Scheme 2.4 that Na_2CO_3 / DMF system was used for **29** instead

of the K_2CO_3 / DMSO used for **27** and **28**. The reason is because it is known[345] that the use of K_2CO_3 / DMSO for **29** leads to the formation of a monosubstituted hydroxyethylthiol product, 4-hydroxy-5-hydroxyethylthiophthalonirile. The reaction with **26** yielding **27 - 29** complexes (Scheme 2.4) is a simple nucleophilic displacement. After recrystallization, no further purification was required and spectroscopic characteristics confirmed good purity. The relatively novel complex **28** showed satisfactory elemental analysis. The ^1H NMR spectra (singlet, 7.00-7.20 ppm) defined the benzene rings, the hydrogen atoms on the phenythiol ring showed two doublets at 6.90 and 8.40 ppm, respectively, while those on the alkyl chains showed appropriate multiplicity according to the n + 1 rule. FTIR spectra (as assigned in the experimental section) showed good agreement with the required values.

3.1.3.2 Metal-free Octasubstituted Thiol-derivatised Metallophthalocyanine Complexes.

Octasubstituted phthalocyanine complexes of zinc

The metal-free phthalocyanine complexes, octabutylthiophthalocyanine, H_2OBTPc (**30**) and octa (methylphenylthio) phthalocyanine, H_2OMPPc (**31**) complexes were synthesized by heating under reflux the corresponding thiophthalonitrile derivatives (**27** and **28**) with 1,8-diazabicyclo[5.4.0]undec-7-ene (DBU), which is a strong organic base, in pentanol for 48 hours as reported for similar complexes, Scheme 2.5, route I.[22] The metallated phthalocyanine complexes, octabutylthiophthalocyaninatozinc(II) (ZnOBTPc) (**32**), octabutylthiophthalocyaninatocobalt(II) (CoOBTPc) (**33**) and octa(4-methylphenylthio)phthalocyaninatozinc(II) ZnOMPPc (**34**), were synthesized by the

metallation of their corresponding metal-free analogues using excess metal acetate. This step was usually complete within 15 min and easily indicated using the UV-Vis spectrophotometer in $CHCl_3$ by observing the total collapse of the split Q-band (700 and 732 nm for **31** and 710 and 737nm for **30**) of the metal-free analogue to the single Q-band. Figure 3.4 shows typical UV-Vis spectra of the metal-free and metallated zinc complexes. The difference in the Q band features is due to the difference in symmetry; metal-free complex possessing lower symmetry (D_{2h}) than the metallated complex, which has a D_{4h} symmetry. The eight peripheral substituents confer on these macromolecules good solubility in common organic solvents (such as chloroform, DMF, tetrahydrofuran and toluene). It is more difficult to purify **34** than **32** by column chromatography using chloroform alone. It was found that **34** could easily be purified by column chromatography using a small amount of DMF (~10%) as co-eluent with $CHCl_3$.

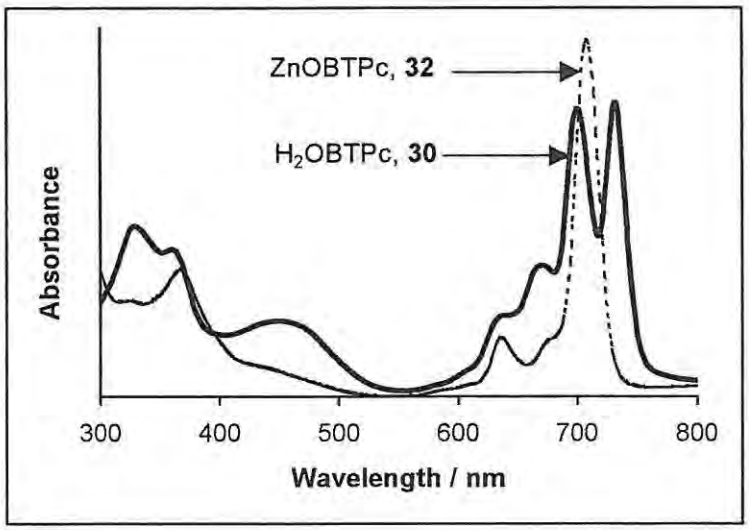

Figure 3.4: Electronic absorption spectra of H_2OBTPc, **30**, and ZnOBTPc, **32**, in chloroform.

A similar observation has been made before[355] and was attributed to the ability of the co-solvent (in this case DMF) to break up the molecular aggregation of **34** thereby increasing its mobility on silica gel columns. The synthetic route employed here is identical to that used for **32**,[26] except for the employment of a different solvent and the shorter reaction time required in this method. The differences in the solvent employed may be responsible for the increased yield observed in this work.

The UV-Vis spectra of **32** and **34** are typical of MPcs with D_{4h} symmetry.[32] The Q band of **34** (715 nm) is shifted slightly to a longer wavelength when compared to **32** (708 nm). Such a red shift is an indication that the energy gap between the highest occupied molecular orbital (HOMO) and lowest unoccupied molecular orbital (LUMO) of **34** is narrower than that for **32**.[32] There was no shifting in peak positions of both the Q and B bands for **34** and **32** (Figure 3.5) over the concentration ($1x10^{-6} - 2x10^{-5}$ mol dm^{-3}) range studied. Deviations from Beer-Lambert law relationship were observed at concentrations

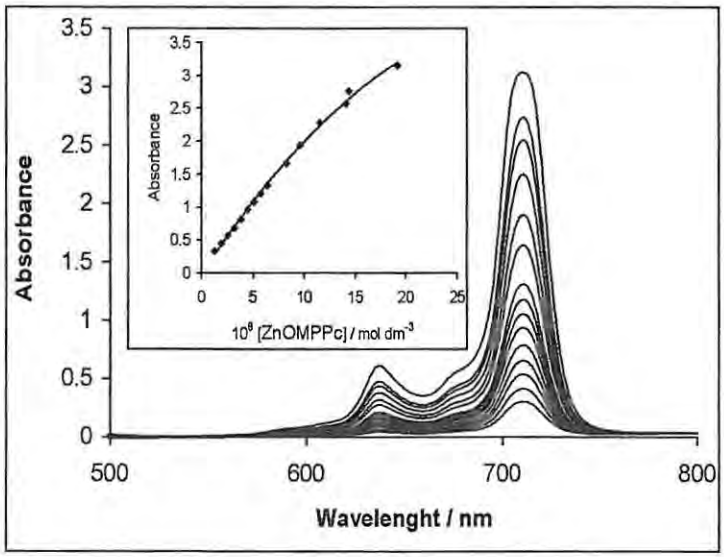

Figure 3.5: Variation of absorbance with concentration and Beer's law behaviour for ZnOMPPc (**34**) in DMF.

higher than $1.2x10^{-5}$ mol dm^{-3}, for **34**, Figure 3.5 (inset), as a result of aggregation of the complex. It has been reported that for **32**, the aggregation behaviour occurs only at concentrations higher than ~$5x10^{-5}$ mol dm^{-3},[26] hence confirming the higher aggregation tendency of **34** compared to **32**, even at low concentrations. This observation can be attributed to the π-π interactions arising from the peripheral benzene rings.[356]

The ^{1}H NMR spectra of both **34** and **32** were recorded in $CDCl_3$ and all showed satisfactory spectra (see assignments in the experimental section). It is worth mentioning here that metallation of the metal-free Pc resulted in the shielding of protons. For example, the aromatic protons observed at 7.98 ppm for **34** and 7.60 ppm for **32** appeared at 8.95 and 8.40 ppm in their corresponding metal-free derivatives. This observation is consistent with literature report for thiol-derivatised ZnPcs.[23] The analytical data of **32** and **34** (as assigned in the experimental section) showed good agreements with the required value of IR, and elemental analyses.

Octasubstituted phthalocyanine complexes of cobalt.

The cobalt octabutylthiophthalocyanine, **33**, was obtained from the metal-free analogue as for the zinc complexes. However, unlike in the synthesis of the zinc analogue, **32**, where the reaction was achieved within 10 minutes at 110°C, the synthesis of **33**, took a longer time (~ 60 minutes) and higher temperature (~ 180°C) to accomplish, implying greater difficulty in the insertion of the central metal into the core of the metal-free phthalocyanine, **30**. Like its zinc analogue, **32**, the electronic absorption spectra of **33** are shifted to longer wavelengths in various solvents (for example, 690 nm in pyridine) when compared to the unsubstituted CoPc (658 nm in pyridine). However,

unlike the **32** (Figure 3.4), the electronic absorption spectrum of **33** in $CHCl_3$ (Figure 3.6) showed the Q band at 704 nm, with a shoulder around 650 nm. The appearance of a shoulder at higher energy of the Q band in apolar solvent, $CHCl_3$, was previously observed for cobalt(II) octahexythiophthalocyanine and was attributed[23] to a possible interaction of the central cobalt ion of one molecule with the thioether groups of another. Since this behaviour was not observed in the zinc analogue, **32,** the involvement of the central $Co^{(II)}$ ion may also be assumed. Cobalt(II) octa(hydroxyethylthio)phthalocyanine, **40**, is known and was synthesized using the established procedure, and gave appropriate spectroscopic characterization. The analytical data of the cobalt phthalocyanine complexes **33** and **40** (as assigned in the experimental section) showed good agreement with the required values for IR and elemental analyses

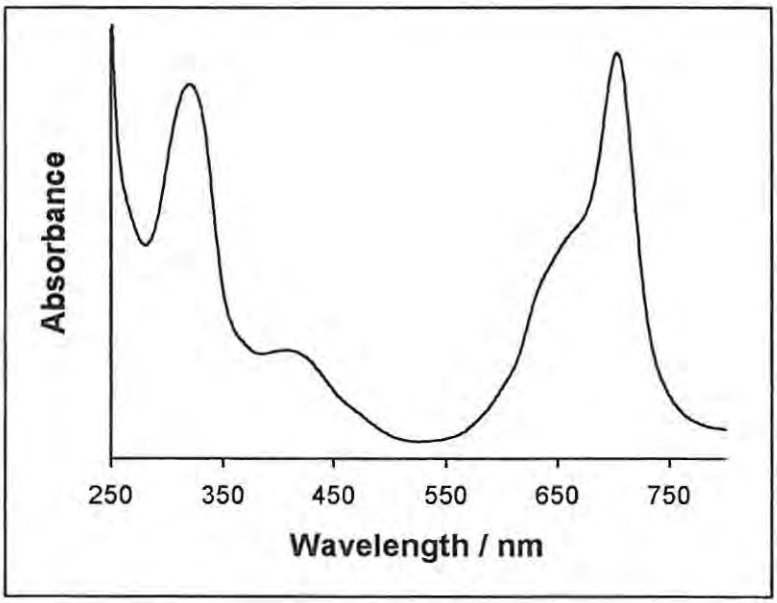

Figure 3.6: Electronic absorption spectrum of CoOBTPc (**33**) in chloroform.

Octasubstituted phthalocyanine complexes of iron

The two iron thiophthalocyanines, octabutylthiophthalocyaninatoiron(II), FeOBTPc (**35**) and octa(hydroxyethylthio)phthalocyaninatoiron(II), FeOHETPc (**36**) studied in this work are not known. Their synthesis was accomplished by a simple direct reaction of their respective thiophthalonitriles, **27** and **29**, with $FeCl_2.4H_2O$ in good yields. The synthesis of these complexes, **35** and **36,** is somewhat interesting since it involves a simple solvent-free, less time-consuming (~ 2hrs) and high yielding (88% for **35** and 70% for **36**) process when compared to the literature methods[23,347] for similar zinc, cobalt and nickel complexes that require expensive high-boiling solvents and longer reaction times (7-22hrs) but low-yielding (28-49%). The solubility characteristics of **35** are similar to those of its zinc (**32**) and cobalt (**33**) analogues, but differ from those of **36,** which is only readily soluble in DMF and DMSO, as in the case for the cobalt analogue, CoOHETPc, **40**.

UV-Vis spectra of **35** and **36** in DMF and DMSO are shown in Figures 3.7 A and B, respectively. Both complexes showed two strong absorption regions, 348-356 nm (Soret or B band) and 676- 684 nm (Q band) that are typical of MPc complexes with D_{4h} symmetry.[32] The spectra in DMF showed an absorption band centered near 450 nm as is typical of low-spin six-coordinate $Fe^{(II)}Pc$ species.[357-363] This band is usually associated with $Fe^{(II)}$-to-ligand charge transfer transitions,[358,360-363] hence its presence is a good indication that the central metal ion remains in the +2 oxidation state.[32,46] This band has also been observed to become more intense as the σ donor strength of the axial ligand increases.[32] Both B and Q bands of these complexes (**35** and **36**) are slightly shifted to longer wavelengths when compared to unsubstituted FePc (330 and 659 nm in DMF).

The Q band of **35** is broad in DMSO and in apolar solvents such as $CHCl_3$, even at very low concentrations ($\sim 10^{-6}$ mol dm^{-3}); a behaviour associated to some intermolecular interactions of the central metal ion of one molecule with the thioether groups of another.[23] These Fe-thioether interactions is less favoured in DMF than in DMSO or apolar solvents, most probably due to enhanced axial coordination with DMF.

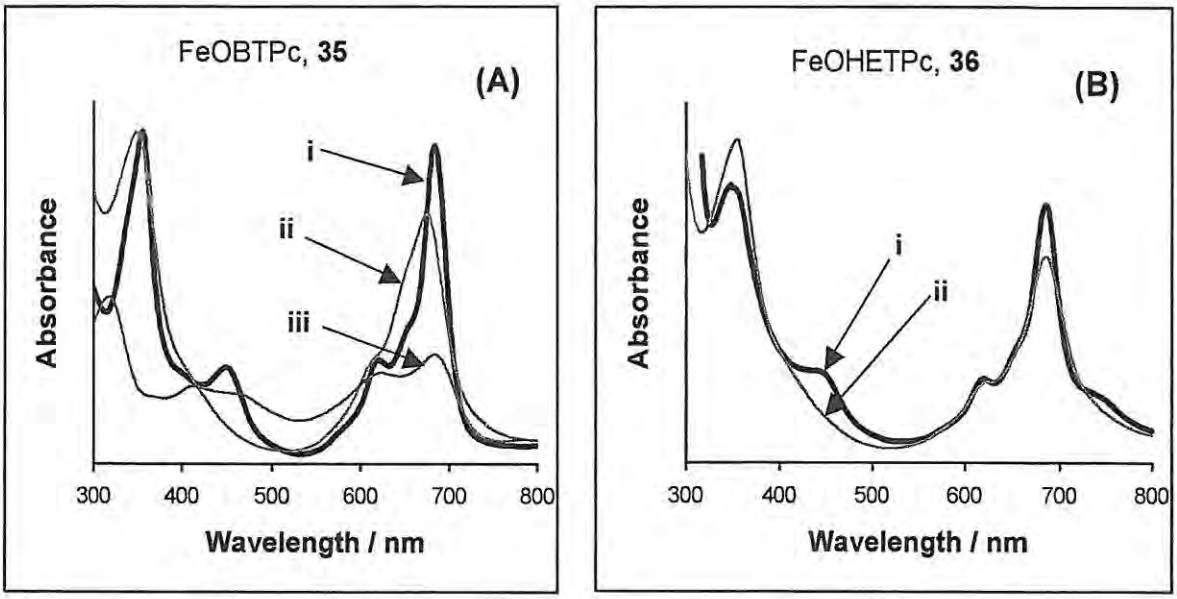

Figure 3.7: Electronic absorption spectra of FeOBTPc (**35**) and FeOHETPc (**36**) in (i) DMF, (ii) DMSO and (iii) $CHCl_3$.

The axially ligated, $((DMF)_2FeOBTPc)$ (**37**) and $((CN)_2FeOBTPc)$ (**38**) complexes of **35** were prepared using the established methods.[29,237] Whereas the solubility of **35** in DMF is extremely poor at room temperature, its axial ligated complexes, **37** and **38,** are soluble in both DMF and DMSO; with the cyano complex **38** also being soluble in water. These data are not surprising since axial ligation often leads to an increase in the solubility of MPc.[253,364] The electronic absorption spectra of the dicyano complex (**38**) in both DMF and DMSO, Figure 3.8 i and ii, respectively, are

typical of a non-aggregated MPc complex. Because of steric constraints a six-coordinate species is not likely to exhibit aggregation in solution. The spectrum of **38** showed a split in the Soret band in both DMSO and DMF, which is typical of such dicyano complexes.[365] The O-bonding of DMF is evidenced by the presence of the distinct Fe-O vibrations[357,366] at 850 cm^{-1} in the IR spectra of **37** (Figure 3.9) but absent in **35** and **38**

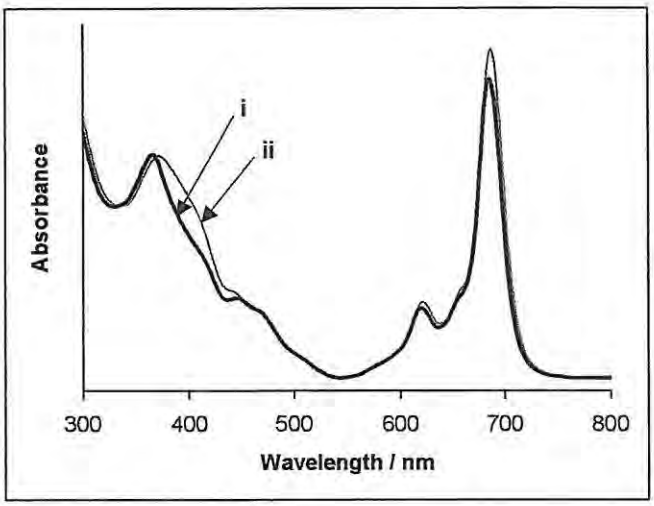

Figure 3.8: Electronic absorption spectra of $[(CN)_2FeOBTPc]$ (**38**) in (i) DMF and (ii) DMSO.

complexes. The ligation of cyanide was confirmed by the FTIR spectrum of the solid complex, $(CN)_2FeOBTPc$, **38**. The Fe-CN vibration is observed at 2169 cm^{-1}, a value in the range reported for M-CN vibrations in $(CN)_2MPc$ and related complexes.[46,367-370] For example, the Fe-CN vibrations for bis(cyano)phthalocyaninatoiron(II), $[(CN)_2FePc]^{2-}$ and bis(cyano)hexadecachlorophthalocyaninatoiron(II), $[(CN)_2FePc(Cl)_{16}]^{2-}$ have been reported[30,46] as 2120 and 2070 cm^{-1}, respectively. Indeed, it is interesting to see how the two different peripheral substituents, chlorine (an electron-acceptor) and butylthiol (an

electron-donor) affect the Fe-CN vibrations with equal but opposite magnitudes (~ ± 50 cm^{-1}). The complexes gave satisfactory spectroscopic (FTIR and UV-Vis) characteristics as well as the elemental analyses results.

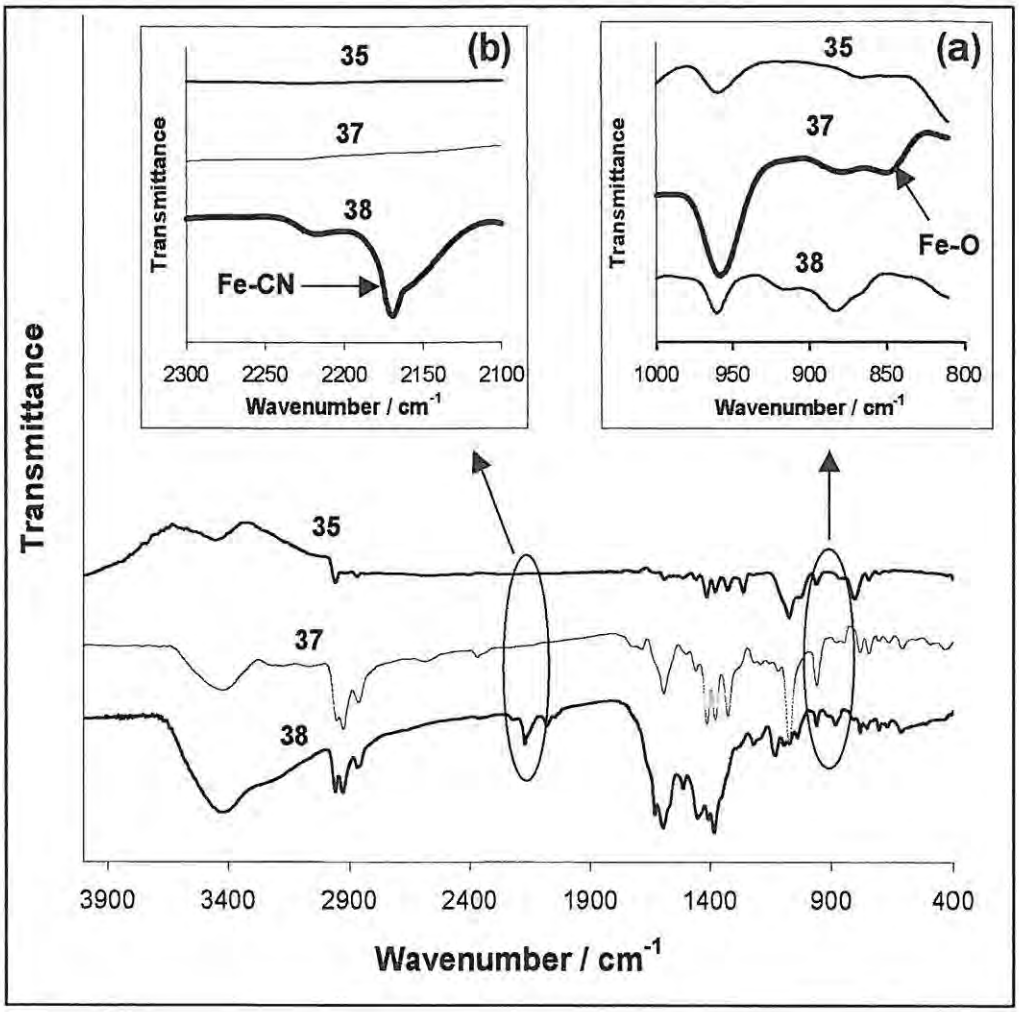

Figure 3.9: Comparative FTIR spectra of FeOBTPc (**35**), $(DMF)_2$FeOBTPc (**37**) and $(CN)_2$FeOBTPc (**38**) showing the characteristic Fe-O (inset a) and Fe-CN (inset b) vibration bands in **37** and **38**, respectively.

3.2 Photochemical Properties

3.2.1 Water-Soluble Metallophthalocyanine Complexes

3.2.1.1 Singlet Oxygen Quantum Yields (Φ_Δ)

The singlet oxygen quantum yields (Φ_Δ) of the six water-soluble metallophthalocyanine complexes (**9, 10, 15 - 21**) were obtained in pH 7 and 10 buffer solutions containing ADMA[198] using the relative method, described by equation 1.28 from Chapter 1.

$$\Phi_{\Delta}^{MPc} = \Phi_{\Delta}^{ref} \frac{(C_o - C_t)^{MPc}(\alpha t)^{ref}[Q]^{ref} I^{ref}}{(C_o - C_t)^{ref}(\alpha t)^{MPc}[Q]^{MPc} I^{MPc}} \qquad 1.28$$

where C_o and C_t are the concentrations of ADMA prior to and after irradiation, respectively. Other symbols have the meanings already described in Chapter 1. The $AlPcS_{mix}$ was used as a standard MPc since its Φ_Δ value (0.38) as a monomer in aqueous solution is known.[371] Initial concentration of ADMA was about 7×10^{-5} mol dm^{-3} and its decay upon irradiation of the Q band of the MPc sensitiser (~ 5×10^{-6} mol dm^{-3}) was monitored at 380 nm. Figure 3.10 is a typical absorption behaviour of ADMA upon irradiation of the Q band of the MPc in a solution containing MPc plus ADMA. The intensity of the light was low enough to ensure that the MPc remains unaffected during the process. The apparent first order kinetics for ADMA photo-oxidation confirmed that the condition $k_d >> (k_r)$[ADMA], equation 1.19 in Chapter 1, applies for the photolysis studies investigated. The Φ_Δ values for all the water-soluble MPc complexes are summarized in Table 3.2. The Φ_Δ values for **9, 15, 20** and **21** are comparable to literature reports,[372] the slight differences in values are due to different experimental conditions

employed. The low Φ_Δ value for **20** had been attributed to its association via hydrogen bonding between the axial hydroxyl groups.[372]

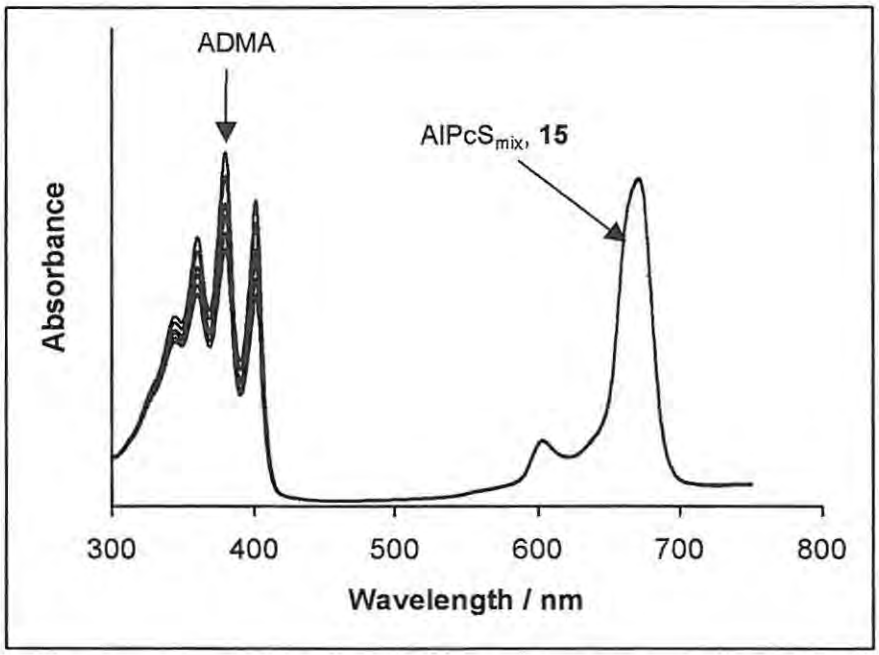

Figure 3.10: Typical decay of ADMA following irradiation of the Q band (λ = 670 nm) of AlPcS$_{mix}$, **15** in aqueous buffer solution at different irradiation times.

The Φ_Δ value for **16** is slightly low in comparison with known data for its monomeric form in organic media,[86,200] most probably due to partial aggregation of this sensitiser in aqueous buffer solutions. The complex, **10**, is highly aggregated; hence its Φ_Δ value is low (less than 0.01) as expected. The literature value is higher for **10** due to addition of CTAC, which monomerises the complex. The Φ_Δ values for **16, 17** and **18** have not been reported before this work, and despite partial aggregation, **16** and **17** show high singlet oxygen quantum yield in water, Φ_Δ = 0.48 and 0.46, respectively (Table 3.2).

Table 3.2: Singlet oxygen quantum yield and percentage photo-degradation data of various water-soluble metallophthalocyanine sensitisers under wavelength (λ) = 670 nm irradiation. pH 10.

MPc Complex	Φ_Δ	Photo-degradation of MPc (%)[a]
$AlPcS_4$, **9**	0.18 (0.07)[b]	0
$ZnPcS_4$, **10**	< 0.01 (0.31)[b]	0.5
$AlPcS_{mix}$, **15**	0.38 (0.38)[c]	0
$ZnPcS_{mix}$, **16**	0.48	35
$SnPcS_{mix}$, **17**	0.46	53
$SiPcS_{mix}$, **18**	0.16	0
AlOCPc, **20**	0.12 (0.15)[d]	1.3
ZnOCPc, **21**	0.52 (0.57)[d]	51

[a]After 180 seconds of irradiation of the Q band with visible light; [b]Values in brackets from reference 200, in the presence of 0.1M CTAC / water / 0.1M NaCl / 3 mM $Na_2S_2O_3$; [c]Value in bracket from reference 371; [d]Values in bracket from references 198 and 372 in alkaline solution.

3.2.1.2 Photostability

In order to assess the properties of these MPc complexes as potential photosensitisers for chlorinated aromatic pollutants in aqueous environments, their photostability was also investigated. Photostability, also known as photobleaching, is a measure of the rate of degradation of the conjugated chromophore structure of the Pc ring.[373] Figure 3.11 shows the photo-degradation pathway for MPc complex. In this pathway (Figure 3.11), photo-degradation of MPc complexes is believed to occur via singlet oxygen cyclo-addition to the phthalocyanine pyrrole units, which leads to the destruction of the macrocyle with

phthalimide as the degradation product. Here, the photostability studies were undertaken in buffer solutions by measuring the percentage decrease of the Q-band of the original MPc spectrum (5 x 10^{-6} mol dm^{-3}) over time, as the solution is photolysed. Table 3.2 gives the percentage photo-degradation of the photosensitisers and shows that the aluminium (**9, 15** and **20**) and silicon (**18**) phthalocyanine complexes are more stable in comparison with the zinc (**10, 16** and **21**) and tin (**17**) phthalocyanine complexes. AlPc and SiPc have been reported[351] to exhibit stable characters, for instance they can exist as μ-oxo dimers unlike the ZnPc complexes, thus explaining their similar photostability.

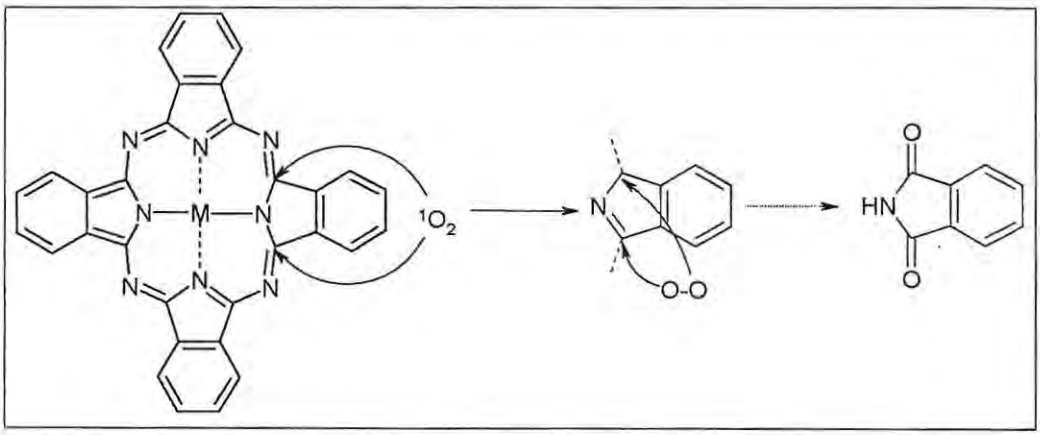

Figure 3.11: Suggested photo-degradation mechanism of MPc.[373]

3.2.2 Thiol-derivatised Zinc Phthalocyanine Complexes

3.2.2.1 Singlet Oxygen Quantum Yields (Φ_Δ)

A similar method for the determination of Φ_Δ for water-soluble complexes described above was also employed here for the thiol-derivatised zinc phthalocyanine complexes, **32** and **34** except that DMF was used as the solvent, ZnPc as the reference and DBPF as scavenger of the singlet oxygen. Figure 3.12 is a typical example of the

degradation of the DBPF as a result of the generation of the highly reactive singlet oxygen by **34** following periodic irradiation of its Q band using visible light. Both **32** and **34** showed no degradation during this process, indicating their high stability and efficiency in the generation of singlet oxygen under the experimental conditions employed. The Φ_Δ values for complexes **32** and **34**, which were obtained at an accuracy of ~10%, are given in Table 3.3. The Φ_Δ value for **32** is slightly higher than that for **34**, implying that the π-π^* interactions of the peripheral benzene promotes more association or aggregation in **34** thereby resulting in lower Φ_Δ in **34** compared to **32**. It is interesting, however, to observe that these values are in the same range as those reported for similar

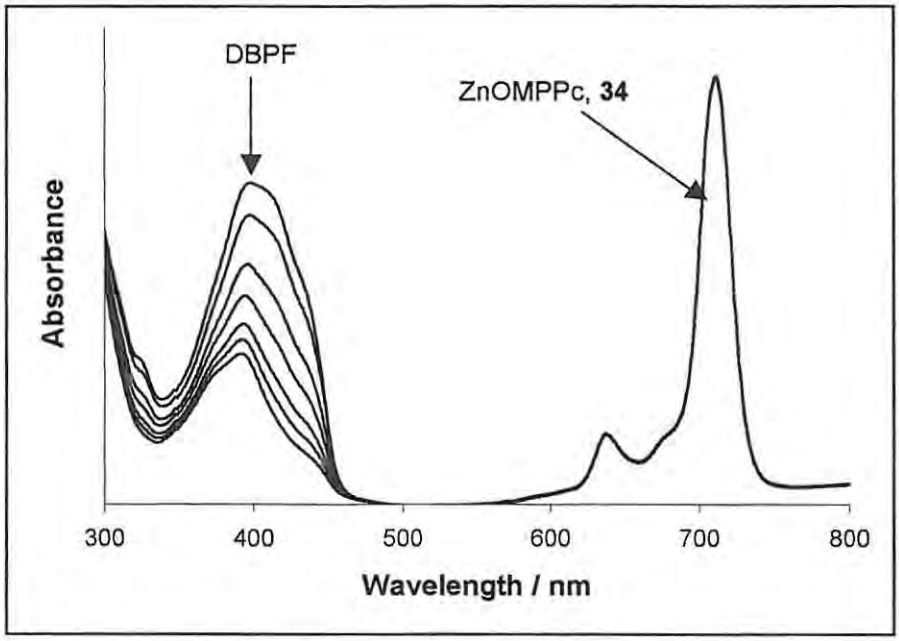

Figure 3.12: Typical decay of DBPF following irradiation of the Q band (λ = 700 nm) of ZnOMPPc, **34** in DMF solution at different irradiation times.

analogues (Table 3.3). The Φ_Δ value reported by Schurpfeil et al.[373] for the long chain octa-alkylthio substituted, $ZnPc(SC_8H_{17})_8$ complex (Φ_Δ = 0.53) is less than that for the short chain analogue, **32** (Φ_Δ = 0.61), suggesting a lowering of Φ_Δ as the chain length of the peripheral alkane-substituent increases.

Table 3.3: Singlet oxygen quantum yields (Φ_Δ) and photobleaching quantum yield (Φ_p) of ZnPc and its thiol-derivatised complexes in DMF.

ZnPc complex	Φ_Δ	$\Phi_p / 10^5$	Reference
ZnPc	0.56 ± 0.08	-	200
ZnOBTPc, i.e. $ZnPc(S\text{-}C_4H_9)_8$ (**32**)	0.61 ± 0.06	5.2±0.5 (air) 6.4±0.5 (oxygen)	This work
ZnOMPPc, i.e. $ZnPc(S\text{-}C_6H_4\text{-}CH_3)_8$ (**34**)	0.54 ±0.05	6.3±0.5 (air) 8.1±0.5 (oxygen)	This work
$ZnPc(S\text{-}C_8H_{17})_8$	0.53 ± 0.08	-	372

3.2.2.2 Photostability

Photostability studies of complexes **34** and **32** were studied in DMF solutions by measuring the decrease of the Q-band over time, as the solution is photolysed. The photobleaching quantum yields (Φ_p) values were determined as before[374,375] using equation 3.1 (similar to equation 1.26),

$$\Phi_P = \frac{(C_o - C_t)V}{I_{abs}t} \qquad 3.1$$

where I_{abs} is obtained using equation 1.27, from Chapter 1

$$I_{abs} = \frac{\alpha SI}{N_A} \qquad 1.27$$

As defined before in Chapter 1, C_o and C_t are the concentrations of the MPc prior to and after irradiation, respectively. V is the volume of the sample in the cell; t is the irradiation or photolysis time. α is the fraction of light absorbed, S is the cell area irradiated, and N_A is the Avogadro's constant. The Φ_p values were calculated to be (6.3±0.5) x 10^{-5} in air and (8.1±0.6) x 10^{-5} in oxygen-saturated solution for **34**, while for **32** the values were (5.2±0.5) x 10^{-5} in air and (6.4±0.5) x 10^{-5} in oxygen-saturated solution. Smaller Φ_p values correspond to a higher photostability. Higher Φ_p values were observed in oxygen, showing that oxidative degradation of the ring occurs. The Φ_p values for **34** are about 20% higher than those of **32** in similar media, in agreement with the previous speculation[373] that benzene rings tend to enhance photobleaching. Figure 3.13 shows the influence of DABCO (a singlet oxygen scavenger) on the photobleaching behaviour of ZnOMMPc, **34**. The photobleaching rates of both complexes were totally inhibited in the presence of DABCO suggesting a self-sensitized photo-oxidation by singlet oxygen as suggested by others.[373] Figure 3.13 also shows kinetic curves for the photobleaching of **34** in DMF, saturated with air or oxygen in addition to kinetic curves in DMF (containing air) in the presence of DABCO. Generally, photobleaching has been reported[194-197] to be either dependent or independent on singlet oxygen. The increase in the photobleaching rate in oxygen (~ 50% higher than in air) suggests the involvement of oxygen in the process. Inhibition of the photobleaching rate by singlet oxygen scavenger, DABCO,

confirmed the involvement of singlet oxygen in the photobleaching process. Similar observation was also made for **32**. It is therefore suggested that photobleaching of these compounds in DMF mainly proceeds, most likely, through a self-sensitized photo-oxidation by singlet oxygen as suggested by others.[373]

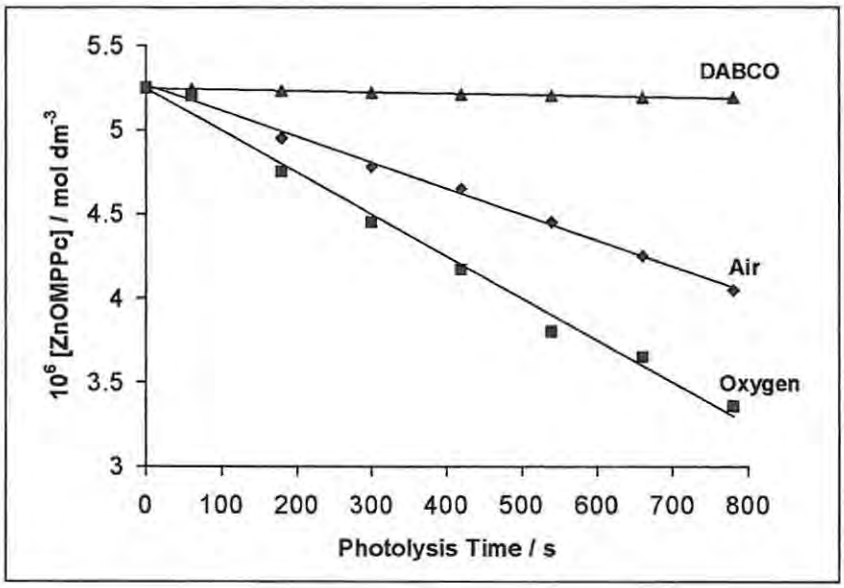

Figure 3.13: The kinetic curves for the photobleaching of ZnOMPPc, **34** in DMF saturated with air and oxygen, and containing $2x10^{-3}$ mol dm^{-3} DABCO (in air).

3.3 Electrochemical Properties

3.3.1 Thiol-Derivatised Zinc Phthalocyanine Complexes

The redox properties of **34** ($1x10^{-4}$ mol. dm^{-3}) were studied in DMF solution containing TBAP (0.1 mol dm^{-3}). From the UV-Vis spectral studies, it is evident that at the concentration of $1x10^{-4}$ mol. dm^{-3} in DMF used for this study, considerable aggregation of **34** occurs. Figure 3.14 is a typical cyclic voltammogram (first scan) of the **34**, showing four clear redox peaks (**I-IV**) and a weak redox couple, **V**, separated from

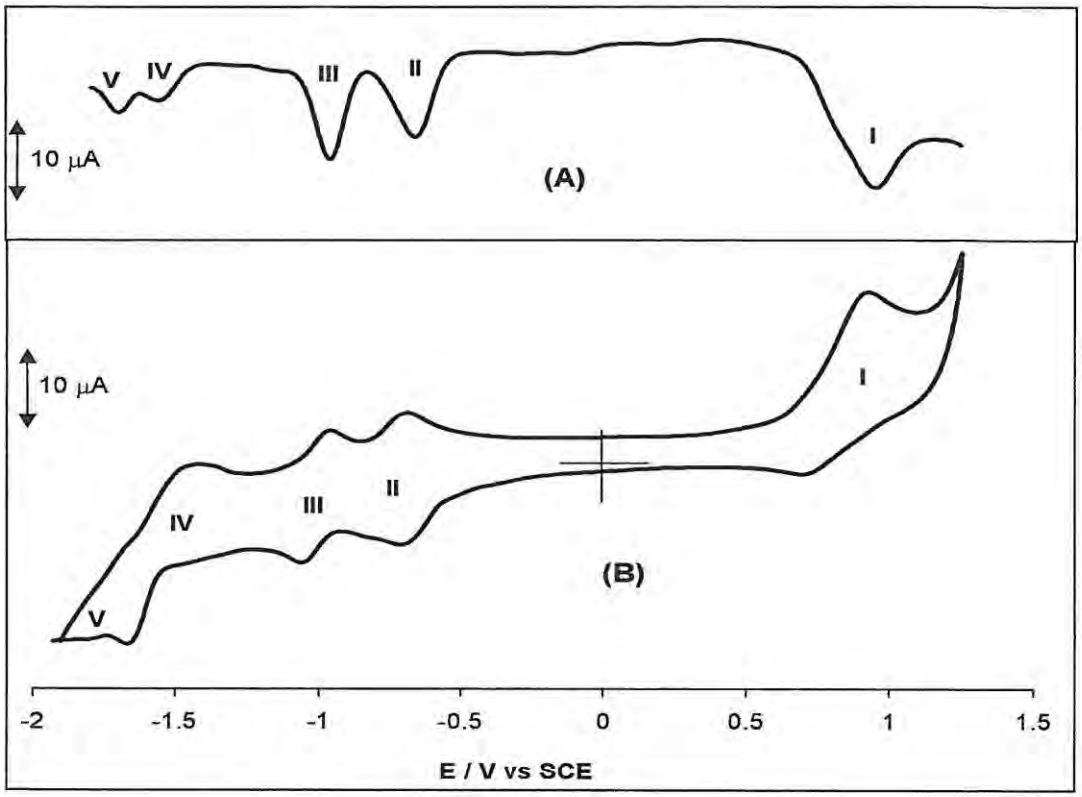

Figure 3.14: The Osteryoung square wave voltammogram (A) and cyclic voltammogram (B) of $1x10^{-4}$ mol dm^{-3} of **34** in DMF containing 0.1 mol dm^{-3} TBAP. Scan rate = 100mV/s.

IV by 0.16 V. Using the Osteryoung square wave voltammetry, which exhibit excellent sensitivity,[209,210] the weak redox couple **V** is clearly observed. Although, the fourth reduction step is not readily observed in MPc complexes, Louati et al.[16] had observed a similar separation value between **IV** and **V** (0.17 V) for the octa-cyano species, $CuPc(CN)_8$. Since the central Zn(II) metal is redox inactive, all oxidation and reduction processes observed are ring-based. The redox behaviour of complex **32** has been reported.[225] In comparison with **32** and other thiol-substituted ZnPc complexes[223,225,316] (Table 3.4), the oxidation process **I** observed at $E_{1/2}$ = 0.75 V vs SCE for **34** is assigned to ZnPc(-1) /ZnPc(-2). The four reduction processes at $E_{1/2}$ = - 0.68 (**II**), - 1.05 (**III**), –1.57 V (**IV**) and –1.73 V (**V**) vs SCE are assigned to ZnPc(-2)/ZnPc(-3), ZnPc(-3)/ZnPc(-4), ZnPc(-4)/ZnPc(-5) and ZnPc(-5)/ZnPc(-6), respectively.

Table 3.4: Comparison of redox potentials for **34** with those for **32** and other ZnPc complexes. Solvent = DMF containing TBAP. Pc(-2) = phthalocyanine dianion.

ZnPc Complex	$E_{1/2}$ (V vs SCE)					Reference
	I Pc^{-1}/Pc^{-2}	**II** Pc^{-2}/Pc^{-3}	**III** Pc^{-3}/Pc^{-4}	**IV** Pc^{-4}/Pc^{-5}	**V** Pc^{-5}/Pc^{-6}	
ZnPc	0.67	-0.86	-1.30	-1.85	-2.25	223
ZnOBTPc (**32**)	0.62	-0.83	-1.18	-	-	225
ZnOMPPc (**34**)	0.75	-0.68	-1.05	-1.57	-1.73	This work
ZnOHETPc[1]	0.64	-0.74	-1.11	-1.76	-	316

[1] value obtained in dimethylsulphoxide

The anodic to cathodic peak separations ($\Delta E_p = E_{pa} - E_{pc}$) were found to range between 60 and 200 mV. The oxidation process **I** was quasi-reversible in that it showed a more enhanced forward (anodic) peak compared to the return (cathodic) peak and a large ΔE_p value (200 mV). Reduction processes **II** and **III** showed a reversible behaviour in that the cathodic to anodic peak currents (i_{pc}/i_{pa}) were unity and ΔE_p ranged between 60 and 80 mV. A ΔE_p value of 80 mV was observed for the ferrocene internal standard. Process **IV** and **V** were found to be quasi-reversible with ΔE_p = 190 mV and i_{pc}/i_{pa} being greater than unity. The lack of total reversibility in some of the reduction couples is most likely due to the disaggregation and decomposition of the complex following a redox process.

The peak currents increased linearly with the square root of scan rates, for scan rates ranging from 5-800mVs^{-1}, suggesting diffusion-controlled reactions. The difference

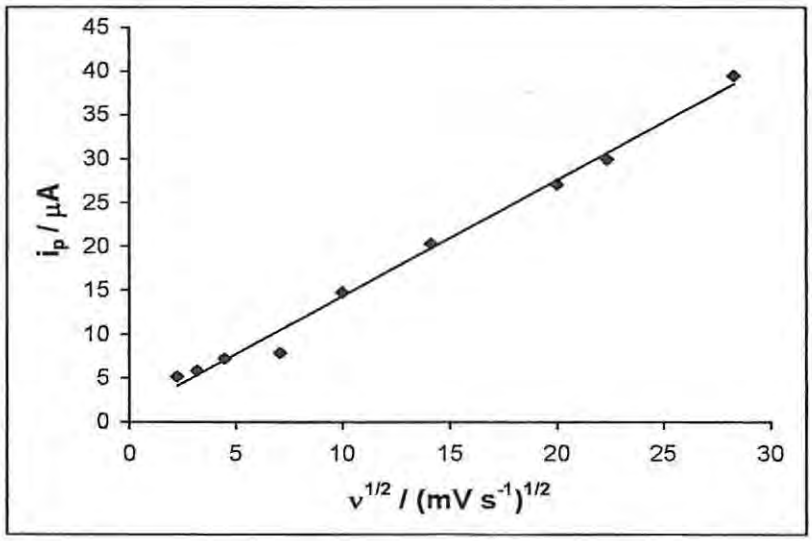

Figure 3.15: Plot of anodic peak current (reduction couple, **III** of ZnOMPPc, **34**) against the square root of scan rate.

between the first and second reduction processes for complex **34**, is 0.37 V, which compares with the average value for the first and second reduction processes of non transition metal phthalocyanine complexes.[223,248,316,376,377] The difference between the second and third reduction processes is 0.52 V, a value that perfectly agrees with literature values of various phthalocyaninatozinc(II) complexes.[223] For the main group metallophthalocyanine complexes, the potential separation between the first ring oxidation and the first ring reduction ($\Delta E^{o'}$), which corresponds to the magnitude of the energy difference between the HOMO and LUMO, is approximately 1.5 V.[32,223] The $\Delta E^{o'}$ value for ZnPcs containing eight peripheral thiol substituents ranges from 1.38 to 1.45 V (Table 3.4). Thus, the $\Delta E^{o'}$ value of 1.43 V observed for **34** falls within the range reported for similar complexes.

Repetitive scanning of the complex, **34**, resulted in considerable negative potential shift (> 0.2 V) of the cyclic voltammogram (CV) wave of the redox process **I**, which stabilized at about five scans (Figure 3.16 B, i to ii). The OSWV (Figure 3.16 A) clearly showed broad peaks, more defined compared to the first scan (Figure 3.14). However, using a fresh working electrode surface, the first scan (shown in Figure 3.16B i) is reproduced. Aromatic systems physisorb onto glassy carbon surfaces, implying that this change in peak shapes after a few scans may in part be attributed to the adsorption and formation of different products on the electrode. The two broad peaks in Figure 3.16A are most likely to be due to the oxidation of the aggregated and non-aggregated species of the ZnPc complex.[223,316] This is a reasonable assumption since the redox processes due to both aggregated and non-aggregated species can simultaneously be

observed as two closely spaced peaks if the aggregation-disaggregation equilibrium is slow in relation to the electrochemical timescale. [223,316]

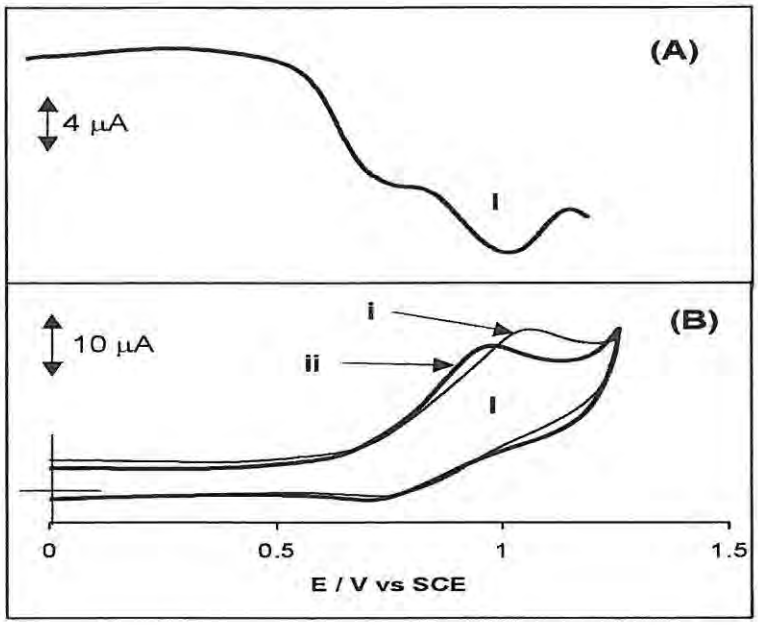

Figure 3.16: Comparative Osteryoung square wave voltammogram (A) and cyclic voltammograms (B) of the oxidation couple **I** of ZnOMPPc, **34** ($1x10^{-4}$ mol dm^{-3}) in DMF containing 0.1 mol dm^{-3} TBAP at first (i) and fifth (ii) scans. Scan rate = $100mVs^{-1}$.

Introduction of electron-donating substituents (such as the butanethiol and phenylthiol being investigated) to MPc ring should lead to an increase on the average electron density on the total conjugated ZnPc system leading to easier oxidation (and more difficult reduction) when compared to the unsubstituted ZnPc.[16] For **34**, contrary to expectation, oxidation is more difficult than for unsubstituted ZnPc. However, **32** is easier to oxidize than ZnPc (Table 3.4). It is surprising that the $E_{1/2}$ values for the reduction processes (**II** and **III**) for **32** do not show a corresponding difficulty in the reduction process, compared to ZnPc. The reason for this behaviour is not understood,

however, as evident from Table 3.4, all available reports show that thiol-derivatised ZnPc complexes tend to be more easily reduced than unsubstituted ZnPc. This abnormal behaviour put to question the actual role of these thiol-substituents on the MPc ligands. It can also be observed from Table 3.4 that this negative effect is more pronounced in the thiophenyl substituents than the alkylthio-substituted derivatives. This observation can be attributed to the delocalisation of the π-electrons of the phenyl ring substituent in **34**. This is perhaps not very surprising since Isaacs et al.[378] have observed similar behaviour where the extra benzene rings in cobalt naphthalocyanine caused strong electron withdrawing effects.

Electronic spectra have been successfully employed [229,379,380] to characterize anion and cation radical species in MPc. *In situ* UV-Vis spectroelectrochemistry using optically transparent thin layer electrode (OTTLE) cell was used to investigate the electrode reactions of **34**. This was performed by carrying out controlled coulometry at potentials corresponding to the $E_{1/2}$ values determined from the voltammetric experiments. The electronic absorption spectra were recorded before the application of the potential and then were periodically monitored as oxidation or reduction proceeded. Figure 3.17 shows the spectral changes observed on reduction of **34** at the applied potential of –0.70 V vs SCE, in the potential range of couple **II**. At this potential, the Q band decreased in intensity, with the formation of a broad band in the 560 to 650 nm region. These bands are characteristic of the monoanion phthalocyanine species, ZnPc(-3).[32,379] Isosbestic points were observed at 348, 412, 630 and 733 and 630 nm indicating uncomplicated conversion of the starting material to the reduced form. Oxidation of the reduced species at 0.00 V resulted in about 90% regeneration of the starting complex, confirming the

cyclic voltammetry data, which showed reversibility of process **II**, and showing that the electrogenerated reduced species is stable in DMF solutions. Oxidation of complex **34** at potentials of process **I** (not shown) also resulted in the decrease of the Q band and formation of a weak broad band near 580 nm, typical of the spectral changes for one-electron oxidation of the phthalocyanine ring to a π-cation radical species.[381] However,

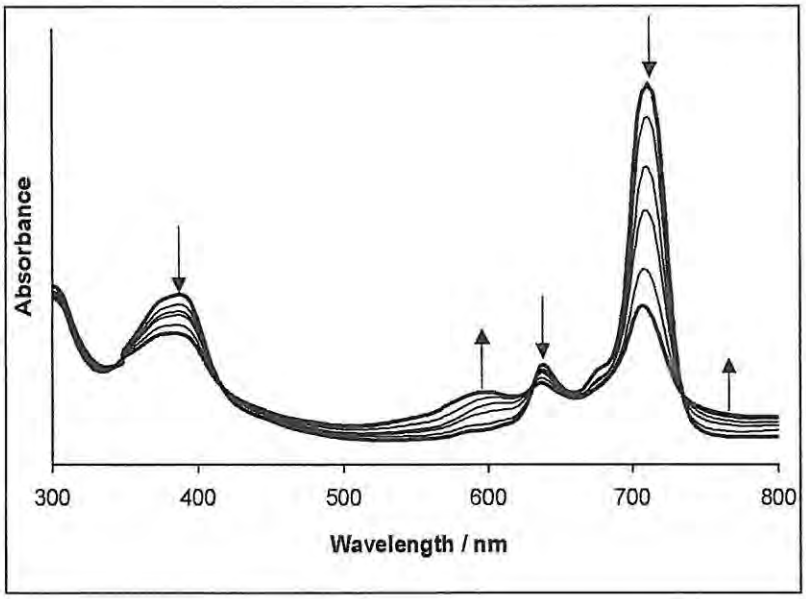

Figure 3.17: Changes in spectral features observed for complex ZnOMPPc, **34** ($1x10^{-4}$ mol dm^{-3} in DMF containing 0.1 mol dm^{-3} TBAP) during the controlled potential reduction at – 0.70 V vs. SCE in the OTTLE cell.

re-reduction of the oxidized species at 0.0 V resulted in about 60 % recovery of the spectra of the starting species, confirming the lack of complete reversibility observed from the cyclic voltammogram (Figure 3.14); an indication of possible loss of the starting material via oxidative decomposition and/or existence of coupled chemical reactions.

3.3.2 Thiol-derivatised Cobalt Phthalocyanine Complexes

Typical cyclic voltammogram of CoOBTPc, **33** (~ 10^{-4} mol dm^{-3}) in DMF containing TBAP is shown in Figure 3.18. Solvents or supporting electrolytes play a

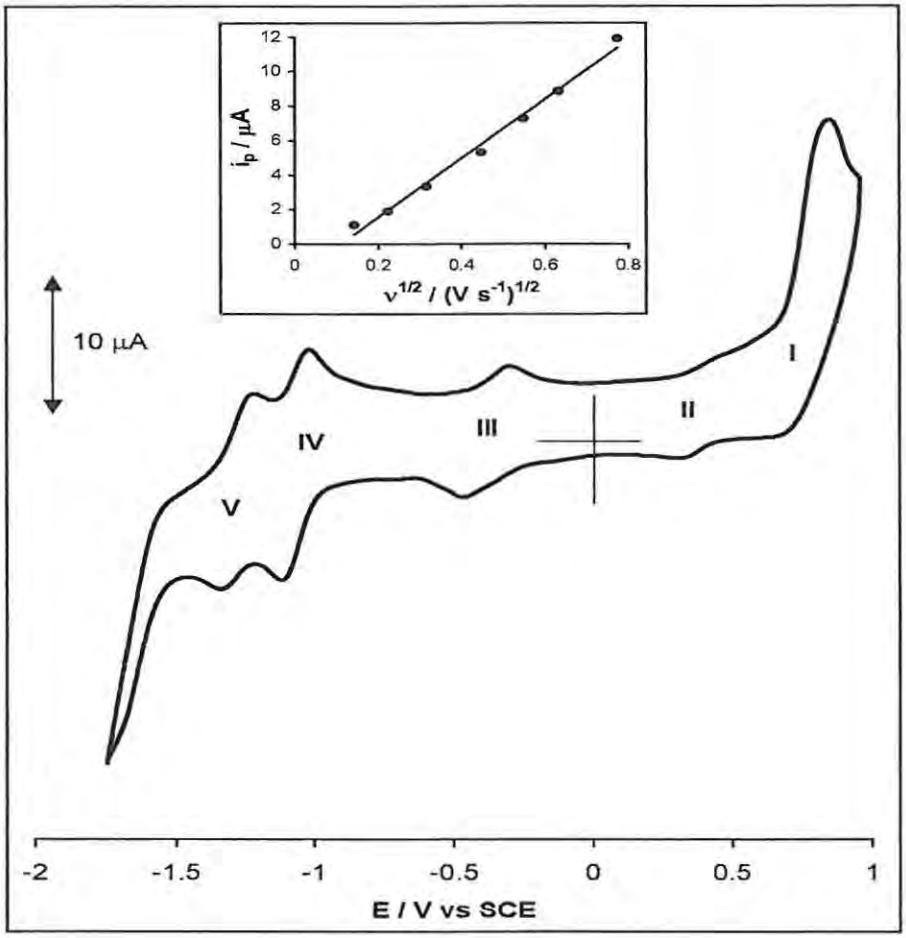

Figure 3.18: Cyclic voltammogram of 1 x 10^{-4} mol dm^{-3} of CoOBTPc, **33**, in DMF containing 0.1 mol dm^{-3} TBAP. Scan rate = 100mV/s. Inset: plot of peak currents (reduction couple **III**) against the square root of scan rate.

major role in the electrochemistry of $Co^{(II)}Pc$ complexes.[223] Donor solvents (such as DMF or DMSO) or coordinating counterions in non-donor solvents (e.g. dichloromethane) strongly favour $Co^{(III)}Pc$ by coordinating along the axis thereby forming the six

coordinate species, $(L)_2Co^{(III)}Pc$. In the absence of strong-donating solvents, the oxidation of $Co^{(II)}Pc$ to $Co^{(III)}Pc$ is inhibited, hence ring oxidation occurs first. Figure 3.18 is a cyclic voltammogram of CoOBTPc(-2), **33** in the presence of a coordinating medium, DMF/TBAP electrolyte system. From the above discussion, therefore, couples **I** and **II** correspond to ring-based $[Co^{(III)}Pc(-1)]^{2+}/[Co^{(III)}Pc(-2)]^{+}$ and metal-based $[Co^{(III)}Pc(-2)]^{+}/[Co^{(II)}Pc(-2)]$ redox couples, respectively. The first reduction couple, **III**, is assigned to metal-based redox couple $[Co^{(II)}Pc(-2)]/[Co^{(I)}Pc(-2)]^{-}$ since $Co^{(II)}$ is reduced before the ring in both donor and non-donor solvents. Redox couples **IV** and **V** are both ring-based $[Co^{(I)}Pc(-2)]^{-}/[Co^{(I)}Pc(-3)]^{2-}$ and $[Co^{(I)}Pc(-2)]^{2-}/[Co^{(I)}Pc(-4)]^{3-}$, respectively. The redox potentials obtained for CoOBTPc(-2), **33** are consistent with those reported in literature (Table 3.5) for other CoPc complexes.

The redox properties of octa(hydroxyethylthio)phthalocyaninatocobalt(II), CoOHETPc, **40**, are known and so were not investigated again here. In a recent study by Özkaya et al.[316] ring oxidation (couple **I**) was not observed for **40** in DMSO. The appearance of couple **I** for **33** was found to coincide with the oxidation side of couple **II** resulting to an ill-defined wave for this couple (**II**). The present study seems to be the first time a ring oxidation couple is observed in alkanethiol-derivatised CoPc. When the potential window was switched between –0.70 and 1.00V vs SCE (CV not shown), the $[Co^{(III)}Pc(-2)]^{+}/[Co^{(II)}Pc(-2)]$ process **II** was improved and showed a scan rate dependent i_{pc}/i_{pa} ratio which approached unity at higher scan rates (scan rate ranging from 10–600 mVs^{-1}). This behaviour has previously been observed for other CoPc complexes[223,316] and was attributed to the changes in the groups axially coordinated to the central cobalt ion upon oxidation.

Table 3.5: Comparison of redox potentials for CoOBTPc and CoOHETPc with those of other CoPc complexes. Solvent = DMF containing TBAP, unless otherwise stated.

$Co^{(II)}Pc$ Complex	$E_{1/2}$ (V vs SCE)				
	I	**II**	**III**	**IV**	**V**
	$[Co^{(III)}Pc(1)]^{2}$/ $[Co^{(II)}Pc(-2)]^{+}$	$[Co^{(III)}Pc(2)]^{+}$ /$[Co^{(II)}Pc(-2)]$	$[Co^{(II)}Pc(2)]$/ $[Co^{(I)}Pc(2)]^{-}$	$[Co^{(I)}Pc(2)]^{-}$/ $[Co^{(I)}Pc(3)]^{2-}$	$[Co^{(I)}Pc(3)]^{2-}$/ $[Co^{(I)}Pc(4)]^{3-}$
CoPc[1]	-	-	-0.37	-1.40	-
CoOBTPc, (**33**)[2]	0.77	0.40	-0.38	-1.07	-1.28
CoOHETPc,(**40**)[3]	-	0.43	-0.34	-1.22	-1.72

[1] ref. 223; [2] this work; [3] value obtained in dimethylsulphoxide , ref. 316

Table 3.5 lists the potentials for processes **I** to **V** (Figure 3.18) for CoOBTPc(-2), **33** and compares them with those reported for unsubstituted CoPc and an alkanethiol-derivatised CoPc, octa(hydroxyethylthio)phthalocyaninatocobalt(II) (CoOHETPc, **40**). For CoOBTPc(-2) the oxidation processes (**I**) and (**II**) were observed at $E_{1/2}$ = 0.77V and 0.40V vs. SCE. The three reduction processes were observed at $E_{½}$ = - 0.38 (**III**), - 1.07 (**IV**) and –1.28 V (**V**) vs. SCE. The anodic to cathodic peak separations ($\Delta E_p = E_{pa} - E_{pc}$) were found to range between 60 and 160mV. The oxidation process (**I**) was quasi-reversible in that it showed a more enhanced forward (anodic) peak compared to the return peak and a large ΔE_p value (160 mV). Reduction processes **III** - **V** showed reversible behaviour in that the cathodic to anodic peak currents (i_{pc}/i_{pa}) were unity and ΔE_p ranged between 60 and 80 mV. A ΔE_p value of 70 mV was observed for the

ferrocene internal standard. The peak currents increased linearly with the square root of scan rates, for scan rates ranging from 10 to 600mVs^{-1}, (Figure 3.18, inset) indicating that the electrode reactions are purely diffusion-controlled.

Table 3.5 shows that both CoOBTPc and CoOHETPc show little difference in their first reduction potentials when compared to CoPc; similar behaviour was observed for the ZnPc complexes described above. These data can only suggest a very weak influence of electron-donating substituents of the alkylthio-substituents on the average electron density of the phthalocyanine ligand.

3.3.3 Thiol-derivatised iron phthalocyanine complexes

Because of good solubility in DMF and high concentration (~10^{-4} mol dm^{-3}) required for the electrochemical investigation, $(DMF)_2$FeOBTPc (**37**), was chosen in preference to FeOBTPc (**35**) for this investigation. The redox properties of $(DMF)_2$FeOBTPc (**37**), (Figures 3.19) and FeOHETPc (**36**) (Figures 3.20) were studied using both CV and OSWV in DMF containing 0.1 mol dm^{-3} TBAP. The purity of these complexes is evident in their well-defined voltammograms. The potential values are listed in Table 3.6. The weak couple **I** is better resolved using OSWV. In comparison with other $Fe^{(II)}Pc$ complexes,[223] the weak couple **I** observed near 1.0V vs SCE is assigned to the ring oxidation couple $[Fe^{(III)}Pc(-1)]^{2+}/[Fe^{(III)}Pc(-2)]^{+}$. Couple **II** is assigned to the metal-based oxidation, $[Fe^{(III)}Pc(-2)]^{+}/[Fe^{(II)}Pc(-2)]$, while the two reduction processes **III** and **IV** are assigned to $[Fe^{(II)}Pc(-2)]/[Fe^{(I)}Pc(-2)]^{-}$ and $[Fe^{(I)}Pc(-2)]^{-}/[Fe^{(I)}Pc(-3)]^{2-}$, respectively. Table 3.6 shows that both FeOHETPc (**36**) and $(DMF)_2$FeOBTPc (**37**) are more easily oxidized than either the unsubstituted FePc or

chloro-substituted complex, $FePc(Cl)_{16}$. Surprisingly again, like in the zinc and cobalt complexes, the $E_{1/2}$ values for the reduction processes **III** and **IV** do not show a corresponding difficulty in the reduction process.

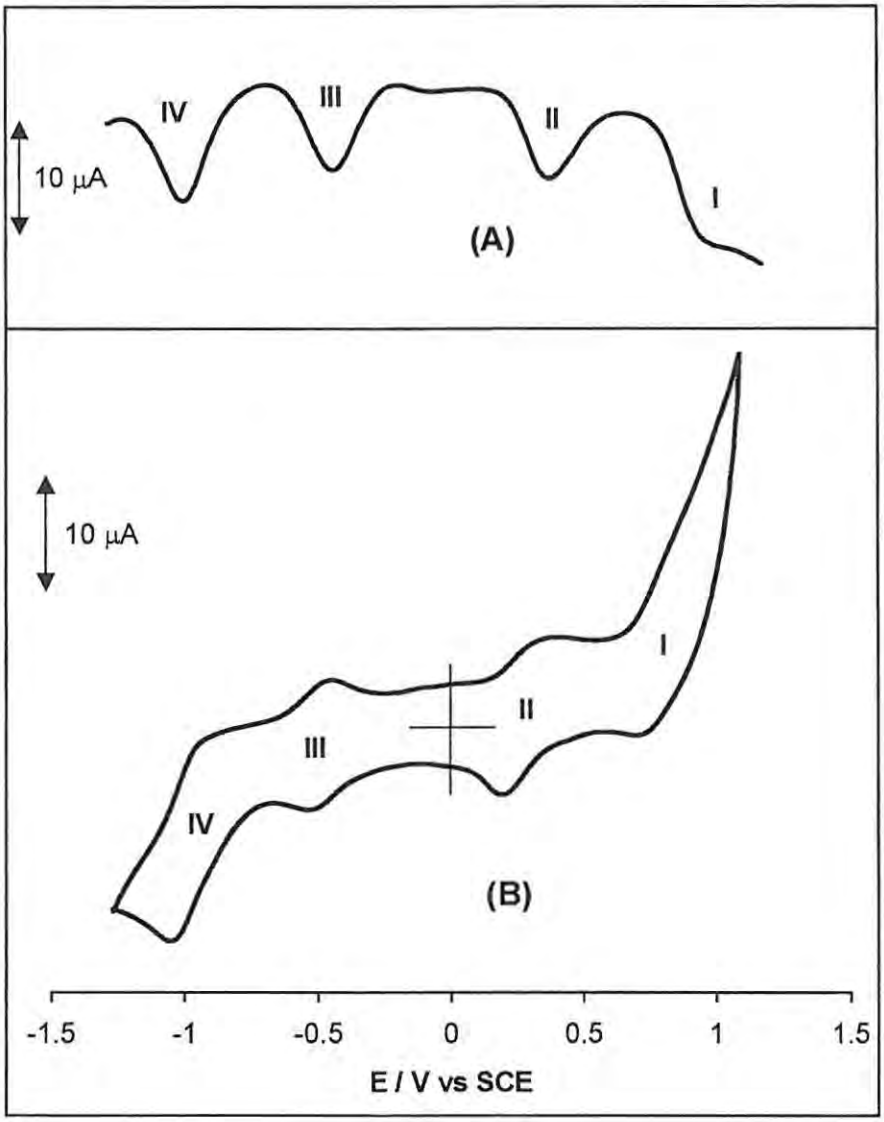

Figure 3.19: (A) Osteryoung square wave voltammogram and (B) cyclic voltammogram of $1x10^{-4}$ mol dm^{-3} of $(DMF)_2FeOBTPc$, **37**, in DMF containing 0.1 mol dm^{-3} TBAP. Scan rate = 100 mV s^{-1}.

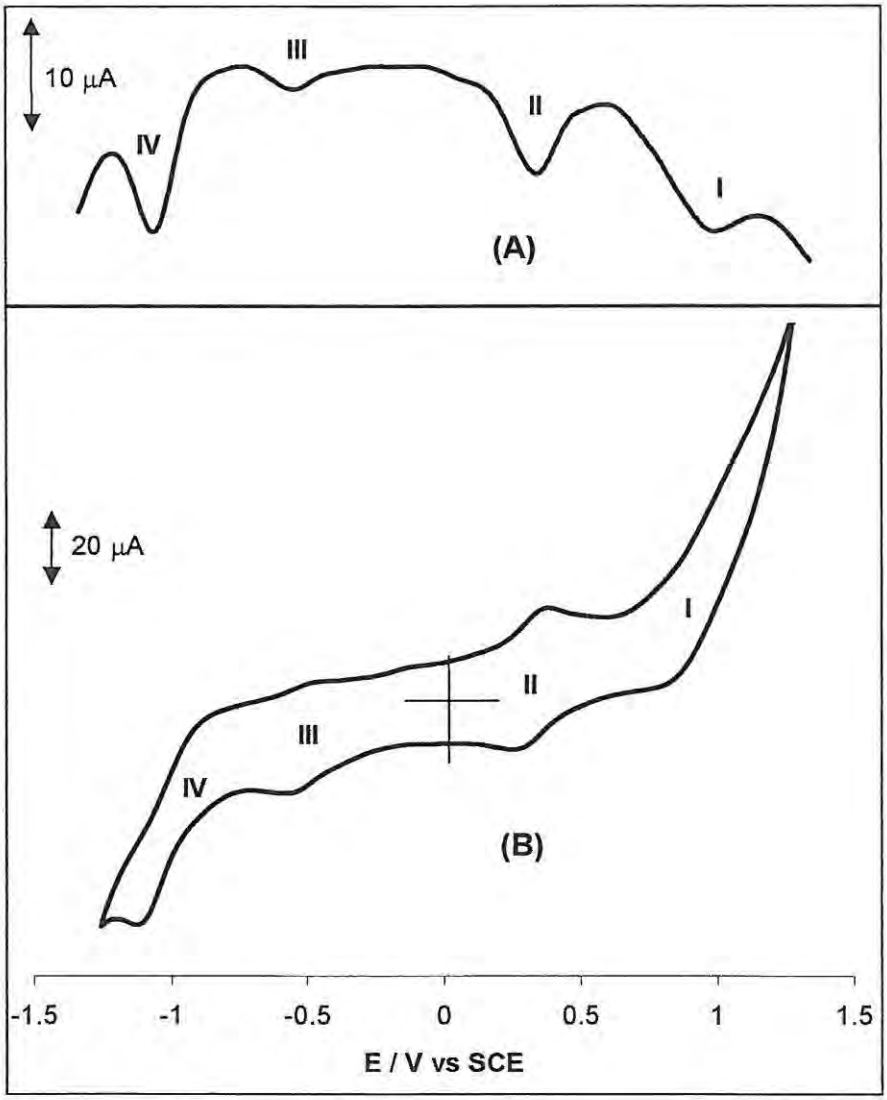

Figure 3.20: (A) Osteryoung square wave voltammogram and (B) cyclic voltammogram of $1x10^{-4}$ mol dm^{-3} of FeOHETPc, **36**, in DMF containing 0.1 mol dm^{-3} TBAP. Scan rate = 100 mV s^{-1}.

Table 3.6: Comparison of redox potentials of $(DMF)_2FeOBTPc$ with those of other FePc and complexes. Pc(-2) = phthalocyanine dianion. Solvent = DMF containing TBAP, unless otherwise stated.

$(L)_2Fe^{(II)}Pc$ Complex	$E_{1/2}$ (V vs SCE)			
	I	**II**	**III**	**IV**
	$[Fe^{(III)}Pc(-1)]^{2+}/[Fe^{(III)}Pc(-2)]^{+}$	$[Fe^{(III)}Pc(-2)]^{+}/[Fe^{(II)}Pc(-2)]$	$[Fe^{(II)}Pc(-2)]/[Fe^{(I)}Pc(-2)]^{-}$	$[Fe^{(I)}Pc(-2)]^{-}/[Fe^{(I)}Pc(-3)]^{2-}$
FePc [1]	-	0.37	-0.55	-1.17
$FePc(Cl)_{16}$ [2]	-	0.73	-	-1.11
$(DMF)_2FeOBTPc$ (**37**) [3]	0.91	0.26	-0.49	-1.00
FeOHETPc (**36**) [3]	0.90	0.31	-0.54	-1.01

[1] ref. 223 (data obtained in dimethylacetamide, DMA); [2] ref. 223; [3] this work

The anodic to cathodic peak separations ($\Delta Ep = E_{pa} - E_{pc}$) were found to range between 60 and 140mV for **36** and **37**. Couples **II** and **IV** showed quasi-reversible behaviour (ΔE_p values 140 and 110mV, respectively) and cathodic to anodic peak currents (i_{pc}/i_{pa}) greater than unity. For couples **II** and **IV**, the peak currents were found to increase linearly with the square root of the scan rates (for scan rates ranging from 10 – 800 mVs^{-1}) indicating that the electrode processes are purely diffusion-controlled. The reduction process **III** showed excellent reversible behaviour for **37** at high scan rates (> 100 mV s^{-1}) in that i_{pc}/i_{pa} equals unity and ΔE_p = 60 mV. For couple **III** of **36**, i_{pc}/i_{pa} deviated slightly from unity, however ΔE_p value equals 60 mV. The ΔE_p value for the ferrocene internal standard was observed at 70 mV.

CHAPTER 4

PHOTOSENSITIZED TRANSFORMATION OF CHLOROPHENOLS IN THE PRESENCE OF WATER-SOLUBLE METALLOPHTHALOCYANINE COMPLEXES*

* The following publications resulted from part of the research work presented in this chapter and they are not referenced further in this thesis:

1. K. Ozoemena, N. Kuznetsova and T. Nyokong, *J. Photochem. Photobiol., A: Chem.*, 2001, **139**, 217.
2. K. Ozoemena, N. Kuznetsova and T. Nyokong, *J. Mol. Catalysis, A: Chem.*, 2001, **176**, 29.

4.1 Photosensitized Transformation of 4-Chlorophenols

The photo-transformation studies for all the chlorophenols investigated in this work (shown in Figure 1.3) were performed in the visible region of the electromagnetic spectrum (i.e. Q band regions of the metallophthalocyanine photosensitisers) using the in-house photochemical set-up shown in Figure 2.1. The experimental conditions (including intensity of absorbed light) were kept constant for all the photosensitisers.

4.1.1 pH Studies

The stability and photosensitising abilities of phthalocyanine photosensitisers are known to be dependent on pH.[86] In micellar solutions, the photosensitizing activities of metallophthalocyanines towards the photo-transformation of phenols were shown to decrease with pH.[86] The quantum yields for the photo-oxidation of 4-CP using $AlPcS_4$ (**9**) $AlPcS_{mix}$ (**15**) and $ZnPcS_{mix}$ (**16**) as photosensitisers were found to increase with pH from pH 7, with a levelling off at pH 10, Figure 4.1. Hence pH 10 was employed for

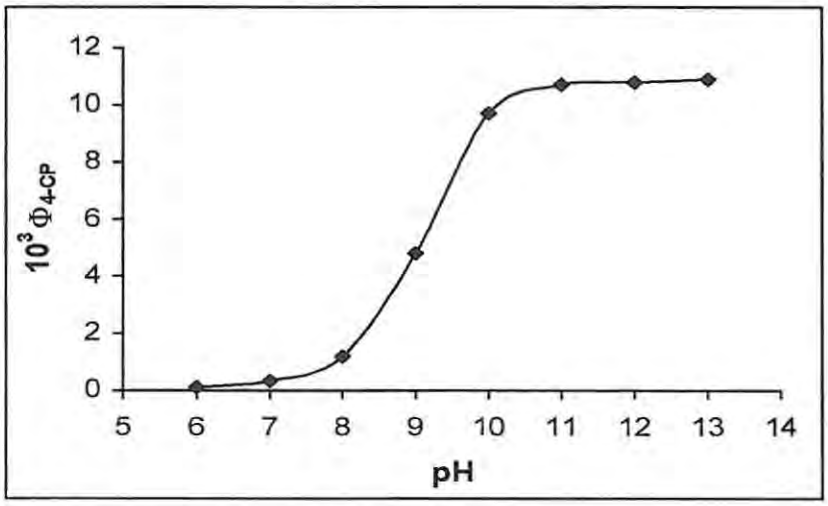

Figure 4.1: Dependence of quantum yield on pH for the transformation of 4-CP in the presence of AlPcSmix, **15**. [4-CP] = 3.5 x 10^{-5} mol dm^{-3}.

subsequent studies. In basic media, 4-CP with pKa = 9.4[207,382] is in its deprotonated phenolate form hence, it is more easily oxidizable, higher quantum yields for the photo-oxidation of 4-CP are thus obtained at high pH. The pH dependence of for transformation of 4-CP demonstrates an insignificant contribution of the unionised form of the 4-CP in the process (Figure 4.1).

4.1.2 Rates and Quantum Yields of 4-CP Photo-oxidation

Figure 4.2 shows the decrease in the concentration of 4-CP with time during irradiation in the presence of the various photosensitisers at pH 10. The disappearance of

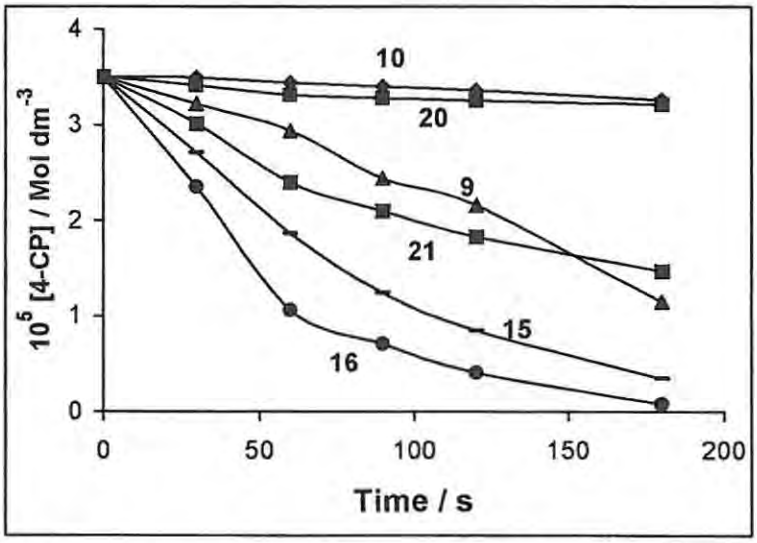

Figure 4.2: The dependence of concentration of 4-CP on time in the presence of the sensitisers; $ZnPcS_4$ (**10**), AlOCPc (**20**), $AlPcS_4$ (**9**), ZnOCPc (**21**), $AlPcS_{mix}$ (**15**) and $ZnPcS_{mix}$ (**16**); pH = 10. Photolysis in the Q band (λ = 670 nm) in the presence of an interference filter.

4-CP was monitored with HPLC. The results show that the photo-oxidation of the 4-CP occurred faster with the photosensitiser, $ZnPcS_{mix}$ (**16**) while the least activity was

observed for the $ZnPcS_4$ (**10**) and AlOCPc (**20**) sensitisers. The observed results show that the rate of the 4-CP photo-transformation depends on the sensitisers as follows:

$ZnPcS_{mix}$, **16** > $AlPcS_{mix}$, **15** > ZnOCPc, **21** > $AlPcS_4$, **9** > AlOCPc, **20** ≈ $ZnPcS_4$, **10**

Values of quantum yields ($\Phi_{4\text{-CP}}$) for 4-CP photosensitised oxidation are summarised in Table 4.1. It was found that two main factors determine photosensitiser activity: efficiency of singlet oxygen generation and sensitiser photostability. The data presented in Table 4.1 show that the rates and $\Phi_{4\text{-CP}}$ for photo-oxidation decrease as the singlet oxygen oxygen quantum yields (Φ_Δ) of the photosensitisers decrease, with the exception of **21**. The relatively low activity of **21** when compared to **16** and **15** is most probably due to high photo-degradation rate (Table 4.1), since its spectral characterization showed monomeric properties and its singlet oxygen quantum yield ($\Phi_\Delta = 0.52$) is relatively high. All the AlPc complexes are relatively stable (Table 4.1) thus degradation is not an important factor in their photosensitising abilities. Aggregation in ZnPc complexes influences photo-transformation of 4-CP since the monomeric complexes (e.g. **21**) show higher degree of transformation of 4-CP than aggregated species (e.g. **10**), Table 4.1. The relatively high efficiency of **16** as shown by Figure 4.2 is surprising considering the fact that this complex shows extensive photo-degradation (35%, Tables 3.1 and 4.1). This could be a result of its relatively high singlet oxygen quantum yield ($\Phi_\Delta = 0.48$). The little activity of the **10** towards the transformation of 4-CP is due to the extensive aggregation in solution (see Figure 3.1). Aggregated MPc complexes are photo-inactive due to rapid energy dissipation after excitation.[182] The aluminium species (AlOCPc, **20**) is also virtually inactive towards the transformation of 4-CP, even though it shows monomeric absorption properties and low degradation. This might be due to the association between

the axial hydroxyl groups in this sensitiser via hydrogen bonding as suggested before,[372] hence the low $\Phi_\Delta = 0.12$.

Table 4.1: Photosensitisation data for 4-CP transformation in the presence of various water-soluble metallophthalocyanine sensitisers under wavelength, $\lambda = 670$ nm irradiation[a].

MPc Sensitiser	Φ_Δ	4-CP Photo-transformation		
		Rate / 10^7 mol dm^{-3} s^{-1}	$\Phi_{4\text{-CP}}$	MPc Photo-degradation[b] %
$AlPcS_4$, **9**	0.18	0.93	0.0040	0
$ZnPcS_4$, **10**	<0.01	< 0.5	< 0.002	0.5
$AlPcS_{mix}$, **15**	0.38	2.70	0.0097	0
$ZnPcS_{mix}$, **16**	0.48	4.07	0.0140	35
AlOCPc, **20**	0.12	< 0.5	< 0.002	1.3
ZnOCPc, **21**	0.53	1.68	0.0059	51

[a] Conditions: pH 10, [4-CP] = 3.5×10^{-5} mol dm^{-3}

[b] After 180 seconds of irradiation of the Q band with visible light

Figure 4.3 shows the change in the absorbance of ZnOCPc (**21**) with photolysis time under the Q band excitation and pH 10 conditions. ZnOCPc (**21**) readily disappeared showing that this complex is not stable. Photo-degradation of **21** was observed in the absence of 4-CP and the effect of 4-CP (1×10^{-4} mol dm^{-3}) on the rate of the degradation was minimal (Figure 4.3). This result shows that the interaction between sensitiser and 4-CP has negligible influence on its photo-degradation under the experimental conditions. When an aqueous solution containing **21** was photolysed in the presence of the singlet

oxygen quencher, sodium azide, NaN_3 (5×10^{-3} mol dm^{-3}), the rate of photo-degradation of **21** did not change, suggesting that a mechanism other than attack by singlet oxygen, $O_2(^1\Delta_g)$ could be involved in its photo-degradation.

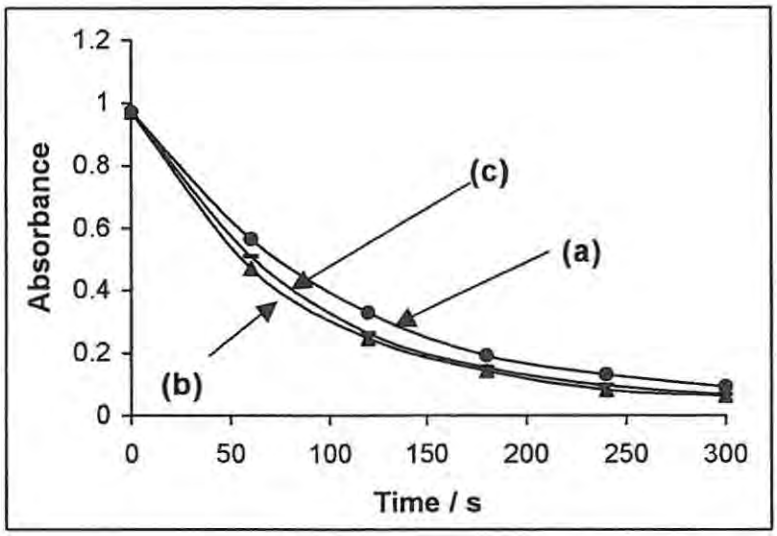

Figure 4.3: Changes in absorbance of ZnOCPc, **21** with time in the absence (a) and presence (b) of 1 $x10^{-4}$ mol dm^{-3} 4-CP; (c) of 5×10^{-3} mol dm^{-3} NaN_3. pH = 10. Photolysis in the Q band (λ = 670 nm) using an interference filter.

For practical applications of these water-soluble photosensitisers, it is important to study the photo-oxidation of 4-CP without the use of the interference filter. The time dependence of the concentration of 4-CP during photolysis in the presence of the various photosensitisers and excitation with light of wavelength, $\lambda > 600$ nm was studied. Under these conditions, both the monomer and dimer components of the Q band were exposed to radiation for complex **10**, while the dimeric component of the Q band was cut off in the presence of the interference filter. Absence of the interference filter did not significantly affect the dependence of 4-CP transformation on the photosensitisers.

The products of photo-transformation of 4-CP were identified using HPLC (Figure 4.4) as explained in the experimental section. A new peak with a retention time of

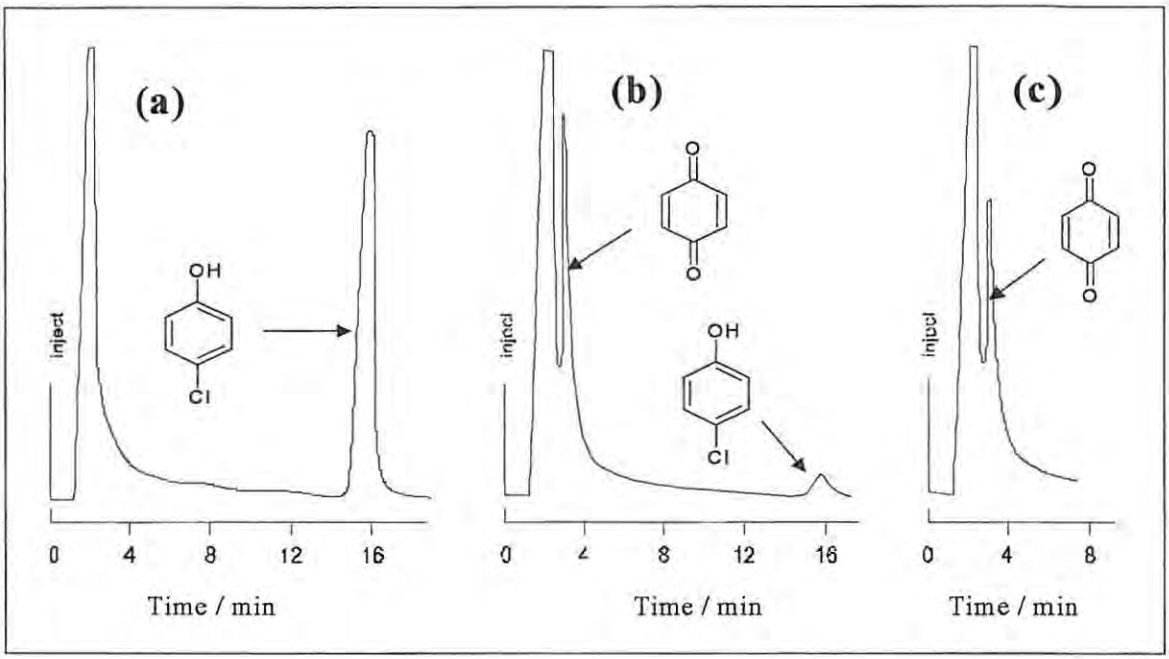

Figure 4.4: Typical HPLC traces for the photo-oxidation of 4-CP (a) before and (b) after 16 min of photolysis; (c) corresponds to the HPLC trace for *p*-benzoquinone used as standard. Photosensitiser = $AlPcS_{mix}$ (**15**) at pH 10.

3 min was observed when 4-CP was photolysed in the presence of **15**, which was identified as *p*-benzoquinone. During oxidation of phenols and 4-CP in alkaline medium, photocatalysed by MPcs, *p*-benzoquinone is the basic intermediate of the substrate photo-degradation.[85,86,383] It is well established[384,385] that *p*-benzoquinone is oxidized easily by oxygen in alkaline aqueous solution even in the absence of catalysts. The photo-transformation of 4-CP was also followed by UV-Vis spectrophotometry, and *p*-benzoquinone was detected after a photolysis time of 4 min by its characteristic absorption at 245 nm. *p*-Benzoquinone was observed only in the presence of oxygen.

4.1.3 Kinetic Studies.

The kinetic studies were performed with the aim of answering some questions about the role of phthalocyanine-type sensitisers in the photo-transformation of 4-CP. The importance of Type I radical pathway and efficiency of Type II photo-oxidation (Scheme 1.9) of 4-CP with **15** and **16** as photosensitisers were investigated.

Singlet oxygen mediated photo-oxidation of 4-CP sensitised by sulphonated metallophthalocyanine complexes is well recognised.[85,86] However, Lang et al.,[85] using laser flash photolysis, have recently found that the interaction of excited singlet state of sulphonated aluminium and zinc phthalocyanine complexes with the 4-CP leads to the formation of phthalocyanine anion and substrate cation radicals, both of which can react with oxygen through the Type I radical pathway. Thus, besides oxidation by singlet oxygen, the interaction of 4-CP with the excited singlet state of the sensitiser is more important than is generally recognised.

To address the question of relative contribution of Type I reaction pathway in the overall quantum yields of 4-CP photo-oxidation, experiments were performed on inhibition of the sensitised reaction by the singlet oxygen quencher, NaN_3 (5×10^{-3} mol dm^{-3}). As shown in Figure 4.5 (A), addition of sodium azide to the oxygen saturated solutions containing low amounts of 4-CP (3.5×10^{-5} mol dm^{-3}) at pH 10 and **15** as a photosensitiser, resulted in strong (92%) inhibition of the transformation of 4-CP, hence proving that the singlet oxygen mediated Type II mechanism is the dominating route under these conditions. At a higher concentration of 4-CP (2.0×10^{-3} mol dm^{-3}) and in oxygen saturated solutions only 70% inhibition of the photo-oxidation of 4-Cp by NaN_3 was observed {Figure 4.5 (B)} hence about 30% of 4-CP is transformed through the

Type I process. The full inhibition of singlet oxygen in these experiments was confirmed by obtaining the same results using 5 x 10^{-3} and 5 x 10^{-2} mol dm^{-3} concentrations of NaN_3. These data show that the contribution of the Type I mechanism to overall quantum yields is concentration dependent and can be neglected only at low concentrations of substrates.

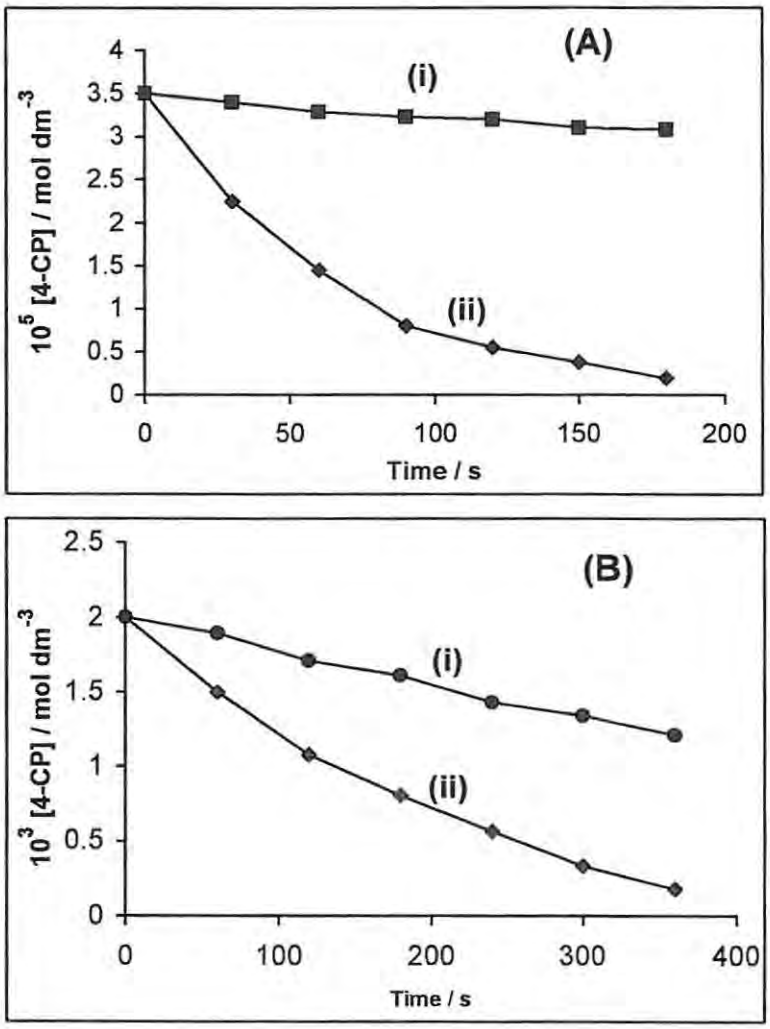

Figure 4.5: Effects of singlet oxygen quencher (sodium azide) on the rate of photo-transformation of (A) 3.5 x 10^{-5} mol dm^{-3} and (B) 2.0 x 10^{-3} mol dm^{-3} of 4-CP in the presence (i) and absence (ii) of 5 x 10^{-3} mol dm^{-3} sodium azide. Sensitiser = $AlPcS_{mix}$, **15**.

The kinetic parameters (k_d, k_q and k_r) described in the introduction section (Equations 1.12 – 1.14, and 1.29 and 1.30) for the chlorophenol photo-transformation were used in determining the 4-CP kinetics. According to equation 1.30, where ChP represents 4-CP,

$$\frac{1}{\Phi_{ChP}} = \frac{1}{\Phi_{\Delta}}\left(\frac{k_r + k_q}{k_r} + \frac{k_d}{k_r[ChP]}\right) \qquad 1.30$$

the plots of $1/\Phi_{4\text{-CP}}$ vs 1/[4-CP] (Figure 4.6) were used for the determination of the limiting value of quantum yields, Φ_∞, for the Type II photo-transformation of 4-CP in the

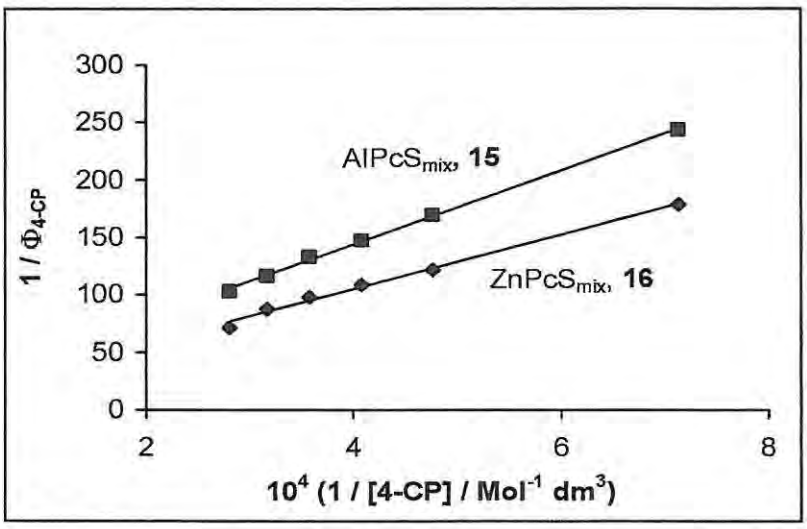

Figure 4.6: Plots of $1/\Phi_{4\text{-CP}}$ vs 1/[4-CP] for the photo-transformation of 4-CP in the presence of $AlPcS_{mix}$, **15** and $ZnPcS_{mix}$, **16.** pH = 10. Photolysis in the Q band (λ = 670 nm) using an interference filter.

presence of the two most efficient photosensitisers, $AlPcS_{mix}$ (**15**) and $ZnPcS_{mix}$ (**16**), under pH 10 conditions and 4-CP concentrations ranging from 1 x 10^{-5} to 5 x 10^{-5} mol dm^{-3} (i.e. mainly Type II mechanism conditions). The values of $\Phi_\infty = 0.10 \pm 0.03$ for **16** and of $\Phi_\infty = 0.07 \pm 0.01$ for **15** sensitised photo-oxidation of 4-CP phenoxide were

determined from the inverse of the y - intercepts of the plots shown in Figure 4.6. These Φ_∞ values are significantly lower than the Φ_Δ values (Table 4.1), indicating that not all the $O_2(^1\Delta_g)$ is involved in the chemical reaction with the quencher, Q (equation 1.13) (in this case, the 4-CP phenoxide). This observation shows that physical quenching of $O_2(^1\Delta_g)$ by the phenolate form of the 4-CP (Equation 1.14) competes strongly with the chemical reaction of $O_2(^1\Delta_g)$. The ratio between the rate constant for reactive quenching (*kr*) and the total quenching constant (*kr* and *kq*) is strongly dependent on the structure of the phenolic compounds,[386] and for 4-CP the value of this ratio is unknown. To compare efficiencies of chemical reaction and total quenching, the corresponding constants were calculated using equation 1.30. From the plots shown in Figure 4.6, slopes of 0.0032 ± 0.0008 mol dm^{-3} were obtained for **15** and 0.0024 ± 0.0001 mol dm^{-3} for **16**. These slopes are equal to $k_d / \Phi_\Delta k_r$ with $k_d = 1 / \tau_\Delta = 3.22 \times 10^5$ s^{-1} ($\tau_\Delta = 3.09 \times 10^{-6}$ s in water[387]). Using values of Φ_Δ in Table 4.1, k_r was calculated for the phenolate ion of 4-CP. From the plots, the values of k_r were (2.65 ± 0.3) x 10^8 mol^{-1} dm^{-3} s^{-1} and (2.80 ± 0.3) x 10^8 mol^{-1} dm^{-3} s^{-1} for **15** and **16** sensitisers, respectively. The closeness of these two values of k_r confirms that the choice of sensitiser has no effect on k_r.

The intercepts of the plots shown in Figure 4.6 equal $(k_q + k_r) / \Phi_\Delta k_r$. The intercepts were found to be 14.33 ± 3.00 for **15** and 9.67 ± 4.00 for **16**. The average value of k_r = (2.7 ± 0.3) x 10^8 mol^{-1} dm^{-3} s^{-1} for the phenolate ion of the 4-CP and Φ_Δ values from Table 4.1 were used to calculate the rate constant $(k_q + k_r)$ for the total quenching of $O_2(^1\Delta_g)$ by deprotonated 4-CP. The calculated values for $(k_q + k_r)$ are (14.7 ± 3.1) x 10^8 and (12.5 ± 5.2) x 10^8 mol^{-1} dm^{-3} s^{-1} with **15** and **16** as sensitisers, respectively giving an average value of (13.5 ± 3.0) x 10^8 mol^{-1} dm^{-3} s^{-1}. The total quenching rate constant (k_q +

k_r) of 4-CP phenolate ion is five times larger than the rate constant, k_r, for the photo-oxidation alone thus, most of the singlet oxygen is scavenged by a quenching process. The situation is similar to that of the other phenols, which quench singlet oxygen more rapidly than react with it.[206]

It is important to note that the chemical quenching constant (k_r) of 4-CP by $O_2(^1\Delta_g)$ in water had been determined earlier by Tratnyek and Holgné.[207] The method used by these authors[207] was based on k_r calculations from rates of phenol photo-oxidation and steady state concentration of $O_2(^1\Delta_g)$ determined separately with furfuryl alcohol. Thus, the k_r constants were obtained for diverse sets of phenols, the value of k_r for the deprotonated 4-CP was reported as 1.93×10^8 mol^{-1} dm^{-3} s^{-1}. However, it was noted that this k_r constant for 4-CP was low due to the depression of steady state concentrations of $O_2(^1\Delta_g)$ through physical quenching by the phenolate ion. Indeed, with steady state concentrations of $O_2(^1\Delta_g)$, determined in the same solution with the 4-CP, values of k_r were as high as 2.7×10^8 mol^{-1} dm^{-3} s^{-1}, and are close to those obtained in this study. The rate constants obtained in this work appear to be more precise than previously reported.[207]

Rates of photo-oxidation of undissociated 4-CP by $O_2(^1\Delta_g)$ were measured at the pH 6.5 (fraction of 4-CP dissociated at this pH is negligible, about 0.1%). The experiments under comparable conditions show that the rate of 4-CP reaction with $O_2(^1\Delta_g)$ is a factor of 20 lower than that for 4-CP phenoxide anion. The estimated k_r value for undissociated 4-CP is about 10^7 mol dm^{-3} s^{-1}, a result which agrees with literature data.[207]

4.2 Photosensitized Transformation of Polychlorophenols

4.2.1 Relative Efficiency of Sensitized Oxidation of Polychlorophenols

Figure 4.7 shows the decrease, with time, of the concentration of trichlorophenol (TCP) in the presence of the various MPc sensitisers at pH 7, on excitation of sensitiser in the Q band. In the absence of sensitiser no transformation of chlorophenol was observed.

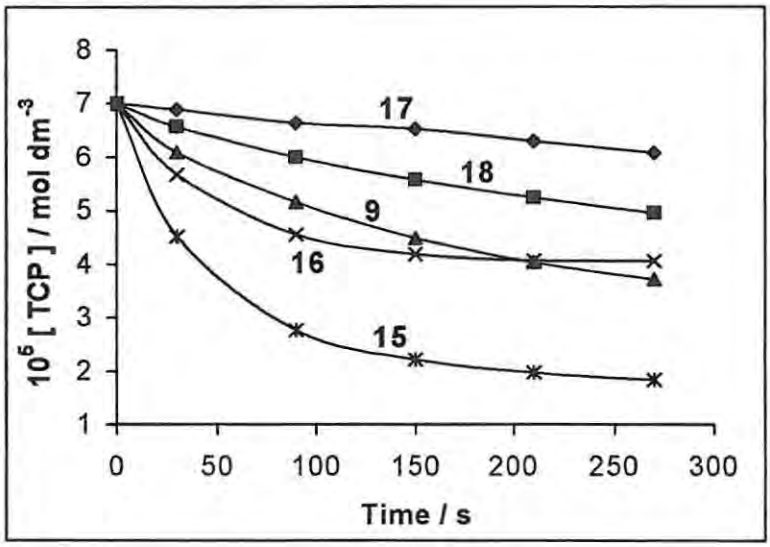

Figure 4.7: Kinetic curves for the photo-oxidation of TCP sensitised by $SnPcS_{mix}$ (**17**), $SiPcS_{mix}$ (**18**), $AlPcS_4$ (**9**), $ZnPcS_{mix}$ (**16**) and $AlPcS_{mix}$ (**15**); pH = 7.

The quantum yields of TCP (Φ_{TCP}) and pentachlorophenol, PCP (Φ_{PCP}) photo-transformation, sensitised by sulphonated MPc complexes were calculated and are listed in the Table 4.2. Values of Φ_{TCP} depend on the sensitiser as follows:

$AlPcS_{mix}$, **15** > $ZnPcS_{mix}$, **16** > $AlPcS_4$, **9** > $SiPcS_{mix}$, **18** > $SnPcS_{mix}$, **17**.

For PCP, the values of Φ_{PCP} depend on the sensitisers as follows:

$AlPcS_{mix}$, **15** > $AlPcS_4$, **9** > $SiPcS_{mix}$, **18** ≈ $ZnPcS_{mix}$, **16** > $SnPcS_{mix}$, **17**.

The trend for Φ_{PCP} is slightly different from that of the Φ_{TCP} since **16** is replaced by **9** in the second place, in the case of Φ_{PCP}.

Table 4.2: Photosensitisation data for the TCP and PCP transformation in the presence of the various water-soluble, sulphonated metallophthalocyanine sensitisers (sens) under wavelength, λ = 670nm irradiation. [TCP], [PCP] = $7x10^{-5}$ mol dm^{-3}.

MPc Sensitiser	Φ_Δ	TCP		PCP	
		$\Phi_{TCP} / 10^3$	% of MPc degradation*	$\Phi_{PCP} / 10^3$	% of MPc degradation*
$AlPcS_4$, **9**	0.18	5.40	< 1	4.50	8
$AlPcS_{mix}$, **15**	0.38	11.80	< 1	6.80	16
$ZnPcS_{mix}$, **16**	0.48	10.50	21	3.92	32
$SnPcS_{mix}$, **17**	0.46	< 2.00	38	< 2	46
$SiPcS_{mix}$, **18**	0.16	3.43	0	4.11	4

*After 270 s of irradiation.

The results of Table 4.2 show that the trend of photosensitiser activity for polychlorophenol oxidation differ from the trend in their Φ_Δ values in that **15** with a lower Φ_Δ than **16** and **17** shows a better Φ_{TCP} and Φ_{PCP}. Apart from the efficiency in $O_2(^1\Delta_g)$ sensitisation, there are other factors that influence the photo-transformation of chlorophenols. One of the important factors is the photostability of photosensitiser. From this point of view and considering TCP transformation, the highest activity, which is observed for $AlPcS_{mix}$, can be explained by its high level of singlet oxygen quantum yield and photostability in aqueous solution. The complex $ZnPcS_{mix}$ is less active despite highest efficiency of $O_2(^1\Delta_g)$ photosensitization (Φ_Δ = 0.48), and this behaviour may be

caused by its enhanced photo-degradation during the course of photolysis (21% photo-degradation for TCP after 270 s of illumination, Table 4.2). The activities of photostable $AlPcS_4$ and $SiPcS_{mix}$ are in accordance with their low Φ_Δ values. $SnPcS_{mix}$ is virtually inactive towards the photo-transformation of the substrates even though it showed a high Φ_Δ. This complex is a characteristic example of an extremely unstable photosensitiser. The slightly different trends in activity observed for photosensitisers towards TCP and PCP oxidation, e.g. the replacement of $ZnPcS_{mix}$ and $AlPcS_4$ complexes from the second place in PCP when compared to TCP, can be attributed to the influence of increased rate of photosensitiser's degradation in the presence of PCP when compared to TCP. The data shown in Table 4.2 and the kinetic curves for photosensitiser photobleaching, presented in Figure 4.8, demonstrate that Si and Al complexes are the most stable of all the sensitisers studied.

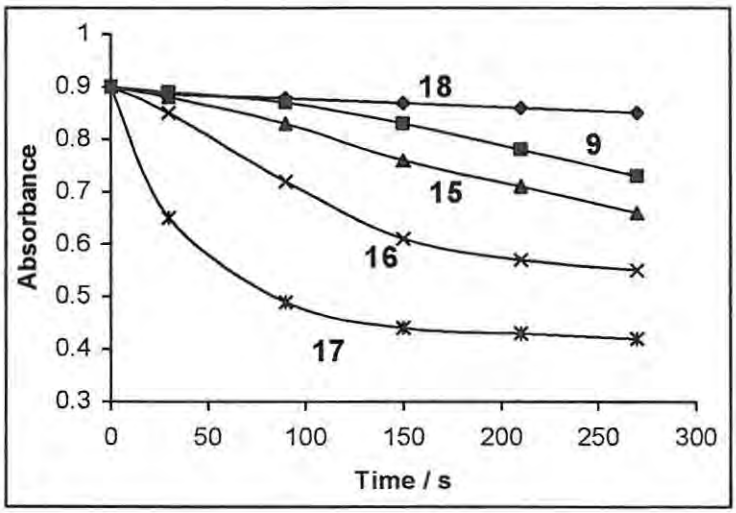

Figure 4.8: Kinetic curves for the photo-degradation of $SiPcS_{mix}$ (**18**), $AlPcS_4$ (**9**), $AlPcS_{mix}$ (**15**), $ZnPcS_{mix}$ (**16**) and $SnPcS_{mix}$ (**17**) in the presence of PCP. pH = 7.

4.2.2 pH Dependence

Polychlorophenols are fairly acidic and dissociate in aqueous solutions (pKa values of TCP and PCP are 6.2 and 4.7 respectively[111,115,207]). There are two species with different properties, which are in equilibrium in PCP or TCP solutions; these are the undissociated phenol (ArOH) and phenoxide ion (ArO^-). Since the equilibrium between these two forms is pH dependent, chemical transformations involving these compounds should be pH dependent as well. The dependence of pH on the following photochemical processes was observed in this work: photosensitised degradation of polychlorophenol, formation of *p*-benzoquinone related photoproducts and photobleaching of sensitiser. The results obtained are discussed below.

The dependence of Φ_{TCP} (using $AlPcS_{mix}$ as sensitiser) on pH (Figure 4.9a) is consistent with literature reports[135,207] and reflects insignificant contribution of the

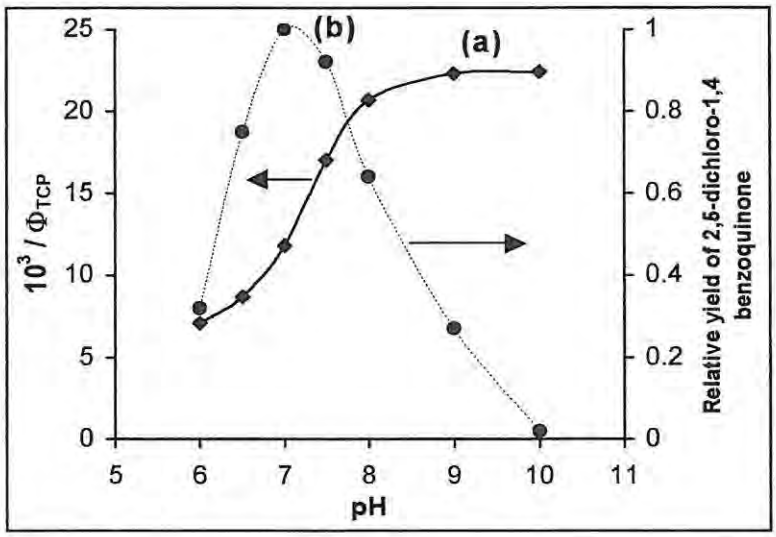

Figure 4.9: The pH dependence of (a) quantum yield for the transformation of 7 x 10^{-5} mol dm^{-3} TCP and (b) relative yields of 2,5-dichloro-1,4-benzoquinone formation using $AlPcS_{mix}$, (**15**) as sensitiser.

unionised form of polychlorophenols in the photo-oxidation. In accordance with pKa values, the rates and quantum yields of transformation of the polychlorophenols increase from pH 6 with a leveling off at pH 8 for TCP and at pH 7 for PCP.

Figure 4.10 represents spectral changes observed on photolysis of TCP and PCP in the presence of **15** under pH 7 conditions. The spectral changes show decrease of PCP absorption peaks at 248 nm and 320 nm and formation of photoproduct with λ_{max} at 290 nm. The TCP peaks at 312 nm decreased with photolysis and a product peak was observed at 272 nm. These transformations proceed with clear isosbestic points, indicating substrate oxidation to the end product with negligible accumulation of intermediates.

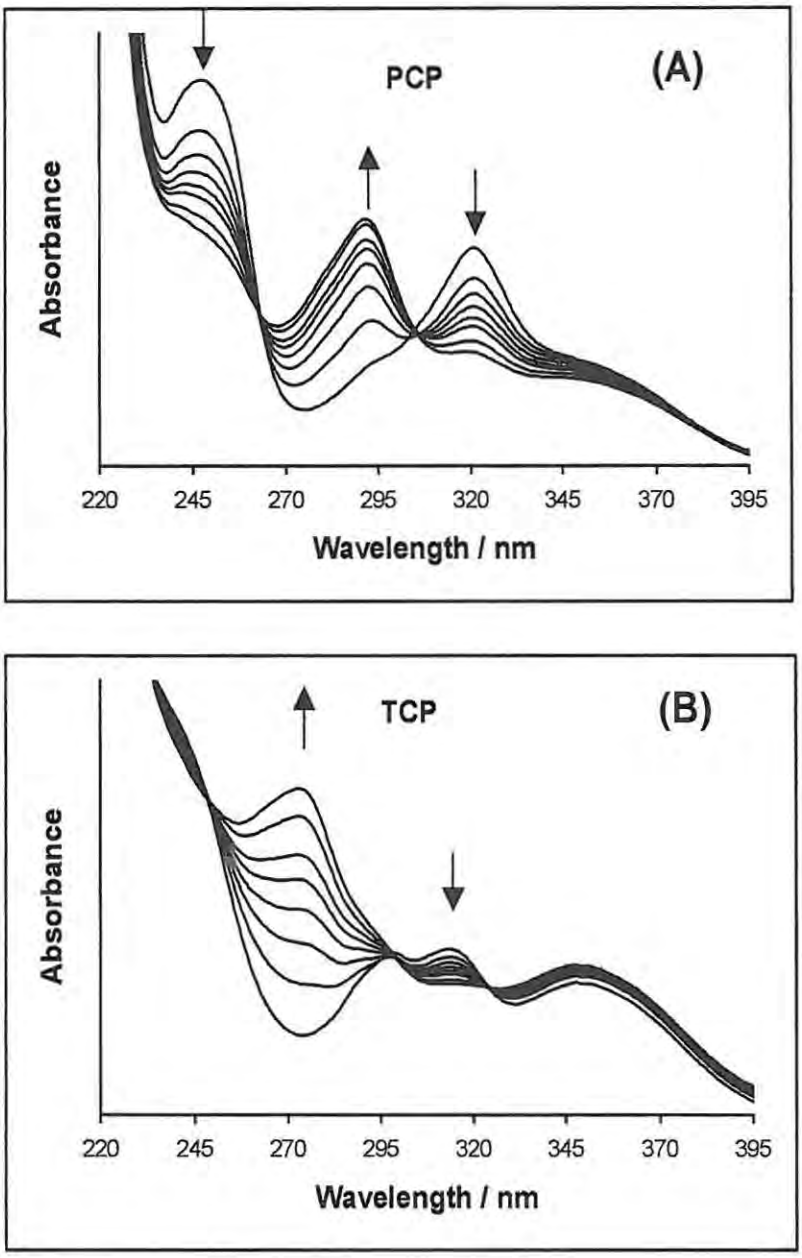

Figure 4.10: Electronic absorption spectral changes observed during photolysis of $7x10^{-5}$ mol dm^{-3} solutions of (A) PCP and (B) TCP in the presence of $AlPcS_{mix}$ (**15**) as sensitiser under pH 7 conditions.

The products for the photo-transformation of polychlorophenol oxidation were confirmed with HPLC studies, by spiking with standards such as 2,3,5,6-tetrachloro-1,4-benzoquinone for PCP and 2,5-dichloro-1,4-benzoquinone for TCP. Further continuous photolysis at pH 7 led to photo-oxidation of the primary products and the formation of new products (HPLC retention times of 5 min for TCP and 8.5 min for PCP (Figure 4.11). The secondary products formed are most likely due to further dechlorination of the ring as has been reported before.[135]

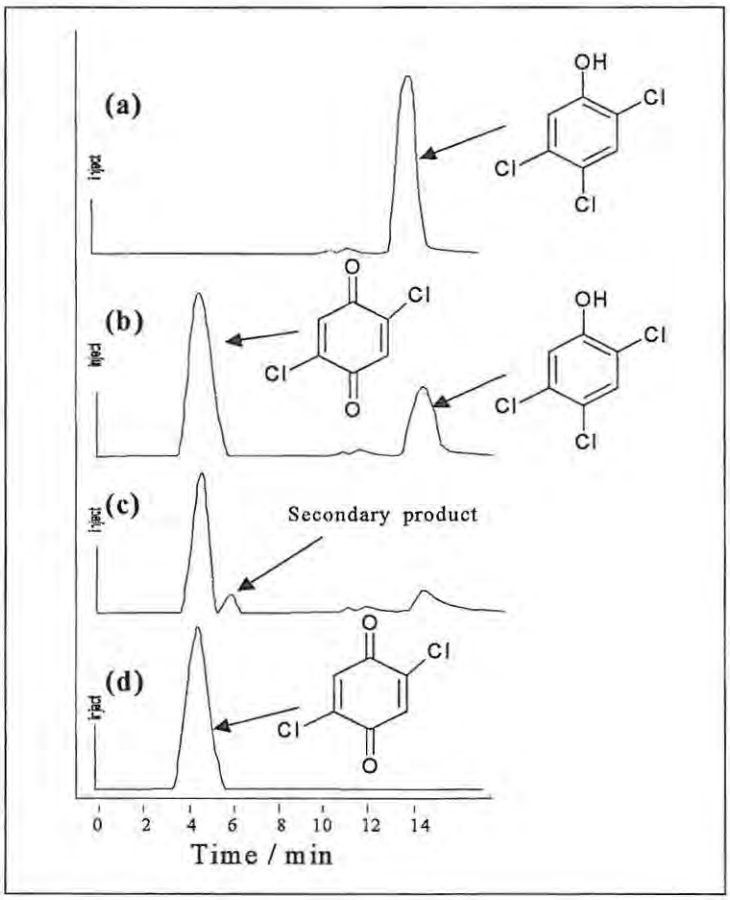

Figure 4.11: Typical HPLC traces for the photo-oxidation of TCP (a) before and, (b) after 3.5 min and (c) 7 min of photolysis using $AlPcS_{mix}$, (**15**) as sensitiser under pH 7 conditions; (d) corresponds to the HPLC trace for 2,5-dichloro-1,4-benzoquinone used as standard.

Photolysis of both TCP and PCP at pH 10 showed diffuse isosbestic points and broad maxima, indicating formation of complicated mixtures of photoproducts absorbing at the same wavelength region. Figure 4.12 shows the spectral changes observed during photolysis of PCP solutions in the presence of $AlPcS_{mix}$ (**15**) as sensitiser under pH 10 conditions. The pH dependence of the relative yield (determined from HPLC traces) for the formation of 2,5-dichloro-1,4-benzoquinone (the photo-oxidation product of TCP) using $AlPcS_{mix}$ (**15**) as a photosensitiser is shown in Figure 4.9b. Maximum selectivity and yield of benzoquinone derivative as a photoproduct was obtained at pH 7 for both PCP and TCP. Thus, the oxidation products of polychlorophenols are pH dependent and at high pH an increase in the rate of further oxidation of primary benzoquinone derivative is possible.

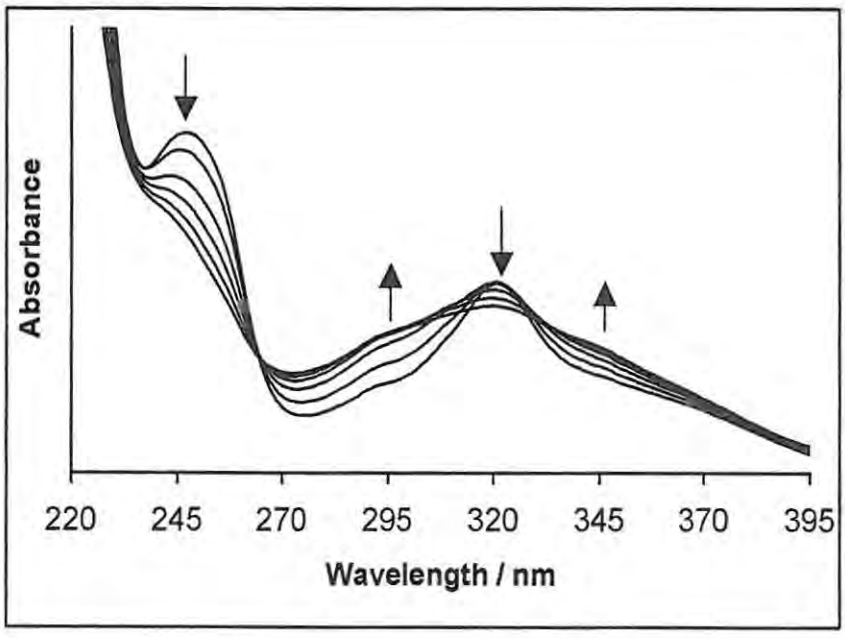

Figure 4.12: Electronic absorption spectral changes observed during photolysis of $7x10^{-5}$ mol dm^{-3} solutions of PCP in the presence of $AlPcS_{mix}$ (**15**) as sensitiser under pH 10 conditions.

Finally, photobleaching of the sensitiser during sensitised polychlorophenol oxidation was also found to be pH dependent. After 270 s of illumination of aqueous solution of $AlPcS_{mix}$ (**15**) containing PCP as substrate, the extent of sensitiser photobleaching was found to be 16% at pH 7 and 6% at pH10. In the absence of PCP no photobleaching of **15** was observed. This may suggest that the PCP or TCP are involved in the photobleaching of MPcs. Studies of the dependence of photobleaching of **15** on the nature of the substrate have shown that photo-degradation of photosensitiser is most pronounced for PCP, decreasing for TCP and being negligible for 4-CP and phenol. This suggests that electron-acceptor properties of phenols are of main importance in the photobleaching process. Electron transfer being directed from the excited sensitiser to polychlorophenol (equation 4.1) may be considered as a primary step in the Pc photobleaching process. It was found that addition of reductants stabilised the sensitiser, probably due to recovery of sensitiser from its semi-oxidised form (equation 4.3). Addition 5% v/v of ethanol as reductant resulted in 60% inhibition of **15** photo-degradation in the presence of PCP transformation. No effect of ethanol on the rate of PCP transformation was observed during this experiment. Similar results were obtained for other reductants such as sodium borohydride. Thus, based on the results obtained, the mechanism of photosensitiser photo-degradation may be represented by the following sequence of reactions 4.1 – 4.3:

$$MPc^* + PCP \longrightarrow MPc^{\bullet+} + PCP^{\bullet-} \qquad 4.1$$

$$MPc^{\bullet+} \longrightarrow \text{products} \qquad 4.2$$

$$MPc^{\bullet+} + red \longrightarrow MPc + red_{ox} \qquad 4.3$$

where red is the reductant. The fate of $PCP^{\bullet-}$ anion radical will be discussed below. This shows that PCP or TCP degrade also by Type I in addition to Type II.

4.2.3 Efficiency of Types I and II Processes

As stated above, at pH 7 polychlorophenols are oxidized to give 1,4-benzoquinone derivatives with high selectivity. Some aspects of the formation of these products were measured by following their appearance spectrophotometrically at 272 nm and 290 nm for TCP and PCP, respectively, using **15** since it is the most active sensitiser used in this work.

Although there is no study yet on the photo-oxidation of the polychlorophenols using the water-soluble sulphonated metallophthalocyanines, singlet oxygen-mediated photo-oxidation of chlorophenols (Type II mechanism) is an established process.[86,135,207] In order to determine the relative contribution of the Type I radical pathway when sulphonated metallophthalocyanines were employed as sensitisers, experiments were carried out in a solution containing the singlet oxygen quencher, NaN_3, in the presence of **15**. The data presented in Figure 4.13 shows that addition of NaN_3 ($2.5x10^{-3}$ mol dm^{-3}) to $7.0x10^{-5}$ mol dm^{-3} solution of PCP, containing **15** resulted in 76% inhibition of photo-transformation of PCP. The same experiments with TCP gave inhibition of Type II mechanism up to 83%. The extent of inhibition of photo-transformation was not changed by increasing the concentration of NaN_3 from 2.5×10^{-3} to 5×10^{-2} mol dm^{-3}, thus confirming the full quenching of $^1O_2(^1\Delta_g)$ in these experiments. The above results show the dominance of the Type II process; with just about 17% for TCP and 24% for PCP of the Type I process under the present experimental conditions. It also suggests the greater

participation of PCP to Type I process than TCP. The negative inductive effects of halogen substituents in aromatic rings results in electron-withdrawal from the benzene nucleus, deactivating it for an electrophilic attack by $O_2(^1\Delta_g)$ and hence decreasing the contribution of Type II pathway as the number of halogen substituents increase.

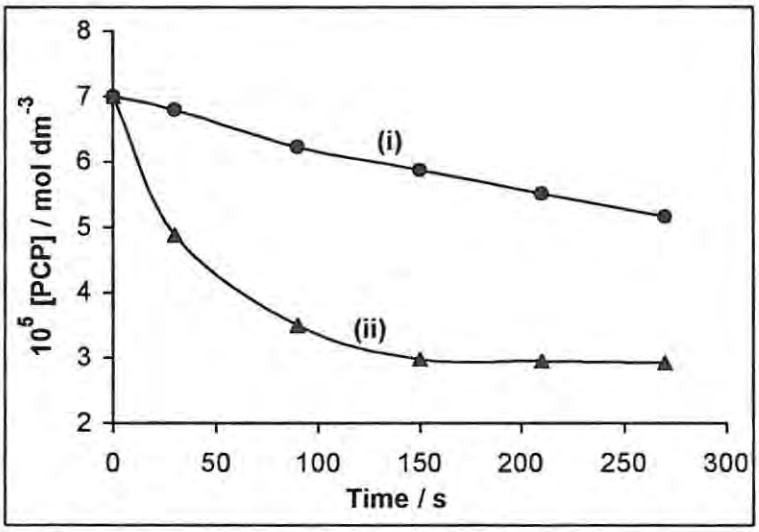

Figure 4.13: Effects of addition of singlet oxygen quencher (sodium azide) on the rate of photo-transformation of 7 x 10^{-5} mol dm^{-3} PCP in the presence (i) and absence (ii) of sodium azide, 2.5 x 10^{-3} mol dm^{-3}. Sensitiser = $AlPcS_{mix}$, **15**

With sulphonated methallophthalocyanines as sensitisers and phenols as substrates for Type I mechanism, the primary electron transfer from ionised substrate to the sensitiser in its excited state has been reported.[85] The formation of anion radical $AlPcS_{mix}^{\bullet-}$ in the presence of phenol was reported before[388] and the formation of this anion may be considered as confirmation of electron transfer from the substrate to the sensitiser. There is no evidence in this work to warrant the rejection of this generally accepted process for phenols. However, in the case of polychlorophenols, due to electron-

withdrawing effect of chlorine substituents the electron-donating ability of substrate is reduced and electron-acceptor ability is increased substantially. So, it is not surprising that results obtained in this work provide evidence for opposite direction of electron transfer – from excited sensitiser to polychlorophenol in the unionised form (see above and equation 4.1). This electron transfer leads to formation of polychlorophenol anion radical and sensitiser cation radical as primary species for Type I mechanism. Scheme 4.1 shows the transformation of the radical anion of polychlorophenol transformation to *p*-benzoquinone derivative, based on reductive dechlorination (reductive defluorination is an established process[388]).

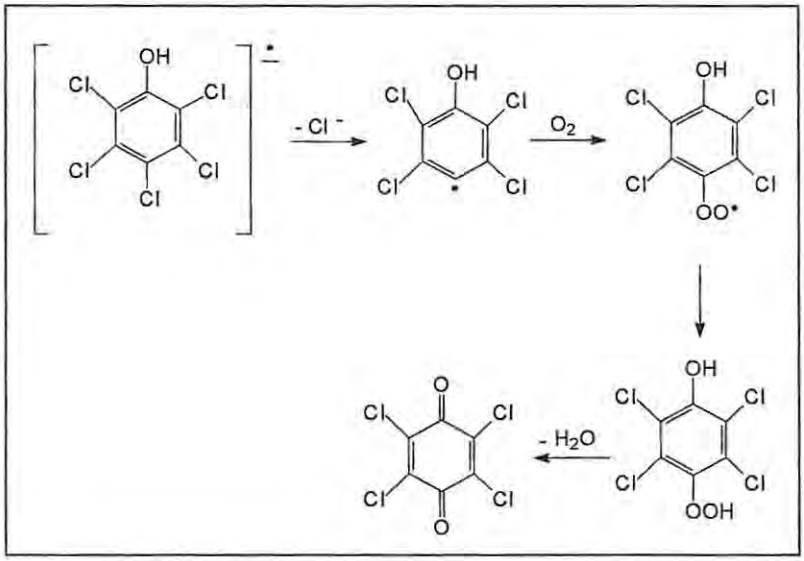

Scheme 4.1: Proposed mechanistic pathway for the photo-transformation of PCP in aqueous solution using MPc sensitiser.

It is worth noting that oxidation of ionised PCP by singlet oxygen remains as the main pathway, resulting in the formation of 1,4-benzoquinone derivatives. The interaction of PCP radical anion with oxygen may result in the recovery of the substrate

and the simultaneous production of the superoxide. In the series of substrates from phenol to 4-CP, TCP and PCP an increase in Type I mechanism was observed, which involves electron transfer from the excited sensitiser to the unionised form of the phenol derivative.

Considering the competitive and dominating Type II pathway, the reaction of singlet oxygen proceeds through processes described by equations 1.12 to 1.14. The quantum yield for the transformation of the polychlorophenol (Φ_{ChP}) is given by Equations 1.29 and 1.30. The overall chlorophenol quantum yields, Φ_{ChP}, involve contributions from both Type I and Type II (dominating) reactions. To determine limiting values of quantum yields Φ_∞ for photo-transformation of the polychlorophenols and other kinetic parameters (k_d, k_q and k_r), similar methods employed for 4-CP studies were also employed here. However, the photosensitiser $AlPcS_4$ (**9**) which is more stable in the presence of PCP or TCP was employed instead of $ZnPcS_{mix}$ (**16**) used for 4-CP. $ZnPcS_{mix}$ (**16**) is not photo-stable in the presence of PCP or TCP solutions. Also, all studies were performed in pH 7 instead of the pH 10 conditions used for the 4-CP. The plots of 1 / Φ_{ChP} vs 1 / [ChP] for TCP and PCP in the concentrations ranging from 2.5 to 7.0 x 10^{-5} mol dm^{-3} show linear relationship (Figure 4.14). Values of Φ_∞ were found for TCP to be: 0.048 ± 0.015 with **9** and 0.07 ± 0.015 with **15**, and for PCP: 0.032 ± 0.005 and 0.031 ± 0.005 with **9** and **15** respectively. Hence, the overall limiting quantum yields, consisting of radical and singlet oxygen contributions, are significantly lower than the Φ_Δ value of sensitisers (Table 4.2). The data again imply that not all the singlet oxygen is involved in the chemical reaction with polychlorophenols and that there is a strong competition

between the physical quenching and the chemical reaction of the $O_2(^1\Delta_g)$ by the phenolate ions.

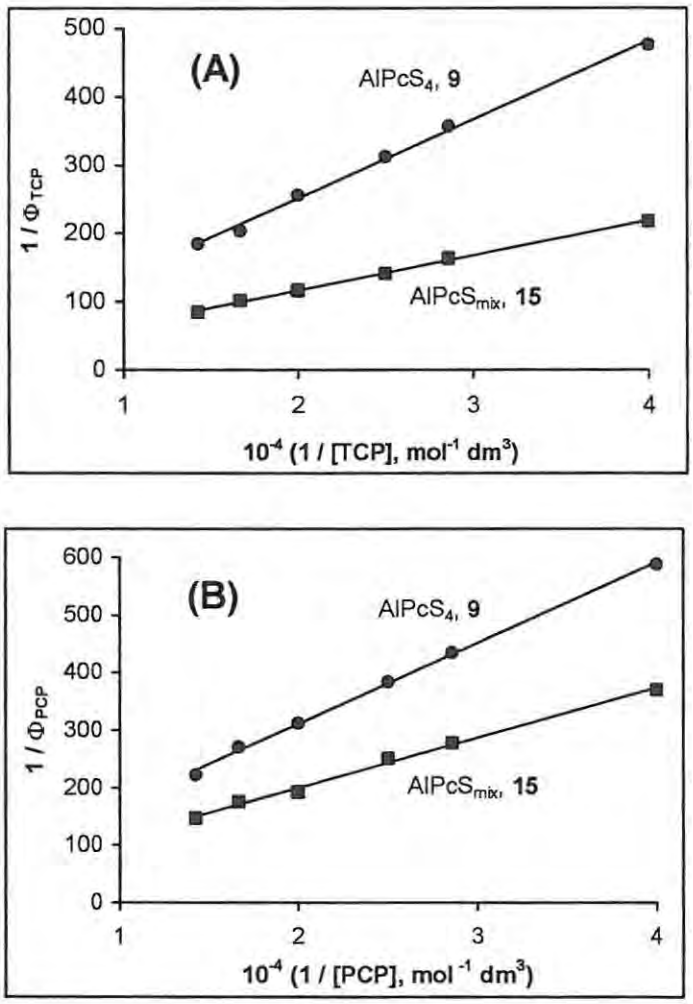

Figure 4.14: Plots of (A) 1 / Φ_{TCP} vs 1 / [TCP] and (B) 1 / Φ_{PCP} vs 1 / [PCP] for the photo-transformation of TCP and PCP in the presence of $AlPcS_4$, **9** and $AlPcS_{mix}$, **15** under pH = 10 conditions.

Neglecting the minor Type I contribution to Φ_{ChP}, the efficiencies of the reactive and physical quenching of $^1O_2$ for TCP and PCP were determined as described above for 4-CP. The ratio $k_q + k_r / k_r$ of the phenolate ion was obtained (with an error of ± 20%) to

be about 5 for TCP and 9 for PCP, implying that most of the $O_2(^1\Delta_g)$ is scavenged by a quenching process. Simply put, PCP for example, can deactivate about 9 molecules of $O_2(^1\Delta_g)$ before being destroyed. The slopes (k_d / Φ_Δ kr) of plots on Figure 4.14 were for TCP: 0.011 ± 0.003 mol dm^{-3} for **9** and 0.005 ± 0.001 mol dm^{-3} for **15**, and for PCP: 0.014 ± 0.002 mol dm^{-3} for **9** and 0.0085 ± 0.001 mol dm^{-3} for **15**. The rate constants k_r calculated for the chlorophenolate ions of the chlorophenols were: for TCP; (1.5 ± 0.2) x 10^8 mol^{-1} dm^3 s^{-1} for the **9** and (1.6 ± 0.2) x 10^8 mol^{-1} dm^3s^{-1} for **15**, while for PCP it was (1.2 ± 0.2) x 10^8 mol^{-1} dm^3 s^{-1} for **9** and (1.0 ± 0.2) x 10^8 mol^{-1} dm^3 s^{-1} for **15**. The reported k_r values for TCP and PCP are within these ranges.[207]

The average values of the total rate constants (k_r + k_q), determined from the intercepts of the plots, for the deprotonated substrates were (7.5 ± 1.5) x 10^8 mol^{-1} dm^3 s^{-1} for TCP and (10 ± 2) x 10^8 mol^{-1} dm^3 s^{-1} for PCP. The low solubility of TCP and PCP in acid media did not permit for the effective estimation of the rate constants, (k_r + k_q), for the protonated forms of these polychlorophenols.

In conclusion, it has been shown in this work that water-soluble metallophthalocyanines, especially the sulphonates, are efficient sensitisers of singlet oxygen generation. The use of these complexes as sensitisers for the photo-oxidative degradation of chlorophenols shows that the efficiency of the process depends not only on the singlet oxygen quantum yields of the sensitiser, but also on its stability and aggregation properties. This explains why, for example, $SnPcS_{mix}$ turned out to have high singlet oxygen quantum yield, but due to low photostability, the efficiency of this photosensitiser for the oxidation of polychlorophenols is low.

CHAPTER 5

SURFACE ELECTROCHEMICAL CHARACTERIZATION OF METALLOPHTHALOCYANINE SELF-ASSEMBLED MONOLAYERS (SAMs) ON GOLD ELECTRODES*

* The following publications resulted from part of the research work presented in this chapter and they are not referenced further in this thesis:

3. K. Ozoemena, P. Wesbroek and T. Nyokong, *J. Porphyrins Phthalocyanines*, 2002, **6**, 98.
4. K. Ozoemena and T. Nyokong, *Electrochim. Acta*, 2002, **47**, 4035.

Voltammetry is regarded as the most popular, convenient and sensitive technique for probing the structural properties of SAMs.[276,277] This is because information concerning the quality of SAM on gold can be conveniently obtained using cyclic voltammetric experiments in simple electrolytes. Electrochemical assessment of SAM on gold surface is based on the knowledge that thiol-derivatised SAMs act as physical barriers, preventing molecules in solution from getting close enough to the underlying gold surface.[276] Thus, cyclic voltammetric experiments in simple electrolytes have conveniently been used to measure the passivation ability of thiol-SAMs to the following Faradaic processes: electrochemical reduction of gold oxide (oxide stripping peak), ion permeation (electrochemical capacitance), underpotential deposition (UPD) of metals (usually copper) and heterogeneous electron transfer processes[276,289,307,309,389] as well as the Nernstian factors for surface-confined electroactive species.[276] These parameters were used in this thesis to interrogate the formation and integrity of the SAMs of the thiol-derivatised MPc complexes of iron (FeOBTPc, **35** and FeOHETPc, **36**), cobalt (CoOBTPc, **33** and CoOHETPc, **40**) and ZnPc (ZnOBTPc, **32** and ZnOMPPc, **34**) studied in this work. Iron and cobalt phthalocyanine, unlike the zinc phthalocyanine complexes, are redox active with respect to their central metals because of the easy accessibility of their d-orbital electrons.

For simplicity, the octabutylthio-metallophthalocyanine complexes (i.e. **32**, **33** and **35**) will herein be referred to collectively as MOBTPc (where M = Fe, Co and Zn) while the octahydroxyethylthio-metallophthalocyanine complexes (i.e. **36** and **40**) as the MOHETPc (where M = Fe or Co). Since only ZnPc complex was studied for the octa(4-methylphenylthio)phthalocyanine ligand, it will be represented as ZnOMPPc.

5.1 Passivation of Gold Surface Reaction

Figure 5.1 shows that in acidic pH, (0.1 mol dm^{-3} H_2SO_4) oxidation of bare gold electrode occurs in the region of 1.2 to 1.3 V vs Ag|AgCl with a well-defined reduction (gold oxide stripping) peak at 0.84 V vs Ag|AgCl. This cyclic voltammogram is consistent with the reported gold surface redox reaction in acidic conditions.[323] Similar CV results were also obtained in neutral conditions. However, unlike in acidic and neutral solutions, it was found in this work that in a 0.01 mol dm^{-3} KOH solution (between –0.2 and +0.6 V vs Ag|AgCl) a clearly defined bare gold redox couple (Figure 5.2 A – C, curves i) could be obtained. This is not surprising given that gold oxidation to the gold oxide is pH-dependent,[390] occurring at less positive potentials with increasing pH. The high positive potential in the acidic and neutral conditions, normally employed[289,389] to bring about the oxidation of bare gold in the pinholes usually present following the formation of SAMs, is known[389] to result in oxidative desorption of the SAM itself.

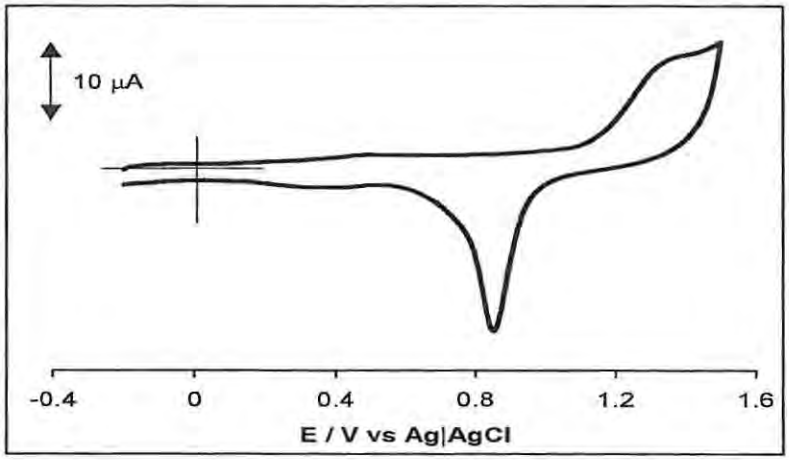

Figure 5.1: Cyclic voltammogram obtained for bare gold electrode (d = 0.8 mm) in blank. Electrolyte = 0.1 mol dm^{-3} H_2SO_4. Scan rate = 100 mV s^{-1}.

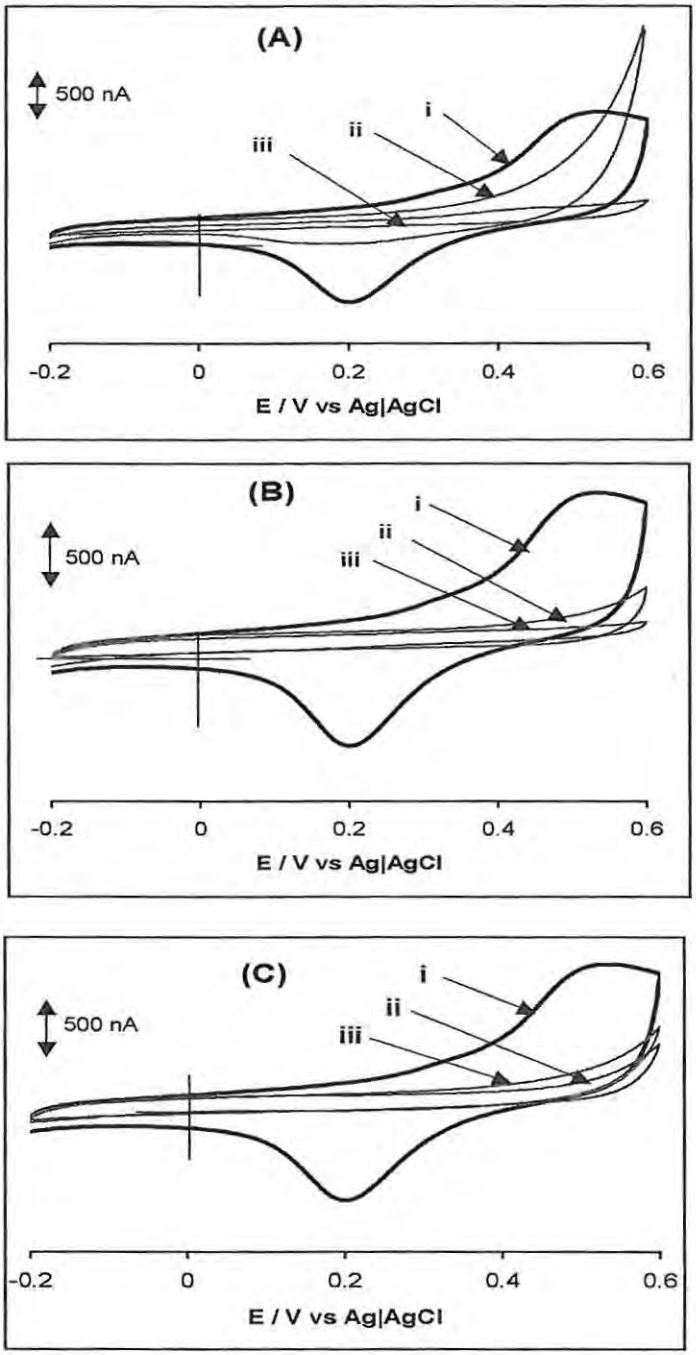

Figure 5.2: Cyclic voltammograms of gold electrode before (i) and after coating with the SAMs of (A) CoOHETPc, **40** (ii) and CoOBTPc, **33** (iii); (B) FeOHETPc, **36** (ii) and FeOBTPc, **35** (iii); (C) ZnOMPPc, **34** (ii) and ZnOBTPc, **32** (iii). Electrolyte = 0.01 mol dm^{-3} KOH. Scan rate = 25 mV s^{-1}.

The stability of all the MPc-SAMs studied in this work is dependent on potential, being stable at potentials less than 1.0V vs Ag|AgCl (see further discussion in section 5.7). It is important, therefore, that a low positive potential window where gold can be oxidized without adversely affecting the SAM is employed. Hence, alkaline pH was chosen for this study. The well-defined gold reduction (cathodic) peak in Figures 5.1 and 5.2A-C (curves i), as mentioned in the introduction {section 1.5.2.3(b)(iv)}, is due to the stripping of the gold oxide, hence the name "oxide removal or stripping peak".[289,389] The area under this cathodic peak is proportional to the amount of gold oxide formed in the forward scan. Hence, the oxide removal peak is regarded as a true measure of the total pinhole area available for an undisturbed penetration of ions present in the working solution. Figure 5.2 shows typical voltammograms obtained in alkaline solution (0.01 mol dm^{-3} KOH) performed on seven independent electrode modifications using the six MPc complexes. For both the bare gold (curves i) and MPc-SAM modified gold electrodes {curves ii for the MOHETPc (M = Co and Fe) and ZnOMPPc, and curves iii for the MOBTPc (M = Co, Fe and Zn) species}, the first and subsequent scans remained approximately the same, indicating electrode stability. It is clearly evident from Figure 5.2 that the broad gold oxidation peak and the corresponding reduction (gold oxide stripping) peak (curve i), are strongly blocked after coating the bare gold electrode with the MPc-SAMs. MOBTPc-SAMs (M = Fe and Co, Figure 5.2A and B, curves iii) showed stronger passivation than those of MOHETPc-SAMs (Figure 5.2A and B, curves ii) in that lower currents were obtained in the former. For ZnPc-SAMs (Figure 5.2C), ZnOMPPc showed slightly stronger blocking than ZnOBTPc. These results indicate that the gold surface is isolated from the aqueous solution, which is the oxygen source for

gold oxide formation by these MPc-SAMs. From equation 1.66 (from Chapter 1), the so-called 'ion-barrier factor', Γ_{ibf},[276] values (summarized in Table 5.1) were obtained.

$$\Gamma_{ibf} = 1 - \frac{Q_{SAM}}{Q_{Bare}} \qquad 1.66$$

The total charge, Q(μC) is obtained by integrating the currents (μAs^{-1}).

Table 5.1: Summary of ion-barrier factor (Γ_{ibf}) and interfacial capacitance (C_s) of the MPc-SAMs on gold electrodes studies in this work. Scan rate = 25 mVs^{-1}.

MPc-SAM	Γ_{ibf}	C_s / μF cm^{-2}
FeOBTPc, **35**	0.998 ± 0.002	1.1 ± 0.1
FeOHETPc, **36**	0.997 ± 0.002	1.2 ± 0.1
CoOBTPc, **33**	0.998 ± 0.004	0.8 ± 0.1
CoOHETPc, **40**	0.975 ± 0.005	1.7 ± 0.2
ZnOBTPc, **32**	0.997 ± 0.002	1.5 ± 0.2
ZnOMPPc, **34**	0.997 ± 0.002	1.5 ± 0.2

The charges under the gold oxide stripping peaks were estimated as ~ 4.0×10^{-6} C for the bare gold (Q_{Bare}) and ~1.0×10^{-7} C for the CoOHETPc-SAM modified electrodes (Q_{SAM}). For the CoOBTPc (Figure 5.2A iii), FePc (Figure 5.2B) and ZnPc (Figure 5.2C) derivatives, it was more difficult to detect any charge due to gold surface reaction after coating with the SAMs (Q_{SAM}), an indication of stronger passivation by CoOBTPc, FePc and ZnPc derivatives than the CoOHETPc-SAM to solvent ions. Table 5.1 suggests that about 2.5% of the gold surface is not covered by the CoOHETPc-SAM. However, since

the Γ_{ibf} values are close to unity for all the SAMs, it implies that these MPc-SAMs provide effective barriers to ion and solvent permeability to gold surfaces. Although the results cannot adequately be compared, as there has been no study on the "ion barrier factor" for any porphyrin or phthalocyanine SAM, it is interesting to note that the Γ_{ibf} value is usually close to unity for long-chain alkanethiol SAMs.[289,389]

5.2 Interfacial Capacitance

As already discussed in the introduction (Section 1.5.2.4), the lower the interfacial capacitance, C_s, the less defects there are in the SAM. From the charging current i_{ch} (A) in the region of 0.0 to -0.2V vs Ag|AgCl (Figure 5.2), the C_s ($\mu F\ cm^{-2}$) value was obtained using equation 1.65 and summarized in Table 5.1

$$C_s = \frac{i_{ch}}{vA} \qquad 1.65$$

where i_{ch} is the charging current (μA), A is the surface area of the electrode. The C_s value of the CoOBTPc (**33**) is lower than that of the corresponding CoOHETPc (**40**). For FeOBTPc (**35**) and FeOHETPc (**36**), and ZnOBTPc (**32**) and ZnOMPPc (**34**) complexes, the C_s values are almost the same for each pair. The C_s values for the MPc-SAMs lie between 23 and 50 times lower than the value (~ 40 $\mu F\ cm^{-2}$) obtained for the bare gold electrodes. Although the real surface area is larger than the geometric area, the specific C_s values obtained here are consistent with literature reports[276] in that the C_s values for most alkanethiol-derivatised SAMs are usually more than an order of magnitude smaller than the typical capacitances for bare gold. These C_s values were also found to be independent of different scan rates studied (10 - 800 mVs^{-1}). These data also imply that the SAMs are relatively free of defects, and with low permeability to the ions of the electrolyte.

In another method, a simple CV experiment of the SAMs were performed in pH 4 containing 1.0 mol dm^{-3} Na_2SO_4 as described elsewhere,[276] and the C_s was also estimated in the same potential region of 0.0 to -0.2V vs Ag|AgCl. As an example, Figure 5.3 shows CV responses of the FePc-SAMs using the pH 4 + 1.0 mol dm^{-3} Na_2SO_4 electrolyte system. Figure 5.3 shows that the presence of the FeOBTPc-SAMs on gold

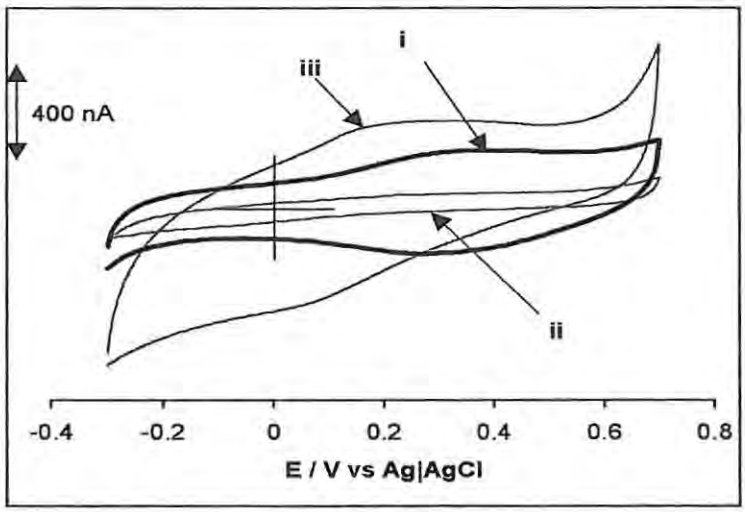

Figure 5.3: Cyclic voltammograms showing charging currents of gold electrode before (i) and after deposition of FeOBTPc-SAM (ii) and FeOHETPc-SAM (iii). Electrolyte = 1.0 mol dm^{-3} Na_2SO_4 + pH 4. Scan rate = 50 mV s^{-1}.

electrode {curve (ii)} led to a dramatic drop in the charging current observed for the bare gold electrode {curve (i)}. However, with the FeOHETPc-SAM (curve iii), much higher background currents were obtained. Similar results were also obtained with the CoPc-SAMs. This electrolyte system is, therefore, not suitable for C_s measurements of the MOHETPc-SAMs since much higher background currents are obtained, characteristic of permeability of the ions of the electrolyte and SAM defects. It has previously been established[276] that the capacitance of thiol-SAMs are affected by their terminal functional groups and increases in the following way: -COOH > -OH > $-CH_3$. In addition, hydrophilic terminal groups are by nature quasi-liquids, while hydrophobic groups are quasi-solids,[276,277,391] meaning that the SAMs of OH-terminated MPc complexes (like MOHETPc) should be more permeable to solution ions than those of CH_3-terminated MPc complexes (like MOBTPc). This observation may also explain the low blocking ability of the MOHETPc to gold surface reaction described above.

5.3 Passivation of Underpotential Deposition of Copper

Figure 5.4 demonstrates another effect of a closed–packed SAMs on Faradaic processes, i.e. inhibition of copper metal deposition on the gold electrode. According to

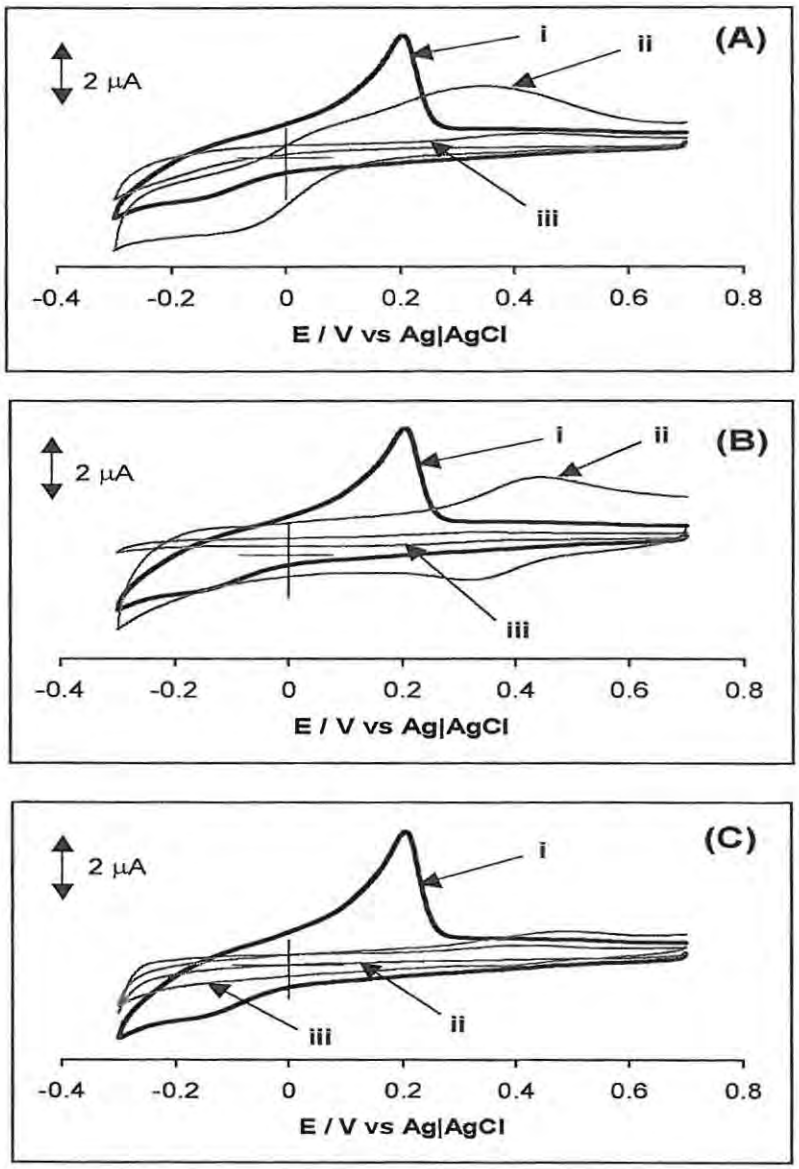

Figure 5.4: Cyclic voltammograms showing the responses of gold electrode to underpotential deposition of copper before (i) after coating with the SAMs (A) CoOHETPc, **40** (ii) and CoOBTPc, **33** (iii); (B) FeOHETPc, **36** (ii) and FeOBTPc, **35** (iii); (C) ZnOMPPc, **34** (ii) and ZnOBTPc, **32** (iii). Electrolyte = 1.0 mmol $CuSO_4$ in 0.5 mol dm^{-3} H_2SO_4. Scan rate = 50 mV s^{-1}.

Finklea,[276] copper metal depositions involve underpotential deposition (UPD) at potentials well positive of the thermodynamic potential. Figure 5.4 shows typical cyclic voltammogram of a 1.0 mmol $CuSO_4$ in 0.5 mol dm^{-3} H_2SO_4 on a bare gold electrode (curves i) and the same electrode after modification with the SAMs of MOHETPc (M = Co and Fe, Figure 5.4A and B, curves ii), MOBTPc (M = Co, Fe and Zn, Figure 5.4A and B curves iii) and ZnOMPPc (Figure 5.4C, curves ii). The bulk deposition of the copper started around –0.1 V vs Ag|AgCl during the negative-going scan. This potential is attributed to the standard potential of the Cu^{2+}/Cu^0 half-reaction.[276] On a return scan, a large UPD stripping peak for the copper metal appeared at +0.20 V vs Ag|AgCl, corroborating the previous observation of Hickey and Riley.[392] Also, the shape of the UPD voltammogram shows good resemblance to that reported by Finklea,[276] who observed the UPD peak around +0.3 V vs saturated calomel electrode (SCE). Thus, voltammograms (i) correspond to the UPD in the forward direction and stripping of a monolayer of copper in the reverse direction. From the much smaller currents of MOBTPc-SAMs {Figure 5.4, curves (iii)} and ZnOMPPc-SAMs {Figure 5.4C, curves (ii)}, compared to the currents obtained using the MOHETPc-SAMs {Figure 5.4A and B, curves (ii)}, it is clear that MOBTPc and ZnOMPPc-SAMs are able to cover the electrode much better than the MOHETPc-SAMs, which is also confirmed by the fact that in Figure 5.4A and B (curves ii) the reduction and oxidation of copper is still visible. This means that the gold surface is still accessible to copper or that the MOHETPc SAMs layers do not cover the gold electrodes properly. The cyclic voltammograms peaks observed in Figure 5.4A and B (curves ii) for SAMs of MOHETPc and MOBTPc (M = Co or Fe) complexes are due to the redox processes centered on the central metal of the

Pc complexes. The ill-defined peak in Figure 5.4A (ii) is due to $Co^{(III)}$ / $Co^{(II)}$ couple whereas in Figure 5.4B (ii) the peak is due to $Fe^{(III)}$ / $Fe^{(II)}$ couple. For curves iii, the weaker peaks due to this process were also observed under magnification. The ZnPc complexes (Figure 5.4C) show weak redox waves in the 0.5V region, attributable to ring-based (Pc^{-1}/Pc^{-2}) couple. These redox assignments are based on the well-known electrochemistry of the CoPc, FePc and ZnPc complexes.[223] The ZnOMPPc shows slightly better coverage than ZnOBTPc, possibly due to the peripheral benzene substituent of the ZnOMPPc, which is lacking in the ZnOBTPc. Figure 5.4 also shows that the MOBTPc (curves iii) and ZnOMPPc (curve ii) SAMs effectively block out bulk copper metal deposition on gold electrodes up to –0.3 V vs Ag|AgCl. This blocking capability indicates that the MOBTPc and ZnOMPPc-SAMs are virtually pinhole-free and defect-free.

The electrical charge Q under the UPD is proportional to the electroactive area of the electrode.[276,392] In the presence of sulphate ions the charge associated with UPD of copper on gold has been reported[393] as 430 μC cm^{-2}. Integration of the UPD stripping peak (Figure 5.4) gave approximately 8.0 μC (for SAMs of MOBTPc and ZnOMPPc) and 5.0 μC (for MOHETPc-SAMs). Since 0.020 cm^2 is the geometric area of the electrode, it means that the MOBTPc and ZnOMPPc-SAMs cover almost completely the electrochemically active gold surface area (~ 0.019 cm^2) while the MOHETPc-SAMs only show partial coverage (~ 0.012 cm^2). Thus, from the electrochemical point of view, the MOBTPc and ZnOMPPc-SAMs are better packed than the MOHETPc. This method of SAM characterization is rare.[276,394] Indeed, this is the first time it is being employed to characterize the SAMs of either a porphyrin or phthalocyanine complex.

5.4 Passivation of Heterogeneous Electron Transfer Processes

Figure 5.5 demonstrates another manifestation of the blocking ability of MPc-SAMs; the suppression of the simple Faradaic processes emanating from the exchange of electrons between gold electrode and solution redox couples. Porter et al.[286] have used the

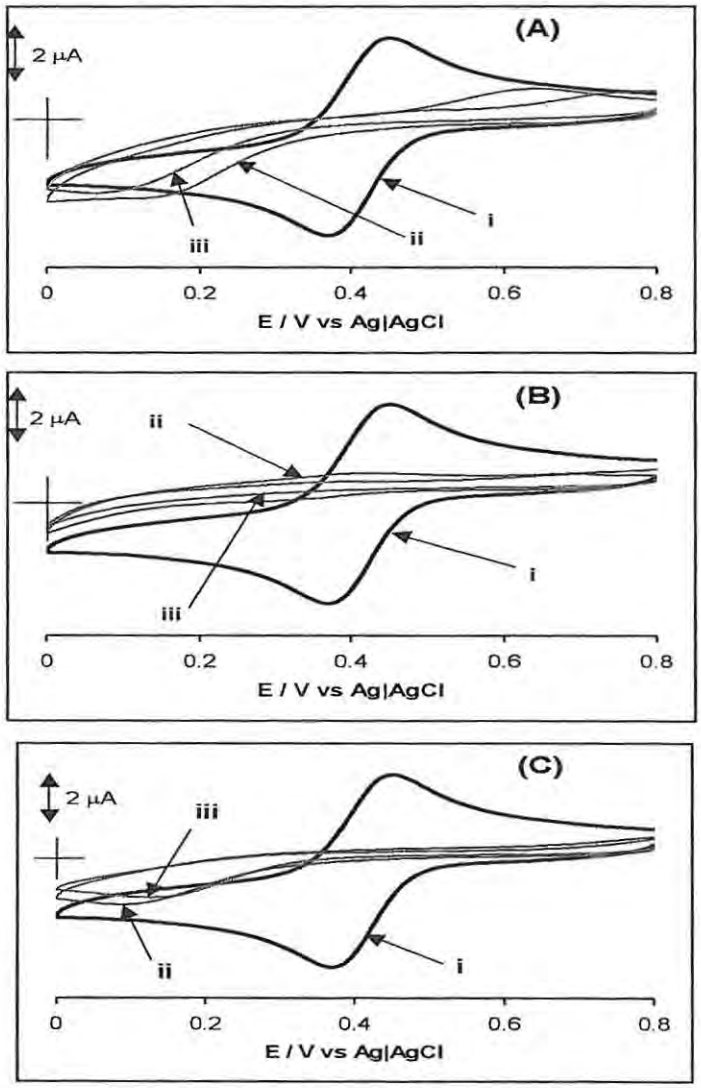

Figure 5.5: Cyclic voltammograms showing the responses of gold electrode to the redox chemistry of 1.0 mmol $Fe(NH_4)(SO_4)_2$ in 1 x 10^{-3} mol dm^{-3} $HClO_4$ before (i) and after coating with SAMs of (A) CoOHETPc, **40** (ii) and CoOBTPc, **33** (iii); (B) FeOHETPc, **36** (ii) and FeOBTPc, **35** (iii); (C) ZnOMPPc, **34** (ii) and ZnOBTPc, **32** (iii). Scan rate = 25 mVs^{-1}.

commercially available salts, $K_3Fe(CN)_6$ or $Fe(NH_4)(SO_4)_2$, in aqueous solutions to study such processes. Figure 5.5 showed the responses of bare gold (curves i) and gold modified the MPc-SAMs in 1.0 mol dm^{-3} $HClO_4$ solution of 10^{-3} mol $Fe(NH_4)(SO_4)_2$. Unlike the reversible $[Fe(H_2O)_6]^{3+}/[Fe(H_2O)_6]^{2+}$ redox couple in 1.0 mol dm^{-3} $HClO_4$ solution, the reversible couple of $[Fe(CN)_6]^{4-}/[Fe(CN)_6]^{3-}$ in 1 mol dm^{-3} KCl showed similar voltammetric waves (i.e. no change in the redox potential and peak current intensities) on both bare and MPc-SAM modified gold electrodes, meaning that the $K_3Fe(CN)_6$ is not a suitable redox probe for characterizing redox active MPc films. This is not surprising as a similar behaviour with the $[Fe(CN)_6]^{4-}/[Fe(CN)_6]^{3-}$ couple was observed recently by Griveau et al.[255] in their study of the electrocatalytic activity of adsorbed cobalt tetra-aminophthalocyanine films. This selective blocking behaviour may be simply explained by the fact that the reversible $[Fe(CN)_6]^{3-}/[Fe(CN)_6]^{4-}$ couple shows a higher heterogeneous electron transfer rate constant than $[Fe(H_2O)_6]^{3+}/[Fe(H_2O)_6]^{2+}$ redox species,[286] so that mass transport determines the reaction rate, even at small overpotentials. Hence, $Fe(NH_4)(SO4)_2$ was chosen as the electrochemical probe for this investigation in preference to the ferricyanide. Figure 5.5A and B shows the CV of a 10^{-3} mol $Fe(NH_4)(SO_4)_2$ in $1x10^{-3}$ mol dm^{-3} $HClO_4$ on a bare gold electrode (curve (i)) and the same electrode modified with the MOHETPc-SAMs {curves (ii)} and the MOBTPc-SAMs (curves iii). Figure 5.5C shows the passivations due to ZnOMPPc (curve i) and ZnOBTPc (curve iii). The ability of these SAMs to act as a barrier to the transport of the $[Fe(H_2O)_6]^{3+}$ / $[Fe(H_2O)_6]^{2+}$ redox species is a good indication that these MPc-SAM films are rather compact and/or that the pinholes are smaller than the electroactive probe ions.

Since $[Fe(CN)_6]^{3-}/[Fe(CN)_6]^{4-}$ is anionic it may be argued that electrostatics play a role in its interaction with the SAM on the electrode compared to the interaction of $[Fe(H_2O)_6]^{3+}/[Fe(H_2O)_6]^{2+}$ with the electrode. However it is important to note the blocking ability of FeOBTPc-SAM is also observed in buffer alone, hence ruling out electrostatics. Figure 5.6 compares the blocking ability of CoOBTPc, **33** (curve b), ZnOBTPc, **32** (curve c), FeOBTPc, **35** (curve d) with that of the metal-free analogue, octabutylthiophthalocyanine H_2OBTPc, **30** (curve e). It is evident from Figure 5.6 that both metallated and unmetallated phthalocyanine complexes exhibit similar blocking behaviour towards $[Fe(H_2O)_6]^{3+}/[Fe(H_2O)_6]^{2+}$ redox species. Figure 5.6 shows some variations in the blocking ability of these SAMs to $[Fe(H_2O)_6]^{3+}/[Fe(H_2O)_6]^{2+}$ redox couple.

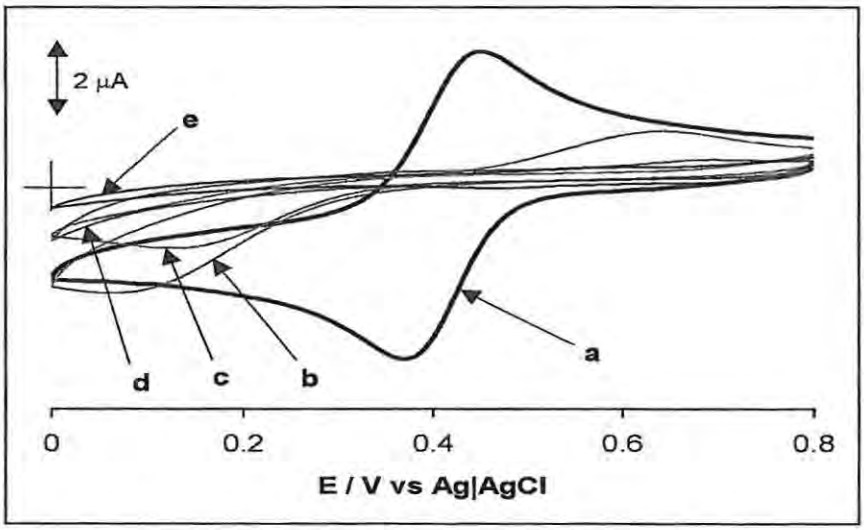

Figure 5.6: Typical comparative cyclic voltammograms showing the responses of gold electrode to the redox chemistry of 1 x 10^{-3} mol $Fe(NH_4)(SO_4)_2$ in 1 x 10^{-3} mol dm^{-3} $HClO_4$ before (a) and after coating with SAMs of CoOBTPc, **33** (b) ZnOBTPc, **32** (c) FeOBTPc, **35** (d) and H_2OBTPc, **30** (e). Scan rate = 25 mV s^{-1}.

The CV curves due to the SAMs of FeOBTPc (curve d) and H_2OBTPc (curve e) are flat-like, indicating that the SAMs provide an effective barrier to the heterogeneous electron transfer. The voltammograms due to the CoOBTPc (curve b) and ZnOBTPc (curve c) complexes are sigmoidal-like, typical of microelectrode array-type responses,[392] which is an indication that the CoPc-SAMs contain some defects. It does also appear that direct oxidation of the $Fe(NH_4)(SO_4)_2$ is accomplished on the CoPc and ZnPc-SAM-modifified electrodes with loss of reversibility. The irreversible nature of the $[Fe(H_2O)_6]^{3+}/[Fe(H_2O)_6]^{2+}$ redox wave obtained on these SAMs is a suggestion that the kinetics of the oxidation and reduction of this redox probe, are much slower when compared with that on a bare gold electrode. Porter et al.[286] postulated three processes through which electron transfer from the solution species in SAMs may occur: (a) through the SAM film via the electron tunneling process, (b) the electroactive species permeating through the monolayer and then reacting at the electrode surface, or (c) the electroactive species diffusing to a bare spot, a pinhole, on the electrode. The values of ion barrier factor which show negligible permeability of the SAM, suggests that paths (b) and (c) may be ignored, hence observation can be attributed to electron-tunneling mechanism (path a) and not directly with the exposed gold surface, path (c). Thus, both the insignificant (flat) and sigmoidal currents observed in Figures 5.5 and 5.6 indicate that electron transfer occurs mostly through the SAMs via the electron-tunneling mechanism and not directly with the exposed gold surface. This passivating ability of the SAMs to the $[Fe(H_2O)_6]^{3+}$ electrochemistry testifies that the SAMs are well packed, thus confirming the results of > 95% barrier to ion permeability.

5.5 Nernstian Factors for Electroactive Monolayer

5.5.1 Reversibility and Activation of the $M^{(III)}Pc$ / $M^{(II)}Pc$ Couple

Unlike ZnPc complexes, the CoPc and FePc-SAMs on gold electrodes are redox active at the metal centers, thus their $M^{(III)}Pc$ / $M^{(II)}Pc$ couples were investigated by surface electrochemistry. Figure 5.7 shows typical surface cyclic voltammograms of the SAMs of MOBTPc and MOHETPc (M = Co or Fe) on gold electrodes in 0.5 mol dm^{-3} H_2SO_4. It is evident from Figure 5.7 that the surface - immobilised species of the

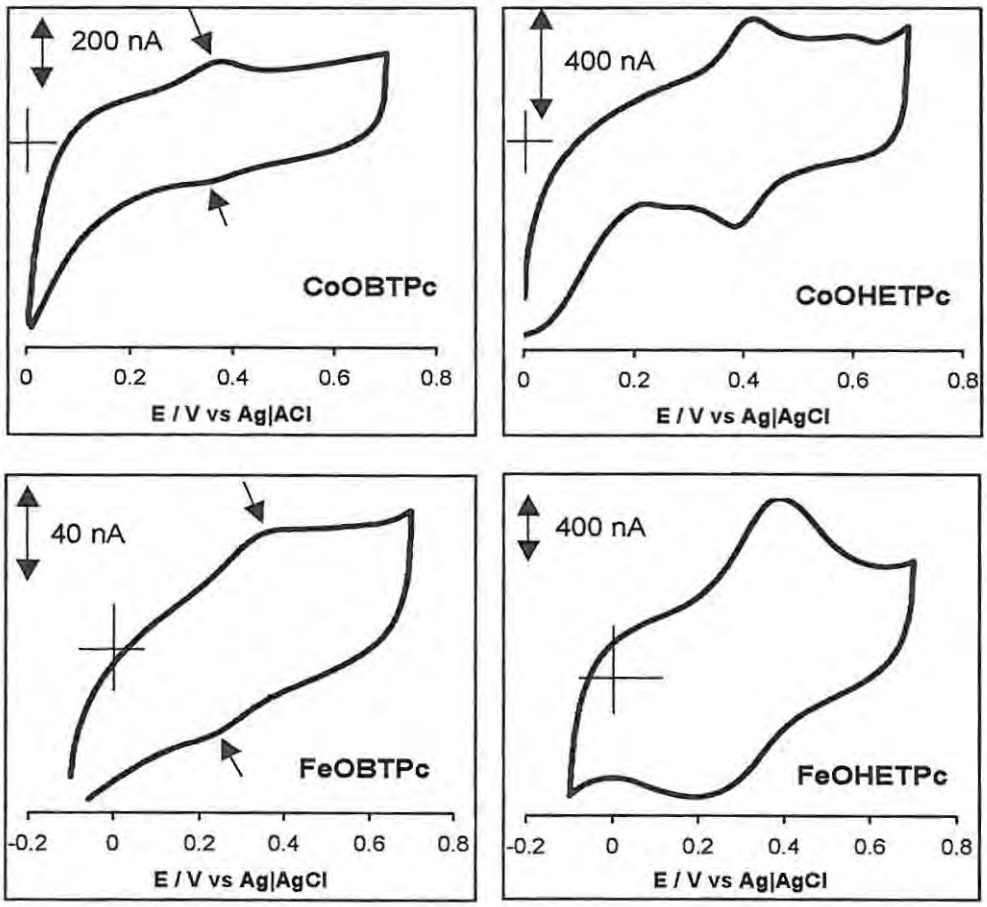

Figure 5.7: Typical surface cyclic voltammograms of the SAMs of MOBTPc and MOHETPc (M = Co or Fe) on gold electrodes in 0.5 mol dm^{-3} H_2SO_4. Scan rates = 25 mV s^{-1}.

MOHETPc showed well-behaved reversible redox couples positive of zero (around $E_{1/2}$ ~ 0.3 V and 0.4 V vs Ag|AgCl for the iron and cobalt complexes, respectively). For the MOBTPc complexes, however, similar redox waves appeared at the same potential regions but are broad and ill-defined. One common feature of a chemically modified electrode is that the formal potential of the surface-bound redox center is close to the formal potential of a solution analogue.[276] Thus, the identity of these redox couples, on the basis of the solution electrochemistry of these FePc and CoPc complexes investigated in this study (Tables 3.5 and 3.6) and literature reports[26,223] are ascribed to the $[M^{(III)}Pc(-2)]^+$ / $[M^{(II)}Pc(-2)]$ (where M = Fe or Co). The difference in the surface cyclic voltammetric responses of the MOBTPc and MOHETPc on gold electrodes is most likely to be the consequence of the different peripheral substituents; the CH_3-terminated MOBTPc species being crystalline-like and hydrophobic while the OH-terminated MOHETPc species being more liquid-like and hydrophilic.[276,391]

The Nernstian features for $[M^{(III)}Pc(-2)]^+/[M^{(II)}Pc(-2)]$ redox couple of the adsorbed monolayer of MOBTPc or MOHETPc were investigated in the acidic pH. As an example, the cyclic voltammetric curves for SAM of CoOHETPc in pH 4 phosphate buffer solution as a function of scan rate are shown in Figure 5.8. The more defined nature for this CV when compared to Figure 5.4A (ii) is due to the different electrolytes, pH effect and the presence of copper ions. Reversibility in Figure 5.8 was confirmed by the fulfilment of the following criteria:

- The ratio of cathodic to anodic peak currents (i_{pc}/i_{pa}) equals unity regardless of the scan rate;

- Linear relationship was obtained between peak current and scan rate, which is indicative of an immobilised monolayer-like behaviour;
- Peak potential did not shift with increasing scan rate, and the difference between anodic and cathodic peak potential (ΔE_p) is about 40 mV (Table 5.2). The ΔE_p values are usually non-zero, but small compared to zero volt expected for the Nernstian reaction of an ideal adsorbed monolayer.

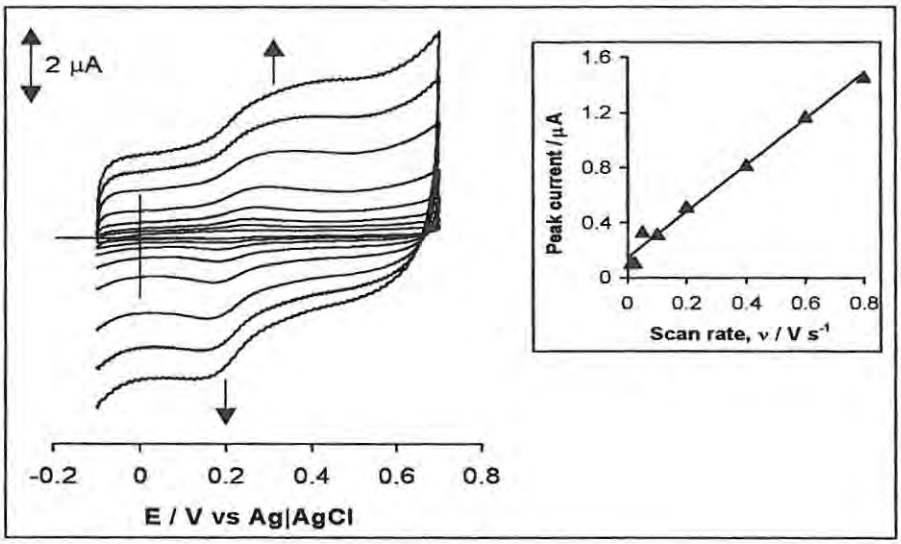

Figure 5.8: Cyclic voltammograms showing the dependence of peak currents on scan rate of the CoOHETPc-SAM-modified gold electrode in pH 4 buffer solution.

From scan rates of about 500 mV s^{-1} deviations from reversibility were observed, as a result of electron tunneling becoming the overall rate determining step in the reaction. This same effect explains why the background current of the SAM increases with scan rate. Peak currents vs scan rate plotted in the inset of Figure 5.8 are the result of the experimental reductive peak currents corrected for the increasing background currents.

Table 5.2: Summary of voltammetric data of the SAMs of MOBTPc and MOHETPc (M = Co, Fe) in aqueous solutions. Scan rate = 25 mVs^{-1}.

MPc-SAM	$E_{1/2}$ / V vs Ag|AgCl	ΔE_p / V vs Ag|AgCl	E_{fwhm} / mV vs Ag|AgCl	Γ (mol cm^{-2}) x 10^{10}
CoOBTPc, **33**	~0.36 (0.40) [a]	0.05 (0.05) [a]	85 (126) [a]	0.96±0.05 (1.02±0.06)[a]
FeOBTPc, **35**	0.26 (~ 0.30) [a]	0.10 (0.04) [a]	162 (97) [a]	~ 0.50 (0.98 ± 0.05)[a]
FeOHETPc, **36**	0.30	0.08	174	2.55 ± 0.10
CoOHETPc, **40**	0.40	0.04	75	2.40 ± 0.10

[a] The values in bracket were obtained from activated SAM-modified gold electrodes

Further surface cyclic voltammetric experiments were performed with a view to investigating the possibility of improving the cyclic voltammograms of the ill-defined $[M^{(III)}Pc(-2)]^+$ / $[M^{(II)}Pc(-2)]$ redox couples of the MOBTPc species in Figure 5.7. Figure 5.9 shows typical cyclic voltammograms in H_2SO_4 of the SAMs of CoOBTPc (Figure 5.9A) and FeOBTPc (Figure 5.9B) on gold electrodes. Curve (i) in Figure 5.9 shows the voltammogram for MOBTPc-SAM modified gold electrode (herein referred to as 'inactivated' electrode) in 0.5 mol dm^{-3} H_2SO_4. Curves (ii) in Figure 5.9 represent the cyclic voltammograms observed on repetitive cycling of the MOBTPc-SAM modified gold electrode in DMF containing $1x10^{-3}$ mol dm^{-3} TBAP for 2 minutes (herein referred to as the 'activated' electrode) and then rinsing thoroughly in a 0.5 mol dm^{-3} H_2SO_4 solution and recording the cyclic voltammograms in 0.5 mol dm^{-3} H_2SO_4. The weakness of the $[M^{(III)}Pc(-2)]^+$ / $[M^{(II)}Pc(-2)]$ redox couples of the MOBTPc species in Figure 5.9, curves i, is perhaps not very surprising. Thiol-derivatised SAMs of metalloporphyrins complexes of cobalt have been reported[276,320,321] to be characterized by very ill-defined

cyclic voltammograms, thus limiting their use to obtain reliable information about surface coverages and possible orientations of these complexes on electrodes. Hence, there has always been the need to improve the voltammetry of such SAMs using simple electrolytes or coordinating solvents. For example, Hutchinson et al.[321] attempted to improve the surface cyclic voltammetry of the cobalt(II)tetra(phenylethoxythio)porphyrin complex ($CoP(aryl\text{-}OC_2SH)_4$) by using NaOH electrolyte and by adding pyridine, but were not successful. It is interesting, therefore, to observe in this work that the activated

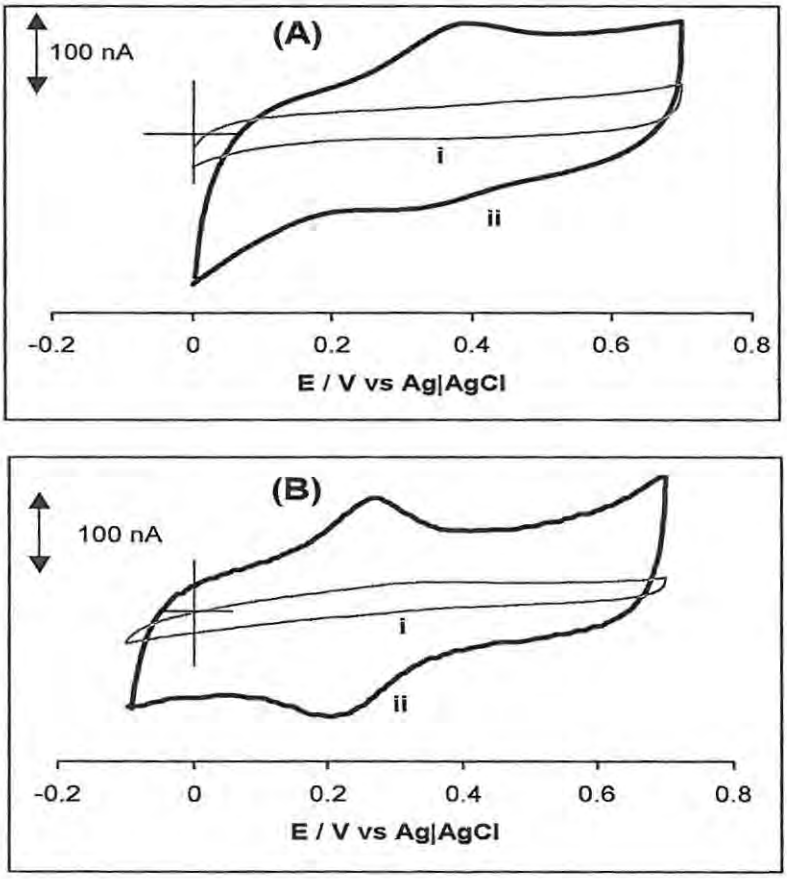

Figure 5.9: Surface cyclic voltammograms of MOBTPc-SAM-modified gold electrode before (i) and after (ii) two minutes of repetitive cycling in DMF containing $1x10^{-3}$ mol dm^{-3} TBAP. M = Co (A) and Fe (B). Electrolyte = 0.5 mol dm^{-3} H_2SO_4. Scan rate = 10 mV s^{-1}.

electrodes obtained on repetitive cycling of the MOBTPc-SAM modified gold electrodes in DMF containing 1 x 10^{-3} mol dm^{-3} TBAP for about 2 minutes as described above, showed well-defined $[M^{(III)}Pc(-2)]^+$ / $[M^{(II)}Pc(-2)]$ redox couple in 0.5 mol dm^{-3} H_2SO_4 solution at $E_{1/2}$ = 0.30 and 0.4 V vs Ag|AgCl for FeOBTPc and CoOBTPc, respectively. Immersion of the MOBTPc-SAM modified gold electrode in the DMF solution containing TBAP for about 10 minutes, without voltammetric cycling, showed no significant improvement on the redox wave obtained in Figure 5.9(i). The well-defined voltammograms obtained for the activated electrode may be attributed to ClO_4^- anion, which is known to bind strongly to $[M^{(III)}Pc(-2)]^+$ and subsequently influence the $[M^{(III)}Pc(-2)]^+/[M^{(II)}Pc(-2)]$ (M = Co or Fe) couple.[223] As is evident from Figure 5.9(ii), clearly defined redox wave following activation was associated with increase in background current of about 60% higher than that for the MOBTPc-SAM modified inactivated electrode (not cycled in the DMF/TBAP system), Figure 5.9(i). However, the background currents shown in Figure 5.9(ii) decayed gradually with cycling and then stabilized to ~ 10% after about 40 repetitive scanning, but the peak current did not decrease. The reason for the high background current in Figure 5.9(ii) may be due to electron tunneling and/or the result of a local concentration of DMF/TBAP at the surface of the SAM. The gradual loss of background current with repetitive scanning may be driven in part by the tendency of the alkane chains of the MOBTPc to aggregate so as to exclude the surrounding DMF/TBAP. Figure 5.10 compares the plots of the peak current (i_p) with scan rate (ν) for the anodic peaks of the $[Fe^{(III)}Pc(-2)]^+/[Fe^{(II)}Pc(-2)]$ redox processes of the activated (i) and inactivated (ii) FeOBTPc species. As in Figure 5.8(inset), the experimental peak currents plotted in Figure 5.10 were corrected for the

increasing background currents. The cyclic voltammetric response of these SAMs is consistent in every respect with that expected for a Nernstian reversible redox reaction of a surface-confined species. Thus, all the activated SAMs { Figure 5. 10 (ii)}, like their

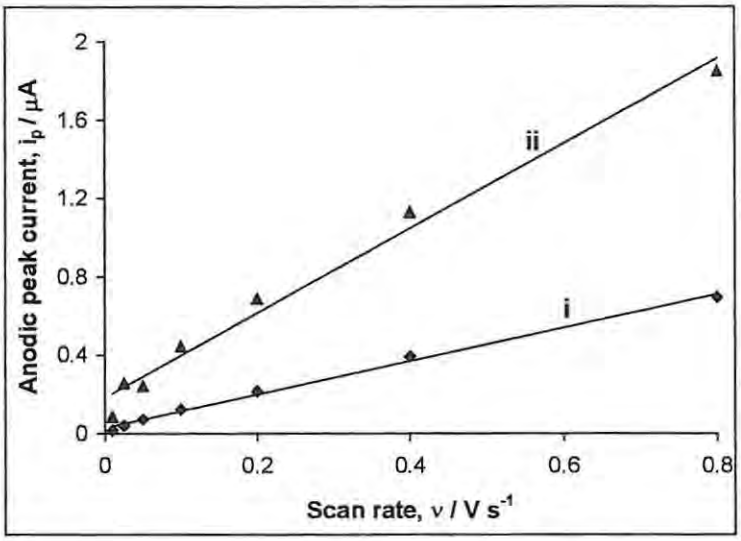

Figure 5.10: Plots of anodic peak current versus scan rate for $[Fe^{(III)}Pc(-2)]^{+}/[Fe^{(II)}Pc(-2)]$ redox processes of the inactivated (i) and activated (ii) FeOBTPc-SAM-modified gold electrode.

inactivated counterparts {Figure 5.10 (i)}, showed features of a surface-confined Faradaic reactions; good linear dependence of peak currents i_p on sweep rates, ν, (in the 10-800 mVs^{-1} range), despite the rather larger background current. These features of surface-confined Faradaic reactions are listed in Table 5.2. From Table 5.2, the anodic-cathodic peak separations (ΔE_p) are between 0.04 and 0.10 V for the inactivated, and 0.04 and 0.05 V vs Ag|AgCl for the activated electrodes at low scan rates ($\leq$ 200 mV s^{-1}); full width at half maximum (E_{fwhm}) are in the range of ca 75 –174 mV vs Ag|AgCl (Table 5.2). At scan rates > 200 mVs^{-1} peak broadening also occurred. These data suggest that the reactions involving the activated electrode may be kinetically hindered.[276]

5.5.2 The pH Effect on the $[M^{(III)}Pc(-2)]^+ / [M^{(II)}Pc(-2)]$ Couple

Osteryoung square wave voltammetry (OSWV), because of its excellent sensitivity,[210] was adopted to study the influence of pH on the electrochemical behaviour of the $[M^{(III)}Pc(-2)]^+ / [M^{(II)}Pc(-2)]$ redox couple of the investigated species. Figure 5.11 is a surface OSWV response of CoOHETPc in pH ranging from 2-9. In this pH range, the

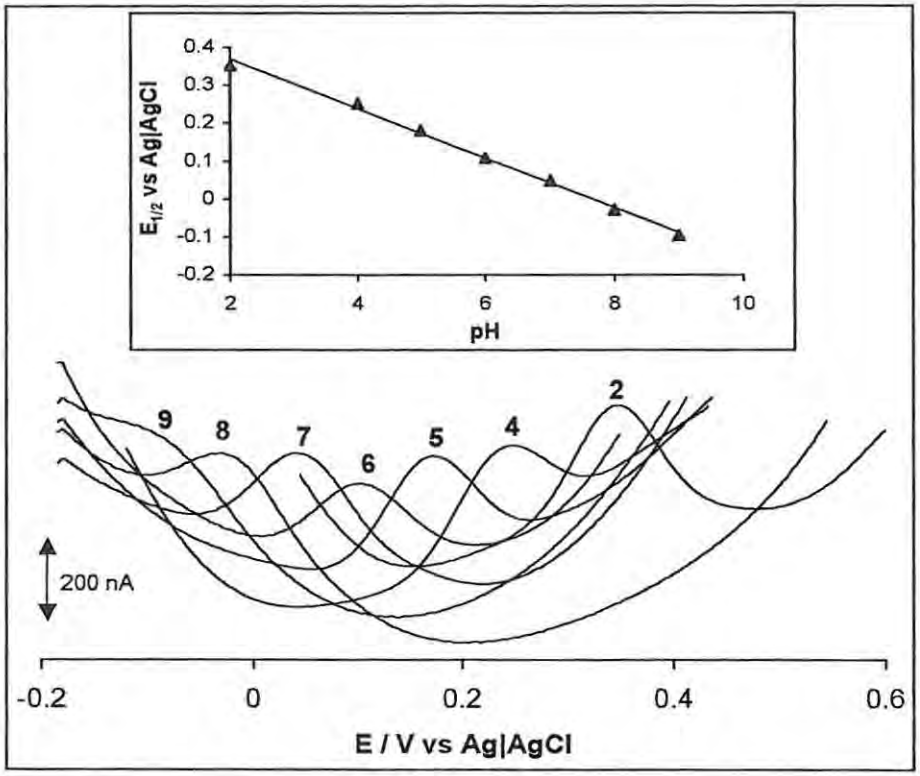

Figure 5.11: Surface Osteryoung square wave voltammetric response of CoOHETPc-SAM-modified electrode with changes in pH (pH 2, 4, 5, 6, 7, 8 and 9, shown as numbers on the peaks). The inset shows the plot of the changes in peak potential with pH.

peak potential ($E_{1/2}$) shifts to a more negative direction with increasing pH with a slope of ca – 64 mV pH^{-1} (inset), suggesting the participation of one proton redox process. A similar value (*ca* – 61 mV pH^{-1}) was also obtained for the CoOBTPc species. The mV

pH^{-1} values for both CoOHETPc and CoOBTPc species are close to the theoretical value of –59 mV per unit pH expected for a Nernstian reaction that involves the reaction of one proton for the transfer of each electron.[395,396] It has previously been reported[322,378,396] that the $[Co^{(III)}Pc(-2)]^{+}$ / $[Co^{(II)}Pc(-2)]$ redox couple in CoPc and substituted CoPc (regardless of the nature of the substituents) shifted *ca.* – 66 mV pH^{-1} for pH > 7.5 only, while for lower pH values, the redox potential is independent of pH. On the other hand, the $[Co^{(II)}Pc(-2)]$ / $[Co^{(I)}Pc(-2)]^{-}$ redox couples in CoPc and substituted CoPc (regardless of the nature of the substituents) gave slope of ca – 64 mV pH^{-1} for pH ≤ 5 but became pH – independent at higher pH values.[322,378,396] The results obtained here for the thioether-linked MPc complexes shows pH dependence of potential throughout the pH range investigated. The slope of ~ – 60 mV pH^{-1} is similar to those reported for $[Co^{(III)}Pc(-2)]^{+}$ / $[Co^{(II)}Pc(-2)]$ and $[Co^{(II)}Pc(-2)]^{+}$ / $[Co^{(I)}Pc(-2)]$ redox couples.[378]

For the activated and inactivated FeOBTPc and FeOHETPc complexes, the shift in peak potentials to the more negative potential with increasing pH was accompanied by a corresponding broadening and decrease in the peak current. As an example, Figure 5.12 shows typical surface OSWV for FeOBTPc {Figure 5.12(A)} and FeOHETPc {Figure 5.12(B)} species at pH 2, 4, 7 and 8. From pH ≥ 6, the OSWV peaks for the FeOBTPc {Figure 5.12(A)} became broader while the FeOHETPc species showed a new peak {labelled (i) for pH 6 and 7, Figure 5.12(B)} that also shifted to a more negative potential with increase in pH. This new peak (i) is probably the same weak redox couple observed by Golovin et al.[397] for the $FePcCl_{16}$ species in alkaline pH and was assigned to the $[Fe^{(II)}Pc(-2)]^{+}$ / $[Fe^{(I)}Pc(-2)]$ redox couple. It does seem that it is the presence of this

couple in the FeOBTPc that might have resulted in the broadening of the $[Fe^{(III)}Pc(-2)]^+$ / $[Fe^{(II)}Pc(-2)]$ redox couple at pH ≥ 6 (Figure 5.12A). Plots of peak potentials of the redox

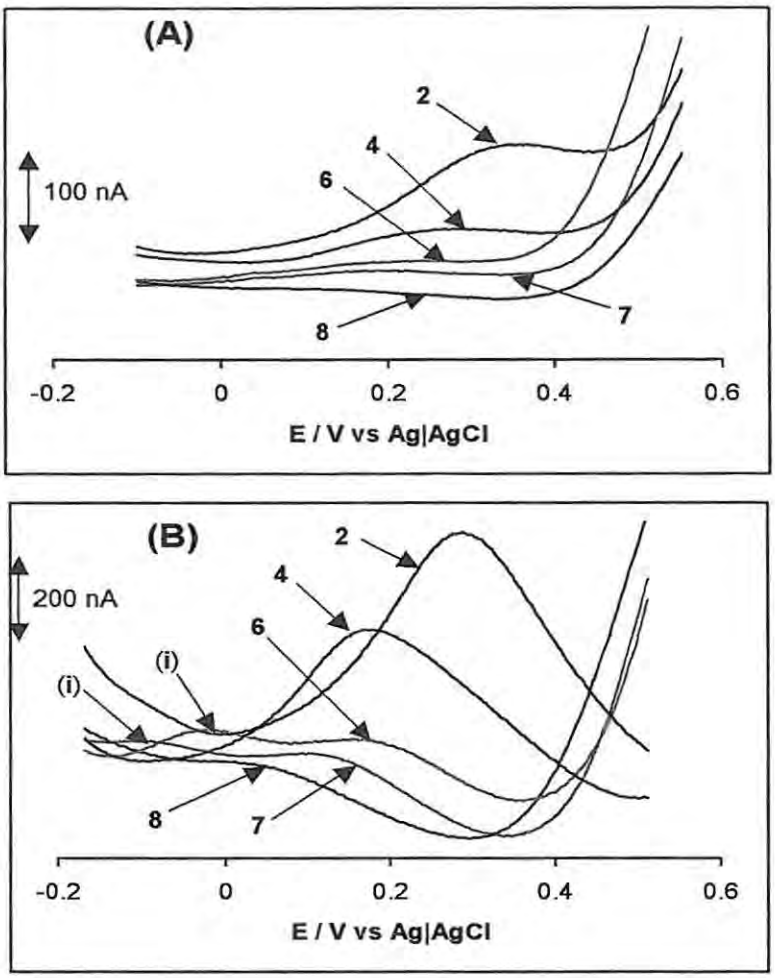

Figure 5.12: Surface Osteryoung square wave voltammetric responses of gold electrode modified with the SAMs of (A) FeOBTPc, **35** and (B) FeOHETPc, **36** with changes in pH (pH 2, 4, 6, 7 and 8, shown as numbers on the peaks).

waves vs pH for the inactivated and activated SAM-modified electrode showed good linearities in the pH range 2-9, with slopes of –58 mV pH^{-1} (for inactivated FeOBTPc), –57 mV pH^{-1} (for activated FeOBTPc) and –61 mV pH^{-1} (for FeOHETPc). These values for the FePc species again are consistent with Nernstian characteristics for a one-proton

redox reaction. It is interesting to realize that similar behaviour had been observed for the perchlorinated iron phthalocyanine ($FePcCl_{16}$)[397] and thioether-linked iron protoporphyrin[307] immobilized on highly oriented pyrolytic graphite (HOPG) and gold electrodes, respectively. In both cases, water (in acidic and neutral conditions) and hydroxyl group (in alkaline pH) were speculated to be coordinated to the Fe^{III} ion center. Thus, it may be assumed that in the present study coordination of hydroxide or water to the iron center also occurs. In the acidic range, however, one might also consider the protonation of the pyrrolic nitrogens of the FeOBTPc ring since the electron-donating butylthio-substituent should increase the basicity of these nitrogen atoms.

5.5.3 Surface Coverage

The orientation of electroactive phthalocyanine or porphyrin SAM on a solid surface can be determined from its surface concentration or coverage, Γ, as described by equation 1.62. MPc substituted with eight peripheral thiols or thioacetate bind to gold surfaces by adopting the so-called 'octopus' orientation.[103,104] The Γ values of all the electroactive MPc species investigated in this work can be estimated from the electrical charge, Q, under the oxidative (or reductive) $[M^{(III)}Pc(-2)]^+$ / $[M^{(II)}Pc(-2)]$ redox peaks using equation 1.62. The background corrected electric charge, Q, under the oxidative peaks (e.g. Figures 5.7 – 5.9) obtained for all the SAMs of MOBTPc and MOHETPc (M = Co or Fe) ranged from 8×10^{-8} to 2×10^{-7} C. These values were essentially independent of ν in the range of 10 – 100 mVs^{-1}, but slightly decreased for higher scan rates, which is consistent with immobilized monolayer-like behaviour. The estimated Γ values obtained from the calculated Q values are listed in Table 5.2. The surface coverage for the

inactivated FeOBTPc (~ 1.0 x 10^{-10} mol cm^{-2}) is more reliable than that (4.5 x 10^{-11} mol cm^{-2}) for the inactivated FeOBTPc due to the broad voltammogram for the latter, Figure 5.9. A surface coverage of ~10^{-10} mol cm^{-2} is expected for a monolayer of MPc complex. However, despite the fact that the surface coverage data obtained for both activated and inactivated CoOBTPc are almost similar, it is interesting to note that a more reliable value (~ 1.0 x 10^{-10} mol cm^{-2}) is obtained for the activated FeOBTPc compared to the inactivated FeOBTPc, which is a clear indication of the importance of this activation process. The values for surface coverage for all the SAMs obtained in this work are (within the limit of experimental error) in the range (~10^{-10} mol cm^{-2}) reported for other metalloporphyrin and metallophthalocyanine macrocycles adsorbed as monolayers.[321,322,328] For example, the surface coverages for the following phthalocyanine and porphyrin complexes; cobalt (II) hexadecyltetrapyridylporphyrin,[326] cobalt (II) tetra (phenylethoxythio) porphyrin[321] and iron (III) protoporphyrin IX adsorbed on gold electrodes have been reported as 8.6 x 10^{-11}, 8.0 x 10^{-11} and 2.5 x 10^{-11} mol cm^{-2}, respectively, while those for cobalt (II) tetrasulphopthalocyanine[324] and cobalt (II) tetra-aminophthalocyanine[325] adsorbed on pyrolytic graphite electrodes were reported as 1.4x10^{-10} and 1.24x10^{-10} mol cm^{-2}, respectively.

Using the surface concentrations of the MOBTPc and MOHETPc in Table 5.2, one can estimate the gold surface occupied by one molecule of the MPc by simply multiplying the Γ values with the Avogadro's constant (N_A). The values obtained are in the region of 150 – 190 $Å^2$ $molecule^{-1}$ for the MOBTPc and ~ 70 $Å^2$ $molecule^{-1}$ for the MOHETPc. In estimating the surface concentrations of these SAMs, it is assumed that the real surface of the electrode is equal to the geometric area, which is generally not the

case. Since the real surface area is larger than the geometric, these estimations set upper limits for the surface concentrations. Hence, if it is assumed that each MPc molecule lies flat on the electrode (connected to the electrode through sulphur of the eight thioether legs resulting in the so-called octopus configuration[103,104]) and occupying the reported[322,325] area of about 200 $Å^2$, it means that the MOBTPc-SAMs contain a monolayer, while those of the MOHETPc-SAM modified electrodes suggest about three monolayers. The different surface coverages shown by the MOBTPc and MOHETPc species can be attributed to their different orientations (octopus or flat orientation for the MOBTPc and perpendicular orientation for the MOHETPc) on gold surface (further discussed in Section 5.7).

Reductive desorption experiments were performed for both CoOBTPc and CoOHETPc-SAM-modified electrodes in 0.5 mol dm^{-3} KOH in the potential window of –0.2 to –1.2V vs Ag|AgCl according to literature.[276,277] Alkanethiol-SAMs are known to desorb quantitatively from gold surfaces at negative potentials in strongly alkaline electrolytes (usually 0.5 mol dm^{-3} KOH) according to equations 1.63[276,277] shown below. During such electrochemical desorption, a reduction peak due to the desorption of the thiolate is obtained.

$$Au\text{-}SC_nX + ne^- + M^+ \longrightarrow Au^o + XC_nS^- M^+ \qquad 1.63$$

The area under the reductive peak corresponds to the coverage of the SAM. Figure 5.13 shows a typical reductive desorption cyclic voltammograms obtained for gold electrodes modified with the SAMs of CoOBTPc (A) and CoOHETPc (B) in 0.5 mol dm^{-3} KOH. The desorption peaks were observed in the –0.50 and –0.95V regions for the MOBTPc and MOHETPc complexes, respectively. Each of the CoPc-SAM-modified electrodes

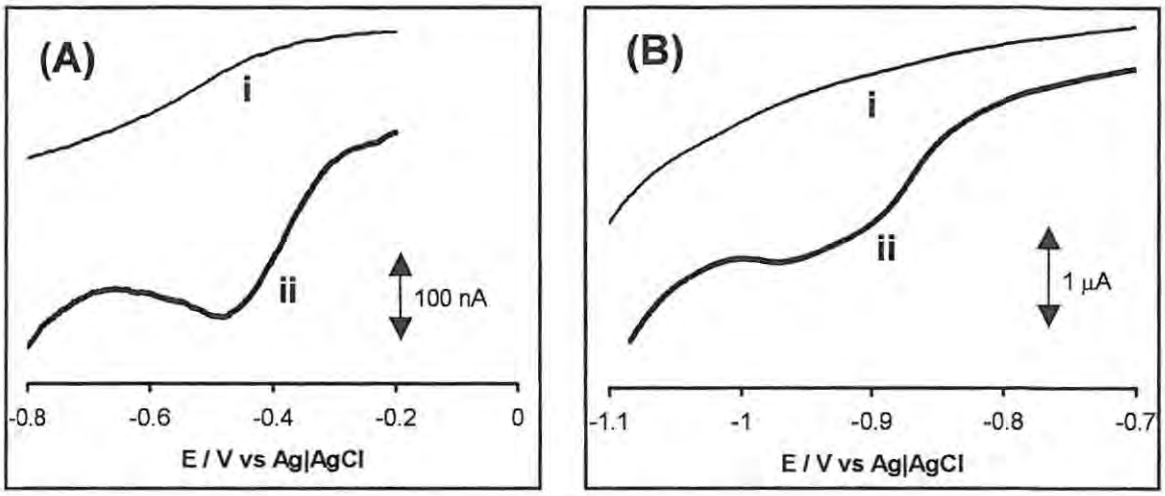

Figure 5.13: Reductive desorption cyclic voltammetry peaks of gold electrodes before (i) and after (ii) modification with the SAMs of (A) CoOBTPc, (B) CoOHETPc. Electrolyte = 0.5 mol dm^{-3} KOH, Scan rate = 25 mVs^{-1}.

was scanned ten times between -0.2 to -1.2V vs Ag|AgCl. In each case, the first scan showed a well-defined reduction peak (around ~ -0.5V for CoOBTPc and ~ -0.95V for CoOHETPc vs Ag|AgCl) due to desorption of the SAM (Figure 5.13, curves ii). The integrated charges under the desorption peak averaged about 1.5 x 10^{-6} C for CoOBTPc-SAMs and 2.0 x 10^{-6} C for the CoOHETPc-SAMs. If correlated with the estimated surface coverages determined from the $[Co^{(III)}Pc(-2)]^{+}$ / $[Co^{(II)}Pc(-2)]$ redox couples, these charges (within the limits of experimental errors) should result in number of electrons, n (or coupling points) ≈ 8 and 4 for MOBTPc and MOHETPc, respectively. These data agree with the proposed possible orientations of these MPc SAMs.

Unlike the CoPc and FePc-SAMs, surface coverage (Γ) of the ZnPc-SAMs cannot be obtained from the $[M^{(III)}Pc(-2)]^{+}$ / $[M^{(II)}Pc(-2)]$ redox couples since ZnPc complexes are redox inactive with respect to the central metal. Thus, the surface coverages of the

ZnPc-SAMs (**32** and **34** complexes) could only be estimated by reductive desorption experiments in 0.5 mol dm^{-3} KOH, between –0.3 and –1.2 V vs Ag|AgCl. The reductive (desorption) peaks (Figure 5.14, curves a and b for **32** and **34**, respectively) were observed at –0.88 V corresponding to the stripping of the thiol. The results of the

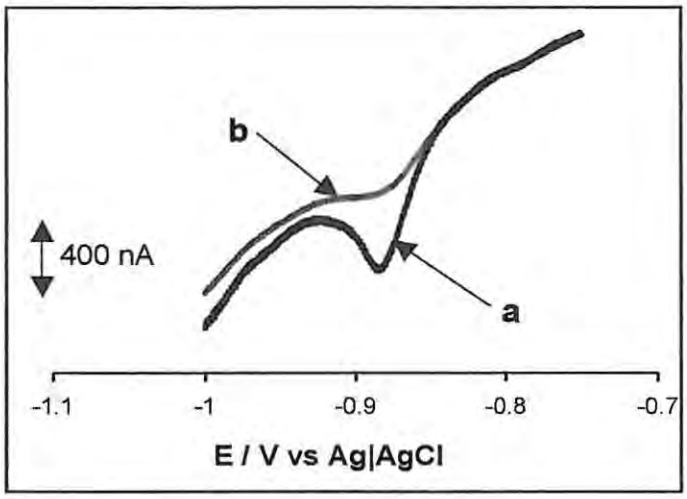

Figure 5.14: Reductive desorption cyclic voltammetry peaks of SAMs of ZnOBTPc (a) and ZnOMPPc (b) on gold electrode. Electrolyte = 0.5 mol dm^{-3} KOH, Scan rate = 25 mVs^{-1}.

desorption experiments obtained here are interesting since the peak potential values for ZnPc and CoOHETPc-SAMs fall within the potential regions (-0.70 to –1.40V vs Ag|AgCl[276]) where alkanethiol SAMs on gold desorb under the same experimental conditions. Integration of the desorption curves gave approximately 1.2×10^{-6} and 0.7×10^{-6} C for **32** and **34**, respectively. Applying the thiol desorptive equation (equation 1.63 above) and then assuming $n \approx 8$ (for the eight thiol substituents per MPc molecule), these electric charge values should give surface coverages of about 8.0×10^{-11} and 5.0×10^{-11} mol cm^{-2} for **32** and **34**, respectively. These estimated surface coverages are (within the

limit of experimental error) in the range (~10^{-10} mol cm^{-2}) reported for other metalloporphyrin and metallophthalocyanine macrocycles adsorbed as monolayers with flat orientations.[321,322,328]

5.6 Reproducibility and Stability of Thio-MPc SAMs

All results discussed in this paper were obtained by six independent electrode modifications using the MPc species and the voltammograms were obtained with a relative standard deviation of ±2%. Straight chain alkanethiols fabricated as SAMs are known to oxidize at the thiolate roots over a period of time, limiting their potential applications in many analytical areas. Alkanethiol-derivatised phthalocyanine SAMs, on the other hand, are known for their good stability.[101,398,399] All the thio-MPc SAMs investigated in this work were found to be stable by storing in pH 4 phosphate buffer solutions, current responses remaining almost unchanged for at least a month. The reason for this long-term stability is not fully understood but may be related to the protection of the sulphur by the macrocyclic ring of the phthalocyanine as suggested by other studies.[101,398,399] The interchain attractive interactions resulting from the alkyl chains may also be a contributing factor to the stability.

Finally, the stability of the SAMs was both dependent on pH of the electrolyte and the applied potential. The monolayers showed remarkable stability from pH 2 to 9 at potentials between –0.2 to +0.7 V vs Ag|AgCl. The SAMs reductively desorb at potentials more negative than –0.2V vs Ag|AgCl and oxidatively at potentials more positive than +0.70V vs Ag|AgCl. Hence, to avoid possible desorptions of the monolayers, the most permissible potential window for their electrocatalytic applications at pH ≥ 10, is within a narrow potential window of –0.20 and +0.70 V vs Ag|AgCl.

5.7 The Fate of Carbon-Sulfur Bond During Self-Assembling

A first indication that cleavage of the R-groups (butyl-, ethylhydroxy- and methylphenyl-) in the MPc does not occur can be found in the interfacial capacitances of the SAM-coated electrodes. Figures 5.2 - 5.7 give first evidence that the R groups in the investigated MPcs are not cleaved, since MOBTPc show lower currents than the MOHETPc complexes. If R-group cleavage occurred, the SAMs of the two types of complexes would show the same electrochemical behaviour. This is clearly not the case as can be seen from Figures 5.2 – 5.7.

The explanation of the non-cleavage of the R groups can be found from the solution electrochemistry of these thiol-derivatised MPc complexes (Tables 3.4 – 3.6). Thiol groups are electron donors and it can be expected that their presence should result in easier oxidation and more difficult reduction of the Pc rings in MPc complexes.[16,223] Surprisingly, however, the opposite is observed for ring reduction (process IV) of a group of thiol-derivatized MPcs (Tables 3.4 – 3.6). For example, the data in Table 3.6 indicate that thiol-derivatized MPcs can be reduced more easily than $FePc(Cl)_{16}$, the latter having substituents with electron withdrawing properties. This result suggests that the R-S substituents show electron-withdrawing effects on the Pc-rings, which tend to strengthen their R-S bonds, hence leading to non-cleavage. It is believed that the redox chemistry of these thiol-substituted MPcs plays a role in the binding process.

Another evidence for the non-cleavage comes from the difference in the surface concentration or coverage, Γ (mol cm^{-2}) of the MOHETPc and MOBTPc. The fact that these complexes possess different surface coverages (hence different areas) implies that the molecules have different orientation or sitting arrangement on gold electrode;

perpendicular/vertical for MOHETPc and flat/parallel (octopus) for MOBTPc (Figure 5.15) and ZnOMPPc. The self-assembly mechanism for alkanethiols has been speculated to follow two stages: initial horizontal adsorption and final lifting up process.[276] If the MOBTPc and MOHETPc complexes follow similar mechanism, it is possible that what is

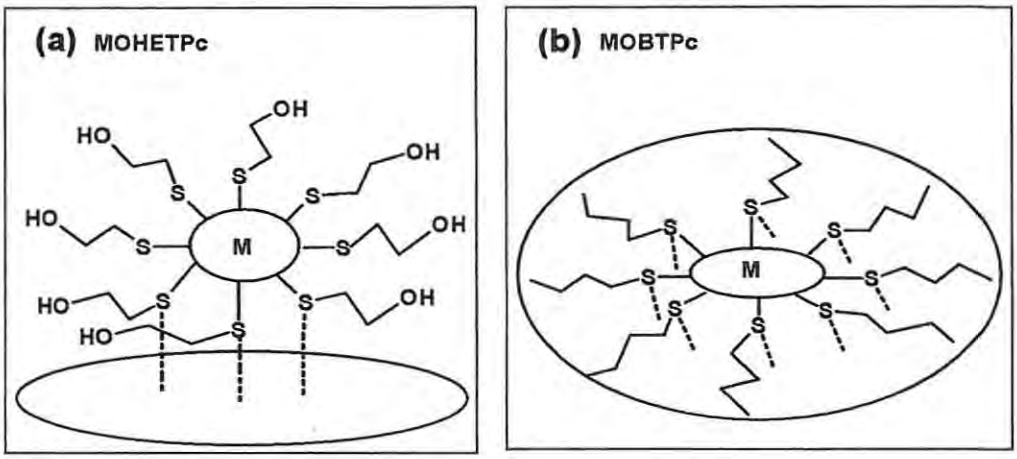

Figure 5.15: Schematic representations of the possible orientations adopted by the SAMs of (a) MOHETPc (perpendicular), and (b) MOBTPc (octopus or flat). M = Co or Fe. The small circles containing the central metal, M, represent the phthalocyanine rings.

being observed here is a type of stereochemical frustration where one Pc ring blocks others from flat binding. This, of course, should be more pronounced in MOHETPc (as observed) where a possible electrostatic repulsion is expected than in MOBTPc complexes. Such a hypothesis can also explain why the blocking abilities of these SAMs to Faradaic processes (Figures 5.2 – 5.6) are less pronounced in MOHETPc than those for the MOBTPc complexes. The difference in orientation of the molecules gives further evidence that these molecules still contain their different R groups. It is interesting to note that these results are consistent with those of several other reports[303,309,400] for the SAMs of thioether-linked species on gold surfaces.

Conclusions:

Functionalised thiol-derivatised pthalocyanine complexes of iron(II), cobalt(II) and zinc(II) capable of forming SAM on gold electrode have for the first time been reported. Since the MOHETPc species are soluble only in DMF and DMSO, their SAMs were deposited onto the gold electrodes using either of the solvents for deposition. MOBTPc-SAMs can be formed on gold electrodes using $CHCl_3$, dichloromethane, toluene or THF. Comparative surface electrochemical investigation of their distinct self-assembling features, with respect to the passivation of Faradaic processes and surface coverages, revealed some pointers that suggest different orientations and non-cleavage of the C-S bonds of these thioether-linked MPc species when adsorbed onto gold surfaces. The chapter (6) that follows investigates the potential electrocatalytic behaviour of the gold electrodes modified with the electroactive SAMs of the MOBTPc and MOHETPc species towards thiols (L-cysteine, homocysteine and penicillamine) and thiocyanate. Since the central metal in ZnPc complexes (ZnOBTPc, **32** and ZnOMPPc, **34**) are electrochemically silent, no further investigation was performed on them. However, it is interesting to observe that these photosensitive ZnPc complexes (see chapter 3), can be immobilized on gold surface as stable SAMs. Without doubt, research on photo-electrochemical application of these thiol-derivatised ZnPc complexes, for example, can provide an efficient technology for the clean up of toxic wastes such as the recalcitrant halogenated aromatic molecules. Future research in this direction is likely to prove rewarding.

CHAPTER 6

ELECTROCATALYTIC BEHAVIOUR OF MPC-SAM-MODIFIED GOLD ELECTRODES TOWARDS THIOLS, THIOCYANATE AND CYANIDE*

* The following publications resulted from part of the research work presented in this chapter and they are not referenced further in this thesis:

5. K. Ozoemena, P. Westbroek and T. Nyokong, *Electrochem. Commun.*, 2001, **3**, 529.
6. K. Ozoemena, T. Nyokong and P. Westbroek, *Electroanalysis,* 2002 (in press).

6.1 Electrocatalytic Oxidation of Thiols

6.1.1 Activation of MPc-SAM-Modified Gold Electrode

Cyclic voltammetric analysis of any of the thiols investigated in this work (i.e. L-cysteine, homocysteine and penicillamine) using a freshly MOBTPc-SAM coated gold electrode (especially prepared using chloroform as deposition solvent) was characterized by an ill-defined catalytic oxidation wave. However, continuous cycling in ~ 10^{-5} mol dm^{-3} acidic solution of the thiol for one to two hours resulted in a well-defined voltammogram due to the catalytic oxidation wave of the thiol with peak potential close to the formal potential value of the $[M^{(III)}Pc(-2)]^{+}/[M^{(II)}Pc(-2)]$ redox couple. As an example, Figure 6.1 shows typical voltammetric responses during 8, 28 and 48 minutes continuous cycling of FeOBTPc-SAM modified gold electrode in a pH 4 phosphate buffer solution containing ~10^{-5} mol dm^{-3} L-cysteine. The broad peak near +0.55 V vs

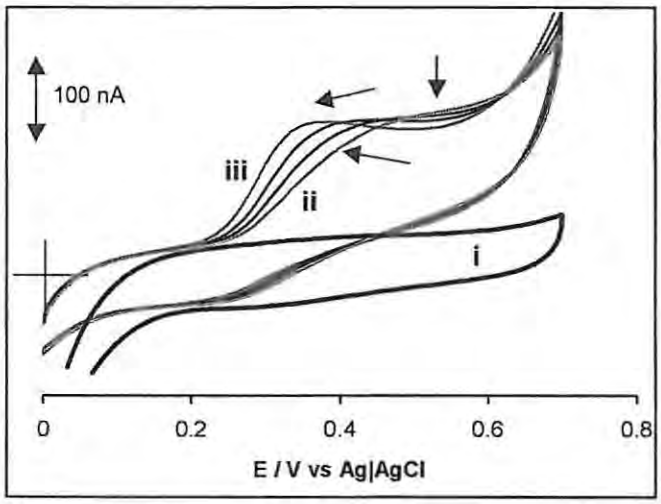

Figure 6.1: Typical cyclic voltammetric responses of FeOBTPc-SAM modified gold electrode in a pH 4 phosphate buffer solution in the absence (i) and presence of ~10^{-5} mol dm^{-3} L-cysteine before (ii) and after 8, 28 and 48 minutes {from inner to outer (iii) wave} of continuous cycling.

Ag|AgCl shifted to a less positive potential of ~ +0.33 V vs Ag|AgCl, following cycling. The final oxidation peak at ~ +0.33 V vs Ag|AgCl is close to the $[Fe^{(III)}Pc(-2)]^{+}$ / $[Fe^{(II)}Pc(-2)]$ redox couple of this species, FeOBTPc at pH 4 (see chapter 5, Figure 5.9). The formal potential ($E^{o'} \sim E_{1/2}$) of the $[Fe^{(III)}OBTPc(-2)]^{+}$ / $[Fe^{(II)}OBTPc(-2)]$ couple was observed (weakly using CV, Figure 5.7A, but clearly with OSWV in pH 2 and 4, Figure 5.12A) at $E_{1/2} \approx 0.28$ V vs Ag|AgCl, and it shifted slightly to 0.33 V vs Ag|AgCl on addition of L-cysteine. Similar behaviour was also observed for the L-cysteine on CoOBTPc-SAM where the initial broad peak around +0.55 V vs Ag|AgCl was finally obtained at ~ +0.40 V vs Ag|AgCl, on cycling. L-Cysteine did not show any peak on unmodified gold within the potential range studied.

Cyclic voltammetric analysis in a pH = 4 buffer solution shows that gold electrode freshly coated with FeOBTPc-SAM exhibits a slightly higher background current in buffer alone (Figure 6.2 curve i) when compared to the same electrode after about 50 minutes of continuous cycling or 'activation' in ~ 10^{-5} mol dm^{-3} L-cysteine in pH 4 solution, then rinsed in buffer and CV recorded in buffer alone (Figure 6.2 curve ii). Continuous cycling of the modified electrode, between 0.0 and +0.7 V vs. Ag|AgCl in a pH = 4 buffer solution alone, for about an hour did not show the appreciable change in the background currents observed in pH 4 buffer solution containing L-cysteine. Also, experiments involving longer deposition time of between two and four days for the SAM onto the electrodes showed noticeable reduction in the background current, although not as much as with the cycling experiments in L-cysteine pH 4 solutions. Figure 6.2 also shows the oxidation waves of L-cysteine in pH 4 solutions before (curve iii) and after the activation of the electrode (curve iv). The electrode was activated in L-cysteine and then

rinsed in buffer. Curves ii and iv show the voltammograms obtained on activated electrode in the absence (i.e. in buffer alone) and presence of L-cysteine, respectively. Curves i and iii are voltammograms obtained on inactivated electrode in the absence and presence of L-cysteine respectively. Although both curves (Figure 6.2, curves iii and iv) show essentially the same current response, there is a remarkable improvement on the shape and the height of the oxidation wave of L-cysteine using the activated electrode.

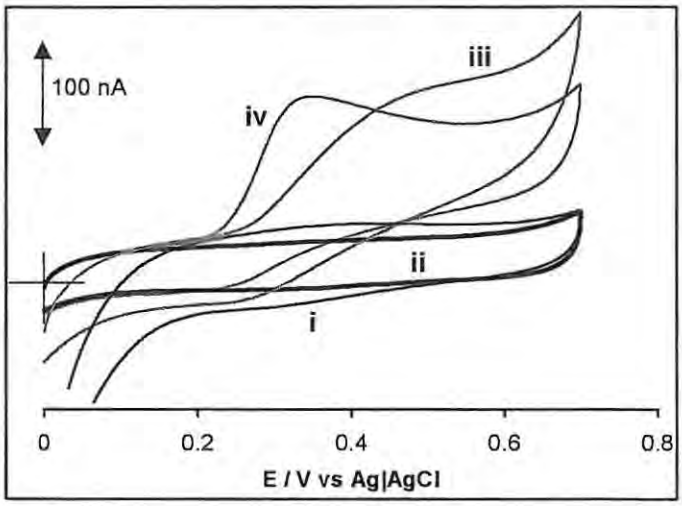

Figure 6.2: Cyclic voltammograms of FeOBTPc-SAM-modified gold electrode in a pH 4 phosphate buffer solution before (i) and after (ii) activation in ~10^{-5} mol dm^{-3} L-cysteine. Curves (iii) and (iv) are L-cysteine waves obtained with inactivated (i) and activated (ii) FeOBTPc-SAM modified gold electrode in a pH 4 phosphate buffer solution.

These observations may be rationalized in terms of the so-called SAM annealing[276] via cyclic voltammetry as described earlier {Chapter 1, Section 1.5.2.3 (f)}. Incorporation of deposition solvent into SAMs of organothiols is known and has been well described by Bain et al.[310] It is most likely that after the deposition some of the deposition solvent molecules are incorporated into the MOBTPc-SAM (hence the high

background currents shown by a fresh SAM modified electrode). Lowering of the background current of the electrode enhances octopus orientation of the SAM as described in the preceding chapter. Thus, the reduction of background currents (Figure 6.2, from curve i to curve ii) suggest possible improvement in self-assembling process (since not all MOBTPc are likely to attain the octopus configuration during the initial self-assembling process), by additional adsorption and consolidation, involving expulsion of included solvent from the monolayer and / or displacement of contaminants.[310] With exceptions of few cases, longer SAM deposition times are known to expel included solvents in a monolayer.[310] This may explain the reduction in the background current observed during longer deposition experiments. Because of the hydrophilic nature of these solvents, they cannot be removed easily from the electrode surface by water. However, during electrocatalysis the thiol complexes (e.g. L-cysteine) and their reaction products can 'shock' the imperfect SAM species on the electrode surface. The organic deposition solvents, which are probably adsorbed weakly, are therefore expelled from the surface. To check if L-cysteine and/or its major oxidation product, cystine, were responsible for this activation, experiments were also carried out by dipping the freshly modified electrodes in ~ 10^{-3} mol dm^{-3} pH 4 solution of each substrate for about an hour. No remarkable improvement was observed in either case. This result is an indication that it may be the result of the synergy achieved by thiols and their reaction products during the potential cycling that could be responsible for this activation.

It was found that by drying (at 80°C for 6 hours) of a freshly prepared MOBTPc-SAM modified gold electrode, the same reduction in background current effect was obtained. This treatment is a type of thermal annealing of SAM[276] {chapter 1, Section

1.5.2.3 (f)}. This confirms that activation of the electrode is, in fact, the expulsion of the included solvents into the SAM during its formation. However, activation of the electrode by cycling in a pH 4 L-cysteine solution is favoured, because its conditions are smoother compared to drying and it is a lot easier to monitor and follow the activation process. The activation time used for cycling is also much shorter than with the drying procedure.

Finally, the reduction in background current was found to be dependent on the deposition solvents since it was more pronounced with chloroform followed by dichloromethane, and least observed with tetrahydrofuran and toluene. This seems to suggest that the less dense deposition solvents such as THF (0.89 g cm^{-3}) and toluene (0.87 g cm^{-3}) are less prone to being included into the SAM than the denser solvents such as chloroform (1.49 g cm^{-3}) and dichloromethane (1.32 g cm^{-3}). This may be due to the low solubility of the MOBTPc in these solvents. Therefore, after deposition of a new MOBTPc monolayer, the modified electrode should be subjected to about an hour activation time before use for electrocatalytic oxidation of thiols, especially if the deposition solvent is chloroform. Continuous cycling of the MOHETPc-SAM modified electrode for about an hour in either pH 4 solution alone or pH 4 solution containing thiol showed essentially similar, but less significant reduction in background currents, compared to MOBTPc. This implies that continuous cycling in acidic pH is sufficient for their activation.

Another effect, herein referred to as the "memory effect", was also observed during analysis of high concentration of thiols ($\geq 10^{-4}$ mol dm^{-3}). After the modified electrode (using either the MOBTPc or MOHETPc) was used for electroanalytical detection of a thiol in a pH = 4 buffer alone, it was found that even in the buffer alone a

very small current signal due to thiol oxidation was observed. This means that in a buffer solution containing a thiol an equilibrium is established between the thiol adsorbed onto the SAM (probably onto the $M^{(II)}$ central metal ion) and thiol in solution. However, the observation described above indicates that desorption of thiol is a relatively slow process. From additional experiments it was found that it takes about 6 minutes of cycling in buffer alone for complete desorption of L-cysteine in a pH = 4 buffer, after the electrode has been used for analysis of high concentration of thiol ($\geq 10^{-4}$ mol dm^{-3}). For smaller concentrations ($\leq 10^{-5}$ mol dm^{-3}), this desorption time is shorter (<1 minute). This memory effect, if ignored, can have some bad consequences for the analytical value of the developed electrode in that it can affect the magnitude of the catalytic currents, thereby influencing detection limits. Therefore, in this work, an equilibration time of at least 6 minutes was allowed between two separate voltammetric experiments with thiol.

6.1.2 Detection of Thiols: L-cysteine, Homocysteine and Penicillamine

At most conventional electrodes the electrocatalytic oxidation of thiols (such as L-cysteine, homocysteine and penicillamine investigated in this work) is characterized with slow electron transfer that leads to oxidation occurring at extreme positive potentials, and poor detection limits.[401] Figure 6.3 shows typical voltammetric responses of L-cysteine at bare gold (curve i) and the same gold electrode modified with the SAM of CoOBTPc (curve ii) following activation. From curve i in Figure 6.3, it can be seen that at a bare gold electrode an ill-defined oxidation wave of L-cysteine is obtained resulting in an inclining limiting current plateau. Migration is ruled out because of the use of an electrolyte, therefore it is clear that the inclination of the plateau is due to slow electron

transfer kinetics. Improvement on the oxidation waves of the thiols was obtained after the gold electrode was modified with the SAMs of any of MOBTPc or MOHETPc species.

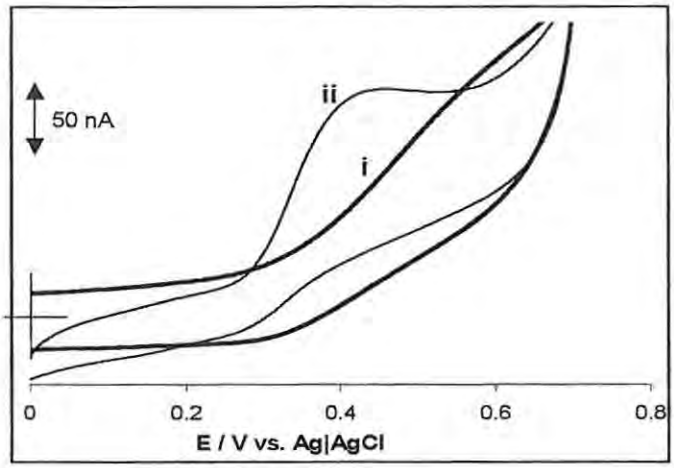

Figure 6.3: Cyclic voltammograms of L-cysteine at (i) bare gold and (ii) the same gold electrode modified with activated CoOBTPc-SAM in pH 4 buffer solution. Scan rate = 100 mVs^{-1}.

Figure 6.4 shows typical voltammograms of FeOBTPc-SAM modified gold electrodes at increasing concentrations of L-cysteine in pH 4 buffer solutions. All the MOBTPc and MOHETPc species when immobilized on gold electrodes as SAMs showed electrocatalytic activities towards L-cysteine, homocysteine and penicillamine studied in this work. The oxidation waves (both CV and OSWV) were well defined with peak potentials in the same range as those reported for other CoPc complexes immobilized on surfaces such as carbon and glassy carbon (Table 6.1). Figure 6.5 (A-D) shows typical cyclic voltammetric responses for the oxidation of homocysteine (Figure 6.5A) and penicillamine (Figure 6.5B) using gold electrodes modified with the SAMs of

CoOBTPc and penicillamine on FeOBTPc-SAM (Figure 6.5C). Figure 6.5D is the Osteryoung square wave voltammogram of penicillamine on FeOBTPc-SAM.

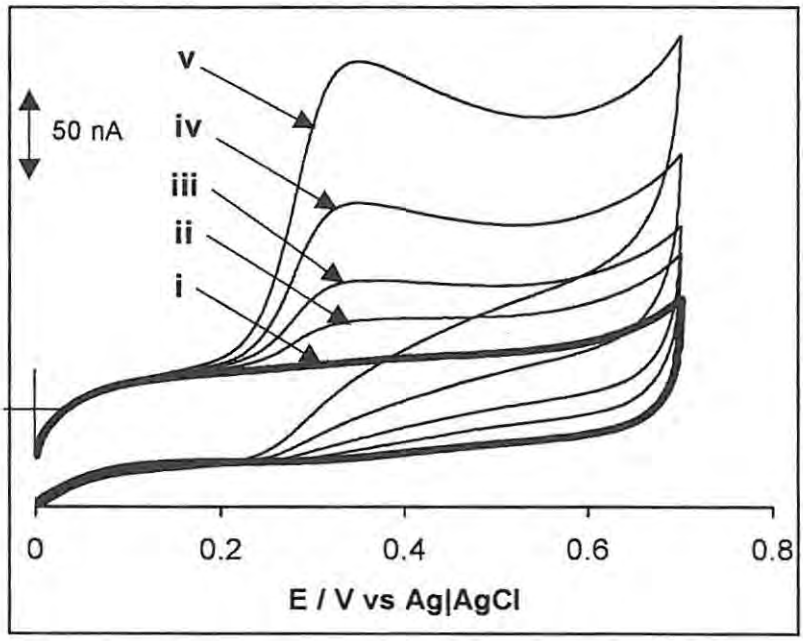

Figure 6.4: Cyclic voltammograms of FeOBTPc-SAM-modified gold electrode in pH 4 solution before (i) and after addition of (ii) 2.66 x 10^{-6} (iii) 5.32 x 10^{-6} (iv) 10.60 x 10^{-6} and (v) 20.90 x 10^{-6} mol dm^{-3} L-cysteine. Scan rate = 25 mVs^{-1}.

Table 6.1: Comparative peak potential (E_p) and limit of detection (LoD) for the electrocatalysed reactions of L-cysteine, homocysteine and penicillamine in acidic conditions using electrodes modified with CoPc and FePc species.

MPc species	Electrode material	Analyte	E_p / V vs (Ag|AgCl)	LoD / mol dm^{-3}	References
CoOBTPc, **33**	SAM-Au	L-cysteine	0.42	$3.1\pm0.8 \times 10^{-7}$	This work
CoOHETPc, **40**	SAM-Au	L-cysteine	0.50	$5.2\pm0.3 \times 10^{-7}$	This work
FeOBTPc, **35**	SAM-Au	L-cysteine	0.33	3.0×10^{-7}	This work
FeOHETPc, **36**	SAM-Au	L-cysteine	0.38	$5.2\pm0.3 \times 10^{-7}$	This work
CoPc	Carbon cement	L-cysteine	0.74	1.0×10^{-7}	402
CoPc	Carbon paste	L-cysteine	0.42	3.1×10^{-8}	174
$CoPcS_4$	Glassy carbon	L-cysteine	0.82	$\sim 1.0 \times 10^{-8}$	78
CoOBTPc, **33**	SAM-Au	Homocysteine	0.52	$5.2\pm0.6 \times 10^{-7}$	This work
CoOHETPc, **40**	SAM-Au	Homocysteine	0.54	$2.3\pm0.8 \times 10^{-6}$	This work
FeOBTPc, **35**	SAM-Au	Homocysteine	0.44	$5.2\pm0.6 \times 10^{-7}$	This work
FeOHETPc, **36**	SAM-Au	Homocysteine	0.45	$2.3\pm0.8 \times 10^{-6}$	This work
CoPc	Carbon cement	Homocysteine	0.62	5.0×10^{-7}	403
CoOBTPc, **33**	SAM-Au	Penicillamine	0.58	$2.7\pm0.6 \times 10^{-6}$	This work
CoOHETPc, **40**	SAM-Au	Penicillamine	0.55	$3.0\pm0.7 \times 10^{-6}$	This work
FeOBTPc, **35**	SAM-Au	Penicillamine	0.45	$2.7\pm0.6 \times 10^{-6}$	This work
FeOHETPc, **36**	SAM-Au	Penicillamine	0.44	$3.0\pm0.7 \times 10^{-6}$	This work
CoPc	Carbon cement	Penicillamine	0.60	9.0×10^{-8}	404

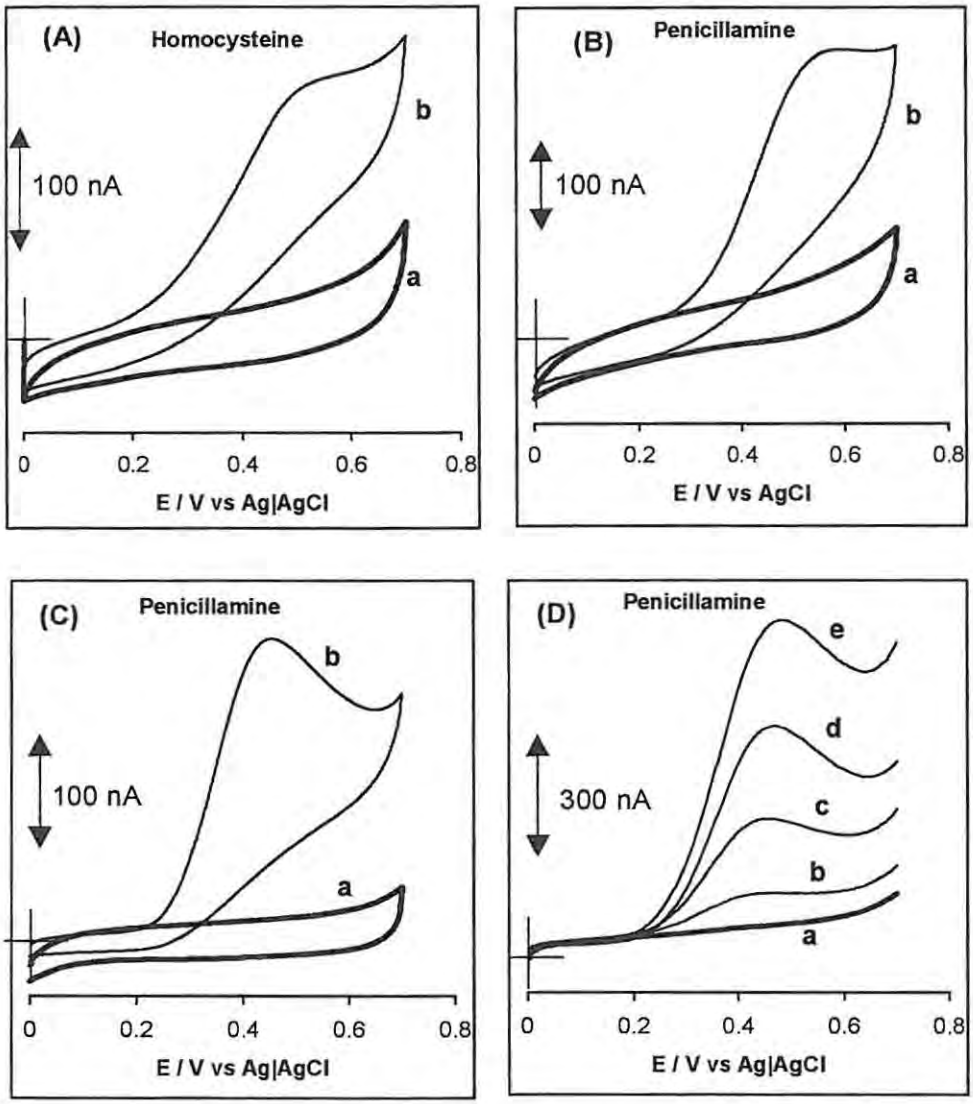

Figure 6.5: Examples of cyclic voltammograms of (A) homocysteine and (B) penicillamine on CoOBTPc-SAM; (C) penicillamine on FeOBTPc-SAM; curves (a) in the absence and (b) presence of ~ 10^{-5} mol dm^{-3} of analyte; (D) Osteryoung square wave voltammograms of penicillamine on FeOBTPc-SAM before (a) and after addition of (b) 5.0 x 10^{-6} (c) 11.0 x 10^{-6} (d) 21.0 x10^{-6} and (e) 40.0 x 10^{-6} mol dm^{-3} penicillamine. Electrolyte = pH 4 buffer solution; Scan rate = 25 mV s^{-1}.

In all cases, the oxidation peak of the thiols occurred positive of the formal potential of the $[M^{(III)}Pc(-2)]^+$ / $[M^{(II)}Pc(-2)]$ redox couple. As a comparison, Figure 6.6 (A-D) gives the representative cyclic voltammograms of L-cysteine, homocysteine and penicillamine obtained using gold electrodes modified with the SAMs of the MOHETPc analogues. Catalytic peaks were observed in all cases, and no peaks were observed for

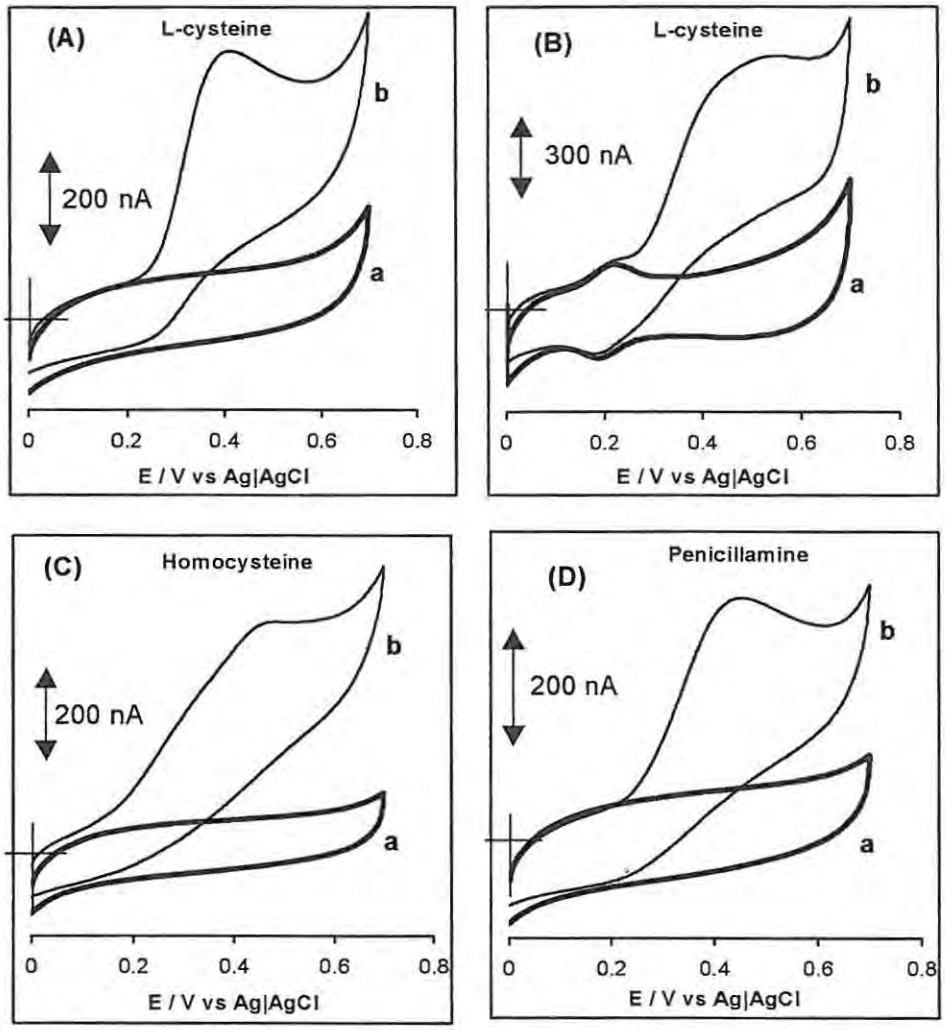

Figure 6.6: Examples of cyclic voltammograms of L-cysteine on (A) FeOHETPc-SAM and (B) CoOHETPc-SAM; (C) homocysteine and (D) penicillamine on FeOHETPc-SAM modified gold electrodes; curves (a) in the absence and (b) presence of ~ 10^{-5} mol dm^{-3} of analyte; Electrolyte = pH 4 buffer solution; Scan rate = 25 mV s^{-1}.

L-cysteine (as already stated) homocysteine and penicillamine on unmodified gold electrode. A broad peak was observed for L-cysteine on MOHETPc -SAMs as shown by Figure 6.6. Homocysteine showed the presence of two peaks at concentrations less than 10^{-5} mol dm^{-3} on both MOHETPc and MOBTPc-SAM modified electrodes, as exemplified in Figure 6.7 using FeOHETPc-SAM modified gold electrode. At higher concentrations of homocysteine ($>10^{-5}$ mol dm^{-3}), the first peak which occurs at approximately the same position as the formal potential of the $[M^{(III)}Pc(-2)]^{+}$ / $[M^{(II)}Pc(-2)]$ redox couple (~ 0.3 V vs Ag|AgCl) becomes less significant while the second peak at

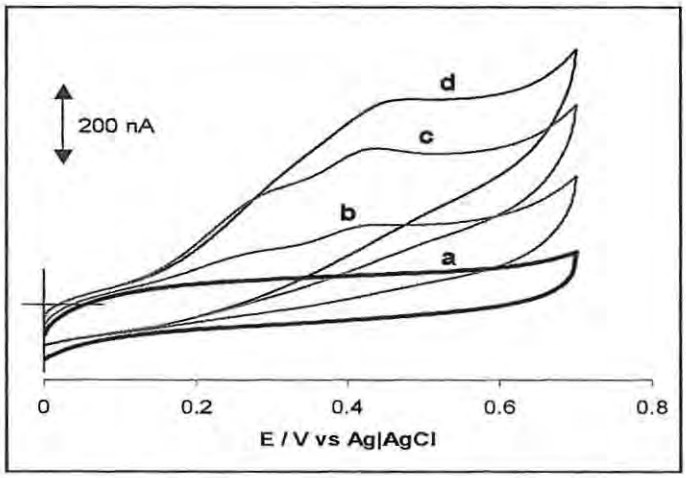

Figure 6.7: Cyclic voltammetric responses of FeOHETPc-SAM before (a) and after addition of (b) 3.0 x 10^{-6} (c) 7.4 x 10^{-6} (d) 1.0 x 10^{-5} mol dm^{-3} of homocysteine; Electrolyte = pH 4 buffer solution; Scan rate = 25 mV s^{-1}.

more positive potential (between 0.40 and 0.50 V vs Ag|AgCl) increased with intensity. This observation seems to suggest that the first peak is likely to be due to the $[M^{(III)}Pc(-2)]^{+}$ / $[M^{(II)}Pc(-2)]$ redox couple and/or that there are two species formed following the oxidation of homocysteine and that only one of the species is catalysed by MPc-SAM.

The penicillamine peak was well-defined, particularly on FeOBTPc. The OSWV was employed to detect penicillamine at low concentrations.

By definition, electrocatalysis requires the mediator system (in this case $[M^{(III)}Pc(-2)]^{+}/[M^{(II)}Pc(-2)]$ redox couple) to be able to increase the rate of electron transfer. This implies that for optimal electrocatalytic process the overall oxidation rate of thiol should be limited by mass-transport. A good indication for mass-transport control is a linear relationship between peak current and square root of the scan rate. As an example, Figure 6.8 gives the plots of oxidation current of L-cysteine vs square root of scan rate. This relationship was obeyed for scan rates ≤ 100 mV s^{-1} at a concentration of $\sim 10^{-6}$ mol dm^{-3} L-cysteine (curves a and b), and at scan rates < 50 mVs^{-1} for curve c, and < 25 mVs^{-1} for curve d).

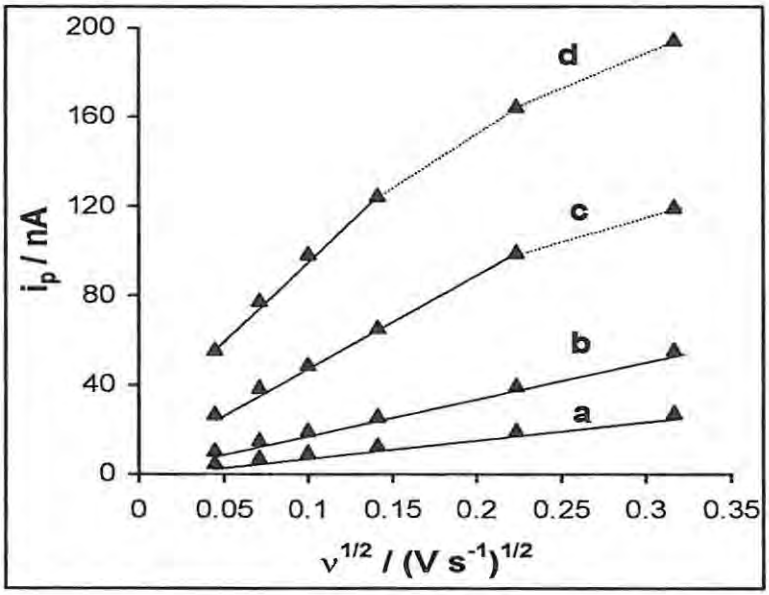

Figure 6.8: Relationship between i_p and $\nu^{1/2}$ at CoOBTPc-SAM modified gold electrode in pH 4 buffer solution containing L-cysteine concentrations of (a) 1.1×10^{-6}, (b) 2.0×10^{-6}, (c) 5.1×10^{-6} and (d) 1.0×10^{-5} mol dm^{-3}.

For higher scan rates deviations from linearity were observed. The background currents were also found to increase remarkably for higher scan rates (> 50 mV s^{-1}). This indicates that capacitive effects become important, possibly due to the presence of relatively large resistance within the monolayer. A possible explanation for this effect is the fact that electron transfer through SAMs of thiols occurs via a tunneling effect.[286] The maximum current that can flow via tunneling is quite limited. An increase in L-cysteine concentration, coupled with increase in the polarization rate (> 50mVs^{-1}) consequently results in higher currents being transferred per unit time through the SAM via electron tunneling. This is confirmed by the fact that at low concentrations (<10^{-5} mol dm^{-3} L-cysteine), the deviation from linearity between peak current and square root of scan rate starts to occur at higher scan rates (Figure 6.8, curves a-c) but at about the same value of peak current (around 100 nA), also known as the "saturation" current. These results mean that if the saturation current is exceeded the overall reaction rate is no longer controlled by mass-transport only. However at currents smaller than the saturation current, mass-transport is the rate-determining step. From the slopes obtained between i_p and $\nu^{1/2}$, recorded at different L-cysteine concentrations, a diffusion coefficient of 4.8×10^{-5} cm^2 s^{-1} (with n = 1) was obtained using the Randles-Sevcik equation,[209,210] a result that agrees with literature data.[161,162] Therefore, it was possible to calculate the theoretical peak current that should be obtained for each concentration of L-cysteine and compare it with the experimental ones. It was found that both theoretical and experimentally obtained peak currents were approximately the same, indicative of the fact that the MPc-SAM is a good electrocatalyst, which is mass transport-controlled at currents below 100 nA.

Plots of oxidation current vs the concentrations of the respective thiol were linear up to ~10^{-4} mol dm^{-3}. The limits of detection (LoD) are in the region of ~ 10^{-7} to 10^{-6} mol dm^{-3} (Table 6.1). The detection limits were obtained at 5 nA higher than the background current. Since the background currents of the SAMs are stable and can be measured accurately, a detection limit at about 1.2 times the background current was employed. Interestingly from Table 6.1, the oxidation of all the thiol species occurred at less positive potential with the FePc than the CoPc complexes. This is expected given that the $[M^{(III)}Pc(-2)]^{+}$ / $[M^{(II)}Pc(-2)]$ redox couple of CoPc generally occur at higher potentials than that of the FePc complexes[223,397] (also see Tables 3.5 and 3.6). The relatively higher LoD observed for the MOHETPc, compared to their MOBTPc counterparts, is ascribed to the high background currents of the former as a result of its liquid-like behaviour described above.

The variation of catalytic peak currents with scan number (25 scans) was also investigated. In all cases, a dramatic decrease in peak currents was observed after first scan. This behaviour is exemplified in Figure 6.9 with the oxidation of penicillamine using FeOHETPc-SAM modified gold electrode. However, after rinsing the electrode in a fresh pH 4 solution and then re-scanning the L-cysteine solution, a peak similar in magnitude with the initial first scan was obtained. This observation may be attributed to the poisoning of the modified electrodes by the oxidation products of the thiols. Similar observations have previously been reported[78,173,175,178] for L-cysteine oxidation in acidic media (pH ~ 4) using MPc – chemically modified electrodes and were attributed to the poisoning of modified electrodes by the adsorbed oxidation product, cystine. The fact that the poisoned electrodes can easily be renewed by simply rinsing in acidic medium

indicates that these oxidation products are physically adhered to the electrode (physisorption) and are soluble in acidic rinsing medium. Cystine is not soluble at pH 4 – 9, hence poisons the electrode. In highly acidic conditions pH < 4, cystine dissolves resulting in improved stability of MPc modified electrodes.[78,173,175]

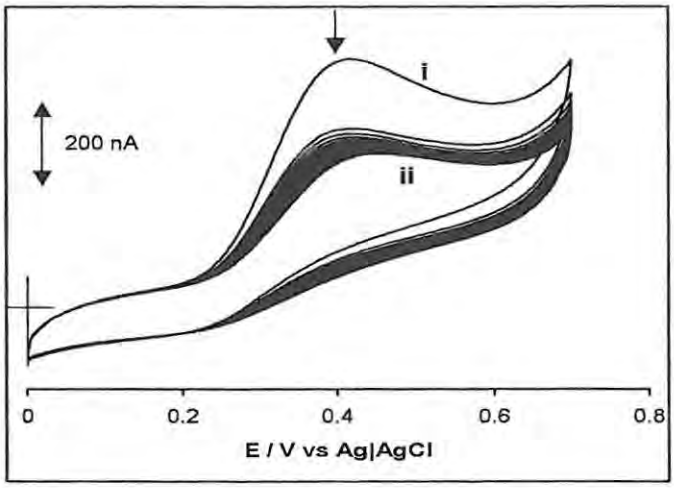

Figure 6.9: Cyclic voltammetric responses of the oxidation peak current of ~ 10^{-5} mol dm^{-3} penicillamine on FeOHETPc-SAM-modified gold electrode on first (i) and after 25 (ii) continuous scans.

Mechanism of thiol oxidation with MPc

Addition of aqueous solutions of the thiols to solutions of the MPc complexes in DMF or DMSO solutions resulted in some shifts in the Q band maximum. For instance, spectroscopic (UV-Vis) interaction of L-cysteine with FeOBTPc in DMF (Figure 6.10A) and FeOHETPc in DMSO (Figure 6.10B) resulted in ~ 8 and 4 nm shifts, respectively. The shift of absorption peak is normally used as an indication of coordination to the $M^{(II)}Pc$ species.[175,178] The generally accepted[78,175,177] mechanism for the electrocatalytic

oxidation of L-cysteine and its derivatives by MPc complexes is oxidation of central metal in $M^{II}Pc$ forming $M^{III}Pc$ followed by electron transfer from the L-cysteine to the latter. Similar mechanism is proposed for the MPc-SAMs catalysed oxidation of all thiols investigated in this work.

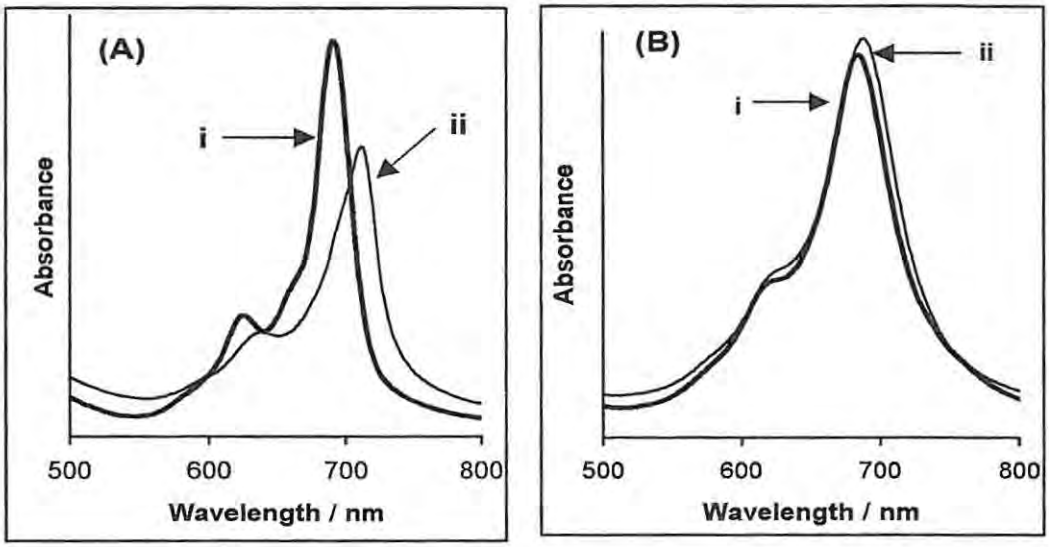

Figure 6.10: UV-Vis spectral changes of (A) FeOBTPc in DMF and (B) FeOHETPc in DMSO before (i) and after (ii) addition of ~ 0.02 ml aqueous solution of L-cysteine.

Thus, catalytic oxidation of thiol by the MPc-SAM may be represented as follows:

$$RSH + M^{II}Pc \rightleftharpoons RS^{-}M^{II}Pc + H^{+} \qquad 6.1$$

$$RS^{-}M^{II}Pc \rightleftharpoons RS^{-}M^{III}Pc + e^{-} \qquad 6.2$$

$$RS^{-}M^{III}Pc \rightleftharpoons M^{II}Pc + RS^{\bullet} \qquad 6.3$$

$$2\,RS^{\bullet} \rightleftharpoons RSSR \qquad 6.4$$

where RSH = thiol (L-cysteine, homocysteine and penicillamine), $^{\bullet}SR$ = thiyl radical, and RSSR = disulphide (e.g. cystine); with equations 6.2 and 6.3 being, most probably, the rapid and the slowest (rate-determining) steps, respectively.[255]

6.2 Electrocatalytic Oxidation of Thiocyanate

Electrocatalytic oxidation of thiocyanate in acidic pH on the gold electrodes modified with the SAMs of MOBTPc and MOHETPc species showed well-defined voltammograms at peak potentials near +0.75 V vs Ag|AgCl (Table 6.2). No peaks were observed for SCN^- on unmodified gold electrodes. Figure 6.11 shows typical voltammetric responses of the SAMs of CoOBTPc (Figure 6.11A and B) and FeOHETPc (Figure 6.11C and D) on gold electrodes following addition of increasing concentrations of thiocyanate in pH 4. Analogous voltammetric features were obtained using electrodes modified with CoOHETPc and FeOBTPc species. In all cases, the catalytic oxidation peaks due to SCN^- occurred at less positive potentials on FePc-SAM modified electrodes than on their CoPc analogues, as was observed above for thiol complexes (Table 6.2).

Table 6.2: Comparative peak potential (Ep) and limit of detection (LoD) for the electrocatalysed reactions of thiocyanate in acidic conditions using electrodes modified with CoPc and FePc species.

MPc species	Electrode material	E_p / V vs (Ag|AgCl)	LoD / mol dm^{-3}	References
CoOBTPc, **33**	SAM-Au	0.78	$1.1\pm0.8 \times 10^{-7}$	This work
CoOHETPc, **40**	SAM-Au	0.75	$9.1\pm0.5 \times 10^{-6}$	This work
FeOBTPc, **35**	SAM-Au	0.76	$1.0\pm0.6 \times 10^{-7}$	This work
FeOHETPc, **36**	SAM-Au	0.74	$9.1\pm0.5 \times 10^{-6}$	This work
FePcCl	PVC membrane	Not stated	$\sim 10^{-6}$	151
CoPc	PVC membrane	Not stated	5.0×10^{-7}	405

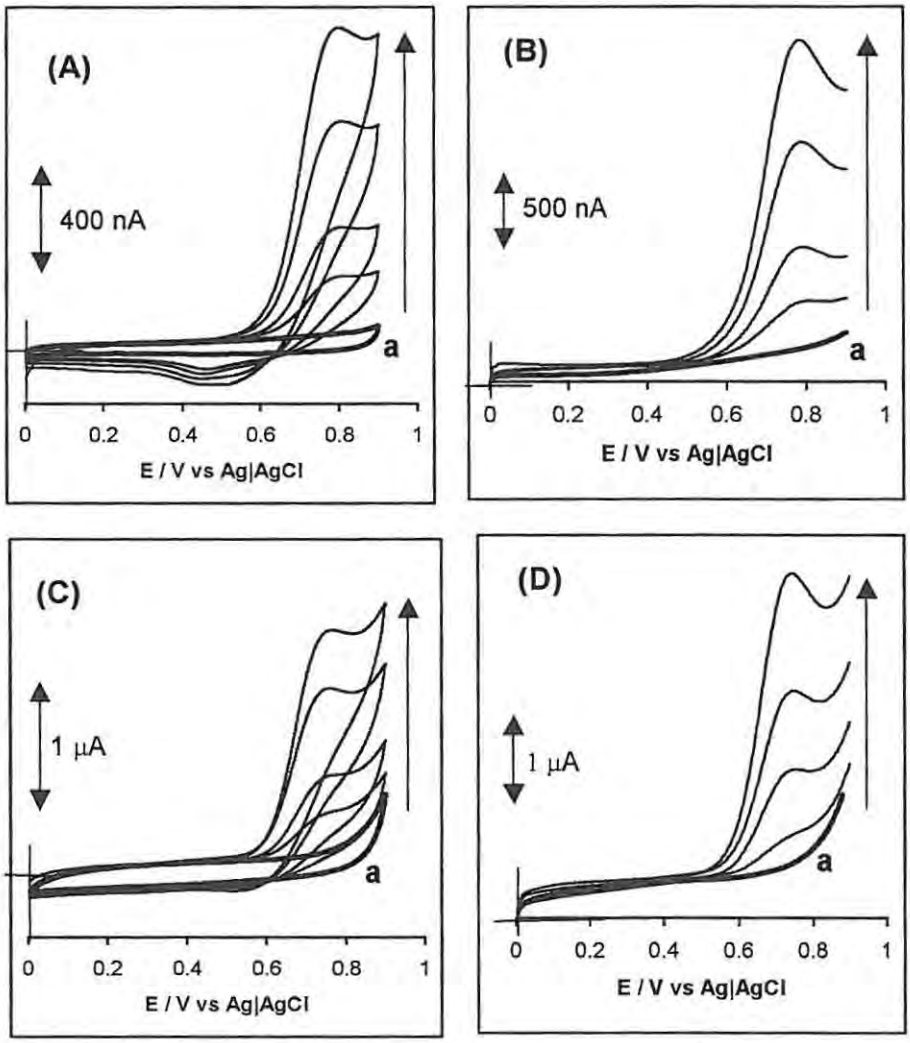

Figure 6.11: Voltammograms of CoOBTPc-SAM (A and B) and FeOHETPc-SAM (C and D) before (a) and on addition of 2.0×10^{-5}, 4.0×10^{-5}, 8.0×10^{-5} and 1.2×10^{-4} mol dm^{-3} (inner to outer curves) thiocyanate in pH 4. A and C = Cyclic voltammograms; B and D = Osteryoung square wave voltammograms.

Figure 6.12 gives the typical linear plot of i_p vs $\nu^{1/2}$ for 6×10^{-5} mol dm^{-3} thiocyanate using CoOBTPc-SAM modified electrode (for scan rates ranging from 10 – 800 mVs^{-1}), which is indicative of diffusion-controlled reaction. Plots of i_p vs [SCN^-]

were linear up to ~10^{-4} mol dm^{-3} (exemplified in Figure 6.13). The LoD are in the region of ~ 10^{-6} mol dm^{-3} and the results are comparable with those in literature (Table 6.2).

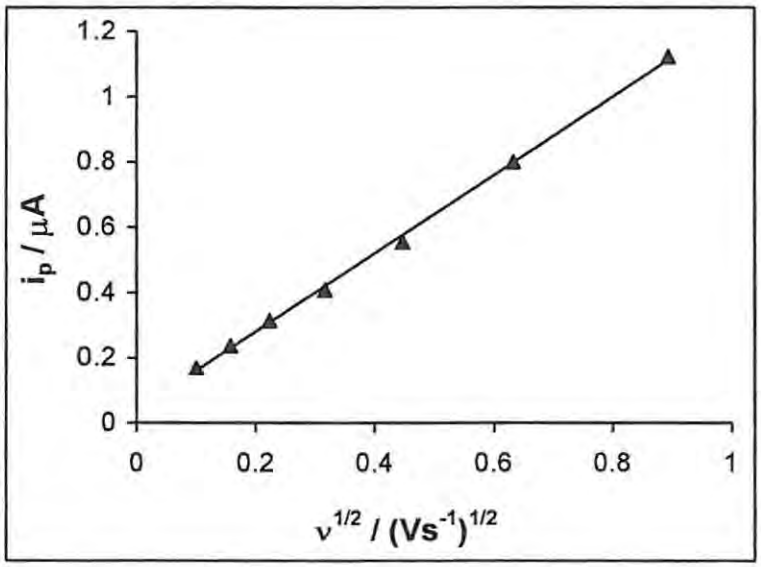

Fig.6.12: Relationship between i_p and $\nu^{1/2}$ at CoOBTPc-SAM in pH 4 buffer solution containing 4.0 x 10^{-5} mol dm^{-3} thiocyanate.

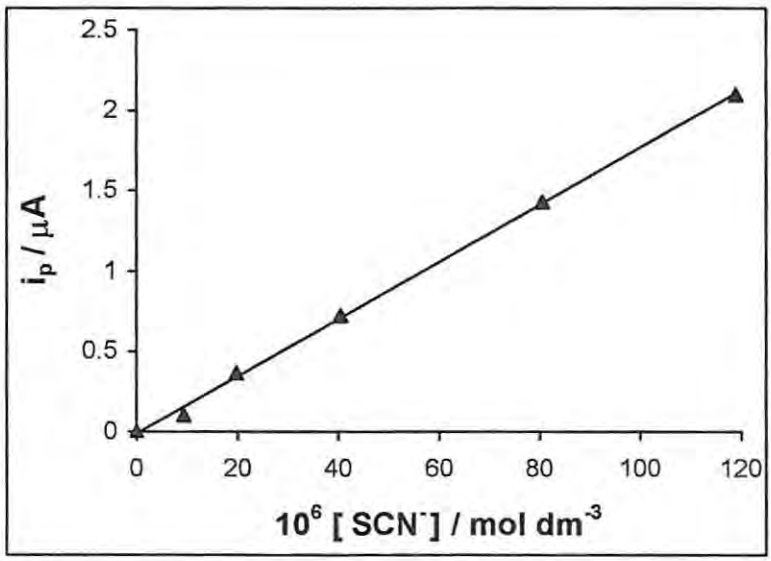

Fig.6.13: Relationship between i_p and [SCN^-] at CoOBTPc-SAM in pH 4 buffer solution.

Repetitive CV cycling of the MPc-SAM modified gold electrodes in aqueous solutions of thiocyante showed no change in voltammograms. Figure 6.14 shows typical repetitive cyclic voltammogram (25 scans) of ~10^{-4} mol dm^{-3} SCN^- using CoOBTPc-SAM modified electrode in the 0.0 to 0.9 V potential window. It is evident from Figure 6.14 that continuous cycling showed no detectable change in the catalytic peak current. Rescanning in fresh pH 4 aqueous solutions, for instance in the pH 4 alone, a peak similar in magnitude with the initial peak due to the adsorbed SAM was obtained. This result is a good indication that the modified electrodes are very stable, i.e. not fouled by the oxidation products of the SCN^-.

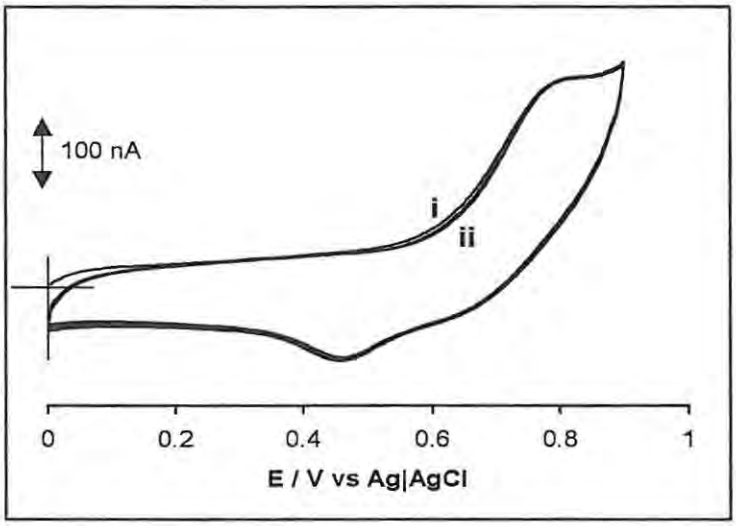

Figure 6.14: Typical cyclic voltammetric responses of 4.0 x 10^{-5} mol dm^{-3} thiocyanate on CoOBTPc-SAM modified gold electrode on first (i) and after 25 (ii) continuous scans. Scan rate = 25 mV s^{-1}.

The effect of pH on the cyclic voltammetric responses of the SCN^- on the MPc-SAM modified gold electrodes was also examined, Figure 6.15. It was found that: (i) oxidative peak potential of the SCN^- was essentially constant in the acidic and neutral

region (pH 2 – 7) but shifted in the negative direction by ~ 100 mV, with peak broadening, at pH ≥ 8; and (ii) a reductive peak appeared near 0.4 V vs Ag|AgCl in the acidic pH but disappeared in the neutral and alkaline media. As an example, Figure 6.15 gives comparative cyclic voltammograms of 4.05 x 10^{-5} mol dm^{-3} SCN^- at pHs of 4 (i) and 9 (ii) using CoOBTPc-SAM modified gold electrode. A similar shift in peak potential at alkaline pH has been observed before[150,151,405] for the oxidation of SCN^- using electrodes modified with PVC-containing MPc and was attributed to increased interference from OH^- ions. The appearance of the reduction peak in the thiocyanate

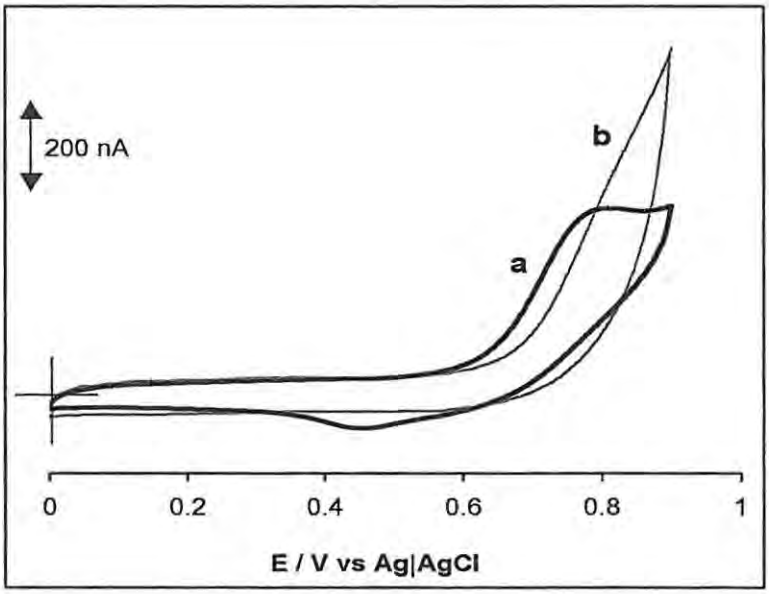

Figure 6.15: Cyclic voltammetric responses of CoOBTPc-SAM modified gold electrodes in the presence of 4.0 x 10^{-5} mol dm^{-3} thiocyanate at (a) pH 4 and (b) pH 9. Scan rate = 25 mV s^{-1}.

electrocatalysed oxidation in acidic medium is most likely to be due to the generation of the thiocyanic acid, HSCN. The lack of a detectable reductive peak in the alkaline

medium is not surprising since it is expected that the generation of the HSCN from KSCN to be much higher in acidic than alkaline pH.

Mechanism of thiocyanate oxidation with MPc

The mechanism for the interaction of MPc complexes with SCN^- is not known. To get a preliminary insight into this, the spectroscopic interaction of the SCN^- with the MOBTPc and MOHETPc using UV-Vis spectroscopy was examined. The electronic spectra of either MOBTPc or MOHETPc (~ 10^{-6} mol dm^{-3}) in DMF or DMSO solutions in the presence of KSCN showed very little (~ 1 nm) or no shifts in wavelength of either the Soret or Q bands, however both bands showed increase in intensity with time. For example, the spectroscopic change of the interaction between CoOHETPc and SCN^- in DMSO (Figure 6.16) showed an increase in intensity of the Q band maximum with negligible shift in wavelength. This spectral change is in good agreement with the

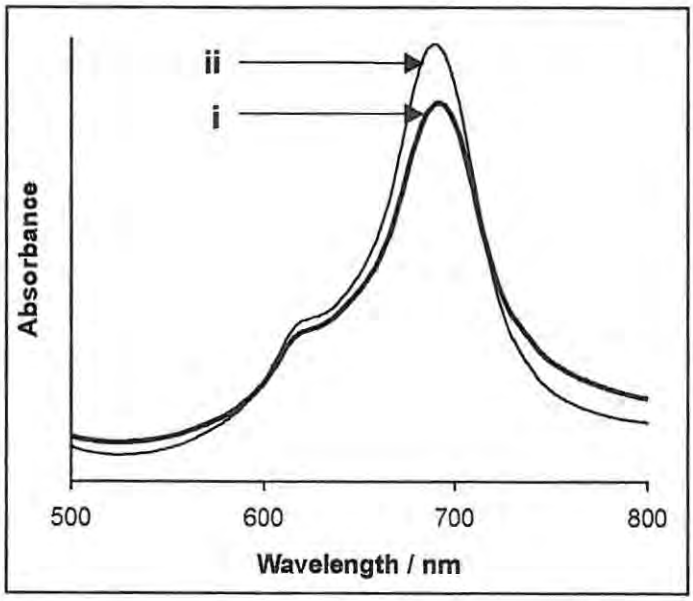

Figure 6.16: UV-Vis spectral changes of CoOHETPc in DMSO before (i) and after (ii) addition of DMSO solution of SCN^-.

observations of Gao et al.[150] on the spectroscopic interaction of SCN^- with the iron center of the μ-oxotetraphenyl porphyrinatoiron, $[(FeTPP)_2O]$ complex. The mechanism for the interaction of SCN^- with PVC-membrane electrodes modified with μ-oxotetraphenyl porphyrinatoiron, $(H_2O)_2(FeTPP)_2O$, is known[150] to be the result of axial ligand exchange reaction of the axially ligated water molecule with the SCN^-. Thus, Equations 6.5 and 6.6 may be used to represent the possible mechanism for the interaction of SCN^- with gold electrodes modified with the SAMs of MOBTPc and MOHETPc species. The observation of the reductive peak due to the HSCN (Figure 6.15) in acidic condition seems to lend more credence to this hypothesis. Further investigations into this mechanism should be undertaken.

$$M^{II}Pc + nSCN^- \rightleftharpoons (SCN)_n\text{-}M^{II}Pc \qquad 6.5$$

$$(SCN)_n\text{-}M^{II}Pc + nH^+ \rightleftharpoons M^{II}Pc + nHSCN \qquad 6.6$$

where n = 1 or 2

Effect of interferent anions on thiocyanate oxidation with MPc

All known reports[149-152,405-408] on electrochemical detection of thiocyanate indicate that some of the possible interferent anions are ClO_4^-, NO_3^-, Br^-, and Cl^-. Anion-selective electrodes made with classical liquid ion exchangers, such as quaternary ammonium salts, respond to anions in the so-called Hofmeister selectivity sequence;[406] $ClO_4^- > SCN^- > NO_3^- > Br^- > Cl^-$. However, it is well established[150,151,405-408] that potentiometric membrane electrodes based on metalloporphyrin and metallophthalocyanine films show greater selectivities for thiocyanate over several other anions (i.e. anti-Hofmeister selectivity sequence). Although the MPc-SAM gold electrodes developed here are not

membrane-based, the effect of the above anions on the detection of SCN^- anion using the developed MPc-SAM modified gold electrodes was investigated. A 100-fold molar ratio (in relation to thiocyanate) of the above common anions did not interfere in the detection of 1×10^{-5} mol dm^{-3} thiocyanate, except for a slight shift to more positive potentials of the catalytic peak. The potential of the catalytic peak shifted to more positive values as follows: $SCN^- > ClO_4^- > Br^- > Cl^- \approx NO_3^-$. This anti-Hofmeister order observed here is similar to those observed by other workers using PVC membrane (potentiometric) thiocyanate-ion selective electrodes based on metalloporphyrin and metallopthalocyanine films. The generally accepted[150,151,405-408] reason for the anti-Hofmeister response is the preferential coordination of the thiocyanate ion (as a fifth or sixth ligand) to the central metal of the metalloporphyrin and metallophthalocyanine complex over other anions. The same reason is proposed for the result observed here for MPc-SAM-modified gold electrodes, as suggested by the UV-Vis (Figure 6.16) and the proposed mechanism (equations 6.5 and 6.6).

6.3 Interaction of Cyanide with MPc-SAM Modified Gold Electrodes

Electrochemical detection of cyanide with bare gold or gold electrode modified with the SAMs of the MOBTPc or MOHETPc (M = Co or Fe) were performed at pH 10 buffer solutions despite the susceptibility of the MPc-SAMs to desorption at pH ≥ 10 (further discussed in Section 6.4 below). This choice is necessary because in acidic pH values cyanide exists mainly as hydrogen cyanide, HCN. At pH 7, cyanide exists as 100% HCN while at pH 10.2 more than 90% of total cyanide is free cyanide.[409] Electro-catalytic oxidation of cyanide occurs at potentials greater than 0.6V,[410,411] thus a potential window of 0.0 and 0.80V vs Ag|AgCl was employed in this study. Figure 6.17 shows typical Osteryoung square wave voltammetric responses of CoOHETPc-SAM modified

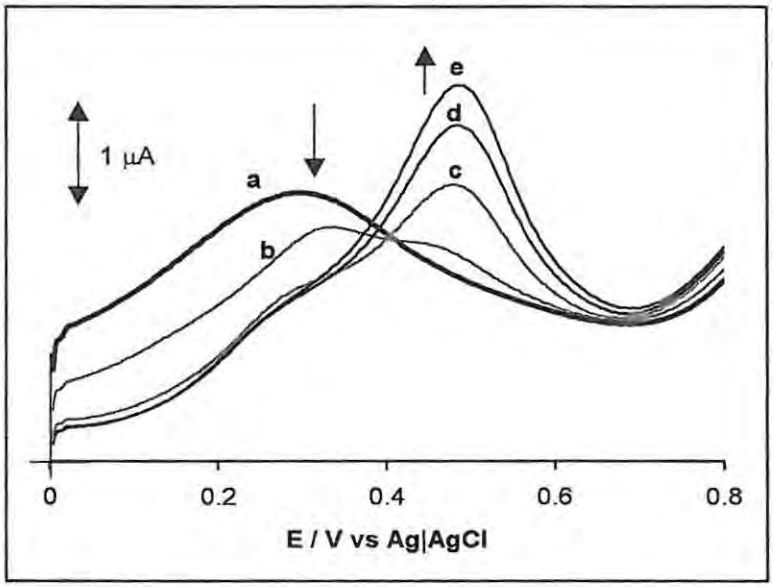

Figure 6.17: Osteryoung square wave voltammetric responses of CoOHETPc-SAM modified gold electrode before (a) and after addition of (b) 5 x 10^{-6} (c) 1.0 x 10^{-5} (d) 2.0 x 10^{-5} and (e) 3.5 x 10^{-5} mol dm^{-3} cyanide solution, pH 10.

gold electrode with increasing concentration of cyanide. In buffer solution alone (curve a), the $[M^{(III)}Pc(-2)]^+$ / $[M^{(II)}Pc(-2)]$ redox couple was observed at ~ 0.3 V vs Ag|AgCl. As the concentration of cyanide was increased (curves b – d), the peak current due to $[M^{(III)}Pc(-2)]^+$ / $[M^{(II)}Pc(-2)]$ redox couple decreased with the formation of a new peak, centered near ~ 0.5 V vs Ag|AgCl. All MPc-SAM modified electrodes showed similar behaviour as for CoOHETPc-SAM above (Figure 6.17), with cyclic voltammetry showing a return peak at $E_{1/2}$ ~ 0.5 V vs Ag|AgCl after cyanide addition, in each case. A peak, almost equal in magnitude as the one at ~ 0.5 V vs Ag|AgCl, was observed with bare gold electrode (for the same concentration range employed in Figure 6.17), indicative of gold-cyanide reaction. Continuous scanning of MPc-SAM in 1.0×10^{-5} mol dm^{-3} cyanide solution resulted in corresponding increase in the peak currents. Thus, the loss of the $[M^{(III)}Pc(-2)]^+$ / $[M^{(II)}Pc(-2)]$ redox couple with corresponding appearance and enhancement of the peak current at ~ 0.5 V may be attributed to coordination of cyanide with the central metal of the MPc-SAM complexes, coupled with etching (gradual desorption) process of gold electrode.

Bare gold is known to undergo rapid etching when immersed in aqueous alkaline cyanide solution,[276,411-416] even at low applied potential (+0.1 V vs Ag|AgCl[276,416]), according to equation 6.7.[415]

$$4Au + 8CN^- + O_2 + 2H_2O \longrightarrow 4[Au(CN)_2]^- + 4OH^- \qquad 6.7$$

The etching process is strongly inhibited by SAMs of certain long-chain alkanethiols {e.g. hexadecanethiol (HDT) and octadecanethiol (OCT)}, presumably because the SAMs blocks access of cyanide to the gold surface.[276] Also, cyanide etching has been

used as an indirect method for detecting pinholes/defects in alkanethiol SAMs.[276,416] Unfortunately, there are only a few alkanethiols that are capable of protecting gold surface from the etching effects of cyanide-based solutions.[417,418] For example, whereas the SAMs of hexadecanethiol (HDT) and octadecanethiol (OCT)[276,415-418] can act as good etch masks against cyanide, SAMs of eicosanethiol (ECT)[418] cannot. Thus, the results obtained in this work for the interaction of MPc-SAMs modified gold electrodes clearly suggest that these MPc-SAMs, like most alkanethiol SAMs,[417,418] cannot protect gold against the etching effect of cyanide solutions, even in nitrogen atmosphere conditions used in this experiment.

6.4 Reproducibility and Stability of MPc-SAM Modified Gold Electrodes

Stability of electrode is extremely important, as it is one of the most decisive parameters for potential usage of the developed electrode in analysis. The stability of the MPc-SAM-modified gold electrode was investigated in several ways. In the first experiment discussed above, Figure 6.9, repetitive cyclic voltammetry resulted in current decrease for thiols but the electrode could be re-newed by dipping/rinsing in acid solution. As described above, the MPc-SAMs can be used for the electro-oxidation of thiocyanate without poisoning of the modified electrodes. Cyanide detection in alkaline medium results in the desorption of SAM and etching of gold surface.

However, a more interesting experiment is to store the electrode in a nitrogen atmosphere for several days and then compare the activity of the electrode with the one obtained before the electrode was stored in nitrogen. Fig. 6.18 shows the cyclic voltammograms of L-cysteine obtained on a gold electrode freshly modified with CoOBTPc (curve i) and at the same electrode stored in nitrogen atmosphere for five days (curve ii). It can be seen that the kinetics of electron transfer is slower after five days of storage, which means that the electrode suffers from an ageing effect during dry storage for a longer period. However the peak current of that wave is almost the same as the one obtained at the freshly prepared electrode. This means that at higher overpotentials, mass transport of L-cysteine still controls the overall oxidation rate and in that potential region, electron transfer is still a much faster process. Despite the observed ageing effect, the electrode can still be used. However, a better approach is to store the modified gold electrode in a buffer solution.

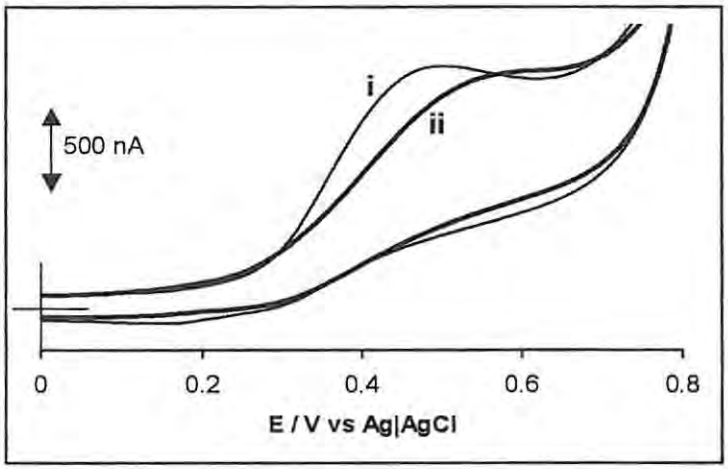

Figure 6.18: Electrocatalytic oxidation of 1.60 x 10^{-4} mol dm^{-3} L-cysteine in pH 4 buffer solution at CoOBTPc-SAM modified gold electrode before (i) and after (ii) 5 days dry storage in nitrogen atmosphere. Scan rate = 100 mV s^{-1}.

Thirdly, stability study was performed by simply storing in aqueous acidic solution before and after use in electrocatalysis experiments with thiols. The calibration plot between peak current and L-cysteine concentration is shown in Figure 6.19 at the start time (curve ii), after 8 (curve iii), 14 (curve iv) and 28 days (curve v) of storing the electrode. Curve i is the theoretical plot (obtained using the Randles-Sevcik equation,[209,210]) with D = 4.8x10^{-5} cm^2 s^{-1} and n = 1. During this period the electrode was stored in a pH = 4 buffer solution. It can be seen that the response of the modified gold electrode is more or less constant as a function of time and meets with the theoretically obtained peak currents. This result shows that the stability of the electrode is very good and is due to the strong bonding of the monolayer at the gold surface.

Finally, the stability of the SAM was studied as a function of pH and applied potential. The most permissible conditions for their electrocatalytic applications are the pH regions ranging from pH 2-9 and at applied potential window between –0.2 to +0.7 V

vs Ag|AgCl. At pH ≥ 10 the SAM reductively desorbs at potentials more negative than –0.2 V vs Ag|AgCl and oxidatively at > +0.70 V vs Ag|AgCl.

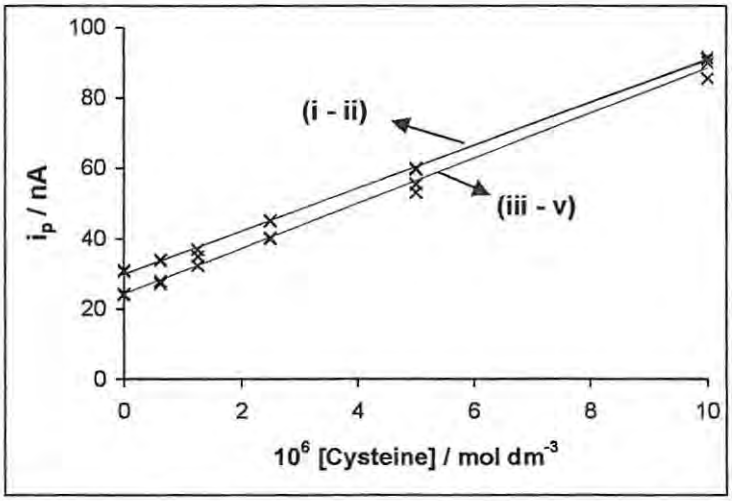

Figure 6.19: Calibration plot between current and L-cysteine concentration at a gold electrode modified with CoOBTPc obtained by calculation using the Randles-Sevcik equation (i) and experimental after (ii) 0, (iii) 8, (iv) 14 and (v) 28 days of storing the modified electrode. In between the electrode was stored in pH = 4 buffer solution.

The high alkaline pH and potential values conditions required for CN^- experiments are not only detrimental to the stability of the MPc-SAMs, as described in Section 6.3 above, but serve as convenient conditions for gold etching by cyanide. These harsh conditions conspired against any further investigations on the electrocatalytic interactions of cyanide with MPc-SAMs, so these results were not followed up. However, to gain an insight on the interaction of cyanide with MOBTPc or MOHETPc (M = Co or Fe) complexes, spectrophotometric technique was employed. The Chapter (7) that follows discusses the kinetics and equilibria of interactions of MOBTPc or MOHETPc, especially FeOBTPc, using UV-Vis spectrophotometry.

CHAPTER 7

SPECTROSCOPIC STUDIES OF THE INTERACTION OF CYANIDE WITH THIOL-DERIVATISED METALLOPHTHALOCYANINE COMPLEXES*

* The following publication resulted from part of the research work presented in this chapter and it is not referenced further in this thesis:

7. K. Ozoemena and T. Nyokong, *J. Chem. Soc., Dalton Trans.*, 2002,1806.

7.1 Interaction with Octabutylthiophthalocyaninatoiron(II)

7.1.1 Spectroscopic Studies

The changes in spectral features observed on addition of cyanide solutions to solutions of FeOBTPc, **35** are shown in Figure 7.1. On addition of DMSO solutions of

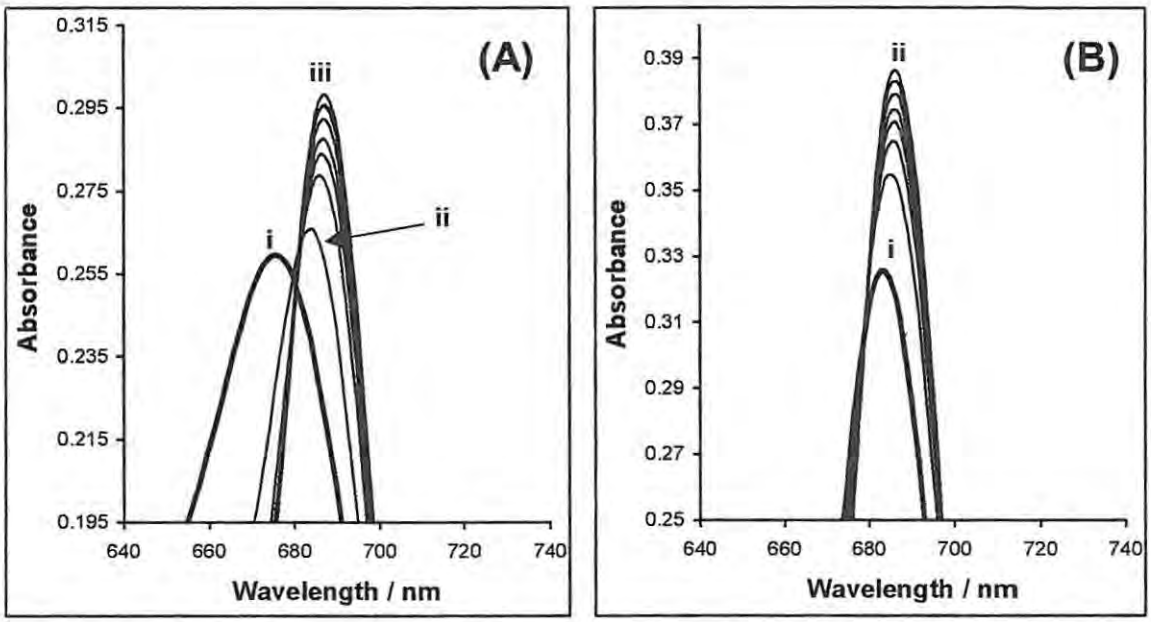

Figure 7.1: Absorption spectral changes observed on addition of (A) cyanide (4.8×10^{-4} mol dm^{-3}) to FeOBTPc, **35** (2.8×10^{-6} mol dm^{-3}) in DMSO, (i) $(DMSO)_2FeOBTPc$, (ii) $[(DMSO)(CN)FeOBTPc]^-$, (iii) $[(CN)_2FeOBTPc]^{2-}$, and of (B) cyanide (5.4×10^{-4} mol dm^{-3}) to $(DMF)_2FeOBTPc$, **37** (2.8×10^{-6} mol dm^{-3}) in DMF (i) $(DMF)_2FeOBTPc$, (ii) $[(CN)_2FeOBTPc]^{2-}$.

cyanide to a DMSO solution of FeOBTPc, **35**, the Q band first shifts from 676 nm to 684 nm, then to 686 nm and increases in intensity with time {(Figure 7.1(A)}. In the DMF system, on the other hand, the Q band shifts from 684 to 686 nm and then increases with time {(Figure 7.1(B)}. In each solvent system, for example DMF (Figure 7.2), the B band splits and shifts to lower energy. The band in the 450 nm regions also splits. The splitting

of the B bands in the UV region and their shifts to lower energy is typical of cyanide coordination.[32] The final spectra for both DMF and DMSO systems are similar to the

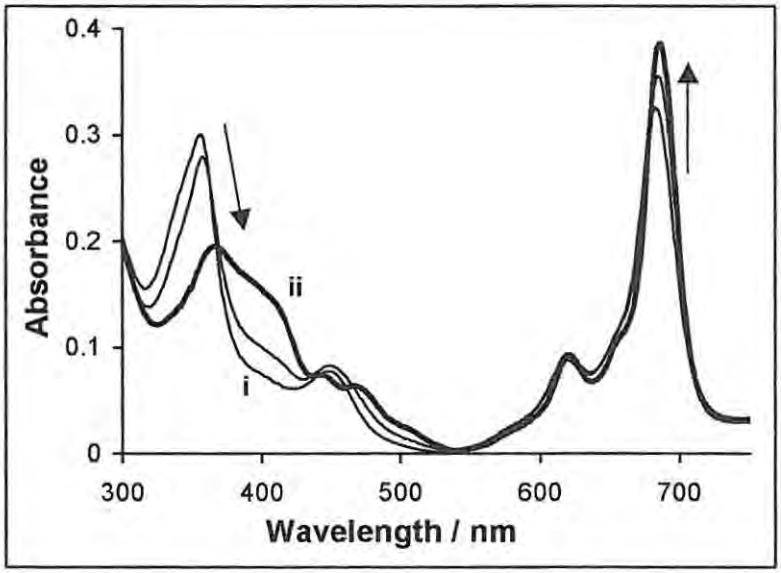

Figure 7.2: Absorption spectral changes observed (i) before and (ii) 15 minutes after addition of cyanide ($5.4x10^{-4}$ mol dm^{-3}) to a solution of $(DMF)_2FeOBTPc$, **37** ($2.8x10^{-6}$ mol dm^{-3}) in DMF.

spectra of the dicyano complexes discussed in Chapter 3 (Section 3.1.3.2, Fig.3.8 i and ii). The new spectra are formed with isosbestic points at 368, 524 and 706 nm for the DMSO system, and 365, 430, and 536 nm for the DMF system. Further addition of cyanide had no effect on the position of the peak maxima. These data indicate that the final spectrum obtained on addition of cyanide to a DMSO or DMF solution of **35** is that of the dicyano complex, $[(CN)_2FeOBTPc]^{2-}$.

Axial ligand substitutions in MPc (and porphyrin) complexes occur in a step-wise manner with the coordination of the first cyanide occurring much faster than that of the second.[30,46,50] The shift in the Q band from 676 to 684 nm before the final shift to 686 nm

in the DMSO system shows the step-wise nature of the cyanide coordination. The first shift to 684 nm is most probably due to the formation of the monocyano species, $[(CN)(DMSO)Fe^{(II)}OBTPc]^-$ and the second to 684 nm due to the dicyano complex, $[(CN)_2FeOBTPc]^{2-}$. The coordination of the first axial ligand in MPc complexes generally occurs at a fast rate causing very minor spectroscopic changes that are difficult to observe.[41,46] This may explain why Figure 7.1B does not show the stepwise change in wavelength observed in Figure 7.1A. It is also most likely that the monocyano species, $[(CN)(DMF)Fe^{(II)}OBTPc]^-$ absorbs at about the same wavelength (684 nm) with the original species, $(DMF)_2FeOBTPc$, **37**. Spectral changes for the formation of the monocyano complexes in both solvent systems could not be followed using the techniques employed in this work since the changes occurred very fast. Hence, equilibria and kinetics could only be determined for the formation of the dicyano complex, $[(CN)_2Fe^{(II)}OBTPc]^{2-}$.

7.1.2 Kinetics and Equilibria

Equilibrium data were determined by the standard spectrophotometric technique using the Hill equation[38] (equation 1).

$$\log [A_{eq} - A_o) / (A_\infty - A_{eq})] = n \log [CN^-] + \log K \qquad 7.1$$

where A_{eq} is the equilibrium absorbance at 686 nm, A_o is the absorbance before the addition of cyanide and A_∞ is the absorbance for the complete formation of the dicyano complex. From the plots of log $[A_{eq} - A_o) / (A_\infty - A_{eq})]$ vs log $[CN^-]$ (Figure 7.3) equilibrium constants [$K = (1.3 \pm 0.2) \times 10^3$ with $n = 1.01 \pm 0.04$ in DMSO and $K = (6.8 \pm$

0.8) x 10^2 dm^3 mol^{-1} with n = 0.99 ± 0.05 in DMF] were obtained. A value of n =1 is an indication of the step-wise nature of the coordination of the second cyanide to these

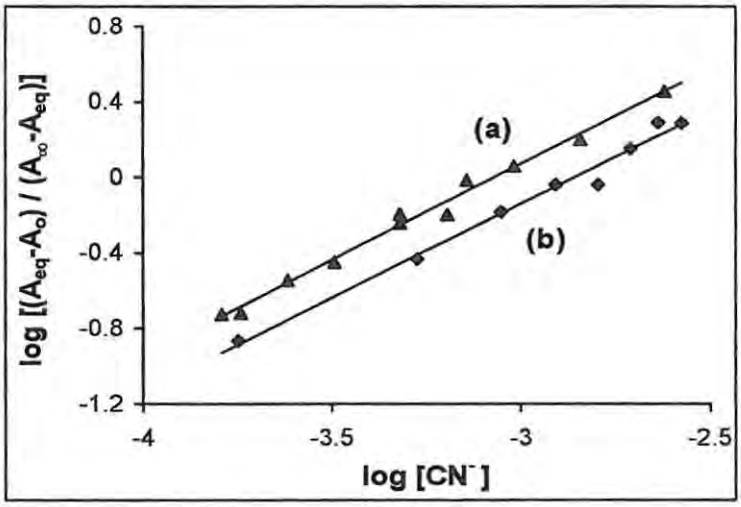

Figure 7.3: Plots of log $[(A_{eq} - A_o)/(A_\infty - A_{eq})]$ vs log $[CN^-]$ for the formation of $[CN)_2FeOBTPc]^{2-}$ in (a) DMSO and (b) DMF.

complexes. K = K_4 (equation below), thus corresponds to the coordination of the second cyanide and formation of the $(CN)_2Fe^{(II)}OBTPc$, **39**, equations 7.2 – 7.5.

$$(L)_2Fe^{(II)}OBTPc \underset{k_{-1}}{\overset{k_1}{\rightleftharpoons}} (L)Fe^{(II)}OBTPc + L \qquad 7.2$$

$$(L)Fe^{(II)}OBTPc + CN^- \underset{k_{-2}}{\overset{k_2}{\rightleftharpoons}} [(L)(CN)Fe^{(II)}OBTPc]^- \qquad 7.3$$

$$[(L)(CN)Fe^{(II)}OBTPc]^- \underset{k_{-3}}{\overset{k_3}{\rightleftharpoons}} [(CN)Fe^{(II)}OBTPc]^- + L \qquad 7.4$$

$$[(CN)Fe^{(II)}OBTPc]^- + CN^- \underset{k_{-4}}{\overset{k_4}{\rightleftharpoons}} [(CN)_2Fe^{(II)}OBTPc]^{2-} \qquad 7.5$$

where L is either DMSO or DMF.

The equilibrium constants obtained in both solvent systems are in the range (within experimental error) for those obtained for the coordination of the second cyanide in FePc complexes[30, 46,47] (Table 7.1). The smaller K_4 value of $(6.8 \pm 0.8) \times 10^2$ dm^3 mol^{-1} in DMF in comparison to the value of $(1.3 \pm 0.2) \times 10^3$ dm^3 mol^{-1} in DMSO is most likely to be due to the stronger O-bonded DMF in comparison to the weaker S-bonded DMSO, hence resulting in the lower lability of the DMF ligand. DMSO is known as a labile ligand because of the weak S-Fe σ-bond.[15] As a π acceptor ligand, DMSO gains extra stability by π back bonding. It has been suggested[40] that this extra stability is reduced in the presence of the electron-withdrawing ring substituents {cf. $K_4 = 1.6 \times 10^3$ dm^3 mol^{-1} for $[(DMSO)(CN)FePc(Cl)_{16}]^-$ compared to $K_4 = 5.7 \times 10^2$ dm^3 mol^{-1} for $[(DMSO)(CN)FePc]^-$ since the electron-withdrawing ligands pull electron density away

Table 7.1: Kinetics and Equilibrium data for the axial exchange reaction of cyanide with iron(II) phthalocyanine complexes in DMSO:

$$[(CN)(L)Fe^{(II)}OBTPc]^- + CN^- \underset{k_{-4}}{\overset{k_4}{\rightleftharpoons}} [(CN)_2Fe^{(II)}OBTPc]^{2-} + L$$

FePc Complex	K_4 / dm^3 mol^{-1}	k_{4f} / dm^3 mol^{-1} s^{-1}	k_{4r} / s^{-1}	Reference
$[(DMSO)(CN)FePc]^-$	5.7×10^2	0.20	3.5×10^{-4}	30
$[(DMSO)(CN)FePc(Cl)_{16}]^-$	1.6×10^3	4.2×10^{-3}	2.3×10^{-6}	46
(CO)(DMSO)FePc	$(6.7 \pm 0.5) \times 10^2$	0.34 ± 0.12	5.9×10^{-4}	47
$[(DMSO)(CN)FeOBTPc]^-$	$(1.3 \pm 0.2) \times 10^3$	$(8.2 \pm 0.3) \times 10^{-2}$	5.5×10^{-5}	This work
$[(DMF)(CN)FeOBTPc]^-$	$(6.8 \pm 0.8) \times 10^2$	$(1.9 \pm 0.1) \times 10^{-2}$	2.5×10^{-5}	This work

from the metal. It would be expected that electron-donating substituents (such as the SC_4H_9-) would result in the increase in stabilization of the Fe-DMSO bond by π back bonding. However, the electron-donating butylthio-group in $[(DMSO)(CN)Fe^{(II)}OBTPc]^-$ results in similar K_4 value as the electron-withdrawing $[(DMSO)(CN)FePc(Cl)_{16}]^-$, again pointing to the weak electron-donating influence of the alkythio-groups.

The rate constants for the formation of the $[(CN)_2Fe^{(II)}OBTPc]^{2-}$ were determined by monitoring the absorption changes at 686 nm. Plots of $\ln(A_\infty - A_t)$ (where A_∞ is the final absorbance at the end of the reaction and A_t is the absorbance at time t) against time were linear for the coordination of cyanide to FeOBTPc as exemplified by Figure 7.4.

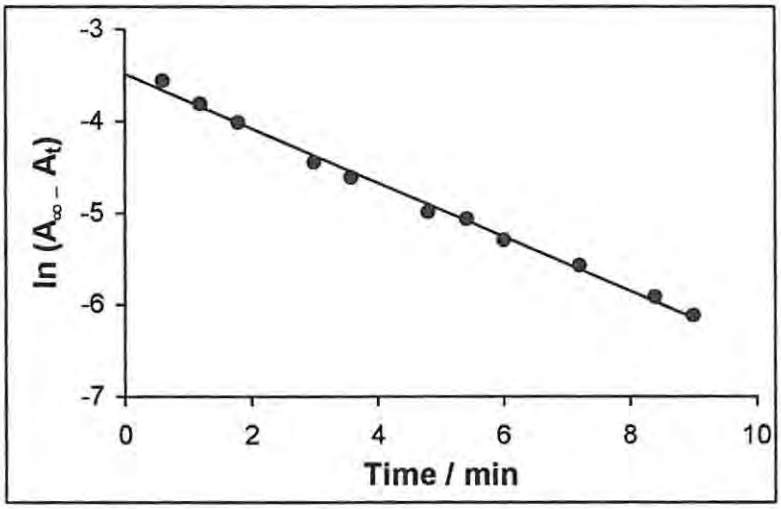

Figure 7.4: Typical plot of ln ($A_\infty - A_t$) vs time for the coordination of CN^- to FeOBTPc, **35** in DMSO

The linearity of the plots is a confirmation that the reaction between FeOBTPc and cyanide is first order with respect to FeOBTPc. The observed rate constant (k_{obs}), which is the slope of the plots of absorbance versus time, was obtained for several concentrations of cyanide. Plots of the observed rate constants against concentrations of

cyanide (Figure 7.5), in either DMSO (Figure 7.5a) or DMF (Figure 7.5b) were linear indicating that the axial ligand exchange reactions are first order with respect to cyanide in both solvent systems.

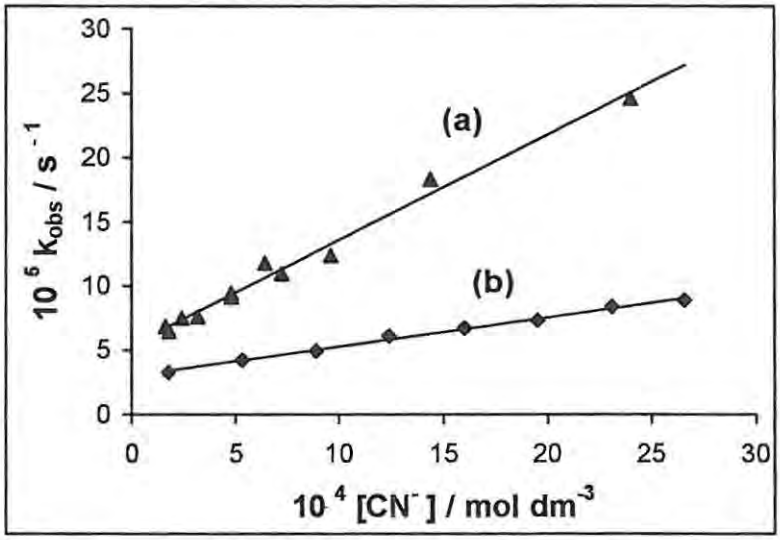

Figure 7.5: The variation of observed rate constants with concentration for the formation of $[CN)_2FeOBTPc]^{2-}$ in (a) DMSO and (b) DMF.

The rate law for the dissociative mechanism is generally given by (equation 7.6) [38-47]

$$k_{obs} = k_{4f}[CN^-] + k_{4r} \qquad 7.6$$

where k_{4f}, the rate constant for the forward reaction, is given by $k_1 k_4 / k_{-1}[L]$ (L =DMSO or DMF) and k_{4r} is the rate constant for the reverse reaction. From the least square analysis of the data presented in Figure 7.5 (summarized in Table 7.1) the values of k_{4f} (obtained from the slopes of the plots) were $(1.9 \pm 0.1) \times 10^{-2}$ dm^3 mol^{-1} s^{-1} in DMF and $(8.2 \pm 0.3) \times 10^{-2}$ dm^3 mol^{-1} s^{-1} in DMSO while k_{4r} values (obtained from the intercepts) were 2.5×10^{-5} s^{-1} in DMF and 5.5×10^{-5} s^{-1} in DMSO. From these values, the

equilibrium constants were estimated from the relationship, $K_4 = k_{4f} / k_{4r} = 7.6 \times 10^2$ dm^3 mol^{-1} s^{-1} in DMF and 1.5×10^3 dm^3 mol^{-1} s^{-1} in DMSO. These values are in good agreement (within experimental errors) with the value of $(6.8 \pm 0.8) \times 10^2$ dm^3 mol^{-1} s^{-1} and $(1.3 \pm 0.2) \times 10^3$ dm^3 mol^{-1} s^{-1} determined directly from equation 7.1 for DMF and DMSO systems, respectively.

It is apparent from Table 7.1 that the rate of coordination of the second cyanide, k_{3f}, to [(DMSO)(CN)Fe$^{(II)}$OBTPc]$^-$ is greater than that for [(DMF)(CN)Fe$^{(II)}$OBTPc]$^-$ by a factor of 4. This is of course due to the higher lability of the DMSO compared to the DMF ligand. However, the k_{4f} value for the coordination of cyanide to [(DMSO)(CN)Fe$^{(II)}$Pc(-2)]$^-$ or (DMSO)(CO)Fe$^{(II)}$Pc(-2) is approximately 3 times greater than that for its coordination to [(DMSO)(CN)Fe$^{(II)}$OBTPc]$^-$ but about 10 times greater than that for the coordination to [(DMF)(CN)Fe$^{(II)}$OBTPc]$^-$. The reason for the discrepancy may not be unconnected to the combined effects of the weak electron-donating influence of the eight peripheral butylthio-substituents and the stronger O-Fe σ-bond arising from DMF ligation. This is consistent with our discussion on electrochemistry concerning the small reducing influence of the alkythio-substituents on the reduction potentials.

7.2 Interaction of Cyanide with other Thiol-derivatised Metallophthalocyanine Complexes of Iron and Cobalt

The possibility of the interaction of cyanide with other thiol-derivatised metallophthalocyanine complexes of iron (FeOHETPc, **36**) and cobalt (CoOBTPc, **33** and CoOHETPc, **40**) was investigated. Addition of cyanide solutions to the solutions of iron complex, **36**, showed similar spectral changes observed for **35** described Section 7.1 above. For example, addition of DMSO solution of cyanide to the DMSO solution of iron complex, **36**, (Figure 7.6) resulted in a shift of the Q band from 685 to 688 nm, then to 692 nm and its increase in intensity with time (Figure 7.6).

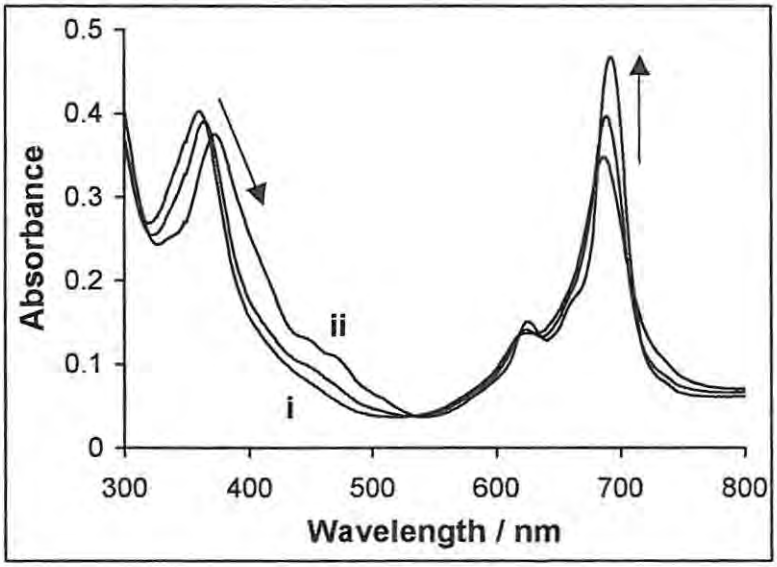

Figure 7.6: Absorption spectral changes observed (i) before and (ii) 20 minutes after addition of cyanide (~ 8 x 10^{-4} mol dm^{-3}) to a solution of FeOHETPc, **36** (~ 5 x10^{-6} mol dm^{-3}) in DMSO.

As was observed for the **35**, the B band also shifted to lower energy (354 to 370 nm) and split, a typical indication of cyanide coordination.[32] The changes in spectral features gave rise to isosbestic points at 368, 530 and 710 nm, for the coordination of CN^- to **36** in

DMSO. The final spectrum of the cyanide coordination with this complex was similar to the spectrum of the dicyano complex $[(CN)_2FeOHETPc]^{2-}$ (**39**), which was synthesized using the established method[29,237] employed in the experimental Section for the **37** and **38** complexes. Although the elemental analysis of $[(CN)_2FeOHETPc]^{2-}$ (**39**) was not satisfactory as the obtained CHN values were much lower than their expected values, it showed satisfactory FTIR with Fe-CN vibrations at 2168 cm^{-1}. Apart from the interaction of CN^- with the central iron of the FeOHETPc complex, there is also the possibility of both the $K^+$and CN^- interacting with the peripheral –OH groups. Such interaction was recently suggested by Drochioiu[419] in his work on the reaction of KCN with the 2,2-dihydroxy-1,3-indanedione. Thus, the equilibria and kinetic studies of the spectral changes shown in (Figure 7.6) were not followed up since any data obtained therefrom will be unreliable. However, the changes indicate interaction of **36** with cyanide.

Interaction of cyanide with the cobalt phthalocyanine, **40** and **33**, complexes were also observed in DMSO. The Q band of **33** shifted from 685 to 700 nm (Figure 7.7), while that of the **40** shifted from 685 to 712 nm. The Q band peak maxima of both complexes increased in intensity very slowly with time, and remained constant after about five hours with no further spectroscopic changes or spectral shifts. These data seem to suggest that the coordination of cyanide to CoPc complexes occurs much slower than for their FePc analogues. The slower coordination of these dicyano CoPc complexes is not surprising since it is known that axial ligand reactions occur faster for FePc than CoPc complexes.[49] Hence, the equilibrium and kinetic studies of the spectral changes observed for these two thio-CoPc complexes were not followed up.

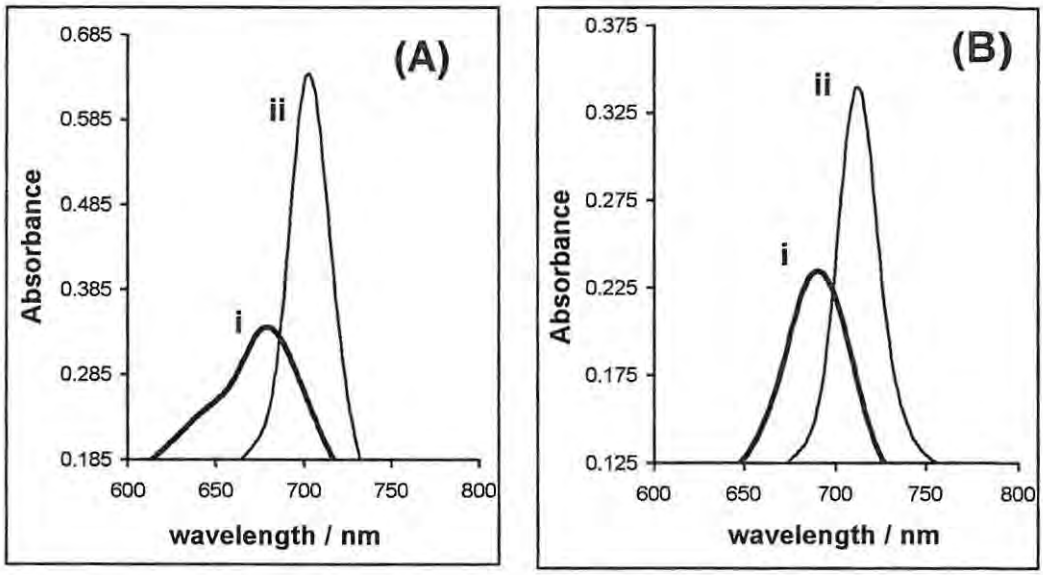

Figure 7.7: Q band absorption spectral changes observed for the DMSO solutions of CoOBTPc, **33** (A) and CoOHETPc, **40** (B) before (i) and after (ii) addition of DMSO solution of cyanide.

Conclusion:

The equilibrium and kinetic data of FeOBTPc for the binding with cyanide are comparable with those reported in literature. The formation of the dicyano species $[(CN)_2Fe^{(II)}OBTPc]^{2-}$ is limited in DMF solution by the weak dissociation of the trans DMF from the central metal iron. Although a direct comparison cannot be made between the rates of cyanide coordination by FePc complexes and the structurally similar iron porphyrin complexes because of differences in experimental conditions, especially with regard to solvent systems, it is worth noting that the rate constant for cyanide binding to iron (II) myoglobin (0.1 dm^{-3} mol^{-1} s^{-1})[420] is approximately the same as cyanide binding to the $[(DMSO)(CN)Fe^{(II)}OBTPc]^-$. This suggests that this complex may offer substantial advantages over the similar analogues reported in the literature.

CONCLUSION

In this work, some metallophthalocyanine complexes (water-soluble and organic-solvent soluble) have been synthesized, characterized and investigated as potential photocatalysts and electrocatalysts. Photochemical properties of the water-soluble sulphonated metallophthalocyanine ($MPcS_4$ and $MPcS_{mix}$, M = Al, Zn, Si or Sn) and octa-carboxymetallophthalocyanine (MOCPc, M = Al or Zn) complexes were investigated. These water-soluble metallophthalocyanine (MPc) complexes, especially the sulphonated aluminium and zinc phthalocyanines, were found to be good photosensitisers for the transformation of the toxic 4-chlorophenol, trichlorophenol and pentachlorophenol in aqueous solutions. The kinetics of the photo-transformation of polychlorophenols depend on a number of factors, and it is essential to establish conditions for the highest degradation efficiency. Results obtained in this work show that the majority of processes (rates of polychlorophenol oxidation and the nature of photoproducts, and sensitiser stability) depend on pH. Hence, substrate ionisation is of crucial importance for any photophysical and photochemical step in the systems investigated. In general, the efficiency of the photo-oxidation of the polychlorophenol, mediated by singlet oxygen, O_2 ($^1\Delta_g$) (Type II reaction mechanism) is lower in comparison with unsubstituted phenol and less chlorinated phenols, due to lower constants of chemical reaction and extensive physical quenching of singlet oxygen by substrates. Trichlorophenol, for instance, is able to deactivate about five molecules of singlet oxygen before it is being destroyed.

Octabutylthiometallophthalocyanine (MOBTPc, where M = Co, Fe or Zn), octa(hydroxyethylthio)metallophthalocyanine (MOHETPc, where M = Co or Fe) and octa(methylphenylthio)phthalocyaninatozinc(II) (ZnOMPPc) complexes were also

synthesized and characterized. The spectral and electrochemical properties of these octa-substituted thiol-derivatised phthalocyanine complexes of cobalt, iron and zinc were comparable to similar complexes in literature. The photochemical properties of the zinc phthalocyanine (ZnOBTPc and ZnOMMPc) complexes in DMF solutions revealed that ZnOBTPc is relatively more stable and more efficient in singlet oxygen generation than ZnOMPPc.

Octa-substituted thiol-derivatised phthalocyanine complexes (MOBTPc, MOHETPc and ZnOMPPc) were, for the first time, immobilized onto gold electrodes using the self-assembling technique. The integrity of these SAMs, with respect to their ability to block certain Faradaic processes, was interrogated using surface electrochemical experiments in aqueous solutions. Results showed that the SAMs provided excellent blocking capability to the Faradaic processes emanating from gold surface oxidation, and for underpotential deposition (UPD) of copper and oxidation of ferric ammonium sulphate in perchloric acid. One of the important revelations of the study was the great improvement of the ill-defined metal-centered reversible couple of the SAM of FeOBTPc and CoOBTPc by simple repetitive cycling of the modified electrode in a DMF solution containing TBAP within a short space of time (ca. 2 minutes). This 'activation' process provides good information concerning the surface coverage and orientation of the monolayer. Surface electrochemistry of the MPc-SAMs suggested that the solid-like MOBTPc and ZnOMPPc assume flat (octopus) orientation while the liquid-like MOHETPc mostly take on the perpendicular orientation. The MPc-SAM electrode modification process is reproducible. The stability of the modified electrodes is dependent on both pH and applied potential, showing greater stability in the

pH 2-9 and at applied potential window between –0.2 to +0.7 V vs Ag|AgCl. At pH ≥ 10, the SAM is prone to both reductive and oxidative desorptions.

Since phthalocyanine complexes of cobalt (CoPc) and iron (FePc) are well established as good electrocatalysts, the gold electrodes modified with the SAMs of CoOBTPc, CoOHETPc, FeOBTPc and FeOHETPc were investigated for possible applications as electrochemical sensors for the detection of thiols (L-cysteine, homocysteine and penicillamine) and cyanides (cyanide and thiocyanate). The modified electrodes showed comparable electrocatalytic behaviour towards the detection of the thiols and thiocyanate in aqueous solutions (acidic pH 4) with detection limits in the range of $\sim 10^{-7}$ and 10^{-6} mol dm^{-3}, respectively. The modification process was reproducible and the modified electrodes showed good stability and, if stored in pH 4 buffer solutions, could be used for the analysis of thiols and thiocyanate for about a month without the need for recalibration. Electrochemical interaction of the MPc-SAM modified gold electrodes with cyanide was hampered by the etching of gold electrodes by cyanide solutions as well as the harsh experimental conditions, high pH and potential values that are detrimental to the stability of the MPc-SAMs, required for this study.

Following the discovery of the adverse etching effect of cyanide against gold, a greater insight on the interaction of cyanide with the MOBTPc and MOHETPc (M = Fe and or Co) was made possible using UV-Vis spectrophotometry. Kinetic and equilibria studies revealed interaction of FeOBTPc with cyanide in non-aqueous solutions. Kinetics and equilibrium measurements for the interaction of cyanide with FeOBTPc in both dimethylsulphoxide (DMSO) and dimethylformamide (DMF) revealed the formation of the bis(cyano)phthalocyaninatoiron(II) complex, $[(CN)_2FeOBTPc]^{2-}$. The kinetic and

equilibria data obtained are comparable with literature reports of cyanide coordination with FePc complexes. This result is interesting since metallopthalocyanines serve as useful models for investigating biological processes involving hemoproteins due to their close structural relationship with porphyrins. FePc is usually considered analogous to the haem group of hemoglobin and myoglobin, hence the study of its axial coordination with cyanide is important in the search for anti-cyanide drugs.

REFERENCES:

1. *Phthalocyanines: Properties and Applications*, eds. C.C. Leznoff and A.B.P. Lever, VCH publishers, New York, 1989, 1993, 1993,1996, Vol.1-4.

2. P. Gregory, *J. Porphyrins Phthalocyanines*, 1999, **3,** 468.

3. N.B. McKeown, *Chem. Ind.,* 1999, 92.

4. R.P. Linstead, *J. Chem. Soc.,* 1934, 1016.

5. J.M. Robertson, *J. Chem. Soc.,* 1935, 615.

6. J.M. Robertson, *J. Chem. Soc.,* 1936, 1195.

7. E. Ough, T. Nyokong, K.A.M. Creber and M.J. Stillman, *Inorg. Chem.,* 1988, **27**, 2725.

8. A.B.P. Lever, S.R. Pickens, P.C. Minor, L. Licoccia, B.S. Ramaswamy and K. Magnell, *J. Am. Chem. Soc.*, 1981, **103**, 6800.

9. H. Sugimoto, T. Higashi and M. Mori, *Chem. Lett.,* 1982, 801.

10. P. Sayer, M. Gouterman and C.R. Connell, *Acc. Chem. Res.,* 1982, **15**, 73.

11. C.C. Leznoff in *Phthalocyanine: Properties and Applications*, eds. C.C. Leznoff and A.B.P. Lever, VCH Publishers, New York, 1989, Vol.1.

12. R.B. Linstead and A.R. Lowe, *J. Chem. Soc.,* 1934, 1022.

13. A. Shaabani, *J. Chem. Res. (S),* 1998, 672.

14. D.M. Maree and T. Nyokong, *J. Chem. Res. (S),* 2001, 68.

15. C.C. Leznoff, S.M. Marcuccio, S. Greenberg, A.P.B. Lever and K.B. Tomer, *Can. J. Chem.,* 1985, **63**, ~~133~~. 623.

16. A. Louati, M.E.I. Meray, J.J. Andre, J. Simon, K.M. Kadish, M. Gross and A. Giraurdeau, *Inorg. Chem.,* 1985, **24**, 1175.

17. D. Wöhrle and V. Schmidt, *J. Chem. Soc., Dalton Trans.*1988, 549.

18. P.D. Hale, W.J. Pietro, M.A. Ratner, D.E. Ellis and T.J. Marks, *J. Am. Chem. Soc.*, 1987, **109**, 5943.

19. D. Schlettwein and N.R. Armstrong, *J. Phys. Chem.,* 1994, **98**, 11771.

20. H. Meeier, W. Albrecht, D. Worhle and A. Hahn, *J. Phys. Chem.*, 1994, **98**, 11771.

21. M. Hanack, P. Haisch and H. Lehman, *Synthesis,* 1993, 387.

22. D. Wöhrle, M. Eskes, K. Shigehara and A. Yamada, *Synthesis*, 1993, 194.

23. A. G. Gürek and Ö. Bekaroğlu, *J. Chem. Soc., Dalton Trans.*, 1994, 1419.

24. J.H. Weber and D.H. Busch, *Inorg. Chem.*, 1965, **4**, 469.

25. S.V. Kudrevich, M.G. Galpern and J.E. van Lier, *Synthesis*, 1993, 779.

26. K. Sakamoto and E. Ohno, *Prog. Org. Coating,* 1997, **31**, 139.

27. R.W. Boyle and J.E. van Lier, *Synlett,* 1993, 351.

28. M. Ambroz, A. Beeby, A.J. MacRobert, M.S.C. Simpson, R.K. Svensen and D. Phillips, *J. Photochem. Photobiol. B: Biol.*, 1991, **9**, 87.

29. J. Metz and M. Hanack, *J. Am. Chem. Soc.*, 1983, **105**, 829.

30. T. Nyokong, *J. Chem. Soc., Dalton Trans.*, 1993, 3601

31. L. Boucher, *Coordination Chemistry of Macrocyclic compounds*, ed. G.A. Melson, Plenium Press, 1979, 461.

32. T. Nyokong and M.J. Stillman in *Phthalocyanines: Properties and Applications,* eds. C.C. Leznoff and A.B.P. Lever, VCH Publishers, New York, 1989, Vol.1.

33. A.B.P. Lever, *Adv. Inorg. Radiochem.*, 1965, **7**, 28.

34. M. Gouterman, in *The Porphyrins, Vol. III, part A, Physical Chemistry*, ed. D. Dolphin, Academic Press, New York, 1978.

35. B.R. Hellebone and M.J. Stillman, *J. Chem. Soc., Faraday Trans. II*, 1978, **74**, 2107.

36. Y. Iyeshida, K. Yakushi and H. Kuroda, *Chem. Phys.*, 1984, **87**, 101.

37. R. Taube, *Pure Appl. Chem.*, 1974, **38**, 427.

38. P. Ascenzi, M. Brunori, P. Pennesi, C. Ercolani and F. Monacelli, *J. Chem. Soc., Dalton trans.*, 1990, 105.

39. G. Pennesi, C. Ercolani. G. Rossi, P. Ascenzi, M. Brunori and F. Monacelli, *J. Chem. Soc., Dalton trans.*, 1985, 1113.

40. G. Pennesi, C. Ercolani. P. Asceni, M. Brunori and F. Monacelli, J. *Chem. Soc., Dalton trans.,* 1985, 1107.

41. D. Y. Stynes, *Inorg. Chem.,* 1977, **16**, 1170.

42. J. Martinsen, M. Miller, D. Trojan and D.A. Sweigart, *Inorg. Chem.,* 1980, **19,** 2162.

43. D. A. Sweigart, *J. Chem. Soc., Dalton trans.,* 1976, 1476.

44. J.G. Jones and M.V. Twigg, *Inorg. Chem.,* 1969, **8**, 2120.

45. K.M. Kadish, L.A. Bottomley and J.S. Cheng, *J. Am. Chem. Soc.,* 1978, **100**, 2731.

46. T. Nyokong, *Polyhedron,* 1995, **14**, 643.

47. A. Boffi, C. Ercolani, F. Monacelli and P. Ascenzi, *Inorg. Chim. Acta*, 1998, **267,** 109.

48. J. Oni and T. Nyokong, *Polyhedron,* 2000, **19**, 1355.

49. T. Nyokong, *Polyhedron,* 1995, **14**, 2325.

50. T. Nyokong and J. Guthrie-Strachan, *Inorg. Chim. Acta,* 1993, **208**, 239.

51. V.N. Nemykin, V. YA. Chernii, S.V. Volkov, N.I. Bundina, O.L. Kaliya, V.D. Li and E.A. Lukyanets, *J. Porphyrins Phthalocyanines,* 1999, **3**, 87.

52. C. Ercolani and F. Monacelli, *J. Porphyrins Phthalocyanines,* 2001, **5**, 668.

53. M.Thamae and T. Nyokong, *Polyhedron,* 2002, **21**, 133

54. C. Chebotareva and T. Nyokong, *J. Coord. Chem,.,* 1999, **46**, 433.

55. M. Sekota and T. Nyokong, *Polyhedron,* 1997, **16**, 3279.

56. S.L. Vilakazi and T. Nyokong, *Polyhedron,* 1998, **17**, 4415.

57. P. Gregory, *High Technology Applications of Organic Colorants*, Plenum Press, New York, 1991.

58. G.C.S. Collins and D.J. Schiffrin, *J. Electroanal. Chem.* 1982, **139**, 335.

59. M.M. Nicholson in *Phthalocyanine: Properties and Applications*, eds. A.P.B. Lever, C.C. Leznoff, VCH Publishers, New York, 1993. Vol. 3.

60. N. Toshina and T. Tominaga, *Bull. Chem. Soc., Jpn*, 1996, **69**, 2111.
61. J.E. Kuder, *J. Imaging Sci.,* 1988, **32**, 51.

62. R. Ao, L. Kummert and D. Haarer, *Adv. Mater.,* 1995, **5**, 495.

63. S. Nalwa and J. A. Shirk in *Phthalocyanine: Properties and Applications*, eds. A.P.B. Lever and C.C. Leznoff, VCH Publishers, New York, 1993, Vol. 4.

64. J. Simon and P. Bassoul in *Phthalocyanine: Properties and Applications*, eds. A.P.B. Lever and C.C. Leznoff, VCH Publishers, New York, 1993, Vol. 2.

65. D.K.P. Ng, Y.-O. Yeung, W.K. Chan and S.-C. Yu, *Tetrahedron Lett.,* 1997, 38, 6701.

66. D. Worhle and D. Meissener, *Adv. Mater.,* 1991, **3**, 129.

67. D. Worhle, L. Kreienhoop and D. Schlettwein in *Phthalocyanine: Properties and Applications*, eds. A.P.B. Lever and C.C. Leznoff, VCH Publishers, New York, 1996, Vol.4.

68. A.B.P. Lever, M.R. Hempstead, C.C. Leznoff, W. Lui, M. Melnik, W.A. Nevin and P. Seymour, *Pure Appl. Chem.,* 1986, **58**, 1467.

69. B. Simic-Glavaski in *Phthalocyanine: Properties and Applications*, eds. A.P.B. Lever and C.C. Leznoff, VCH Publishers, New York, 1993, Vol.3.

70. J. Simon and J.J. Andre, *Molecular Semiconductors,* Springer, Berlin, 1985.

71. J. Simon and T. Toupance in *Comprehensive Supramolecular Chemistry.* Vol. 10: *Supramolecular Technology*, ed. D.N. Reinhoudt, Pergamon, London, 1996.

72. N.B. Mckeown in *Phthalocyanine Materials: Synthesis, Structure And Function. Chemistry of Solid State Materials,* Cambridge University Press, New York, 1998.

73. M . Iwamoto, *J. Mater. Chem.*, 2000, **10**, 99.

74. K. Morishige, S. Tomoyasu and G. Iwano, *Langmuir*, 1997, **13**, 5184.

75. A.W. Snow and W.R. Barger in *Phthalocyanine: Properties and Applications*, eds. A.P.B. Lever and C.C. Leznoff, VCH Publishers, New York, 1989, Vol.1.

76. S. Vilakazi and T. Nyokong, *Polyhedron,* 2000, **19**, 229.

77. R.K. Sen, J. Zagal and E. Yeager, *Inorg. Chem.,* 1977, **16**, 3379.

78. J. Limson and T. Nyokong, *Electroanalysis,* 1997, **9**, 255.

79. K. Hanabusa and H. Shirai in *Phthalocyanine: Properties and Applications*, eds. A.P.B. Lever and C.C. Leznoff, VCH Publishers, New York, 1993, Vol.2.

80. H. Kasuga in *Phthalocyanine: Properties and Applications*, eds. A.P.B. Lever and C.C. Leznoff, VCH Publishers, New York, 1996, Vol.4.

81. B. Meunier and A. Sorokin, *Acc. Chem. Res.*, 1997, **30**, 470.

82. M. Thamae and T. Nyokong, *J. Electroanal. Chem.*, 1999, **470**, 126.

83. J.R. Harbour, J. Tromp and M.L. Hair, *J. Am. Chem. Soc.*, 1980, **102**, 1874.

84. J.D. Spikes, *J. Photochem. Photobiol.* 1986, **43**, 691.

85. K. Lang, D.M. Wagnerová and J. Brodilová, *J. Photochem. Photobiol. A: Chem.* 1993, **72**, 9.

86. R. Gerdes, D. Wörhle, W. Spiller, G. Schneider, G. Schnurpfeil and G. Schulz-Ekloff, *J. Photochem. Photobiol. A: Chem.* 1997, **111**, 65.

87. E. Ben-Hur and I. Rosenthal, *Int. J. Radiat. Biol.*, 1985, **47**, 145.

88. E. Ben-Hur and I. Rosenthal, *J. Photochem. Photobiol.*, 1985, **42**, 129.

89. I. Rosenthal and E. Ben-Hur, in *Phthalocyanine: Properties and Applications*, eds. A.P.B. Lever and C.C. Leznoff, VCH Publishers, New York, 1989, Vol.1.

90. D. Phillips, *Pure Appl. Chem.*, 1995, **67**, 117.

91. I. J. MacDonald and T. Dougherty, *J. Porphyrins Phthalocyanines,* 2001, **5**, 105.

92. S. Baker, M.C. Pretty, G.G. Roberts and M.V. Twigg, *Thin Solid Films*, 1983, **99**, 53.

93. D.G. Zhu, M.C. Petty and M. Harris, *Sens. Actuators B,* 1990, **2**, 265.

94. D. Crouch, S.C. Thorpe, M.J. Cook, I. Chambrier and A.K. Ray, *Sens. Actuators B,* 1994, **18-19**, 411.

95. M.J. Cook, *J. Mater. Chem.*, 1996, **6**, 677.

96. M.J. Cook, *Pure Appl. Chem*, 1999, **71**, 2145

97. M. Nicoli, B. Rey, T. Torres, C. Mingotaud, P. Delhaes, M.J. Cook and S.C. Thorpe, *Synth. Metals*, 1999, **102**, 1462.

98. I. Chambrier, M.J. Cook and D.A. Russell, *Synthesis*, 1995, 1283.

99. M.J. Cook, R. Hersans, J. McMurdo and D.A. Russell, *J. Mater. Chem.*, 1996, **6**, 149.

100. T.R.E. Simpson, D.J. Revell, M.J. Cook and D.A. Russell, *Langmuir*, 1997, **13**, 460.

101. D.J. Revell, I. Chambrier, M.J. Cook and D.A. Russell, *J. Mater. Chem.*, 2000, **10**, 31.

102. Z. Li and M. Lieberman, *Supramol. Science,* 1998; **5:** 485.

103. Z. Li and M. Lieberman in *Fundamental and Applied Aspects of Chemically Modified Surfaces,* eds. J.P. Blitz and C.B. Little, Royal Soc. Chem., Lettchworth, U.K. 1999; pp24-35

104. Z. Li, M. Lieberman and W. Hill, *Langmuir*, 2001, **17**, 4887.

105. *Pentachlorophenol*, World Health Organisation, Geneva, 1987.

106. J. Paasivitra, *Water Sci. Technol.*, 1988, **20**, 119.

107. R.B. Clark, *Halogenated Hydrocarbons in Marine Pollution*, 2nd ed. Oxford Science publications, Oxford, 1989.

108. D. Henscher, *Angew. Chem., Int. Ed. Engl.*, 1994, **33**, 1920.

109. *Directive 76/464/EEC*, European Community Law, 1976.

110. *Toxic Substance Control Act*, United States Environmental Protection Agency, Washington, D.C., 1979.

111. D.G. Crosby, K.I. Beynon, P.A. Greve, F. Korte, G.G. Sztill and J.W. Vonk, *Pure Appl. Chem.*, 1981, **53**, 1051.

112. M.L. Hitchman, R.A. Spackman, N,C. Ross and C. Agra, *Chem. Soc. Rev.*, 1995, **24**, 423.

113. M. Alexander, *Science*, 1981, **211**, 132.

114. W. Reineke in *Microbial Degradation of Aromatic Compounds*, ed. D.T. Gibson, Marcel Dekker, New York, 1984.

115. B. Winter, W. Zimmermann in *Metal Ions in Biological Systems, Vol. 28, degradation of Environmental Pollutants by Micro-organisms and their Metalloenzymes,* eds. H. Sigel and A. Sigel, Marcel Dekker, New York, 1992.

116. H. Al-Ekabi and N. Serpone, *J. Phys. Chem.*, 1988, **92**, 5726.

117. H. Al-Ekabi, N. Serpone, E. Pelizzetti, C. Minero, M.A. Fox and R.B. Draper, *Langmuir*, 1989, **5**, 250

118. G. Al-Sayyed, J.-C. D'Oliveira and P. Pichat, *J. Photochem. Photobiol. A: Chem.*, 1991, **58**, 99.

119. A. Mills and S. Morris, *J. Photochem. Photobiol. A: Chem.*, 1993, **71**, 75.

120. A. Mills, S. Morris and R. Davies, *J. Photochem. Photobiol. A: Chem.*, 1993, **70**, 183.

121. A. Mylonas and E. Papaconstantinou, *J. Mol. Catal.*, 1994, **92**, 267.

122. U. Stafford, K.A. Gray and P.V. Kamat, *J. Phys. Chem.*, 1994, **98**, 6343.

123. A. Mills and R. Davies, *J. Photochem. Photobiol. A: Chem.*, 1995, **85**, 173.

124. A. Haarstrick, O. M. Kut and E. Heinzle, *Environ. Sci. Tech.*, 1996, **30**, 817.

125. J.M. Kesselman, O. Weres, N.S. Lewis and M.R. Hoffman, *J. Phys. Chem. B*, 1997, **101**, 2637.

126. E. Leyva, E. Moctezuma, M.G. Ruiz and L. Torres-Martinez, *Catal. Today*, 1998, **40**, 367.

127. X. Li, J. W. Cubbage, T.A. Tetzlaff and W.S. Jenks, *J. Org. Chem.*, 1999, **64**, 8509.

128. X. Li, J. W. Cubbage and W.S. Jenks, *J. Org. Chem.*, 1999, **64**, 8525.

129. N. Nensala and T. Nyokong, *J. Mol. Catal. A: Chem.*, 2000, **164**, 69.

130. S. Vollmuth, A. Zajc and R. Hiessner, *Environ. Sci. Tech.*, 1994, **28**, 1145.

131. J.R. Plimmer and U.I. Kligebiel, *Science*, 1971, **174**, 407.

132. J. Hong, D.-G. Kim, C. Cheong, S. –Yjung, M.-R Yoo, K.-J. Kim, T.-K. Kim and Y.-G. Park, *Anal. Sci.*, 2000, **16**, 621.

133. M. Fukushima, K. Tatsumi and K. Morimoto, *Environ. Toxicol. Chem.*, 2000, **19**, 1711.

134. N. Nensala and T. Nyokong, *Polyhedron*, 1997, **16**, 2971.

135. Y.I. Skurlatov, L.S. Ernestova, E.V. Vichutinskaya, D.P. Samsonov, I.V. Semenova, I.Y. Rod'ko, V.O. Shvidky, R.I. Pervunina and T.J. Kemp, *J. Photochem. Photobiol. A: Chem.*, 1997, **107**, 207.

136. M. Nowakowska and K. Szczubiaka, *J. Photochem. Photobiol. A: Chem.*, 1995, **91**, 81.

137. M. Nowakowska, K. Szczubiaka and S. Zapotoczny, *J. Photochem. Photobiol. A: Chem.*, 1996, **97**, 93.

138. A. Sorokin, J.-L. Séris and B. Meunier, *Science*, 1995, **268**, 1163.

139. A. Sorokin, S. De Suzzoni-Dezard, D. Poullain, J. –P. Noel and B. Meunier, *J. Am Chem. Soc.*, 1996, **118**, 7410.

140. A. Sorokin and B. Meunier, *Chem. Eur. J.* 1996, **2**, 1308.

141. A. Hadash, A. Sorokin, A. Rabin and B. Meunier, *New J. Chem.*, 1998, 45.

142. B. Meunier and A. Sorokin, *Acc. Chem. Res.*, 1997, **30**, 470.

143. K. Kasuga, K. Mori, T. Sugimori and M. Handa, *Bull. Chem. Soc. Jpn.*, 2000, **73**, 939.

144. B. Ballantyne and T.C. Marrs in *Clinical and Experimental Toxicology of Cyanides*, eds. B. Ballantyne and T.C. Marrs, Wright publishers, Bristol, 1987.

145. D.A. Labianca, *J. Chem. Educ.*, 1979, **56**, 788.

146. T.C. Marrs in *Clinical and Experimental Toxicology of Cyanides*, eds. B. Ballantyne, T.C. Marrs, Wright publishers, Bristol, 1987.

147. A.H. Hall, W.H. Doutre, T. Ludden, K.W. Kulig and B.H. Rumak, *Clin. Toxicol.*, 1987, **25**, 121.

148. R. Rahimi and P. Hambright, *J. Porphyrins Phthalocyanines,* 1998, **2**, 493.

149. J.A.Cox and T. Gray, *Anal. Chem.*, 1988, **60**, 1710.

150. D. Gao, J-Z. Li, R-Q. Yu and G-D. Zheng, *Anal. Chem.* 1994, **66**, 2245.

151. M.K. Amini, S. Shahrokhian and S. Tangestaninejad, *Anal. Chim Acta,* 1999, **402**, 137.

152. A. Abbaspour, M.A. Kamyabi, A.R. Esmaeilbeig and R. Kia, *Talanta*, 2002, **57**,859.

153. W.A. Kleinman and J.P. Richie, *Biochem. Pharm.*, 2000, **60**, 19.
154. E. Bald, E. Kaniowska, G. Chwatko and R. Glowacki, *Talanta*, 2000, **50**, 1233.

155. P.C. White, N.S. Lawrence, J. Davies and R.G. Compton, *Electroanalysis*, 2002, **14**, 89.

156. A.A. Al-Majed, *Anal. Chim. Acta,* 2000, **408**, 169.

157. L.S. Stryer in *Biochemistry,* 3rd ed., W.H. Freeman and Co., New York, 1988.

158. M.T. Goodman, K. McDuffe, B. Hernandez, L.R. Wilkens and J. Selhub, *Cancer*, 2000, **89**, 376.

159. C.R. Chong and D.S. Auld, *Biochemistry,* 2000, **39**, 1015.

160. R. Saetre and D.L. Rabenstein, Anal. Chem., 1978, **50**, 276.

161. I.M Kolthoff and C. Barnum , *J. Am. Chem. Soc.,* 1940, **62**, 3061.

162. I.M Kolthoff and C. Barnum, *J. Am. Chem. Soc.,* 1941, **63**, 520.

163. I.M Kolthoff, W. Stricks and N. Tanaka, *J. Am. Chem. Soc.,* 1955, **77**, 5215.

164. G.D Christian, E.C. Knoblock and W.C. Purdy, *Biochem. Biophys. Acta*, 1963, **66**, 415.

165. M.T. Stankovich and A.J. Bard , *J. Electroanal. Chem*, 1977, **75**, 487.

166. F.G. Banina, J.C. Moreira and A.G. Fogg , *The Analyst*, 1994, **119**, 309.

167. D.G Davis and E. Bianco, *J Electroanal. Chem.,* 1966, **12**, 254.

168. J. Koryta and J. Prodac, *J Electroanal. Chem.,* 1968, **17**, 185.

169. J.A. Reynaud, B. Maltoy and P. Canessau, *J Electroanal. Chem.*, 1980, **114**,195.

170. R. Eggli and R. Asper, *Anal. Chim Acta*, 1978, **101**, 253.

171. N. Spătaru, B. Sarada , E. Popa , D.Tryk and A. Fujishima, *Anal. Chem.*, 2001, **73**, 514.

172. P. Vasuvedan, N. Poughat and A.K. Shuklat, *Appl. Organomet. Chem.,* 1996, 591.

173. M. Sekota and T. Nyokong, *Electroanalysis,* 1997, **9**, 1257.

174. T.J. O'Shea and S.M. Lunte, *Anal. Chem.,* 1994, **66**, 307.

175. T.J. Mafatle and T. Nyokong, *J. Electroanal. Chem.,* 1996, **408**, 213.

176. M. Sekota and T. Nyokong, *J. Porhyrins Phthalocyanines,* 1999, **3**, 477.

177. M.K. Halbert and R.P. Baldwin, *Anal. Chem.,* 1985, **57**, 591.

178. S. Maree and T. Nyokong, *J. Electroanal. Chem.,* 2000, **492**, 120.

179. J.G. Calvert and J.N. Pitts Jr., *Photochemistry,* John Wiley, New York, 1967.

180. D.R. Arnold, N.C. Baird, J.R. Bolton, J.C.D. Brand, P.W.M. Jacobs, P. de Mayo and W.R. Ware, *Photochemistry: An Introduction*, Academic Press, New York, 1974.

181. P. Suppan, *Chemistry and Light*, 1st ed. Royal Soc. Chem., Cambridge, 1994.

182. J.R. Darwent, P. Douglas, A. Harriman, G. Porter and M.-C. Richoux, *Coord. Chem. Rev.,* 1982, **44**, 83.

183. E.A. lissi, M.V. Encinas, E. Lemp and M.A. Rubio, *Chem. Rev.,* 1993, **93**, 699.

184. G. Ferraudi, in *Phthalocyanine: Properties and Applications*, eds. A.P.B. Lever and C.C. Leznoff, VCH Publishers, New York, 1989, Vol.1.

185. X. Zhang and H. Xu, *J. Chem. Soc., Faraday Trans.* 1993, **89**, 3347.

186. D. Dhami and D. Phillips, *J. Photochem. Photobiol. A: Chem.* 1996, **100**, 77.

187. V. Iliev, V. Alexiev and L. Bilyarrska, *J. Mol. Catalysis A: Chem.*, 1999, **137**, 15.

188. W.A. Nevin, W. Liu, S. Greenberg, M.R. Hempstead, S.M. Maruccio, M.M. Melnik, C.C. Leznoff and A.B.P. Lever, *Inorg. Chem.*, 1987, **26**, 291.

189. Z. Li and M. Lieberman, *Inorg. Chem.,* 2001, **40**, 932.

190. K. Kasuga and M. Tsutsui, *Coord. Chem. Rev.*, 1980, **32**, 67.

191. N. Nensala and T. Nyokong, *Polyhedron,* 1996, **15**, 867.

192. N. Nensala and T. Nyokong, *Polyhedron,* 1998, **17**, 3467.

193. O.T.E. Sielcken, M.M. van Tilborg, M.F.M. Rocks, R. Hendricks, W. Drenth and R.J.M. Nolte, *J. Am. Chem. Soc.*, 1987, **109**, 4261.

194. I.Geigakoudi and T.H. Foster, *J. Photochem. Photobiol.* 1998, **67**, 612.

195. J.D. Spikes and J.C. Bommer, *J. Photochem. Photobiol.*, 1993, **58**, 346.

196. T.J. Dougherty, *Adv. Photochem.*, 1992, **17**, 275.

197. J.D. Spikes, *J. Photochem. Photobiol.*, 1992, **55**, 797.

198. N. Kutznetsova, N. Grestova, O.Yuzhakova, V. Negrimovsky, O. Kaliya and E. Lukyanets, *Zh. Obsch. Khim.*, 2000, **71**, 39.

199. M.G. Lagorio, L.E. Dicellio and E.A. San Roman, *J. Photochem. Photobiol., B: Biol.*, 1989, **3**, 615.

200. W. Spiller, H. Kliesch, D. Worhle, S. Hackbarth, B. Roder and G. Schnurpfiel, *J. Porphyrins Phthalocyanines,* 1998, **2**, 145.

201. I.B.C. Matheson, *Photochem. Photobiol.*,1979, **29**, 875.

202. C.S. Foote, SPIE Institute Series, 1990, **6**, 115.

203. I. Kraljic and S. El Mohsni, *Photochem. Photobiol.*,1978, **28**, 577.

204. K. Kasuga, A. Fujita, T. Miyazako, M. Handa and T. Sugimori, 2000, **3**, 634.

205. C.S. Foote, T-Y. Ching and G.G. Geller, *Photochem. Photobiol.*, 1974, **20**, 511.

206. M.J. Thomas and C.S. Foote, *Photochem. Photobiol.*, 1978, **27**, 683.

207. P.G. Tratnyek and J. Holgné, *Environ. Sci. Tech.*, 1991, **25**, 1596.

208. A.E. Kaifer and M. Gómez-Kaifer, *Supramolecular Electrochemistry*, Wiley-VCH, New York, 1999.

209. J. Wang, *Analytical Electrochemistry*, VCH Publishers Inc., New York, 1994.

210. P.T. Kissinger, C.R. Preddy, R.E. Shoup and W.R. Heineman in *Laboratory Techniques in Electroanalytical Chemistry*, 2nd ed., P.T. Kissinger and W.R. Heineman, Eds.; Marcel Dekker Inc., New York, 1996.

211. D.B. Hibbert, *Introduction to Electrochemistry,* Macmillan, London, 1993.

212. P.A. Christensen and A. Hamnett, *Techniques and Mechanism in Electrochemistry*, 1st ed., Blackie Academic & Professional, London, 1994.

213. A.J. Bard and L.R. Faulkner, *Electrochemical Methods; Fundamentals and Applications,* John Wiley and Sons, New York, 1996.

214. C.M.A. Brett and A.M.O. Brett, *Electrochemistry, Principles, Methods and Applications*, Oxford University Press, Oxford, 1993.

215. F.M. Hawkridge in *Laboratory Techniques in Electroanalytical Chemistry*, 2nd ed., eds. P.T. Kissinger and W.R. Heineman,. Marcel Dekker Inc., New York, 1996.

216. E.R. Brown and R.F. Large, in *Physical Methods of Chemistry, Vol.1-Part IIA: Electrochemical Methods*, eds. A. Weissberger and B. Rossiter, Willey-Interscience, New York, 1971.

217. R.S. Niccholson, *Anal. Chem.*, 1965, **37**, 1351.

218. W.R. Heineman and P.T. Kissinger in *Laboratory Techniques in Electroanalytical Chemistry*, 2nd ed., eds. P.T. Kissinger and W.R. Heineman, Marcel Dekker Inc., New York, 1996.

219. J.G. Osteryoung, *Acc. Chem. Res.*, 1993, **26**, 77.

220. J.G. Osteryoung and R.A. Osteryoung, *Anal. Chem.*, 1985, **57**, 101A

221. R.Cieslinski and N.R. Armstrong, *Anal. Chem.*, 1979, **51**, 565.

222. F. Hartl, K.M. Deněk, *J. Electroanal. Chem.*, 1991, **317**, 179.

223. A.B. P Lever, E.R. Milaeva and G. Speier, *Phthalocyanines: Properties and Applications*, eds. A.P.B. Lever and C.C. Leznoff, VCH Publishers, New York, 1993, Vol.3.

224. T. Nyokong, *Synth. Met.*, 1994, **6,** 107.

225. K. Takahashi, M. Kawashima, Y. Tomita and M. Itoh, *Inorg. Chim. Acta*, 1995, **232**, 69.

226. G. Ferraudi, T. Nyokong, M. Feliz, M. Perkovic and D.P. Rillema, *Inorg. Chim Acta*, 1994, **215**, 27.

227. T. Nyokong, *Polydehron*, 1994, **13**, 215.

228. T. Nyokong, *Polydehron*, 1994, **13**, 2067.

229. M. Sekota and T. Nyokong, *Polydehron*, 1996, **15**, 2901.

230. W.A. Nevin, N. Liu, M. Melnil and A.B.P. Lever, *J. Electroanal. Chem.*, 1986, **213**, 217.

231. J.F. Myers and R.G.W. Canham, A.B.P. Lever, *Inorg. Chem.*, 1975, **14**, 461.

232. D. Dolphin, B.R. James, A.J. Murray and J.R. Thornback, *Can. J. Chem.*, 1980, **321**, 309.

233. P.C. Minor, M. Gouterman and A.B.P. Lever, *Inorg. Chem.*, 1985, **24**, 1894.

234. T. Nyokong, Z. Gasyna and M.J. Stillman, *Inorg. Chim. Acta*, 1986, **112**, 11

235. T. Nyokong, Z. Gasyna and M.J. Stillman, *Inorg. Chem.*, 1987, **26**, 548.

236. E. Ough, Z. Gasyna and M.J. Stillman, *Inorg. Chem.,* 1991, **30**, 2301.

237. T. Nyokong, *Polydehron*, 1993, **12**, 375.

238. D.W. Clack and J.R. Yandle, *Inorg. Chem.*, 1972, **11**,1739.

239. D.W. Clack, N.S. Hush and I.S. Woosley, *Inorg. Chim. Acta,* 1976, **19**, 129.

240. L.D. Rollman andR.T. Iwamoto, *J. Am. Chem. Soc.,* 1968, **90**, 1455

241. D.W. Clack and N.S. Hush, *J.Am. Chem. Soc.,* 1965, **87**, 4238.

242. R.H. Felton and H. Linschitz, *J. Am. Chem., Soc.,* 1966, **88**, 1113.

243. R.O Loufty andC. Chang, *J. Chem., Phys.,* 1980, **73**, 2902.

244. A.B.P. Lever and J.P. Wilshire, *Can. J. Chem.,* 1976, **54**, 2514.

245. A. Giraudeau, A. Louati, M. Cross, J.J. Andre, J. Simon, C.H. Su and K.M. Kadish, *J. Am. Chem. Soc.,* 1983, **105**, 2917.

246. G. Fu, Y-S. Fu, K. Kayaraj and A.B.P. Lever, *Inorg. Chem.,* 1990, **29**, 4090

247. T. Nyokong, Z. Gasyna and M.J. Stillman, *Inorg. Chem.,* 1987, **26**, 1087.

248. R.H. Campbell, G.A. Heath, G.T. Hefter and R.C. McQeen, *J. Chem. Soc. Chem. Commun.*, 1983, 1128.

249. H. Li and T.F. Guarr, *J. Chem. Soc. Chem. Commun.,* 1989, 832.

250. C.C. Leznoff, S. Greenberg, S.M. Marcuccio, P.C. Minor, P. Seymour and A.B.P.Lever, *Inorg. Chim. Acta,* 1984, **89**, L35.

251. R.J. Blagrove, *Austr. J. Chem.*, 1973, **26**, 472.

252. W. Liu, M.R. Hempstead, W.A. Nevin, M. Melnik, A.B.P. Lever and C.C. Leznoff, *J. Chem. Soc. Dalton Trans.*, 1987, 2511.

253. T. Nyokong, Z. Gasyna and M. Stillman, *ACS, Symp. Ser.*, 1986, **321**, 309.

254. A.B.P. Lever, *J. Porphyrins Phthalocyanines*, 1999, **3**, 488.

255. S. Griveau, G. Pavez, J.H. Zagal and F. Bedioui, *J. Electroanal. Chem.*, 2001, **497**, 75.

256. N. Grootboom and T. Nyokong, *Anal. Chim. Acta,* 2001, **432**, 49.

257. J. Oni and T. Nyokong, *Anal. Chim. Acta,* 2001, **432**, 9.

258. J.H. Zagal, M.A. Gulppi and G. Cárdenas-Jirón, *Polydehron*, 2000, **19**, 2255.

259. J.H. Zagal, *Coord. Chem. Rev.,* 1992, **119**, 89.

260. N. Kobayashi and W.A. Nevin, *Appl. Organomet. Chem.*, 1996, **10**, 579.

261. IUPAC Recommendation, 1997, *Pure and Appl. Chem.*, 1997, **69**, 1317.

262. R.F. Lane and A.T. Hubbard, *J. Phys. Chem.*, 1973, **77**, 1401.

263. C.M. Elliot, R.W. Murray, *Anal. Chem.*, 1976, **48**, 1247.

264. C.R. Martin, C.A. Foss Jr. in *Laboratory Techniques in Electroanalytical Chemistry*, 2nd ed., P.T. Kissinger and W.R. Heineman, Eds.; Marcel Dekker Inc., New York, 1996.

265. A.J. Bard, *J. Chem. Ed.*, 1983, **60**, 303.

266. J.J. Gooding and D.B. Hibbert, *TrAC,* 1999, **18**, 52

267. B.F. Watkins, J.R. Behling, E. Kariv and L.L. Miller, *J. Am. Chem. Soc.*, 1975, **97**, 3549.

268. L. Netzer and J. Sagiv, *J. Am. Chem. Soc.*, 1983, **105**, 674.

269. J. Wang, T. Golden, K. Varughese and I. El-Rayes, *Anal. Chem.*, 1989, **61**, 509.

270. M.B. Gilbert and D.J. Curran, *Anal. Chem.*, 1986, **58**, 1028.

271. T.J. Mafatle and T. Nyokong, *J. Electroanal. Chem.* 1996, **408**, 213.

272. J. Oni, *Ph.D Thesis*, Rhodes University, 2002.

273. J. Oni, P Westbroek and T. Nyokong, *J. Electrochem. Commun.*, 2001, **3**, 524.

274. T-F. Kang, G-L. Shen and R-Q, Yu, *Anal. Chim. Acta*, 1997, **356**, 245.

275. M.A. Ruiz, M.G. Blazquez and J.M. Pingarron, *Anal. Chim. Acta*, 1995, **305**, 49.

276. H.O Finklea in *Electroanalytical Chemistry*, A.J. Bard and I. Rubinstein, Eds., Marcel Dekker: New York, 1996; Vol. 19, pp109-335.

277. H.O. Finklea in *Encyclopedia of Analytical Chemistry: Applications, Theory and Instrumentations*, ed. R.A. Meyers, Wiley & Sons, Chichester, 2000, Vol. 11.

278. J. Sagiv, *J. Am. Chem. Soc.*, 1980, **102**, 92.

279. E.E. Polymeropoulos and J. Sagiv, *J. Chem. Phys.*, 1978, **69**, 1836.

280. R. Maoz, and J. Sagiv, *J. Colloid. Interface Sci.*, 1984, **100**, 465.

281. H.O. Finklea, L.R. Robinson, A. Blackburn, B. Richter, D. Allara and T. Bright, *Langmuir*, 1986, **2**, 239.

282. D. L. Allara and R.G. Nuzzo, *Langmuir*, 1985, **1**, 45

283. D. L. Allara and R.G. Nuzzo, *Langmuir*, 1985, **1**, 52.

284. R.G. Nuzzo and D.L Allara, *J. Am. Chem. Soc.*, 1983, **105**, 4481.

285. R.G. Nuzzo, F.A. Fusco and D.L Allara, *J. Am. Chem. Soc.*, 1987, **109**, 2358.

286. M.D. Porter, T.B. Bright, D. Allara and C.E.D. Chidsey, *J. Am. Chem. Soc.*, 1987, **109**, 3559.

287. H.O. Finklea, S. Avery, M. Lynch and T. Furtsch, *Langmuir*, 1987, **3**, 409.

288. E. Sabatani, I. Rubinstein, R. Maoz and J. Sagiv, *J. Electroanal. Chem.*, 1987, **219**, 365.

289. E. Sabatani and I. Rubinstein, *J. Phys. Chem.*, 1987, **91**, 6663.

290. E.B. Troughton, C.D. Bain, G.M. Whitesides, R.G. Nuzzo, D.L. Allara and M.D. Porter, *Langmuir*, 1988, **4**, 365.

291. L. Strong and G.M. Whitesides, *Langmuir*, 1988, **4**, 546.

292. C.D. Bain and G.M. Whitesides, *J. Am. Chem. Soc.*, 1988, **110**, 3665.

293. C.D. Bain and G.M. Whitesides, *J. Am. Chem. Soc.*, 1988, **110**, 5897.

294. C.D. Bain and G.M. Whitesides, *J. Am. Chem. Soc.*, 1988, **110**, 6560.

295. C.D. Bain and G.M. Whitesides, *Science,* 1988, **240**, 62.

296. C.A. Widrig, C. Chung and M.D. Porter, *J. Am. Chem. Soc.*, 1991, **310**, 335.

297. D.E. Weisshar, B.D. Lamp and M.D. Porter, *J. Am. Chem. Soc.,* 1992, **114**, 5860.

298. C-J. Zhong, J. Zak and M.D. Porter, *J. Electroanal. Chem.*, 1997, **421**, 9.

299. A. Dalmia, C.C. Liu and R.F. Savinell, *J. Electroanal. Chem.*, 1997, **430**, 205.

300. S.E. Creager and G.K. Rowe, *J. Electroanal. Chem.*, 1997, **420**, 291.

301. T. Wink, S.J. van Zuilen, A. Bult and W.P. van Bennekom, *Analyst*, 1997, **122**, 43R.

302. G. Che, Z. Li, H. Zhang and C.R. Cabrera, *J. Electroanal. Chem.*, 1998, **453**, 9.

303. C-J. Zhong, R.C. Brush, J. Anderegg and M.D. Porter, *Langmuir* 1999, **15**, 518.

304. P. Diao, D. Jiang, X. Cui, D. Gu, R. Tong and B. Zhong, *J. Electroanal. Chem.*, 1999, **464**, 61.

305. W. Yang, J.J. Gooding and D.B. Hibbert, *J. Electroanal. Chem.*, 2001, **516**, 10.

306. W.C. Bigelow, D.L. Pickett and W.A. Zisman, *J. Colloid Sci.*, 1946, **1**, 513.

307. D.L. Pilloud, X. Chen, P.L. Dutton and C.C. Moser, *J. Phys. Chem. B*, 2000, **104**, 2868.

308. P.E. Laibinis, G.M. Whitesides, D. Allara, Y-T. Tao, A.N. Parikh and R.G. Nuzzo, *J. Am. Chem. Soc.,* 1991, **113**, 7152.

309. K. Nishiyama, S-I. Tahara, Y. Uchida, S. Tanoue and I. Taniguchi, *J. Electroanal. Chem.*, 1999, **478**, 83.

310. C.D. Bain, E.B. Troughton, Y-T. Tao, J. Eval, G.M. Whitesides and R.G. Nuzzo, *J. Am. Chem. Soc.,* 1989, **111**, 321.

311. R.G. Nuzzo, B.R. Zegarski and L.H. Dubois, *J. Am. Chem. Soc.*, 1987, **109**, 733.

312. L.H. Dubois and R.G. Nuzzo, *Ann. Rev. Phys. Chem.*, 1992, **43**, 437.

313. R.L. Garrell, J.E. Chadwick, D.L. Severance, N.A. McDonald, D.C. Myles, *J. Am. Chem. Soc.*, 1995, **117**, 11563.

314. G.M. Whitesides and P.E. Laibinis, *Langmuir*, 1990, **6**, 87.

315. A. Ulman, *An Introduction to Ultrathin Organic Films from Langmuir-Blodgett to Self-assembly,* Academic Press, San Diego, 1991.

316. A.R. Özkaya, E. Hamurryudan, Z.A. Bayir and Ö. Bekaroğlu, *J. Porphyrins Phthalocyanines,* 2000, **4**, 689.

317. G. Kalyuzhny, A. Vaskevich, G. Ashkenasy and A. Schanzer, I. Rubinstein, *J. Phys. Chem.*, B, 2000, **104**, 8238.

318. D.A. Offord, S.B. Sachs, M.S. Ennis, T.A. Eberspacher, J.H. Griffin, C.E.D. Chidsey and J.P. Collman, *J. Am. Chem. Soc.*, 1998, **120**, 4478.

319. Z. Zhang, S. Hou, Z. Zhu and Z. Liu, *Langmuir*, 2000, **16**, 537.

320. J. Zak, H. Yuan, M. Ho, L.K. Woo and M.D. Porter, *Langmuir*, 1993, **9**, 2772.

321. J.E. Hutchison, T.A. Postlethwaite and R.W. Murray, *Langmuir*, 1993, **9**, 3277.

322. N. Kobayashi, P. Janda and A.B.P. Lever, *Inorg. Chem.*, 1992, **31**, 5172.

323. K. Juodkazis, J. Juodkazyté, B. Šebeka and A. Lukinskas, *Electrochem. Commun*, 1999,**1**, 315.

324. A. Elzing, A. van der Putten, W. Vissler and E. Barendrecht, *Electroanal. Chem.*, 1987, **99**, 95

325. Y-H. Tse, P. Janda, H. Lam, W.J. Pietro and A.B.P. Lever, *J. Porphyrins phthalocyanines*, 1997, **1**, 3.

326. D.A. Van Galen and M. Majda, *Anal. Chem.*, 1988, **60**, 1549.

327. J.H. Zagal, M. Paez, A.A. Tanaka, J.R. dos Santos and C.A. Linkous, *J. Electroanal.Chem.*,1992, **339**, 13.

328. J.H. Zagal, M.A. Guilppi, C. Depretz and D. Lelievre, J. *Porphyrins phthalocyanines*, 1999, **3**, 355.

329. D. Losic, J.G. Shapter and J.J. Gooding, *Langmuir*, 2001, **17**, 3307.

330. H.O. Finklea, D.A Snider and J. Fedyk, *Langmuir*, 1990, **6**, 371.

331. L. Zhang, T. Lu, G.W. Gokel and A.E. Kaifer, *Langmuir*, 1993, **9**, 786.

332. U.K. Sur and V. Lakshminarayanam, *J. Electroanal. Chem.*, 2001, **516**, 31.

333. J.M.D. Rodriguez, J.A.H. Melián and J.P. Peña, *J. Chem. Educ.*, 2000, **77**, 1195.

334. H.O. Finklea and D.D. Hansheu, *J. Am. Chem. Soc.*, 1992, **114**, 3173.

335. A.M. Becka and C.J. Miller, *J. Phys. Chem.*, 1992, **96**, 2657.

336. J.J. Gooding, V. Praig and E.A.H. Hall, *Anal. Chim Acta*, 1998, **70**, 2396.

337. M. Mrksich, G.M. Whitesides, *Annu. Rev. Biomol. Struct.*, 1996, **25**, 55.

338. I. Willner, R. Blonder and A. Dagan, *J. Am. Chem. Soc.*, 1994, **115**, 4935.

339. V.W. Jones, J.R. Kenseth, M.D. Porter, C.L. Mosher and E. Henderson, *Anal. Chem.*, 1998, **70**, 1233.

340. Y. Okahata, Y. Matsunobu, K. Ijiro, M. Mukae, A. Murakami and K. Makino, *J. Am. Chem. Soc.*, 1992, **114**, 8299.

341. I. Willner, M. Lion-Dagan, S. Marx-Tibbon and E. Katz, *J. Am. Chem. Soc.*, 1995, **117**, 6581.

342. T.R.E. Simpson, D.A. Russell, I. Chambrier, M.J. Cook, A.B. Horn and S.C. Thorpe, *Sens. Actuators B*, 1995, **29**, 353.

343. T.R.E. Simpson, M.J. Cook, M.C. Petty, S.C. Thorpe and D.A. Russell, *Analyst*, 1996, **121**, 1501.

344. C.W. Dirk, T. Inabe, K.F. Schoch Jr, T.J. Marks, *J. Am. Chem. Soc.*, 1983, **105**, 1539.

345. A. G. Gürek and Ö. Bekaroğlu, *J. Porphyrins Phthalocyanines*, 1997, **1**, 67.

346. A. G. Gürek and Ö. Bekaroğlu, *J. Porphyrins Phthalocyanines*, 1997, **1**, 227.

347. Z.A. Bayir, E. Hamuryudan, A. G. Gürek and Ö. Bekaroğlu, *J. Porphyrins Phthalocyanines*, 1997, **1**, 349.

348. A.I. Vogel, *A textbook of Quantitative Inorganic Analysis Including Elementary Instrumental Analysis*, 3rd ed., Longman, London, 1968.

349. T. Nyokong, *S. Afr. J. Chem.*, 1995, **48**, 23.

350. J.R. Darwent, I. McCubbin and D. Phillips, *J. Chem. Soc., Faraday Trans. 2,* 1982, **78**, 347.

351. P.C. Martin, M. Gouterman, B.V. Pepich, G.E. Renzoni and D.C. Schindele, *Inorg. Chem.*, 1991, **30**, 3305.

352. R. Edrei, V. Goofried, J.E. van Lier and S. Kimel, *J. Porphyrins Phthalocyanines,* 1998, **2,** 191.

353. G. Schneider, D. Wöhrle, W. Spiller, J.Stark and G. Schult-Ekloff, *Photochem. Photobiol.,* 1994, **60,** 333.

354. D.R. Boston and J.C. Bai, *Inorg. Chem.*, 1972, **11**, 1578.

355. M.T.M. Choi, P.S.P. Li and K.P. Ng, *Tetrahedron,* 2000, **56,** 3881.

356. C. F. van Nostrum, S.J. picken, A.-J. Schouten, R.J.M. Nolte, *J. Am. Chem. Soc.,* 1995, **117,** 9957.

357. J. Metz, O. Schneider and M. Hanack, *Inorg. Chem.,* 1984, **23**, 1065.

358. B.W. Dale, *Trans. Faraday Soc.*, 1969, **65**, 331

359. M.J. Stillman and A.J. Thomson, *J. Chem. Soc., Faraday Trans.* 2, 1974, **70**, 790.

360. A.B.P lever and J.P. Wilshire, *Inorg. Chem.*, 1978, **17**, 1145.

361. N. Kobayashi, M. Koshiyama, K. Funayama, T. Osa, H. Shirai and K. Hanabusa, *J. Chem. Soc., Chem. Comm.,* 1983, 913.

362. N. Kobayashi, H. Shirai and N. Hojo, *J. Chem., Soc., Dalton Trans.*, 1984, 2107.

363. N. Kobayashi and Y. Nishiyama, *J. Phys. Chem.*, 1985, **89**, 1167.

364. N.P. Farrell, A.J. Murray, J.R. Thornback, D.H. Dolphin and B.R. James, *Inorg. Chim. Acta,* 1978, **28**, L144.

365. M.J. Stillman and A.J. Thomson, *J. Chem., Soc., Faraday Trans.2*, 1974, **70**, 805.

366. C. Ercolani. M. Gardini, F. Monacelli, G. Pennesi and G. Rossi, *Inorg. Chem.*, 1983, **22**, 2584.

367. R. Behnisch and M. Hanack, *Synth. Met.*, 1990, **36**, 387.

368. Y. Orihashi, H. Ohno, E. Tsuchida, H. Matsuda, H. Nakanishi and M. Kato, *Chem. Lett.*, 1987, 601.

369. M. Scxhartz, W.E. Hatfield, M.D. Joesten, M. Kanack and A. Datz, *Inorg. Chem.*, 1985, **24**, 4198.

370. D.B. Leznoff, B-Y. Xue, B.O. Patrick, V. Sanchez and R.C. Thompson, *Chem. Commun.*, 2001, 259.

371. J.M. Fernandez, M.D. Bilgin and L.I. Grossweiner, *J. Photochem. Photobiol. B: Biol.*, 1997, **37**, 131.

372. N. Kutznetsova, N. Grestova, V. Derkacheva, O.Yuzhakova, S. Mihailenko, L. Solovieva, O. Kaliya and E. Zukyanets, *Zh. Obsch. Khim.*, 2000, **72**, 325.

373. G. Schnurpfeil, A.K.Sobbi, W. Spiller, H. Kliesch and D. Wöhrle, *J. Porphyrins phthalocyanines*, 1997, **1**, 159.

374. M.D.Maree, N. Kuznetsova and T. Nyokong, *J. Photochem. Photobiol. A: Chem.*, 2001, **140**, 117.

375. I. Seotsanyana-Mokhosi, N. Kuznetsova and T. Nyokong, *J. Photochem. Photobiol. A: Chem.* 2001, **140**, 215.

376. N. Kobayashi, H. Lam, W.A. Nevin, P. Janda, C.C. Leznoff and A.B.P. Lever, *Inorg. Chem.*, 1990, **29**, 3415.

377. A.R. Özkaya, A. Gurek, A. Gul and O Bekaroglu, *Polyhedron*, 1997, **16**, 1877.

378. M. Isaacs, M.J. Aguirre, A. Toro-Labbe, J. Costamagna, M. Paez and J.H. Zagal, *Electrochim. Acta*, 1998, **43**, 1821.

379. Y. Kaneko, Y. Nishimura, T. Avai, H. Sakuraji, K. Tokumaru and D. Matsunaga, *J. Photochem. Photobiol. A: Chem.*, 1995, **89**, 37.

380. T. Nyokong, *J. Chem. Soc., Dalton Trans.*, 1994, 1359.

381. M.J. Stillman in *Phthalocyanines: Properties and Applications*, eds. C.C. Leznoff, A.B.P. Lever, VCH, New York, 1993, Vol.3.

382. A.-P. Durand, R. G. Brown, D. Worrall and F. Wilkinson. *J. Photochem. Photobiol. A: Chem.*, 1996, **96,** 35.

383. T. Sehili, P. Boule and J. Lemaire, *J. Photochem. Photobiol. A: Chem.*, 1989, **50,** 117.

384. T. Matsuura, N. Yoshimura, I. Saito, *Tetrahedron*, 1972, **28**, 4933.

385. V. Iliev, *J. Photochem. Photobiol. A: Chem.*, 2002, **151,** 195.

386. D. Martire, S. Braslavsky and N. Garcia, *J. Photochem. Photobiol. A: Chem.*, 1991, **61,** 113.

387. S. Egorov, V. Kamalov, N. Koroteev, A. Krasnovsky, B. Toleutaev and S. Zinukov, *Chem. Phys. Lett.* 1989, **163**, 421.

388. L.Shoute and J.Mittal. *J. Phys. Chem.* 1996, **100**, 3016.

389. K.V. Gothelf, *J. Electroanal. Chem.*, 2000, **494,** 147.

390. A.M. Bond, S. Kratsis, S. Mitchell and J. Mocak. *Analyst*, 1997, **122**, 1147.

391. C.E.D. Chidsey and D.N. Loiacono, *Langmuir* 1990, **6**, 682.

392. S.G. Hickey and D.J. Riley, *Electrochem. Commun.* 1999, **1**, 116.

393. R.J. Nichols, E. Bunge, H. Meyer and H. Boumgärtel, *Surf. Sci.*, 1995, **335,** 110.

394. I. Rubinstein, S. Steinberg, Y. Tor and A. Shanzer, J. Sagiv, *Nature*, 1988, **332,** 426.

395. C. Rocchicciolli-Deltcheff, N. Fournier, R. Frank and R. Thouvenot, *Inorg. Chem.* 1983, **22**, 207.

396. D. Schlettwein and T. Yoshida, *J. Electroanal. Chem.*, 1998, **441**, 139.

397. M.N. Golovin. P Seymour, K. Jayaraj, Y. Fu and A.B.P. Lever, *Inorg. Chem.* 1990, **29**, 1719.

398. J.E. Chadwick, D.C. Myles and R.L. Garrell, *J. Am. Chem. Soc.*, 1993, **115,** 10364.

399. R.L.Garrell, J.E. Chadwick, D.L. Severance, N.A. McDonald and D.C. Myles, *J. Am. Chem. Soc.*, 1995, **117,** 11563.

400. S. Steinberg, Y. Tor, E. Sabatani and I. Rubinstein, *J. Am. Chem. Soc.* 1991, **113**, 5176.

401. W.R. LaCourse and G.S. Owens, *Anal. Chim. Acta*, 1995, **307**, 301.

402. X. Huang and W.T. Kok, *Anal. Chim Acta,* 1993, **273**, 245.

403. X. Huang and W.T. Kok, *J. Chromatogr.,* 1995, **716**, 347.

404. G. Favaro and M. Fiorani, *Anal. Chim Acta,* 1996, **332**, 249.

405. M.K. Amini, S. Shahrokhian and S. Tangestaninejad, *Anal. Lett.* 1999, **32**, 2737.

406. N.A. Chaniotakis, A.M Chasser, M.E. Meyerhoff and J.T. Groves, *Anal. Chem.*, 1988, **60**, 185.

407. S. Duunert, S. Wallace, A. Florido and L.G. Bachas, *Anal. Chem.*, 1991, **63**, 1676.

408. J.H. Khorasani, M.K. Amini, H. Motaghi, S. Tangestaninejad and M. Moghadam, *Sens. Actuators B*, 2002, **87**, 448.

409. J. Marsden and I House in *The Chemistry of Gold Extraction,* Ellis Horwood, Chichester, England, 1992.

410. A. Starvat and A.V. Lierde, *J. App. Electrochem.*, 2001, **31**, 469.

411. H. Tatsuta, T. Nakamura and T. Hinoue, *Anal. Sci.,* 2001, **17**, 991.

412. D.W. Kirk, F.R. Foulkes and W.F. Graydon, *J. Electrochem. Soc.*, 1978, **125**, 1436.

413. D.W. Kirk, F.R. Foulkes and W.F. Graydon, *J. Electrochem. Soc.*, 1980, **127**, 1962.

414. C.P. Thurgood, D.W. Kirk, F.R. Foulkes and W.F. Graydon, *J. Electrochem. Soc.*, 1981, **128**, 1680.

415. A. Kumar, H.A. Biebuyck, N.L. Abbott and G.M. Whitesides, *J. Am. Chem. Soc.*, 1992, **114**, 9188.

416. L.Sun and R.M. Cooks, *Langmuir*, 1993, **9**, 1951.

417. L. Libioulle, A. Bietsch, H. Schmid, B. Michel, E. Delamarche, *Langmuir*, 1999, **15**, 300.

418. R.B. Bass and A.W. Lichtenberger, unpublished results.

419. G. Drochioiu, *Talanta*, 2002, **56**, 1163

420. E. Olivas, D. de Wall and R. Wilkins, *J. Biol. Chem.*, 1977, **252**, 4038.